University of California
Los Angeles

An Infrared Search for Substellar Companions to Nearby White Dwarfs

A dissertation submitted in partial satisfaction
of the requirements for the degree
Doctor of Philosophy in Physics

by

Jay Farihi

2004

The dissertation of Jay Farihi is approved.

John T. Wasson

Stuart E. Brown

Ian S. McLean

Benjamin M. Zuckerman

Eric E. Becklin, Committee Chair

University of California, Los Angeles

2004

To my mother JoAnn...

who showed me, by her example,

how to succeed

Table of Contents

List of Figures

List of Tables

Acknowledgments

My thanks goes first and foremost to Eric Becklin for giving me the opportunity to work on this project. When no one else would, he gave me the chance I needed. I owe both Eric Becklin and Ben Zuckerman a debt of gratitude for teaching me how to be a careful scientist.

I am sincerely grateful for the help of former fellow graduate students Chris McCarthy and Patrick Lowrance – they, more than anyone, jumpstarted my career in stellar astrophysics. Other UCLA astronomy colleagues, researchers and faculty to whom I owe thanks for dozens of questions, conversations, and overall good advice include; Lisa Prato, Inseok Song, Gaspard Duchene, David Reitzel, Ralph Shuping, Adam Burgasser, James Colbert, Samir Salim, Brad Hansen, Mike Jura, Ian McLean, Mark Morris, and James Larkin.

I am indebted to Steward Observatory for their generosity with telescope time to our group, without which this thesis would not exist.

The Lick Observatory Staff deserves so many thanks for taking care of me for more days than I care to remember. I thank Rem Stone, Elinor Gates and Tony Misch for nearly unending and ever-needful help with instrument support, instruction, and especially troubleshooting. Wayne Earthman, Keith Baker, Kostas Chloros, John Morey, and Bernie Walp all helped me on countless nights with both telescope and instrument support. I also thank Orfa Campbell and Karen St. James for making sure I was properly fed.

Vita

1970	Born, Los Angeles, California
1988	Graduated with High Honors, Cerritos High School, Cerritos, California
1990-96	Electrocardiogram Telemetry Technician, Pioneer Hospital, Artesia, California
1995	Inducted into the National Physics Honor Society, Sigma Pi Sigma
1995	Parker Fellowship recipient
1996	Graduated with High Honors, California State Polytechnic University, Pomona, B.S. in both Physics and Mathematics
1996-99	Teaching Assistant, Physics & Astronomy Department, U.C. Los Angeles
1998	Lead Laboratory Teaching Assistant, Co-Supervisor and Co-Author of Undergraduate Physics Electromagnetism Laboratory, U.C. Los Angeles
1999	Leader of PDP/Excel Innovative Tutorial Workshop on Physics, U.C. Los Angeles
1999	M.S. in Physics, U.C. Los Angeles

2000-2004 Graduate Student Researcher, Physics & Astronomy Department, U.C. Los Angeles, under the guidance of Eric Becklin

Publications

"The Search for Brown Dwarfs Around White Dwarfs", J. Farihi, E. Becklin, & B. Zuckerman 2003, in Proceedings of IAU Symposium 211: Brown Dwarfs, ed. E. Martn (San Francisco: ASP), 289

"Mid-Infrared Observations of van Maanen 2: No Substellar Companion", J. Farihi, E. Becklin, & B. Macintosh, B. 2004, ApJ, 608, L109

"Discovery of an Ultracool White Dwarf Companion", J. Farihi 2004, ApJ, 610, 1013

"A Possible Brown Dwarf Companion to the White Dwarf GD1400", J. Farihi & M. Christopher 2004, AJ, 128, 1868

Abstract of the Dissertation

An Infrared Search for Substellar Companions to Nearby White Dwarfs

by

Jay Farihi

Doctor of Philosophy in Physics

University of California, Los Angeles, 2004

Professor Eric E. Becklin, Chair

This paper presents the results of an extensive search for substellar companions to white dwarfs in the solar neighborhood. The work consists of two major components. The first part is a survey conducted with the Keck I 10 meter telescope of 86 white dwarfs. This deep near field search was sensitive to companions orbiting between roughly $50-1100$ AU of the primary star. The second part is a wide field survey conducted with the Bok 2.3 meter and Shane 3 meter telescopes of 261 white dwarfs. This latter search was sensitive to companions orbiting between roughly $100-5000$ AU. The entire sample has a median distance of around 57 pc.

The J band, centered at 1.25 μm, was chosen as the appropriate wavelength to conduct this search. This atmospheric window lies near the peak in luminositiy of substellar objects, commonly called brown dwarfs. The mass limits of the searches are dependent on the age of the white dwarfs in the sample because brown dwarfs cool as they evolve. The exact ages of the target primaries cannot be known because of their uncertain main sequence progenitor lifetimes. However,

for white dwarfs about 3 Gyrs old, a reasonably conservative median age estimate, companions more massive than 0.06 $M_{\odot}$ in the wide field search and more massive than 0.03 $M_{\odot}$ in the deeper near field search were detectable.

In neither component of the survey were any brown dwarf candidates detected. This implies a brown dwarf companion fraction of less than 0.3% for white dwarfs. In stark contrast, the stellar companion fraction of white dwarfs as measured by this survey is 22%. Moreover, most of the known and suspected stellar companions to white dwarfs are low mass stars whose masses are only slightly greater than the masses of brown dwarfs. This result has strong implications for binary star formation.

Twenty previously undiscovered stellar companions were detected, five of which are confirmed or likely white dwarfs themselves. The remaining fifteen detected companions are confirmed or likely low mass stars.

CHAPTER 1

Introduction

Until less than a decade ago and despite many searches, scientists had no direct evidence of astrophysical objects with masses in between that of stars and planets. Yet the missing link between these two, dubbed brown dwarfs, are now a field of study unto themselves. There remains much to learn about these failed stars, especially their astrophysical niches, origins and destinies.

1.1 Defining Brown Dwarfs

Brown dwarfs are gravitationally bound spheres of gas that never acheive the core temperatures required to ignite hydrogen fusion due to insufficient total mass (Kumar 1963). The mass corresponding to this cutoff has been calculated to be a little less than 0.080 $M_{\odot}$ for solar metallicity (Burrows et al. 1997; Chabrier et al. 2000).

These failed stars have no sustainable energy source – they cool off and dim as they age. While most of their energy comes from gravitational contraction, brown dwarfs receive an ephemeral brightening from fusing light elements such as lithium and deuterium. The process of gravitational collapse is eventually halted by electron degeneracy pressure at approximately 1 R_{Jup}.

In this thesis brown dwarfs are defined as having mass in the range 0.012 $M_{\odot} < M < 0.075\ M_{\odot}$. Since companion objects are the focus of this research,

anything with less mass than 0.012 $M_{\odot}$ in orbit around a star will be called a giant planet. Objects more massive than 0.075 $M_{\odot}$ are full fledged stars.

1.2 Brown Dwarf Searches

There are essentially three places to look for brown dwarfs: in the field, in clusters, and in orbit around nearby stars. Each search venue offers its own advantages, and, with the exception of the radial velocity technique, all search strategies involve imaging.

1.2.1 Companion Searches

Searching for brown dwarfs as companions to stars offers the opportunity to search systems very near to the Sun and requires less time than field and cluster searches covering a relatively large portion of the sky. The very first serious brown dwarf candidate was discovered as a companion to the white dwarf GD 165 (Becklin & Zuckerman 1988). GD 165B ($M \sim 0.072\ M_{\odot}$, $T_{\rm eff} = 1900$ K) remained unique for a number of years but eventually became the prototype for a new spectral class of cool stars and brown dwarfs, the L dwarfs (Kirkpatrick et al. 1999a). The first bona fide brown dwarf was also discovered as a companion to another star, Gl 229 (Nakajima et al. 1995). Coincidentally enough, Gl 229B ($M \sim 0.040\ M_{\odot}$, $T_{\rm eff} = 950$ K) also remained unique for a time and became the prototype T dwarf (Marley et al. 1996; Kirkpatrick et al. 1999b), the coolest known spectral class, all of whose members are brown dwarfs.

Including the searches which discovered the first L and T dwarfs, there have been several dedicated searches for brown dwarfs as companions to nearby stars (Zuckerman & Becklin 1987a, 1992; Henry & McCarthy 1990; Marcy & Butler

1994; Macintosh 1994; Nakajima et al. 1994; Oppenheimer et al. 2001; Lowrance 2001; Schroeder et al. 2000; Hinz et al. 2002; Potter, Martín, & Cushing 2003; Carson et al. 2003; Marois et al. 2003; McCarthy & Zuckerman 2004). The general strategy is to image in the near infrared and followup any candidate objects spectroscopically and for common proper motion with the primary star. There are a few variations on the basic technique; the use of a coronagraph to diminish the contaminating light of the primary star, imaging at one infrared and one optical wavelength to obtain a color as a discriminator, searching for photometric excess flux above the primary star's continuum radiation due to an unresolved brown dwarf, and very high angular resolution imaging to probe the smallest separations possible.

Radial velocity searches monitor spectral lines in a star for variable shifts due to the induced reflex motion from a massive orbiting body. This technique is quite sensitive to brown dwarfs orbiting within ~ 5 AU but has found very few. Butler et al. (2000) estimates the brown dwarf companion frequency to be less than 0.5%. This figure includes the search of several hundred stars and is thus a very good measure for the innermost orbital separations.

Direct imaging searches have also produced a dearth of brown dwarf companions to main sequence stars (relative to stellar companions) at wider separations (Zuckerman & Becklin 1987a, 1992; Henry & McCarthy 1990; Macintosh 1994; Nakajima et al. 1994; Oppenheimer et al. 2001; Schroeder et al. 2000; Hinz et al. 2002; Potter, Martín, & Cushing 2003; Carson et al. 2003; Marois et al. 2003; McCarthy & Zuckerman 2004). The separation range corresponding to the peak in the stellar companion distribution for both G and M dwarf primaries is roughly $10-100$ AU (Duquennoy & Mayor 1991; Fischer & Marcy 1992). In Figure 1.1 is plotted the period distribution for nearby G dwarfs. This range has been searched

quite extensively by the aforementioned surveys and very few brown dwarfs have been found. The most optimisitic estimate for the brown dwarf companion frequency to main sequence star is $\sim 2\%$, although most studies conclude that it is less than 1%. The only exception to this being the case when the primary star is a very low mass star or brown dwarf ($M < 0.10\ M_{\odot}$). For these low mass primaries, the binary fraction is estimated to be $\sim 20\%$, although no system wider than 20 AU has been observed (Reid et al. 2001; Close et al. 2002, 2003; Siegler et al. 2003; Allen et al. 2003; Burgasser et al. 2003; Gizis et al. 2003). Thus it appears that the brown dwarf companion frequency is a strong function of primary mass.

1.2.2 Cluster Searches

The first brown dwarfs identified in significant numbers were found in the Pleiades nearby open cluster (Basri, Marcy, & Graham 1996; Rebolo et al. 1996). For the most part, the first searches were deep imaging searches at two optical wavelengths, with spectroscopic followup for candidates identified by their red colors. At the *sim*100 Myr age of the Pleiades , low mass stars will have fused all their lithium while brown dwarfs will have retained detectable amounts. In this way it was demonstrated that all objects later than spectral type M6.5 still exhibit lithium in their spectra and are hence brown dwarfs (Stauffer, Schultz, & Kirkpatrick 1998).

Subsequent studies of the Pleiades, deeper surveys including infrared imaging as well, have discovered upwards of two dozen brown dwarfs and many more candidates (Martín et al. 1998, 2000, 2003; Schultz 1999; Nagashima et al. 2003; Schwartz, Becklin, & Zuckerman 2003). Similar searches of other open clusters, such as IC 348, Orion, ρ Ophiucus, Trapezium, Praesepe, and α Persei, have also

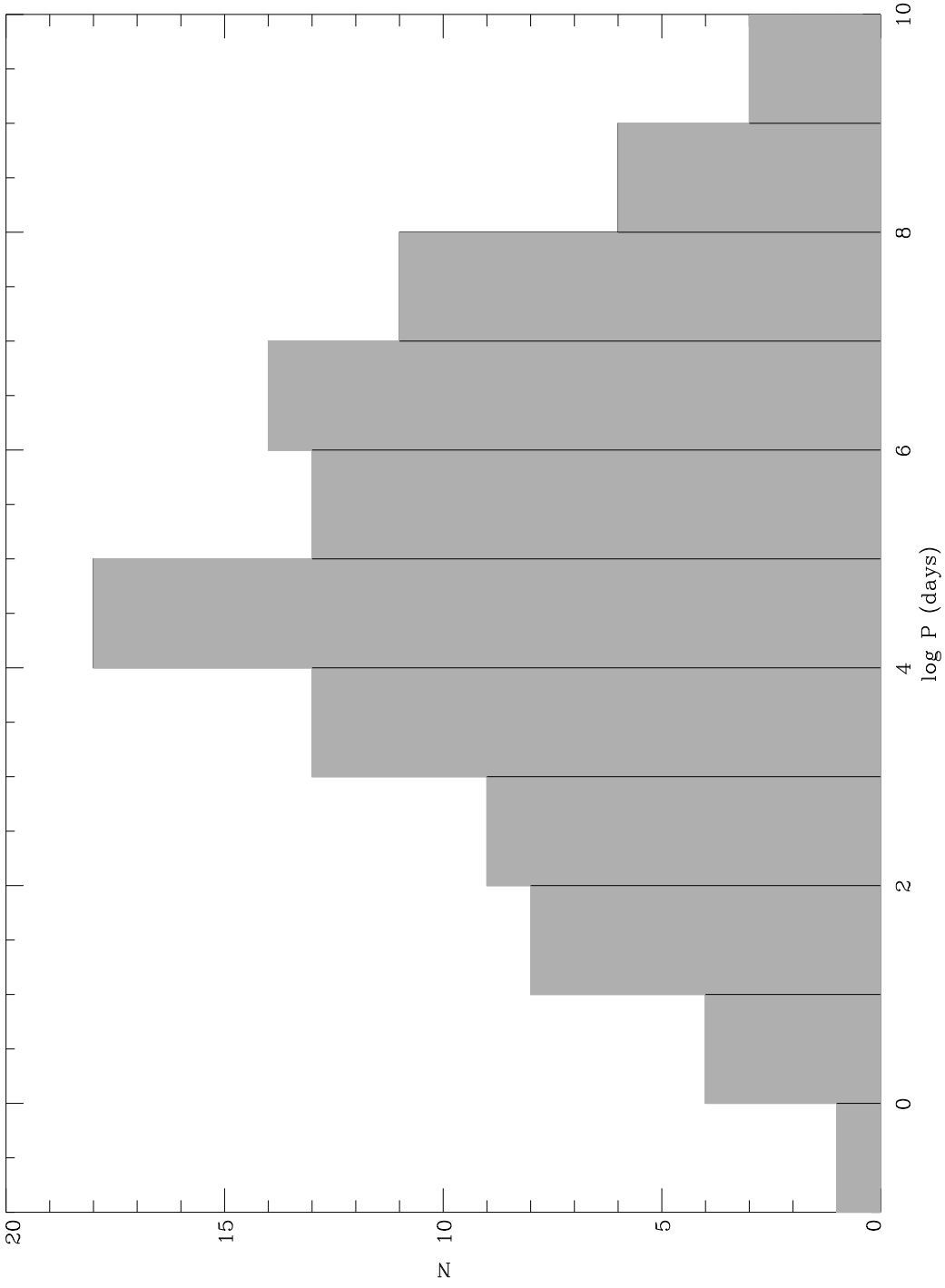

Figure 1.1: The period distribution for nearby binary systems with G dwarf primaries as measured by (Duquennoy & Mayor 1991). The peak corresponds to 30 AU for a total binary system mass of 1.5 $M_{\odot}$.

successfully identified candidate and confirmed brown dwarfs – some down to the deuterium burning limit (Magazzù et al. 1998; Martín, Basri, & Zapatero-Osorio 1999; Zapatero-Osorio et al. 1999; Stauffer et al. 1999; Lucas & Roche 2000; Tej et al. 2002). The advantage of searching in open clusters is that they are generally young ($\tau < 1$ Gyr) and hence substellar objects will still be relatively luminous.

1.2.3 Field Searches

Surveys like the Two Micron All Sky Survey (2MASS), the Deep Near Infrared Sky Survey (DENIS), and the Sloan Digital Sky Survey (SDSS) have revolutionized the discovery and classification of very low mass stars and brown dwarfs. These three surveys combined have discovered more low mass stars and brown dwarfs than any other type of survey. They have the advantage of covering a significant portion of the entire sky or, as in the case of 2MASS, the whole sky. The method is simply to image at multiple optical and/or infrared wavelengths in order to distinguish cool objects by their unique colors. All told there are over 200 field L and T dwarfs discovered from these surveys and subsequent followup studies, most but not all of which are brown dwarfs. Future space infrared all sky surveys have a high probability of detecting even cooler brown dwarfs.

The defining objects for the L spectral class came exclusively from 2MASS, while both 2MASS and SDSS provided defining objects for the T spectral class (Kirkpatrick et al. 1999b; Burgasser 2001). Field stars, stars with no cluster association, are generally suspected of being relatively old ($\tau > 1$ Gyr). If no age or mass estimate is available, then spectral class is used to determine whether a field dwarf is substellar in nature. The best models predict that 'stars' with $T_{\rm eff} < 1750$ K, corresponding to spectral types later than L4, are substellar (Burrows et al. 1997; Kirkpatrick et al. 1999b).

There has been an ongoing search for main sequence companions to 2MASS field L and T dwarfs (Gizis et al. 2001; Gizis 2003). However, it can be trivially demonstrated that this is not statistically equivalent to searching for brown dwarf companions to main sequence stars. Specifically, the number of main sequence stars without L and T dwarf companions is not measured in any way.

1.3 Brown Dwarf Formation

Brown dwarfs, when hypothesized for the first time, were theorized to form just like stars – from gravitational collapse of dust and gas. While this is still the accepted mechanism for their formation, it is clear that they *can* form in disks as evidenced by the few brown dwarfs which have been discovered by the radial velocity technique to be in close orbits around solar type stars (Butler et al. 2000). As stated in the beginning of this chapter, no formation dependence in the definition of brown dwarfs is used here. What is of interest for this thesis is to constrain theories of formation and evolution for low mass stellar and substellar companions to white dwarfs.

Single or binary brown dwarfs should, in general, form like stars. Density perturbations in molecular clouds can cause a small protostellar core to develop which will in turn gravitationally attract surrounding material. Once started, this runaway process culminates in the birth of a star or brown dwarf. The most accepted mechanism for the formation of binaries and multiple systems is fragmentation in the protostellar core before significant accretion occurs. These fragments then accrete fully into a binary or multiple system of stars and/or brown dwarfs.

1.3.1 Field Brown Dwarfs

The idea that brown dwarfs form like stars is supported by the initial mass function as measured in the field. This is a measurement of the number of objects that form in a given volume as a function of mass or dN/dM. The initial mass function is normally expressed as $\psi(M) \propto M^{-\alpha}$ where α is a positive number determined from observations. The negative slope implies a rising trend toward lower masses. The classical value for the initial mass function as determined by Salpeter (1955) is $\alpha = 2.35$

Until recently the initial mass function was not well known in the regime of very low mass stars and brown dwarfs. With the completion of 2MASS and DENIS, researchers were finally able to compute an estimate down into substellar masses. Reid et al. (1999) calculate a value of $\alpha = 1.5 \pm 0.5$, where they state in a note added in proof that values near the lower limit are favored due to recent field T dwarf detections. At a value of $\alpha = 1.3$, brown dwarfs are twice as common as main sequence stars but contribute no more than $\sim 15\%$ of the total mass of the disk – hence they are ubiquitous but not a major component of Galactic dark matter.

1.3.2 Cluster Brown Dwarfs

Also of interest is the determination of the initial mass function in open clusters. In the Pleiades it appears to be flat or rising across the stellar/substellar boundary (from masses just under 0.07 $M_{\odot}$) with at most a gradient of $\alpha = 0.7$ (Hambly et al. 1999). Another study found $\alpha = 0.6$ over an almost identical mass range (Bouvier et al. 1998). Both of these studies are consistent with a more recent study which extends to even lower masses, where it was found that the initial mass function in the Pleiades is well represented by $\alpha = 0.41 \pm 0.08$ for 0.035

$M_\odot < M < 0.30\ M_\odot$ (Jameson et al. 2002). For IC 348, a value of $\alpha = 0.5$ is derived in a study that was complete over the mass range $0.015\ M_\odot < M < 0.70\ M_\odot$ (Najita, Tiede, & Carr 2000). In the Trapezium cluster, an HST/NICMOS study found an intial mass function that is flat or slowly rising from well into the substellar regime (Luhman et al. 2000). That study was complete over the mass range $0.020\ M_\odot < M < 0.60\ M_\odot$. The same study compared the results for the Trapezium with their own ground based work on IC 348 and ρ Ophiucus and found no significant difference in the initial mass function between these three different regions across the stellar/substellar boundary (Luhman et al. 2000). Lastly, similar results have come from a study in the Orion Nebula Cluster. For masses down to $0.02\ M_\odot$, a value of $\alpha = 0.43$ was found (Hillenbrand & Carpenter 2002). Very similar results have been reported in α Persei and σ Orionis (Béjar et al. 2001; Barrado y Navascués et al. 2002)

It is considered something of a holy grail to find an initial mass function that varies significantly from those mentioned above. Is there a universal initial mass function or does it depend on ambient conditions within each star forming environment? The Hyades appears to have a real dearth of low mass objects relative to other open clusters. Several studies have confirmed this observational fact (Macintosh 1994; Reid & Gizis 1997; Gizis, Reid, & Monet 1999). There may also be some preliminary evidence for a nonuniversal substellar mass function in the Taurus star forming region (Briceño et al. 2003). It remains to be seen if further evidence of this will be found.

1.3.3 Companion Brown Dwarfs

The seminal work of Duquennoy & Mayor (1991) supported the idea of binary star formation by random pairing of two stars formed with the same initial mass

function. This was due to the similarity of the secondary masses in their nearby G dwarf sample with the mass function for low mass field stars which shows an increase toward lower masses (Kroupa, Tout, & Gilmore 1990). If this were true, one would expect roughly the same number of substellar and low mass stellar companions to main sequence stars. As mentioned earlier in this chapter, there is a real dearth of brown dwarf companions to main sequence stars at both close and wide separations. This may also be true within the Hyades cluster as well as in the field. More than one survey has turned up a scarcity of brown dwarf companions to both white dwarf and low mass main sequence primaries in the Hyades (Macintosh 1994; Reid & Gizis 1997).

To explain this deficit and the flattening of the low mass end of the initial mass function, it has been proposed that brown dwarfs are ejected stellar embryos (Reipurth & Clarke 2001). That is, brown dwarfs may be lost through dynamically unstable interactions in multiple protostellar systems before they can accrete enough material to reach the minimum hydrogen burning mass. It is not clear that ejection is consistent with the observational fact that roughly 20% of all brown dwarfs are binaries. Another mechanism proposed to explain the lack of close brown dwarf companions is differential accretion in a protobinary disk (Bate 2000). In this scenario, each component in a tight protobinary accretes equally and produces a mass ratio near one; whereas one component in a wider protobinary can accrete most of the surrounding disk material and leave the other component with a substellar mass. Hence, this predicts low mass stellar and substellar companions to main sequence stars should be more common at wide separations. However, there have been two studies of very young binary systems in which the distribution of mass ratios was found to have no dependence on component separation nor primary mass (Woitas 1999; Prato et al. 2002). It should be noted that Bate, Bonnell, & Bromm (2002) currently favor the ejection

mechanism for the formation of brown dwarfs.

This thesis will show that the initial mass function for companions to intermediate mass stars, the progenitors of white dwarfs seen today, does *not* follow the same as those measured in the field and in clusters. Specifically, there is a dearth of brown dwarf *and* very low mass stellar companions relative to stellar companions with $M \geq 0.10\ M_{\odot}$.

1.4 Brown Dwarf Cooling

In order to understand the implications of detection or nondetection in any search for brown dwarfs, one must understand how they cool with age. Unlike stars, substellar objects change their spectral type throughout their lifetime as they radiate their ephemeral energy into space. It is mass that ultimately determines substellarity (the state of being a brown dwarf) and not temperature. However, there is a consensus among researchers that stars are incapable of achieving effective temperatures below 1300 K, the beginning of the T spectral class, and any object with such a temperature must be a brown dwarf.

In Figure 1.2 is plotted one of the most often cited cooling models for brown dwarfs. After burning any lithium and deuterium, brown dwarfs possess only thermal energy which they radiate away until reaching equilibrium with their surrounding environment (normally around 5 K). In this completely thermal phase, luminosity decreases linearly with age. This means given two brown dwarfs of identical mass, one that has cooled twice as long as the other will be half as luminous.

Of course, brown dwarfs still cool while they are young, just not in a perfectly linear fashion. Even main sequence stars are much brighter when they are very

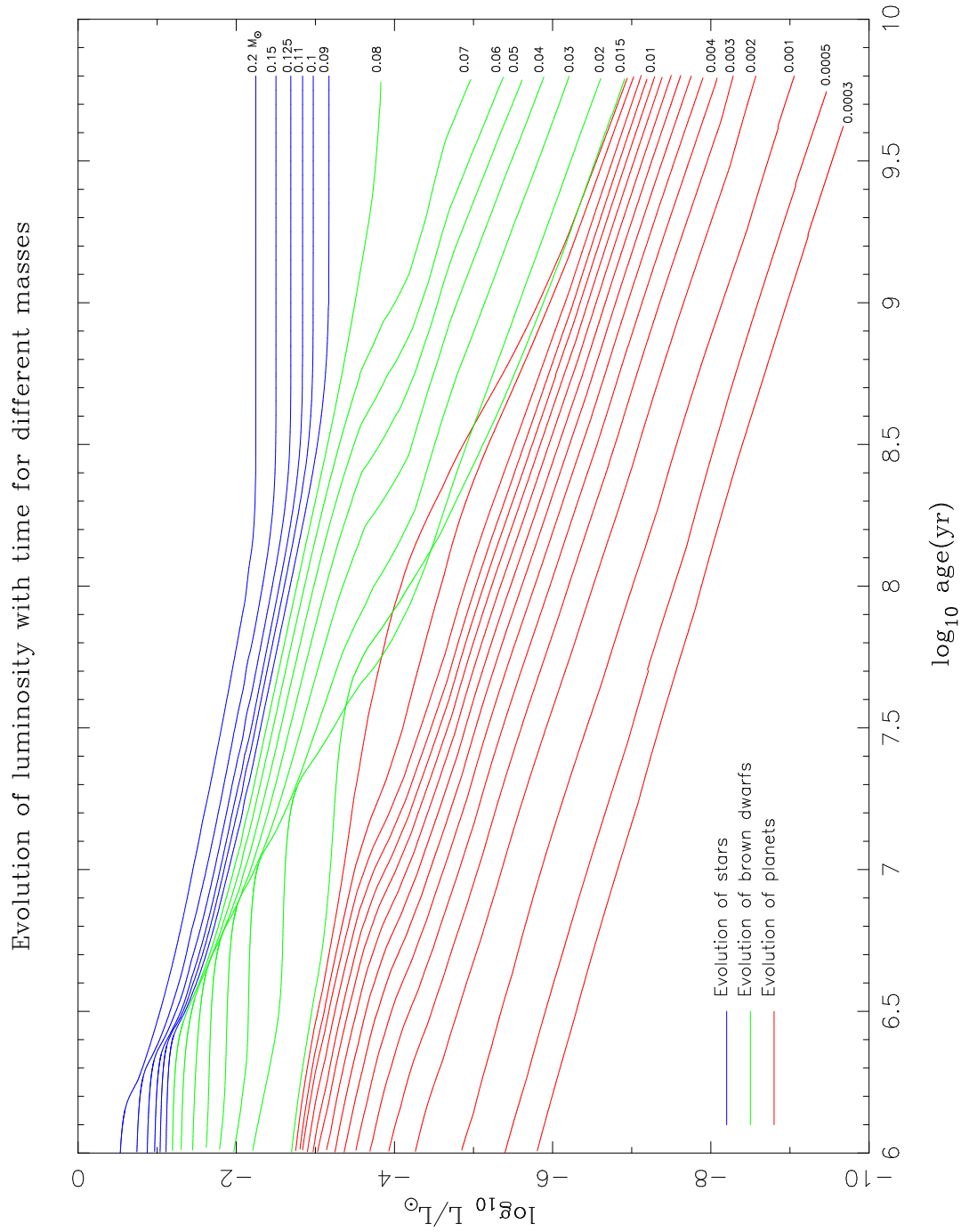

Figure 1.2: Luminosity versus age for stars, brown dwarfs and giant planets from Burrows et al. (1997).

young. This fact does come up in any study of brown dwarfs, not just those of older brown dwarfs. For example, it was thought there was an apparent over-abundance of multiple T Tauri systems in Taurus relative to other young clusters and this may have been a selection effect due to the fact that 'pre main sequence' brown dwarfs are more detectable and may have been missed by 'main sequence' surveys. But there have been two studies in Taurus which determined masses for 88 and 57 components of multiple systems respectively, with no indication that this is the case. In fact a total of four substellar candidates were found between the two surveys (Woitas & Leinert 1998; White & Ghez 2001). Cooling models are absolutely critical to the interpretation of results from any search for brown dwarfs, but especially so for those that may exist aroung evolved stars such as white dwarfs.

1.5 Companion Brown Dwarfs to Nearby White Dwarfs

There are several motivating factors behind the search for brown dwarf companions to nearby white dwarfs. They will be discussed each in turn.

1.5.1 Astrophysical Motivation

The first and foremost reason to search white dwarfs is their intrinsic low luminosities. With typical radii of 0.01 $R_{\odot}$ or roughly one earth radius, their luminosity ($L = 4\pi\sigma R^2 {T_{\rm eff}}^4$) is significantly less that a main sequence star of the same temperature. A 15,000 K white dwarf is 53,000 times fainter than a 15,000 K main sequence star and a 10,000 K white dwarf is 29,000 times fainter than a 10,000 K main sequence star. Their luminosities are so low that a brown dwarf companion can be seen at 2.2 μm merely as infrared excess emission above the

continuum produced by the white dwarf (Zuckerman & Becklin 1987a,b). This is exactly how GD 165B was detected – as 61% excess flux at K band (Becklin & Zuckerman 1988; Zuckerman & Becklin 1992).

Another reason this strategy works is due to the large difference in effective temperatures between a white dwarf and a brown dwarf. A typical white dwarf has $T_{\rm eff} \sim 10,000$ K and a typical brown dwarf has $T_{\rm eff} < 2000$ K. This means their Wein peaks occur at $\lambda \sim 0.29$ μm and $\lambda > 1.45$ μm respectively. This difference provides a further gain in contrast for searches conducted in the near infrared ($1-5$ μm). In this way unresolved low mass stars and brown dwarfs can be detected at very close orbital separations, photometrically.

For wider separations, those which can be probed by direct imaging, there is a further advantage that white dwarfs have to offer. Any object in orbit at $a \geq 5$ AU when the white dwarf was on the main sequence will have its orbit expanded by a factor of $M_{\rm ms}/M_{\rm wd}$ (typically around 3 but can be as large as 7, Weidemann 1987, 1990, 2000; Bragaglia, Renzini, & Bergeron 1995) due to primary mass loss on the asymptotic giant branch (Jeans 1924; Zuckerman & Becklin 1987a). Hence objects orbiting the white dwarf progenitor between $10-50$ AU will typically end up between $30-150$ AU – a directly detectable range for objects within 50 pc. If white dwarf progenitors had binary parameters similar to that of G dwarfs (Figure 1.1) then one might expect the middle region to be swept out and the resulting distribution to look like Figure 1.3. Objects originally orbiting within ~ 2 AU are thought to spiral inward due to frictional interaction with the asymptotic giant's slowly expanding photosphere and wind, called the common envelope (Bond 1985; Bond & Livio 1990; Livio & Soker 1984; Livio 1996; Iben & Livio 1993).

The foregoing motivating factors are really astrophysical and instrumental

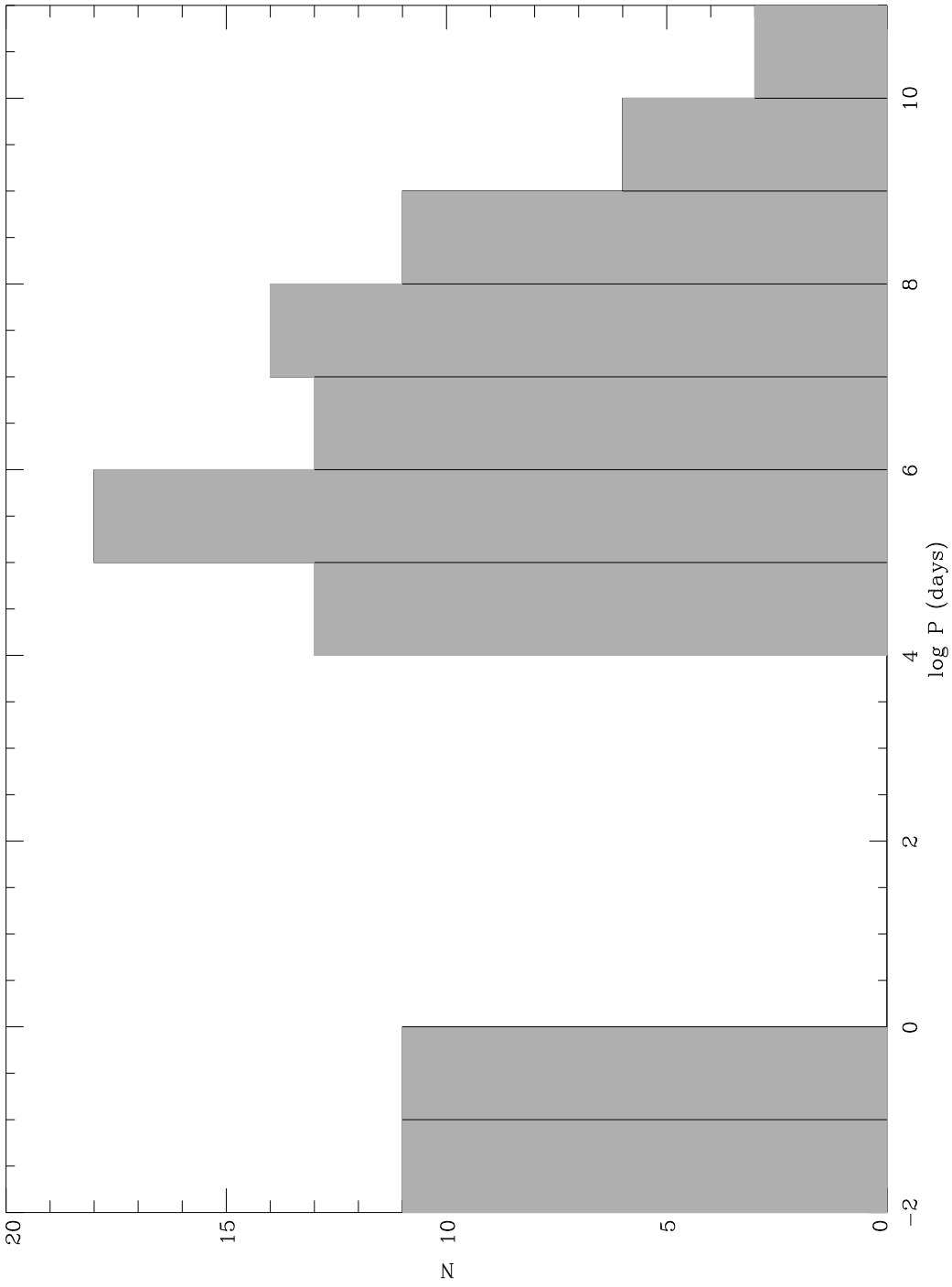

Figure 1.3: Possible binary separation distribution for white dwarfs. Now the peak occurs near 150 AU – a separation directly detectable from the ground for primaries at $d < 100$ pc.

advantages rather than scientific motivation. Why look for brown dwarfs to begin with? This is a question that must be answered and provides the proper perspective for understanding the larger astrophysical picture. The following are the motivating science issues.

1.5.2 Scientific Motivation

The main reason to look for brown dwarfs around other stars is to seek a moderate but important part of the answer to the question: what is the composition of galaxies? It was thought at one time that brown dwarfs may be a significant component of Galactic dark matter (Trimble 1986, 1987). This is no longer the case for various reasons that will not be discussed here in detail. The main reason is because the measured mass function in the field and clusters does not produce enough brown dwarfs to contribute significantly to the Galactic mass budget (Chabrier, Segretain, & Méra 1996; Chabrier & Méra 1997; Tinney 1999). Still brown dwarfs and low mass stars are a critical component of galaxies and any understanding of the universe must include them.

For stellar and planetary astrophysicists, the key question is: what forms around stars? How often does a binary star form? How often does a single star with planets form? Understanding when and where brown dwarfs form can help to answer these questions in part; by understanding how often objects in between the size of stars and planets form. Simply put, studies of this type constrain theories of star and planet formation.

By searching for substellar companions to evolved stars such as white dwarfs, one explores an age regime when it is likely that brown dwarfs have cooled significantly. With few exceptions, most brown dwarf searches have concentrated on systems likely to be young to enhance detectability. This study and its pre-

decessors have specifically targeted evolved stars and are unique for that reason (Zuckerman & Becklin 1987a, 1992; Farihi, Becklin, & Zuckerman 2003). There was the potential for two very unique observations in these studies. One would be the discovery of a minimum mass star – still a relatively bright early L dwarf (according to models) around an old white dwarf. GD 165B may be such an object. According to models it lies in the transition region between stars and brown dwarfs mainly because its age is unknown (Kirkpatrick et al. 1999a). Were GD 165 a much cooler white dwarf and the binary system confirmed to be much older, then GD 165B would certainly have been deemed a minimum mass star. The flipside of this would be the discovery of an old brown dwarf around an old white dwarf, the other potentiality unique to this work. Since the ages of field L and T dwarfs are not well constrained, there really have not been any tests of brown dwarf cooling models; at present their masses are uncertain. Detections of brown dwarfs in young clusters do not provide much of a test either, as these objects have not cooled significantly. This study, had it discovered any old brown dwarfs, would have provided the first data points constraining cooling theories at several billion years.

Lastly, by studying companions to white dwarfs one can hope to learn something about the effects of the asymptotic giant phase on binary parameters. Although the sample is relatively small and the regions probed narrow, one may begin to construct the binary separation distribution of companions to white dwarfs and compare it to predictions such as Figure 1.3. Also, since this work is focussed on the initial mass function, only those companions which did not experience a common envelope phase with the asymptotic giant should be included in any initial mass determinations. It is possible, but still uncertain and under debate, that close companions can accrete matter from the common envelope (Maxted et al. 1998; Drake & Sarna 2003). However, below a roughly

estimated mass ($\sim 0.02\ M_{\odot}$) it is thought that the asymptotic giant branch star will cannibalize any close brown dwarf or giant planetary companions (Livio & Soker 1984; Iben & Livio 1993). This work could provide some initial clues to the answers to these and related questions – something that may have an impact on our understanding of the ultimate fate of the planets in our solar system.

CHAPTER 2

The Search

This chapter will describe the particulars of surveys conducted at Keck Observatory and Steward Observatory for low mass stellar and substellar companions to nearby field white dwarfs. Although the results of a previous phase of this search have already been published by Zuckerman & Becklin (1992), there has been substantial data gathered in the last decade which changes some of their conclusions. In chapters 4 & 5, an update on the companion systems previously published will be provided and then synthesized into the overall results and implications.

2.1 The Steward Survey

The core work completed for this thesis was the analysis of images obtained at Steward Observatory. Beginning in 1991 and continuing through 2003, a program to image nearby white dwarfs at 1.25 μm was conducted on the Bok 2.3 meter telescope at Kitt Peak, Arizona. Images of 273 white dwarf targets were acquired using the first and then later generations of NICMOS infrared arrays (Rieke et al. 1993). This detector is a 256 x 256 HgCdTe array with 0.647$''$ pixels and hence has a 165.6$''$ field of view.

2.1.1 Signal Detection

Near infrared array detectors, such as the one employed in the Bok facility camera, are two dimensional arrangements of submillimeter sized photodiodes (more commonly called pixels) which operate at $1 - 5$ μm. This two dimensional grid is bonded at each photodiode to a silicon readout array. Basically, incoming photons eject electrons via the photoelectric effect (Einstein 1905). The photoelectrons are sequestered by an electric field, migrate via indium bumps onto the silicon chip, and then each pixel is read out individually.

2.1.2 Data Acquisition and Reduction

The imaging procedure was to acquire J band images (1.25 μm) in a 5-point dither pattern with 90 seconds integration per dither position for a total exposure time of 7.5 minutes. The dither pattern consisted of an initial position with the white dwarf centered on the detector and then four positions with the white dwarf at each corner of a square centered at the first position. The spacing along the sides of the square was $15''$.

Dark frames were taken at identical integration times to the science images with a blocking filter in front of the camera. Flat frames were acquired by shining a light on the interior of the dome with the J band filter in place (identical frames were taken with the light off to remove any background, essentially flat darks).

Image reduction proceeded as follows. Flat and flat dark frames were each averaged, then the flat dark subtracted from the flat. This final flat image was then normalized to one. The darks were averaged and the resulting dark subtracted from each J band science image (dark subtracted). These images were then each divided by the normalized flat (flat fielded). A sky frame was created for each

image by taking the median value of the other 4 frames. Each sky frame was then subtracted from each of the 5 dark subtracted, flat fielded J band images. These reduced 5 images were all normalized to the central image, shifted, registered, and then averaged.

For a given pixel, its final value in the reduced image can be expressed by the following formula

$$p = \sum_{i=1}^{5} \frac{\alpha_i h_i}{5} \tag{2.1}$$

Here, α_i is the normalization factor of the i^{th} frame and h_i is the shifted pixel value of the i^{th} frame, where

$$h_i = \frac{g_i - m_{j \neq i}}{q} \tag{2.2}$$

In this last equation, g_i is the initial pixel value for frame i, $m_{j \neq i}$ is the median pixel value of all frames but frame i (i.e. the sky), and q is the quantum efficiency of the pixel, where

$$q = N(f - fd) \tag{2.3}$$

q has a median value of 1 over all pixels by convention, N is the normalization factor, f and fd are the flat and flat dark pixel values, respectively.

2.1.3 Signal to Noise and Completeness

The signal to noise of any imaging program with a given instrument and telescope is basically determined by seven things: the collecting area of the telescope, the detector's intrinsic quantum efficiency, the throughput of the optics, atmospheric transmission, atmospheric background emission, image size, and exposure time. All of these parameters should remain more or less constant with the exception of the atmosphere.

In order to calculate J magnitudes for imaged objects, it is necessary to determine a quantity called the zero point – defined as the magnitude corresponding to source that yields one count per second on the detector. The zero point, J_0, can be determined by imaging standard stars and comparing their total measured fluxes (instrumental magnitudes) to the known values. Corrections must be made to account for any differences between standards and targets observed at different airmases. For an object imaged at an airmass of 1.0, the formula

$$J = J_0 - 2.5\log(F) \tag{2.4}$$

gives the J magnitude for an object with flux, F, in counts per second. The zero point of the camera used on the Bok is $J_0 = 20.3$ mag. This camera was installed in 1994 and all data taken from that date forward reflects the improved sensitivity of the later generation NICMOS arrays.

In order to determine the completeness of the Steward Survey, it was necessary to measure the flux of the faintest reliably detectable sources in images taken over the entire length of the study. Figure 2.1 shows the number of objects detected with a signal to noise ratio (SNR) ≥ 3 as a function of J magnitude in images representative of each observing run conducted at Steward Observatory. There was often sensitivity to $J = 19$ mag objects but the survey was complete to $J = 18.0$ mag. In addition, it is estimated that 37% of $J = 18.5$ mag and 57% of $J = 19.0$ mag objects were missed.

2.1.4 Supplementary Data

In the last two years of this survey phase, supplementary data were gathered at Lick Observatory on the Shane 3 meter telescope with the GEMINI camera (McLean et al. 1993). GEMINI sits behind a telescope that is 70% larger than the Bok telescope and employs nearly identical detector technology. The J band

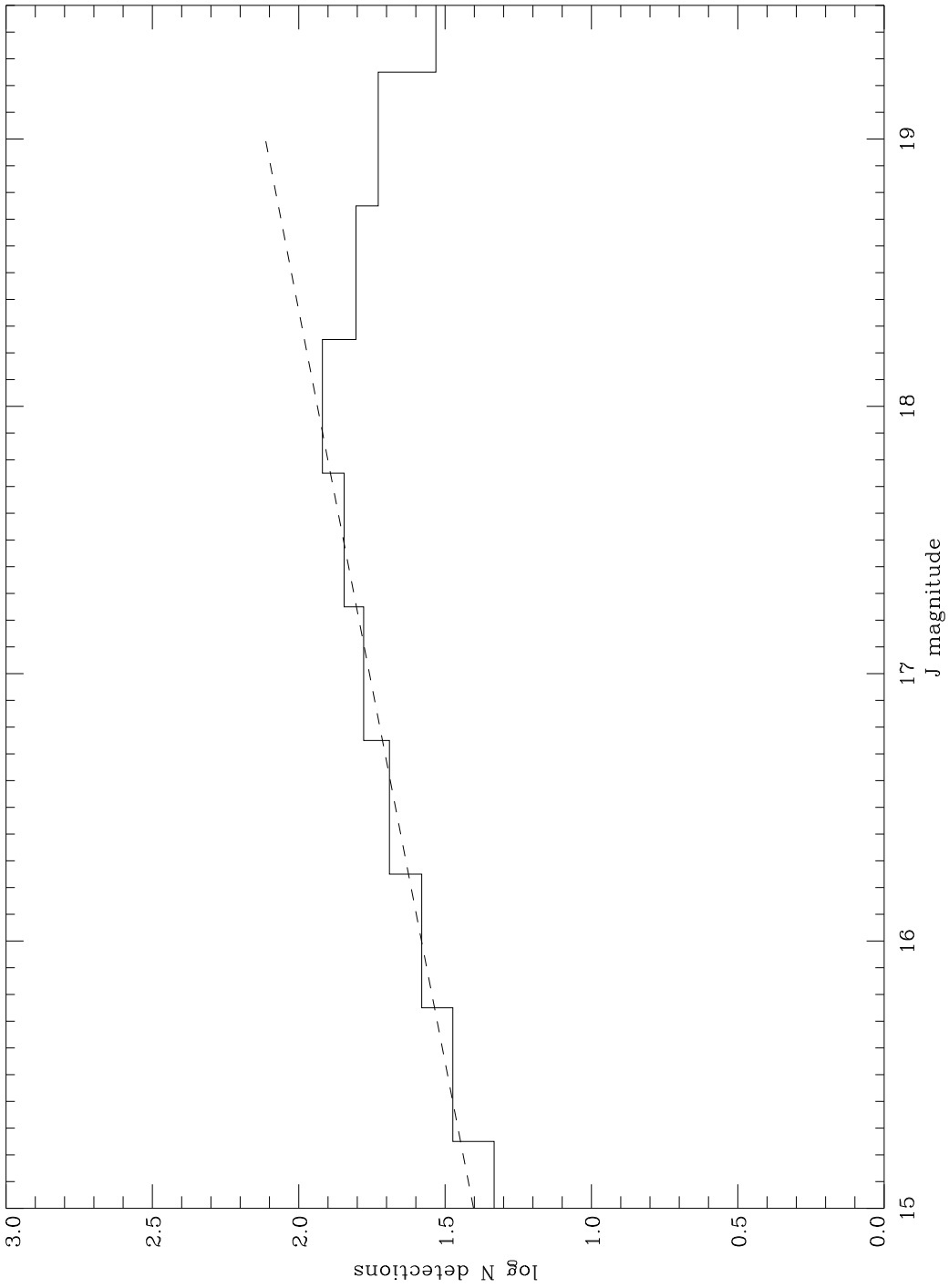

Figure 2.1: Number of objects detected as a function of J magnitude for typical images from every observing run at Steward Observatory. It is determined from the plot that the completeness limit is $J = 18$ mag.

zero point of GEMINI is $J_0 = 21.4$ mag and hence data acquired with this camera generally went about 1 magnitude deeper, providing greater sensitivity to $J \sim 19$ mag objects. However, the completeness limit of the wide field survey remains at $J = 18.0$ mag. Since any survey is limited by its completeness, all calculations will be restricted to this edge.

2.1.5 Analysis of Steward Data – Measuring Proper Motions

The Steward survey was a common proper motion companion search. By imaging the field around a target white dwarf at two epochs separated by a sufficient interval of time, the proper motion of the white dwarf can be measured and compared to any motions exhibited by stars in that field.

GEOMAP, a program within the Image Reduction and Analysis Facility (IRAF) was used for this task. This program creates a general transformation between two sets of coordinates corresponding to sources in the same field at two different epochs. Proper motion stars can be identified by their residuals from this mapping and their motions measured against the near zero motion of background stars and galaxies, which provide a measure of the standard error.

A typical white dwarf with 5 or more field stars produces a map with a standard deviation in the residuals of approximately 0.2 pixels or $0.13''$ on the Steward camera. With a typical time baseline of 5 years, proper motions as small as $0.08''$ yr^{-1} can be measured at the 3σ level. These are characteristic values – the actual measurement values and errors depend on the following factors: an individual white dwarf's proper motion, the number of field sources with good SNR, the quality of the images at each epoch, and the time baseline between epochs (which varies between 2 and 10 years).

Additionally, many proper motions for white dwarf targets and candidate

companions were measured using the digitized versions of large sky survey photographic plates, such as the Palomar Observatory Sky Survey I and II. Although the spatial resoultion of these scans is much lower ($1.0 - 1.7''$ pixel^{-1}) than the near infrared camera data, the epochs are separated by $\sim$ 40 years and hence they provide slightly better measurements and smaller errors (§4.3.2).

2.2 The Keck Survey

From 1995 to 2001, a similar program to image nearby white dwarfs at near infrared wavelengths was conducted on the Keck I 10 meter telescope at Mauna Kea, Hawaii. Images of 91 degenerate targets were acquired using NIRC (Matthews & Soifer 1994). This detector is a 256 x 256 InSb array with $0.150''$ pixels and hence has a $38.4''$ field of view.

2.2.1 Data Acquisition and Reduction

The NIRC data were not taken in an analagous way to the Steward data. In general, each target was observed at J and usually one or more other of the following bands in order of descending usage: z (1.03 μm), K (2.21 μm), H (1.66 μm). A typical total integration time was $60 - 80$ seconds times 5 dithers at J band. Data at all wavelengths were reduced in a manner identical to the Steward data (§2.1.2).

2.2.2 Sensitivity and Completeness

It is not possible to establish a completeness limit in the same way as was done for the Steward data. The main reason for this is the relatively small Keck field of view did not produce images containing lots of background sources to use for

such a determination.

An analysis was performed on several images representative of each observing run from 1995 – 2001. After determination of the zeropoint by measuring instrumental magnitudes for standard stars, J magnitudes and signal to noise ratios were measured for faint but reliably detected objects in the images. The result being that $J = 21.0$ mag or brighter objects were consistently detected with SNR > 10. Therefore, the NIRC survey is likely complete down to $J = 21$ mag.

2.2.3 Analysis of Keck Data – Colors and Astrometry

The $z - J$ and/or $J - K$ color of point sources in the near field of the white dwarf, together with their flux relative to the primary at these wavelengths, were used to filter out uninteresting background stars and discriminate candidate companions. Data were taken at z and J for about 75% of the white dwarfs in this survey. For the remainder of the sample, data were taken at K unless there were no point sources in the field around the white dwarf seen in the J band images. The $z - J$ color is the most indicative of low mass stars and brown dwarfs because it is monotonically increasing with decreasing $T_{\rm eff}$, unlike $J - K$ (Leggett et al. 2002).

If a candidate could not be ruled out based on these criteria, then a followup image was taken at a later epoch in order to perform astrometry and search for common proper motion.

2.3 Companion Data Acquisition and Analysis

For each confirmed or candidate common proper motion companion, optical photometry and spectroscopy, in addition to near infrared photometry, was performed

in order to identify or constrain its temperature and class. The discussion of companions discovered in this work will be deferred until chapter 4, but here will be described the followup observations and data analysis.

There exist various imaging and spectroscopic data on the potential and confirmed companions taken with miscellaneous instruments by department colleagues, advisors and generous astronomers. None of these were used sufficiently to merit a full description of the observing here but will be detailed as necessary. These include the Low Resolution Imaging Spectrograph (LRIS) on the Keck I telescope, the Near Infrared Spectrograph (NIRSPEC) on the Keck II telescope, the Prime Focus Camera on the Shane telescope, the Boller & Chivens Spectrograph on the Bok telescope, and some grism data with NIRC.

2.3.1 Near Infrared Data

Infrared JHK data were acquired using the same instruments used for the wide field survey, namely the Steward and GEMINI cameras. Images were taken and reduced in a more or less identical manner to the J band survey observations, the difference being only in the integration times, number of coadds and frames.

2.3.2 Optical Data

Optical $BVRI$ data were obtained at Lick Observatory using the Nickel 1 meter telescope CCD camera. The detector is a 2048 x 2048 element array with $0.18''$ pixels and a $6.1'$ field of view. The pixels were binned 2 x 2 and only the central quarter of the array was read out for efficient observing. In general, exposures were $1-10$ minutes depending on conditions and the individual target brightness. A depth of $21^{\rm st}$ magnitude is attainable at all wavelengths in approximately 10 minutes under good conditions with this instrument. Flat frames were taken on

either the twilight sky or the dome interior. Images were cleaned of bad pixels in the area of interest, bias subtracted, flat fielded and averaged if there were multiple frames.

Optical spectroscopic data were acquired at Lick Observatory using the Kast dual spectrograph on the Shane 3 meter telescope. This instrument utilizes two complete spectrographs for simultaneous measurements in both the blue and red portions of the optical regime. Either side of the spectrograph can be used alone or both at once with a dichroic beamsplitter in between to separate the blue and red light. The exact set up of both sides of the instrument varied but all observations were done at low resolution ($\sim$ 500) – the ostensible aim being to firmly establish companionship rather than perform line measurements for precise spectral typing. On the red side, a 300 line per mm grating was used, blazed at 7500 Å. This provided 5520 Å of coverage than could be centered at any chosen wavelength. On the blue side, a 452 line per mm grism was used, blazed at 3306 Å. This covered the region from $3200-5600$ Å and was not adjustable. Additional spectroscopy was performed at Steward Observatory using the Boller & Chivens spectrograph on the Bok 2.3 meter telescope, with a 300 line per mm grating blazed at 3306 Å providing coverage from $4200 - 8300$ Å. Spectral flats were taken by shining a light on the dome interior and allowing that light to travel through the spectrograph onto the CCD's. All optical spectra were reduced using standard IRAF software. The spectral images were bias subtracted, cleaned of bad pixels and cosmic rays and flat fielded. For each target, two spectra of the sky were extracted, averaged and subtracted from the extracted target spectrum. The resulting spectra were wavelength and flux calibrated by comparison with observed lamp spectra and standard stars. No attempt was made to remove telluric features.

2.3.3 Photometry

Optical and near infrared magnitudes and colors were used as the main source of constraints for stellar classification and spectral typing of the discovered companions. Aperture photometry was performed on all companion imaging data in the following manner.

Using a circular aperture centered on the target star and an annulus on the surrounding sky, both the flux and SNR was calculated for a range of apertures from one to four full widths at half maximum. The target flux was measured at or near the aperture size which produced the largest SNR. In this way the flux of all targets was measured, including photometric standard stars. A fairly large aperture was used for all calibrators, and flux measurements for science targets were corrected to this standard aperture to account for the smaller percentage of the total flux contained within apertures smaller than the standard. Optical and infrared standard stars were taken from Landolt (1983), Hunt et al. (1998), and Hawarden et al. (2001).

2.4 The IRTF Survey

As mentioned in the introduction to this chapter, there was a previous phase to the search for substellar companions to white dwarfs that began in late 1986 (Zuckerman & Becklin 1992). Although carried out on several different telescopes and instruments, the majority of the data were obtained at the NASA Infrared Telescope Facility (IRTF). Because some results of the IRTF survey were previously published, the details will not be discussed here. However, the results will be updated in chapters 4 & 5 and the white dwarfs surveyed at the IRTF will be included in the overall sample and statistics. Of the over 150 white dwarfs

observed during this early phase, 66 were later re-observed at either Keck or Steward Observatory. There were 84 white dwarf targets observed only at the IRTF and not elsewhere.

2.5 A Search for Infrared Excess

Although data at both J and K were taken for about one fourth to one third of the stars surveyed, all 372 white dwarfs in the sample were searched for near infrared excess emission. A digital finding chart of each white dwarf was overlaid with the 2MASS point source catalog data. The measured JHK_s values for the the white dwarf were then compared to the model predicted values extrapolated from optical data based on the effective temperature of the star. Stars with excess emission at one or more of these near infrared wavelengths (and good SNR) were noted as possible or probable binaries.

CHAPTER 3

The White Dwarf Sample

This chapter addresses a few issues that will later become important in interpreting the results of this work; ages, distances, temperatures, and possible selection effects. These will all affect, to lesser or greater degrees, just what implications the survey has for the existence of companions as a function of mass – the quantity which discriminates substellarity.

3.1 Target Selection

Every target observed for this thesis project can be found in either current or preceding versions of the white dwarf catalog of McCook & Sion (1987, 1999). The catalog is mostly composed of stars selected by one of two criteria: (1) faint proper motion stars; (2) stars with ultraviolet excess. Most of these stars were spectroscopically confirmed to be white dwarfs, but there remains some contamination by nondegenerate stars. Hot subdwarfs (helium burning stars), blue horizontal branch stars, BL Lacertae objects, and Population II stars all display at least one of the two above characteristics and can have spectra difficult to differentiate from that of a white dwarf with older photographic techniques.

The result of this overall identification process is a catalog filled primarily with two types of objects; hotter white dwarfs identified by ultraviolet excess, and cooler white dwarfs identified by the combination of a large proper motion

relative to their apparent brightness. It should be immediately obvious that this is not a homogeneous sample by any means. One absolutely cannot treat the sample as a whole because the objects in this study share only one characteristic; degeneracy.

3.1.1 Wanted: Nearby Hot Young Degenerates

A sample of nearby hot and massive white dwarfs is ideal to search for substellar companions. Proximity to the Sun is desirable for the ability to partially or totally resolve close companions from the primary star and because flux falls off inversely as the square of the distance, d. Hot white dwarfs are "recently deceased" and are therefore younger than their cooler counterparts. A typical white dwarf of $M = 0.6\ M_{\odot}$ that has $T_{\rm eff} = 20,000$ K has been cooling for only $\tau = 70$ Myr (Bergeron, Saumon, & Wesemael 1995). Most massive white dwarfs ($M \geq 0.9\ M_{\odot}$) are thought to descend from main sequence progenitors with masses, $6\ M_{\odot} < M < 8\ M_{\odot}$ (Bergeron et al. 1991; Bergeron, Saffer, & Liebert 1992; Bragaglia, Renzini, & Bergeron 1995; Weidemann 1987, 1990, 2000). Hence massive white dwarfs have a total age on par with their cooling age because the main sequence lifetime of the progenitor would have been relatively short. Although a large ($N \sim 100$) sample with all three characteristics does not exist, these attributes were guiding principles in selecting stars for the survey.

3.1.2 Wanted: Slow Movers

Proper motion can be an indicator of age relative to the three basic kinematic populations of the Galaxy; young disk ($\sim 1-2$ Gyr), old disk ($\sim 5-10$ Gyr), and halo stars ($\sim 10-15$ Gyr). Ages between $2-5$ Gyr are considered intermediate disk ages. In general, the UVW space velocities (and perhaps more important,

velocity dispersions) of stellar populations increase with increasing age. This is primarily due to gravitational upscattering for disk objects, while the halo is a distinctly separate kinematical group in every sense. The halo is not corotational with the disk and experiences a different gravitational potential than does the Sun (which defines the origin of the UVW system). Therefore in general, smaller values of (U, V, W) and $(\sigma_U, \sigma_V, \sigma_W)$, for a given kinematical sample, are correlated with younger objects (Wielen 1974; Mihalas & Binney 1981; Leggett 1992; Jahreiß & Wielen 1997; Binney & Merrifield 1998).

Although it is three dimensional space motion that determines kinematic populations and indicates likely membership for an individual star, proper motion is often used as a proxy because the radial velocity is not known. In addition, it is particularly challenging to measure the radial velocity of white dwarfs due to their large, pressure broadened line profiles and intrinsic faintness. However, two studies have compared the UVW space motions of over 100 white dwarfs in wide binaries calculated with and without the assumption $v_{rad} = 0$ (Silvestri et al. 2001; Silvestri, Oswalt, & Hawley 2002). With accurate radial velocities obtained from a widely separated main sequence component in each binary, there were two major conclusions: (1) the overall kinematics of their sample were consistent with the old, metal poor disk population; (2) assuming $v_{rad} = 0$ did *not* significantly affect the results (Silvestri et al. 2001; Silvestri, Oswalt, & Hawley 2002). This is an important result because, in the end, the sample of white dwarfs in the present work can only be tied together with kinematics, if anything.

3.2 Target List

Table 3.1 lists all 395 target stars observed at all facilities beginning in 1990. The first column lists the white dwarf number from McCook & Sion (1987, 1999),

except where noted. The second column lists the facility or facilities at which the white dwarf was observed; S = Steward, K = Keck, I = IRTF. The third and fourth columns are the proper motion, μ, in arcseconds per year, followed by the position angle, θ, in degrees. These quantities were taken from the most accurate and reliable source available. In decreasing order these are: the Tycho 2 catalog (Høg et al. 2000), the UCAC catalogs (Zacharias et al. 2000, 2004), the USNO B1.0 catalog (Monet et al. 2003), and the white dwarf catalog of McCook & Sion (1999) and references therein. A few proper motions were measured for this work. The fifth column lists the spectral type of the white dwarf: DA stands for an atmosphere showing hydrogen Balmer lines in absorption; DB for helium lines, DO for helium II lines; DC for no lines; DZ for metallic lines; DQ for carbon features; P and H for magnetic fields present with and without detectable polarization; E for emission lines; and finally V denotes variability (McCook & Sion 1987, 1999). The integer value in column five represents the effective temperature index, $\mathrm{Q_{eff}}$, defined as $10 \times \theta_{\mathrm{eff}}$, where $\theta_{\mathrm{eff}} = 5040/T_{\mathrm{eff}}$ (McCook & Sion 1987, 1999). The sixth column lists the distance, d, in parsecs as determined photometrically or by trigonometric parallax. The seventh column lists the Galactic UVW space velocity, corrected for the solar motion $(U, V, W) = (-9, +12, +7)$ (Wielen 1974; Mihalas & Binney 1981) to the local standard of rest (LSR) in km s^{-1}. These quantities were calculated from the vector $(\alpha, \delta, d, \mu, \theta, v_r)$ where α is the right ascension, δ the declination, and $v_r = 0$ was assumed to provide a uniform treatment of the sample. U is taken to be positive toward the Galactic anticenter, V positive in the direction of Galactic rotation, and W positive toward the North Galactic Pole.

Table 3.1: List of Observed White Dwarfs

WD#	Survey	μ	θ	ST	d	(U,V,W)	Name
0000−170	K,I	0.246	91.0	DB4	39.6	(31,-10,-2)	G266-32
0000−345	S	0.772	169.2	DAH7	13.2	(-22,-35,11)	LHS 1008
0002+729	S	0.253	57.4	DBZ4	34.7	(19,-7,21)	GD 408
0009+191†	S	-	-	sdB	-	-	PG
0009+501	S	0.713	219.8	DAP7	11.0	(-36,20,-17)	LHS 1038
0011+000	S	0.457	114.2	DA5	30.4	(30,-36,-14)	G31-35
0013−241	S	0.149	276.9	DA3	70.5	(-49,41,14)	Ton 147
0016−220	S,K	0.085	230.1	DA4	72.8	(-38,7,8)	GD 597
0017+061	I	0.049	243.4	DA2	133.0	(-39,16,3)	PHL 790
0018−339	S	0.198	88.8	DA3	57.5	(38,-13,1)	GD 603
0028−274†	S,K	-	-	sdO	-	-	GD 617
0031−274	S,K,I	0.004	223.9	DA1	53.5	(-10,12,7)	GD 619
0032−175	S	0.608	90.0	DA5	30.9	(67,-33,2)	G266-135
0033+016	S	0.393	202.1	DA4	29.8	(-51,-15,-17)	G1-7
0034−211	I	0.348	227.8	DA3	63.4	(-112,-7,4)	LTT 0329
0037−006	S	0.017	93.1	DA4	39.2	(-6,10,7)	PG
0038−226	S	0.600	231.2	DC9	9.9	(-37,9,6)	LHS 1126
0041−102	S	0.196	226.9	DAP2	49.5	(-54,5,-1)	Feige 7
0046+051	S	2.975	155.5	DZ7	4.4	(-13,-42,-24)	LHS 7
0048−202†	S	-	-	sdB	-	-	GD 656
0050−332	S,K	0.045	300.8	DA1	59.9	(-15,23,6)	GD 659
0058−044	S,I	0.111	69.9	DAP3	69.2	(26,3,13)	GD 9
0100−068	S,K	0.187	166.7	DB3	39.4	(-20,-19,-5)	G270-124
0101+048	S,K	0.395	54.1	DA5	13.5	(15,11,16)	G1-45
0102+095	S	0.049	258.4	DA2	71.1	(-24,19,4)	PHL 972

Table 3.1: List of Observed White Dwarfs

WD#	Survey	μ	θ	Type	d	U, V, W	Name
0103−278	S	0.261	105.1	DA4	58.3	(38,-43,11)	G269-93
0106+372	S	0.152	108.4	DA2	127.1	(57,-49,-13)	GD 11
0106−358	S	0.028	194.4	DA2	95.5	(-19,4,9)	GD 683
0107+267	S	0.264	124.9	DA4	59.8	(29,-45,-23)	GD 12
0107−342†	S,K	-	-	sdB	-	-	GD 687
0113−243	S	0.006	111.0	DA6	29.8	(-9,11,7)	GD 693
0112+104	S	0.049	211.8	DB2	75.9	(-23,7,-3)	PG
0115+159	S	0.651	181.8	DQ5	15.4	(-28,-17,-26)	G33-49
0115+521	S	0.164	260.2	DA5	50.4	(-40,33,-4)	GD 275
0125−236	S	0.296	78.3	DB5	41.1	(43,-12,16)	G274-39
0126+101	S	0.408	200.7	DA6	35.6	(-54,-17,-36)	G2-40
0126+422	I	0.102	124.6	DA2	82.8	(15,-16,-9)	GD 13
0131−163	I	0.038	50.3	DA1	120.2	(12,13,12)	GD 984
0133−116	S	0.480	104.2	DAV4	31.5	(35,-44,14)	G271-106
0134+833	S,K	0.147	311.8	DA3	25.6	(-24,19,14)	GD 419
0136+768	S	0.198	141.2	DA3	67.6	(36,-8,-32)	GD 420
0142+312	S	0.339	114.8	DA6	35.5	(26,-32,-2)	G72-31
0143+216	S	0.217	235.1	DA5	40.0	(-41,19,-18)	G94-9
0148+467	S,K	0.124	0.6	DA4	15.9	(-9,15,16)	GD 279
0155+069	S,I	0.093	288.1	DA2	83.2	(-30,42,5)	GD 20
0156+155	S	0.082	265.8	DC6	46.1	(-23,22,1)	PG
0210+168†	S	-	-	sdG	-	-	PG
0213+396	S	0.180	237.5	DA6	25.1	(-22,18,-9)	GD 25
0213+427	S	1.010	125.2	DA9	19.9	(45,-62,-17)	LHS 153
0227+050	S	0.075	109.1	DA3	24.3	(-5,5,9)	Feige 22

Table 3.1: List of Observed White Dwarfs

WD#	Survey	μ	θ	Type	d	U, V, W	Name
0230−144	S	0.680	177.8	DA9	15.6	(-38,-27,-5)	LHS 1415
0231+570	S	0.204	97.9	DA5	21.5	(5,-2,12)	GD 283
0231−054	S	0.256	69.0	DA3	29.5	(20,0,35)	GD 31
0232+525	S	0.245	134.0	DA3	28.2	(10,-12,-4)	G174-5
0250−026	K,I	0.042	295.3	DA3	36.3	(-11,19,5)	KUV
0253+508	S,I	0.034	305.5	DAP2	78.7	(-17,22,9)	KPD
0257+080	S	0.181	129.7	DAP8	27.8	(-4,-11,7)	G76-48
0302+027	S,K	0.154	198.9	DA1	132.4	(-68,-35,-54)	GD 41
0308+096	I	0.091	158.0	DA2	100.9	(-15,-29,-8)	PG
0308+188	S	0.182	170.5	DA4	34.1	(-13,-12,-10)	PG
0319+055†	S	-	-	sdB	-	-	PG
0322−019	S	0.903	163.8	DAZ10	17.5	(-34,-55,13)	LHS 1547
0339−035	S	0.230	79.9	DA4	61.7	(27,-23,52)	GD 47
0346−011	K	0.173	158.3	DA1	29.6	(-16,-11,3)	GD 50
0347−137	S,I	0.186	70.1	DA2	83.6	(36,-15,57)	GD 51
0348+339	I	0.181	118.1	DA4	66.1	(13,-39,19)	GD 52
0349+247	S,I	0.054	164.9	DA2	141.3	(-9,-19,-11)	LB 1497
0352+096	I	0.168	88.6	DA4	45.7	(6,-11,31)	HZ 4
0354+463	S,I	0.135	276.0	DA6	41.1	(-20,31,-8)	Rubin 80
0357−233	S	0.018	358.4	DA1	278.0	(9,27,11)	Ton S 392
0401+250	S	0.253	148.6	DA4	27.0	(-5,-19,0)	G8-8
0406+169	K,I	0.107	103.0	DA3	57.2	(0,-11,22)	LB 227
0407+179	K,I	0.111	139.4	DA3	38.2	(-8,-8,7)	HZ 10
0408−041	S,K	0.126	177.3	DA3	67.3	(-30,-19,-8)	GD 56
0410+117	S,K	0.098	150.8	DA3	37.7	(-11,-5,4)	HZ 2

Table 3.1: List of Observed White Dwarfs

WD#	Survey	μ	θ	Type	d	U, V, W	Name
0413−077	I	4.079	213.3	DA3	4.9	(-73,-11,-59)	40 Eri B
0416+272	S,I	0.098	137.5	DAV4	47.2	(-5,-10,7)	V411 Tau
0416+334	S	0.190	155.1	DA3	60.8	(1,-39,-11)	GD 60
0416+701	S	0.168	135.5	DA4	44.7	(14,-15,8)	GD 429
0421+162	I	0.113	103.3	DA3	47.0	(-3,-8,21)	VR 7
0423+120	S	0.249	201.3	DC8	16.2	(-16,3,-8)	G83-10
0425+168	I	0.082	111.5	DA2	41.7	(-6,-2,14)	VR 16
0431+126	I	0.099	97.6	DA2	47.3	(-4,-4,22)	HZ 7
0435−088	S	1.520	171.2	DQ7	9.5	(-47,-42,-11)	LHS 194
0435+410	I	0.102	184.5	DBAZ3	54.5	(-5,-6,-12)	GD 61
0437+138	K,I	0.096	100.8	DA3	33.1	(-6,1,16)	EGGR 316
0438+108	I	0.091	96.9	DA2	50.8	(-5,-3,22)	HZ 14
0453+418	S	0.220	174.8	DA4	37.6	(0,-20,-15)	GD 64
0516+365	S	0.027	208.6	DA2	95.9	(-8,7,-4)	KPD
0517+307	S	0.132	155.8	DAV4	57.8	(-7,-23,0)	GD 66
0532+414	S	0.146	285.9	DA7	18.3	(-10,21,-1)	GD 69
0543+579	S	0.136	107.1	DA5	50.6	(-5,-11,29)	GD 290
0549+158	S,K	0.187	155.9	DA1	49.7	(-19,-31,2)	GD 71
0612+177	S	0.358	190.2	DA2	36.1	(-20,-35,-31)	G104-27
0625+415	S,I	0.111	186.2	DA3	83.2	(1,-25,-15)	GD 74
0627+299	I	0.018	3.9	DA5	22.9	(-9,14,8)	KUV
0631+107	I	0.110	199.7	DA2	56.5	(-16,-7,-15)	KPD
0637+477	S,I	0.171	185.4	DAP5	40.0	(1,-16,-7)	GD 77
0644+375	S,K,I	0.965	193.8	DA2	15.4	(4,-44,-33)	G87-7
0710+741	S,I	0.132	129.5	DA3	92.0	(-1,-30,45)	GD 448

Table 3.1: List of Observed White Dwarfs

WD#	Survey	μ	θ	Type	d	U,V,W	Name
0710+216	S	0.179	221.9	DA5	40.7	(-6,-5,-23)	GD 83
0713+584†	S,K	-	-	sdB	-	-	GD 294
0714+458	S,I	0.201	213.2	DQ6	33.1	(3,-7,-15)	GD 84
0716+404	S,K	0.171	127.4	DBA3	57.8	(-18,-27,32)	GD 85
0730+487	S,K	0.231	217.3	DA3	38.5	(10,-13,-21)	GD 86
0743+442	S	0.182	208.3	DA4	39.6	(4,-13,-12)	GD 89
0751+578	I	0.438	189.2	DC5	31.9	(20,-46,-4)	G193-78
0752−146	I	0.320	191.9	DA3	35.0	(-36,-13,-26)	LTT 2980
0802+386	S	0.304	186.8	DZ5	46.6	(0,-52,-12)	G111-54
0802+413	S	0.037	221.1	DA1	139.3	(1,-3,-9)	KPD
0811+644	I	0.193	262.9	DA4	61.4	(24,15,-39)	GD 457
0816+376	S,K	0.150	228.2	DAP4	47.4	(5,-6,-17)	GD 90
0817+386	S	0.105	228.1	DA2	113.8	(16,-19,-33)	PG
0824+288	S	0.050	272.9	DA1	119.1	(7,17,-16)	PG
0826+455	S,K	0.147	132.1	DA5	47.6	(-20,-13,26)	GD 91
0836+404	S	0.136	267.5	DA3	38.4	(6,13,-13)	KUV
0840+262	S,K	0.122	248.9	DB3	48.3	(5,4,-16)	Ton 10
0843+358	S	0.169	245.7	DZ6	23.1	(1,6,-7)	GD 95
0846+346	S	0.121	275.7	DA7	28.3	(1,15,-5)	GD 96
0853+163	S	0.041	227.0	DBA2	91.6	(-4,2,-7)	PG
0856+331	I	0.322	270.7	DQ5	20.5	(12,14,-17)	G47-18
0858+363	S,K	0.206	209.7	DAV4	35.0	(1,-17,-8)	GD 99
0859−039	S,K	0.016	304.6	DA2	38.7	(-7,13,6)	RE
0900+554†	S,K	-	-	sdB	-	-	PG
0901+140	S,K	0.113	260.9	DA5	52.2	(9,9,-16)	PG

Table 3.1: List of Observed White Dwarfs

WD#	Survey	μ	θ	Type	d	U, V, W	Name
0912+536	S	1.553	224.1	DC7	10.3	(35,-42,-23)	G195-19
0913+442	S	0.265	177.6	DA6	30.5	(-9,-26,10)	G116-16
0913+103	S	0.191	116.0	DC6	39.8	(-38,-1,25)	LP 487-21
0914+547†	S	-	-	sdOB	-	-	SBSS
0915+526	S,K	0.025	166.0	DC6	74.5	(-9,4,10)	PG
0922+162	S	0.066	266.0	DA2	118.7	(17,8,-20)	PG
0930+294	S	0.236	221.0	DA6	32.1	(3,-16,-12)	G117-25
0933+025	I	0.062	181.9	DA2	133.7	(-26,-18,-11)	PG
0933+729	S	0.075	228.2	DA3	96.4	(17,-9,0)	PG
0938+286	S	0.154	315.5	DA4	75.2	(28,47,-14)	Ton 20
0938+550	S,K	0.068	256.4	DA3	53.5	(4,7,-3)	PG
0939+071	S	0.014	273.3	DA2	18.9	(-8,12,6)	PG
0943+441	I	0.290	0.0	DA4	34.0	(-7,58,2)	G116-52
0945+245	K,I	0.119	211.3	DA3	41.4	(-5,-8,-4)	PG
0946+534	S	0.262	263.9	DA6	23.0	(13,6,-10)	G195-42
0947+325	K	0.068	269.1	DA1	72.1	(9,9,-8)	Ton 458
0947+639†	I	-	-	sdB	-	-	PG
0950+185	I	0.010	210.1	DA2	201.4	(-8,4,2)	PG
0955+247	S	0.415	220.3	DA6	24.4	(5,-27,-17)	G49-33
0956+045	I	0.146	169.8	DA3	112.7	(-55,-47,-16)	PG
0959+149	S,I	0.339	272.1	DC7	22.2	(20,8,-14)	G42-33
1000+220	S	0.0	0.0	DA6	38.9	(-9,12,7)	Ton 1145
1001+203	S,I	0.095	247.8	DA2	117.5	(23,-14,-26)	Ton 1150
1005+642	K	0.131	232.4	DA3	44.9	(11,-7,1)	GD 462
1011+570	S,K	0.132	135.6	DBZ4	44.7	(-24,-3,24)	GD 303

Table 3.1: List of Observed White Dwarfs

WD#	Survey	μ	θ	Type	d	U,V,W	Name
1013−010	S	0.515	273.6	DA7	26.2	(45,3,-27)	G53-38
1013−050	S	0.095	276.1	DAO1	108.1	(33,7,-17)	RE
1015+161	S,K	0.126	239.4	DA2	83.9	(-16,-19,-23)	PG
1015+076	S	0.037	220.6	DA2	179.5	(-3,-12,-13)	PG
1017+125	S	0.029	215.8	DA2	111.7	(-7,0,-1)	PG
1017+366	I	0.126	193.8	DAH3	64.6	(-9,-26,4)	GD 116
1019+129	K,I	0.084	238.6	DA3	85.5	(8,-9,-14)	PG
1019+637	S	0.377	53.2	DA7	16.5	(-29,33,12)	G235-67
1026+002	S	0.090	141.3	DA3	38.2	(-23,5,7)	PG
1026+023	K,I	0.123	232.9	DA4	34.5	(-1,-1,-6)	LP 550-292
1031−114	K,I	0.344	265.5	DA2	31.0	(31,-2,-21)	EGGR 70
1033+464	I	0.074	184.6	DA2	84.7	(-11,-17,12)	GD 123
1034+492	K	0.063	97.4	DA2	78.7	(-29,15,19)	GD 304
1038+633	K	0.090	233.1	DA2	57.3	(7,-6,4)	PG
1039+747	S	0.067	233.5	DA2	165.2	(30,-24,6)	PG
1042−690	I	0.176	269.4	DA3	36.5	(17,4,-8)	LTT 3943
1046−017	S	0.117	186.9	DBZ5	56.2	(-21,-11,-10)	GD 124
1046+281	K	0.059	222.3	DA4	42.7	(-5,1,3)	Ton 547
1049+103	I	0.097	199.2	DA2	109.1	(-16,-32,-15)	PG
1052+273	S,K	0.143	257.9	DA3	37.5	(10,0,-4)	GD 125
1055−072	S	0.821	276.3	DA7	12.2	(34,2,-10)	LHS 2333
1056+345	S	0.291	219.6	DB5	49.0	(12,-50,-8)	G119-47
1057+719	S	0.050	246.5	DA1	132.4	(16,-7,3)	PG
1101+385†	I	-	-	BLL	-	-	PG
1102+748	S,K	0.120	258.5	DA3	51.5	(16,-2,-1)	GD 466

Table 3.1: List of Observed White Dwarfs

WD#	Survey	μ	θ	Type	d	U,V,W	Name
1104+602	K	0.249	228.9	DA3	43.9	(21,-31,8)	G197-4
1105−048	S,K	0.451	189.0	DA3	25.8	(-29,-28,-25)	G163-50
1108+475	S	0.137	232.1	DA5	43.7	(6,-12,4)	GD 129
1115−029	S	0.582	292.7	DQ5	38.0	(95,7,-7)	G10-11
1115+166	S	0.021	270.0	DA2	132.4	(2,7,2)	PG
1116+026	K,I	0.097	288.1	DA4	49.4	(13,10,2)	GD 133
1119+385	I	0.088	313.2	DA3	85.5	(21,25,-5)	PG
1121+216	S	1.039	268.9	DA7	13.4	(48,-13,-15)	LHS 304
1123+189	I	0.029	236.3	DA1	114.8	(-1,-1,1)	PG
1125−025	I	0.045	271.7	DA2	109.6	(12,4,0)	PG
1126+185†	S	-	-	sdG	-	-	PG
1129+155	K	0.069	131.5	DA3	36.3	(-20,9,8)	PG
1133+293	S,I	0.050	216.9	DA2	88.7	(-5,-8,4)	Feige 45
1134+300	S,K,I	0.148	265.8	DA2	15.3	(0,7,4)	GD 140
1143+321	S	0.283	202.0	DA3	31.6	(-11,-30,5)	G148-7
1154+186	S,K	0.328	276.0	DZ5	29.9	(34,-4,-2)	G57-29
1159+803	S	0.201	255.0	DAV4	63.1	(39,-24,8)	G255-2
1201−001	K	0.099	254.8	DA2	60.3	(11,-6,-1)	PG
1202−232	K	0.228	9.1	DA6	11.2	(-6,19,17)	EC
1202+308	I	0.048	182.4	DA2	110.7	(-20,-11,8)	Ton 75
1204+450	S	0.064	257.3	DA2	92.9	(12,-6,4)	PG
1208+576	S	0.629	132.0	DA9	20.0	(-61,1,34)	G197-47
1210+464	I	0.051	159.4	DA2	139.3	(-32,-9,19)	PG
1210+533	I	0.035	166.8	DAO1	103.3	(-19,0,15)	PG
1214+267	I	0.030	246.9	DA1	211.8	(9,-12,3)	PG

Table 3.1: List of Observed White Dwarfs

WD#	Survey	μ	θ	Type	d	U,V,W	Name
1220+234	S	0.064	262.9	DAP2	44.7	(2,4,5)	Ton 610
1225−079	S	0.125	250.4	DZ5	26.3	(1,1,3)	PG
1230+417	S	0.102	280.2	DA3	102.3	(37,-5,1)	GD 317
1232+479	S	0.162	145.0	DA3	45.5	(-39,-1,18)	GD 148
1234+481	S	0.101	236.3	DA1	134.9	(20,-45,17)	PG
1237−028	S	0.213	284.7	DA5	37.8	(27,0,10)	LP 615-183
1240+754	I	0.190	262.7	DA3	81.7	(50,-32,11)	LB 261
1241−010	I	0.186	196.9	DA2	88.7	(-25,-54,-29)	PG
1241+235	I	0.020	101.3	DA2	110.2	(-19,16,7)	PG
1242−105*	S	0.348	257.7	DA6	18.0	(13,-8,2)	LP 736-4
1244−125	K	0.206	277.9	DA4	43.9	(29,-7,10)	EC
1247+553†	K	-	-	sdB	-	-	GD 319
1254+233	S,K	0.196	188.2	DA1	67.0	(-35,-44,2)	GD 153
1257+037	S	0.966	206.6	DC9	16.1	(-14,-57,-18)	LHS 2661
1257+047	I	0.123	215.8	DA2	78.3	(-6,-30,-6)	GD 267
1257+278	S	0.328	283.0	DA6	34.6	(41,-7,9)	G149-28
1258+593	S	0.087	28.9	DA3	60.3	(-8,34,-5)	GD 322
1307+354	I	0.228	275.8	DAV5	44.3	(33,-11,10)	GD 154
1309+853	S	0.324	140.5	DC9	18.1	(-31,13,24)	G256-7
1310+583	S,I	0.210	112.4	DA5	21.1	(-29,18,9)	PG
1314−153	S	0.709	198.2	DA3	58.6	(-30,-142,-114)	LHS 2712
1319+466	S,K	0.258	289.1	DA3	38.0	(35,-3,7)	G177-34
1327−083	S	1.207	246.9	DA4	18.0	(48,-73,-2)	LHS 354
1328+343	S,I	0.062	209.1	DA3	75.5	(-12,-9,11)	PG
1330+473	I	0.028	262.9	DA2	92.5	(0,3,9)	PG

Table 3.1: List of Observed White Dwarfs

WD#	Survey	μ	θ	Type	d	U, V, W	Name
1333+005*	S	0.307	244.1	DC6	86.3	(52,-98,2)	LP 618-14
1334+039	S	3.880	252.8	DZ9	8.2	(80,-110,14)	LHS 46
1335+700	S,K,I	0.084	298.4	DA2	92.9	(26,1,1)	PG
1337+705	S,K	0.405	266.3	DA2	24.8	(26,-19,18)	G238-44
1344+106	S	0.906	261.6	DA7	20.0	(48,-50,22)	G63-54
1344+572	K,I	0.273	315.9	DA4	24.0	(21,12,1)	G223-24
1345+238	S	1.490	274.9	DC9	12.1	(60,-35,26)	LHS 361
1349+144	K,I	0.094	266.3	DA3	85.5	(18,-14,15)	PG
1349+545	S	0.090	270.0	DAP5	77.3	(-34,33,-1)	SBSS
1350−090	S	0.512	134.7	DA3	14.7	(-38,10,-14)	LP 907-37
1353+409	I	0.050	130.1	DA2	136.1	(-41,13,5)	PG
1407+425	S	0.015	256.7	DA5	31.2	(-8,10,8)	PB 1549
1408+323	S	0.243	176.2	DA3	39.5	(-42,-19,9)	GD 163
1422+095	S,K,I	0.255	233.9	DAV4	31.5	(-1,-25,11)	GD 165
1424+240†	I	-	-	BLL	-	-	PG
1428+373	S	0.086	169.2	DA5	96.8	(-42,-9,9)	PG
1430+427†	I	-	-	sdB	-	-	PG
1433+538	I	0.141	284.8	DA2	150.7	(74,-38,35)	GD 337
1444−096	I	0.170	164.3	DB3	63.4	(-36,-15,-28)	PG
1449+003†	I	-	-	sdM	-	-	G66-36
1449+168	I	0.057	10.1	DA2	101.4	(6,35,11)	PG
1450+432†	I	-	-	BHB	-	-	PG
1501+032	I	0.069	312.0	DA4	71.1	(9,12,22)	PG
1503−070	S	0.205	264.4	DAH7	25.9	(4,-6,18)	GD 175
1507+220	I	0.071	248.5	DA3	78.3	(-2,-11,18)	PG

Table 3.1: List of Observed White Dwarfs

WD#	Survey	μ	θ	Type	d	U, V, W	Name
1507−105	S	0.150	278.5	DA5	50.8	(12,-8,28)	GD 176
1508+637	S,K,I	0.129	220.6	DA4	32.4	(-14,-2,20)	GD 340
1509+322	S,K	0.180	290.9	DA4	47.6	(23,-4,26)	GD 178
1521+310	S	0.058	136.4	DA2	100.9	(-34,12,-4)	Ton 229
1531−022	S,K	0.141	206.9	DA3	31.6	(-13,-8,3)	GD 185
1537+651	S,K	0.205	324.9	DA5	27.2	(17,7,7)	GD 348
1539−035	S,I	0.106	105.4	DA5	34.5	(-18,20,-5)	GD 189
1539+530*	S	0.0	0.0	DA2	173.0	(-9,12,7)	PG
1542−275	S	0.246	235.9	DB4	52.2	(10,-45,14)	LP 916-27
1542+182	S,K,I	0.118	177.1	DB2	53.5	(-30,-7,-1)	GD 190
1548+149	I	0.052	184.4	DA2	80.2	(-21,-3,2)	PG
1550+183	S,K	0.192	309.5	DA4	40.0	(19,9,30)	GD 194
1553+353	S,I	0.046	145.6	DA2	87.5	(-27,11,0)	PG
1554+215	I	0.060	158.6	DA2	121.9	(-38,-1,-8)	PG
1606+422	S	0.170	314.0	DA5	26.3	(10,9,16)	C2
1607−251*	S,I	0.194	312.5	DA5	38.2	(2,13,40)	LTT 6451
1608+118	I	0.040	135.0	DA2	89.9	(-21,11,-5)	PG
1609+044	I	0.026	240.9	DA2	116.9	(-8,-1,13)	PG
1609+135	S	0.546	178.7	DA5	18.3	(-40,-20,-8)	LHS 3163
1612−111	I	0.110	158.6	DB2	69.8	(-24,-5,-21)	GD 198
1614+136	I	0.040	180.0	DA2	131.2	(-25,-5,-1)	PG
1614+270†	I	-	-	sdO	-	-	PG
1615−154	S,K	0.236	226.8	DA2	48.8	(-5,-42,13)	G153-41
1619+123	S	0.098	135.8	DA3	58.6	(-27,11,13)	PG
1620−391	K,I	0.074	88.1	DA2	12.8	(-10,15,4)	EGGR 274

Table 3.1: List of Observed White Dwarfs

WD#	Survey	μ	θ	Type	d	U,V,W	Name
1625+093	S	0.468	189.3	DA7	23.4	(-38,-29,-6)	G138-31
1626+368	S,K,I	0.893	326.7	DZ6	15.9	(51,15,37)	G180-57
1630+618†	I	-	-	sdB	-	-	GD 354
1631+396	I	0.061	172.4	DA3	43.8	(-21,8,5)	KUV
1631+781	S,I	0.067	247.2	DA1	57.3	(-11,2,22)	RE
1632+177	S,K,I	0.089	108.4	DA5	15.1	(-12,14,2)	PG
1633+433	S,I	0.378	144.0	DA8	15.1	(-33,14,-4)	G180-63
1636+160	I	0.072	155.6	DA4	49.7	(-22,6,-3)	GD 202
1636+351	I	0.036	289.4	DA1	115.3	(1,4,21)	PG
1637+335	S,I	0.470	182.5	DA5	28.6	(-63,-21,2)	G180-65
1639+153	S	0.672	178.8	DA7	29.8	(-75,-49,-24)	G138-56
1639+537	S	0.220	212.4	DAEH6	21.1	(-24,0,18)	GD 356
1641+387	S,I	0.167	9.5	DA4	29.9	(11,24,5)	GD 357
1643+143	S,I	0.036	34.4	DA2	150.0	(2,35,3)	PG
1644+198	I	0.108	150.1	DB4	50.1	(-28,6,-9)	PG
1645+325	S,K	0.162	178.0	DBV2	36.6	(1,-3,29)	GD 358
1647+375	S	0.061	287.2	DA2	78.7	(2,2,24)	PG
1647+591	S,K	0.328	155.6	DAV4	11.0	(-26,14,4)	G226-29
1654+160	I	0.047	320.2	DBV2	166.0	(15,16,35)	PG
1654+637	I	0.150	233.3	DA4	90.8	(-37,-22,54)	GD 515
1655+215	S,K,I	0.577	177.4	DA5	23.3	(-58,-24,-12)	LHS 3254
1658+440	S	0.106	344.6	DAP2	24.2	(3,14,10)	PG
1659+303*	S	0.063	170.8	DA5	53.5	(-23,6,2)	PG
1705+030	S,I	0.386	180.0	DZ7	17.5	(-26,-11,-7)	G139-13
1708−147	S,I	0.409	134.4	DQ5	27.4	(-23,4,-44)	LTT 6847

Table 3.1: List of Observed White Dwarfs

WD#	Survey	μ	θ	Type	d	U, V, W	Name
1709+230	I	0.164	176.5	DB2	59.2	(-45,-12,-8)	GD 205
1713+332	I	0.170	142.2	DA2	85.5	(-62,12,-37)	GD 360
1713+695	S,K,I	0.345	189.4	DA3	27.7	(-52,10,21)	G240-51
1748+708	S	1.678	311.3	DQ8	6.1	(22,-12,36)	G240-72
1756+827	S	3.610	336.7	DA7	15.6	(217,-122,54)	LHS 56
1809+284	I	0.168	347.0	DA4	59.2	(-47,-3,-17)	GD 375
1820+609	S	0.710	168.0	DA11	12.8	(-50,19,-6)	G227-28
1822+410	S,I	0.138	359.2	DBAZ4	41.9	(16,18,15)	GD 378
1824+040	S	0.378	220.0	DA4	54.9	(-60,-69,29)	G21-15
1826−045	I	0.298	178.1	DA6	28.7	(-26,-19,-13)	G21-16
1827−106	I	0.282	141.9	DA3	35.6	(-16,-6,-36)	G155-19
1829+547	S	0.392	317.7	DQ7	15.0	(8,4,28)	G227-35
1840+042	I	0.128	299.0	DA6	24.9	(-8,12,22)	GD 215
1844−223	S	0.090	119.4	DA2	58.1	(-5,10,-17)	RE
1855+338	S,I	0.353	7.5	DAV4	32.8	(40,32,22)	G207-9
1858+393	I	0.234	169.6	DA6	34.7	(-41,6,-13)	G205-52
1900+705	S,K	0.510	9.1	DAP5	13.0	(22,5,8)	G260-15
1910+047	I	0.112	185.1	DA2	157.0	(-57,-48,-25)	WD
1914+094	I	0.050	196.3	DA2	148.6	(-33,-13,0)	KPD
1917−077	S	0.174	200.6	DBQA5	11.2	(-13,4,6)	EGGR 131
1917+386	S	0.250	174.7	DC8	11.7	(-21,9,0)	G125-3
1918+110	I	0.107	159.2	DA3	133.7	(-40,-20,-44)	GD 218
1935+276	S,I	0.442	87.7	DAV4	18.0	(8,23,-25)	G185-32
1936+327	S,I	0.153	207.0	DA2	34.8	(-32,2,6)	GD 222
1940+374	S,I	0.222	356.6	DB3	49.3	(34,22,35)	EGGR 133

Table 3.1: List of Observed White Dwarfs

WD#	Survey	μ	θ	Type	d	U,V,W	Name
1950+250	S,I	0.150	1.5	DAV4	38.0	(12,23,20)	GD 385
1952−206	S,I	0.392	165.8	DA4	51.8	(-16,-69,-45)	LTT 7873
1953−011	S,K,I	0.833	212.0	DAH6	11.4	(-38,-22,10)	LHS 3501
2006+481†	I	-	-	sdO	-	-	KPD
2007−219	S,I	0.331	161.7	DA5	18.2	(-9,-12,-9)	LTT 7983
2007−303	S,K	0.428	233.5	DA4	15.4	(-23,-10,24)	LTT 7987
2009+622	I	0.164	202.2	DA2	134.3	(-112,27,-6)	GD 543
2025+554	S,I	0.107	51.8	DA2	115.4	(47,14,-10)	GD 546
2028+390	S,I	0.176	59.4	DA2	41.7	(22,19,-7)	GD 391
2032+248	S,I	0.693	215.7	DA3	14.8	(-54,-7,7)	G186-31
2032+188	I	0.145	182.2	DA3	107.7	(-60,-25,-32)	GD 231
2039−202	S,K,I	0.368	105.4	DA3	21.1	(10,6,-24)	EGGR 141
2047+372	S,I	0.213	44.3	DA4	18.4	(9,15,5)	G210-36
2048+263	S	0.518	234.1	DC9	20.1	(-55,-1,20)	G187-8
2055+221†	S	-	-	sdM	-	-	G187-9
2058+181	K	0.112	108.8	DA4	54.0	(3,8,-19)	GD 232
2058+342	S,I	0.168	42.6	DB4	57.8	(36,21,5)	GD 392
2058+506	S,I	0.114	208.4	DA5	34.0	(-27,12,3)	GD 393
2059+316	I	0.399	214.9	DQ5	34.5	(-72,-4,1)	G187-15
2111+261	I	0.395	165.0	DA6	31.9	(-37,-10,-41)	G187-32
2115+010	S	0.028	12.4	DA2	122.5	(1,24,12)	PG
2116+736	S	0.061	218.4	DA1	161.4	(-53,28,5)	KPD
2117+539	S	0.213	336.4	DA3	19.7	(-2,10,25)	G231-40
2123−229	I	0.201	141.9	DA4	58.6	(5,-31,-26)	LP 873-45
2126+734	S,K	0.289	168.8	DA3	21.2	(-22,24,-16)	G261-43

Table 3.1: List of Observed White Dwarfs

WD#	Survey	μ	θ	Type	d	U,V,W	Name
2131+066	I	0.018	210.4	DO1	398.1	(-37,-6,3)	PG
2134+218	K,I	0.100	274.6	DA3	47.0	(-24,14,23)	GD 234
2136+229	S,I	0.292	65.3	DA5	42.0	(46,18,-12)	G126-18
2140+207	S,I	0.690	197.5	DQ6	12.5	(-42,-5,-10)	G126-27
2144−079	S	0.285	117.1	DB4	69.4	(37,-32,-62)	G26-31
2147+280	I	0.262	108.1	DB4	35.3	(14,3,-29)	G188-27
2149+021	K,I	0.301	177.3	DA3	25.1	(-26,-14,-11)	G93-48
2151−015	I	0.404	180.3	DA6	19.6	(-27,-17,-9)	LTT 8747
2154+408	I	0.045	237.7	DA2	92.5	(-29,13,9)	KPD
2200+085†	I	-	-	sdK	-	-	PG
2207−303	S	0.066	142.4	DA2	108.1	(1,-17,-6)	RE
2207+142	S	0.361	44.8	DA6	25.5	(33,24,8)	G18-34
2244+031	I	0.008	113.2	DA1	407.4	(0,4,-3)	PG
2246+223	S,I	0.528	83.3	DA5	19.0	(34,2,-10)	G67-23
2246+154†	S	-	-	sdB	-	-	PG
2249−105	S	0.192	146.9	DC8	53.2	(-4,-30,-17)	LP 761-114
2251−070	S	2.576	105.3	DZ11	8.1	(60,-36,-44)	LHS 69
2253−062	S,K	0.073	99.5	DBA4	54.7	(6,4,-2)	GD 243
2256+249	I	0.152	119.0	DA4	51.3	(10,-5,-20)	GD 245
2303+242	S	0.088	129.5	DAV4	52.5	(-1,1,-10)	PG
2307+636	S	0.368	171.9	DA2	53.8	(-29,25,-84)	G241-46
2309+105	S,K	0.142	94.0	DA1	69.8	(30,-6,-13)	GD 246
2309+258	I	0.007	167.0	DA4	34.8	(-9,11,6)	KUV
2311−068	S,I	0.381	243.3	DQ6	25.1	(-54,9,14)	G157-34
2316+123	S,I	0.102	95.6	DAP4	53.3	(12,1,-4)	KUV

Table 3.1: List of Observed White Dwarfs

WD#	Survey	μ	θ	Type	d	U, V, W	Name
2316−173	S,K	0.238	93.4	DBQA4	27.7	(19,3,-3)	LP 822-50
2317−185*	I	0.013	344.0	DA4	32.9	(-9,14,8)	GD 1295
2319+691	S	0.134	265.7	DA3	63.9	(-43,26,17)	GD 559
2322−181	S	0.240	87.6	DA2	88.1	(80,-21,-25)	G273-40
2323+157	S	0.116	201.3	DC5	37.3	(-25,4,-3)	GD 248
2324+060	S,I	0.120	164.6	DA4	70.8	(-19,-19,-18)	PB 5379
2326+049	K,I	0.482	237.0	DAV4	13.6	(-40,10,6)	G29-38
2328+107	S,I	0.068	245.7	DA2	109.6	(-44,15,8)	KPD
2328+510	S	0.173	67.6	DB2	50.4	(30,-2,10)	GD 406
2329+267	S	0.444	86.4	DAH5	38.6	(64,-17,-14)	G128-72
2329+407	S	0.280	110.9	DA3	34.1	(22,-7,-20)	G171-2
2329−291	I	0.019	95.3	DA2	45.0	(-6,10,6)	GD 1669
2333−049	S	0.240	235.5	DA5	50.1	(-66,5,8)	G157-82
2341+322	S,K	0.229	252.2	DA3	17.6	(-27,17,7)	G130-5
2342+806	S,K	0.028	278.1	DAO1	64.0	(-16,15,10)	GD 561
2349+286	I	0.062	215.8	DA1	234.4	(-67,6,-29)	PG
2351−335	S	0.500	216.5	DA5	20.0	(-46,-8,16)	LHS 4040
2352+401	S	0.566	158.2	DQ5	25.8	(-9,-15,-57)	G171-27
2357+296	I	0.061	131.0	DA1	191.4	(13,-21,-31)	PG
2359−434	K,I	1.020	135.2	DA6	7.8	(4,-24,9)	LHS 1005

* Not listed in McCook & Sion (1999). The WD number is unofficial.

† Not a white dwarf (see §3.3).

3.3 Sample Contamination

In the white dwarf literature, there are often objects misclassified as white dwarfs. These include, but are not limited to, hot subdwarfs (helium burning stars such as sdO, sdB), blue horizontal branch stars, cool subdwarfs (metal poor stars such as sdG, sdK), quasi stellar objects, and BL Lacertae objects. Hot subdwarfs and blue horizontal branch stars have strong, pressure broadened hydrogen or helium lines and can be mistaken for white dwarfs with low signal to noise and low resolution spectroscopy. A typical misclassification is an sdB star mistaken for a DA white dwarf, both of which show hydrogen Balmer lines although the features of a degenerate star are more significantly pressure broadened by its higher surface gravity (Finley, Koester, & Basri 1997). Cool subdwarfs exhibit very weak features due to their low metallicity and can be mistaken for featureless white dwarfs with low signal to noise and low resolution spectroscopy. They are often identified as white dwarf candidates due to their combination of low luminosity and high proper motion (Salim & Gould 2002). A typical misclassification is an sdG star mistaken for a DC white dwarf, both of which can appear featureless at certain optical wavelengths (Smart et al. 2003). The same reasoning applies to quasi stellar and BL Lacartae objects because their spectra are essentially featureless in the optical (Fleming et al. 1993). 23 targets included in Table 3.1 were subsequently revealed to be misclassified, leaving 372 white dwarfs observed.

3.4 Sample Kinematics

The Galactic UVW space motions and statistics for the white dwarf sample was calculated in order to evaluate the most probable range of stellar ages. As stated above, smaller values of UVW and their dispersions, implying more circular

Galactic orbits, correlate with younger stellar populations that have experienced fewer gravitational events since their birth in and around the spiral arms (Mihalas & Binney 1981; Binney & Merrifield 1998). Table 3.2 contains the kinematical properties calculated for the white dwarf sample. The quantity T is the total space velocity with respect to the LSR ($T^2 = U^2 + V^2 + W^2$), and σ_T is the total disperion in space velocity ($\sigma_T^2 = \sigma_U^2 + \sigma_V^2 + \sigma_W^2$).

Somewhat unexpectedly, the sample does not appear to consist primarily of old, metal poor disk stars. It seems likely that the sample contains a significant fraction of stars with intermediate and young disk kinematics – stars with ages less than ~ 5 Gyr.

In Figure 3.1, the white dwarf sample is plotted in the UV and WV planes. Also shown in the figure are the 1 and 2 σ velocity ellipsoids for old, metal poor disks stars from Beers et al. (2000) – a kinematical study of the halo and thick disk utilizing a large sample of nonkinematically selected metal poor stars. The ellipsoid parameters in Figure 3.1 were taken from the first row of Table 1 in Beers et al. (2000), 141 stars with $-0.6 \leq$ [Fe/H] ≤ -0.8 and $|Z| < 1$ kpc. Z is the scale height above the Galactic plane, and hence this old disk sample is unlikely to be contaminated by halo stars. The ellipsoids are centered at $(U, V, W) = (0, -35, 0)$ km s^{-1} with axes $(\sigma_U, \sigma_V, \sigma_W) = (50, 56, 34)$ km s^{-1}. From the Figure 3.1 and Table 3.2, it is clear that the white dwarf sample is centered much closer to $(U, V, W) = (0, 0, 0)$, values that represent the undisturbed circular Galactic disk orbits of younger stars (Mihalas & Binney 1981; Binney & Merrifield 1998). Older disk stars lag behind the Galactic rotation of the LSR and hence have increasingly negative V velocities with increasing age (Beers et al. 2000).

Comparing the values in Table 3.2 with the values for kinematical populations of known ages from *Hipparcos* measurements of nearby stars, there is further

evidence that the white dwarf sample contains younger disk stars. The average UVW, their dispersions, and the total velocity dispersion (σ_T) values of the entire sample are consistent with those of disk stars of intermediate age ($2-5$ Gyr), but actually inconsistent with stars of age 5 Gyr due to the relatively small negative value of $\langle V \rangle$. This comes from a direct comparison of Table 3.2 with Table 5 & Figures 3-5 of Wielen (1974), and with Table 4 of Jahreiß & Wielen (1997). In fact, the subsample in Table 3.2, white dwarfs with $\mu < 0.50''$ yr^{-1}, is quite consistent with stars of age $\sim$ 2 Gyr by the same comparisons (Wielen 1974; Jahreiß & Wielen 1997).

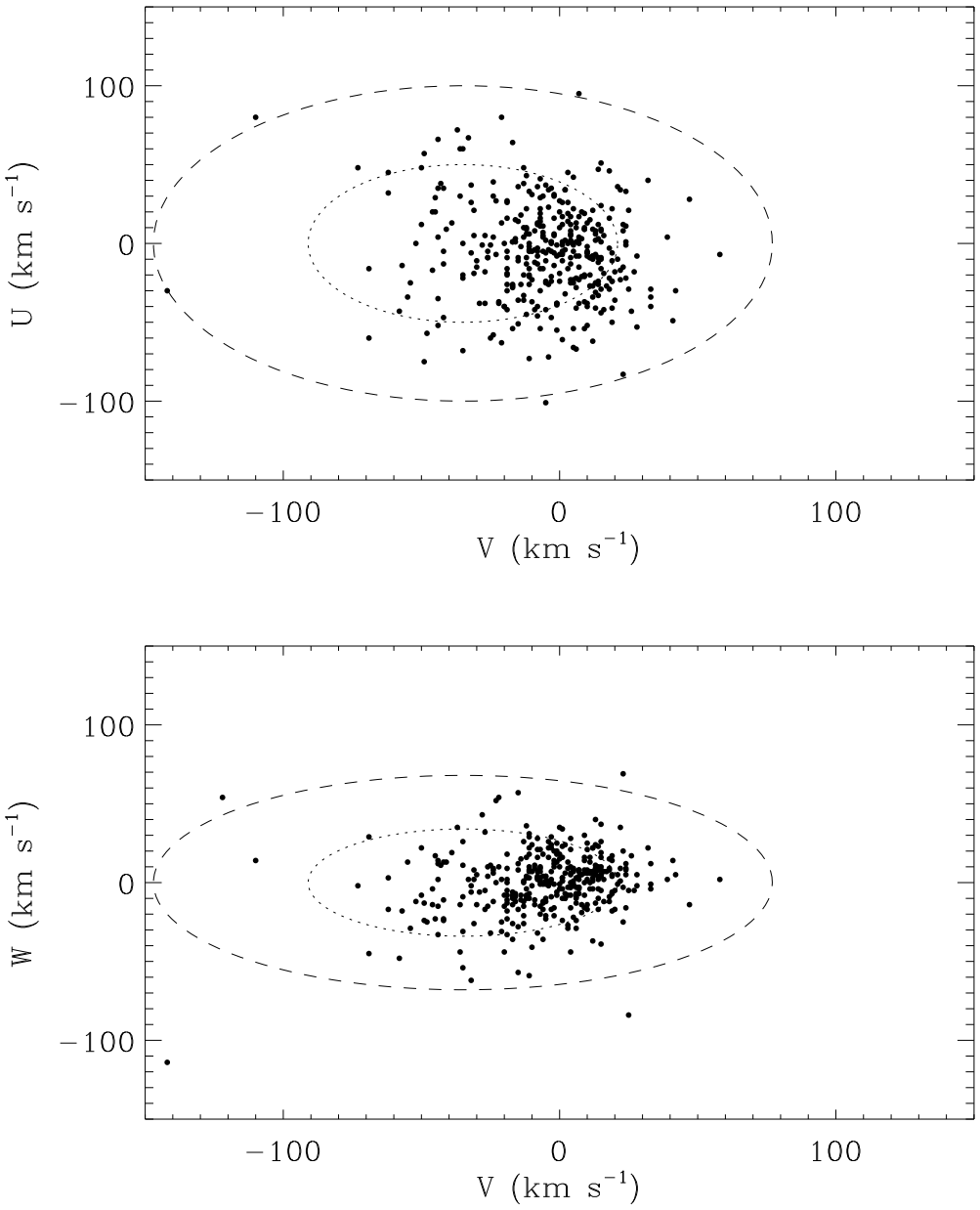

Figure 3.1: Galactic space velocity distribution in the UV and WV planes for all 372 white dwarfs in the sample. The ellipses represent the 1 and 2 σ contours for old, metal poor disk stars from (Beers et al. 2000).

Table 3.2: Sample Kinematics

All 372 Stars	
$\langle U \rangle = -5$ km s^{-1}	$\sigma_U = 32$ km s^{-1}
$\langle V \rangle = -6$ km s^{-1}	$\sigma_V = 24$ km s^{-1}
$\langle W \rangle = 0$ km s^{-1}	$\sigma_W = 20$ km s^{-1}
$\langle T \rangle = 37$ km s^{-1}	$\sigma_T = 44$ km s^{-1}
$\langle \mu \rangle = 0.27''$ yr^{-1}	$\sigma_\mu = 0.45''$ yr^{-1}
$\langle d \rangle = 56.6$ pc	$\sigma_d = 47.1$ pc

330 Stars with $\mu < 0.5$	
$\langle U \rangle = -6$ km s^{-1}	$\sigma_U = 26$ km s^{-1}
$\langle V \rangle = -3$ km s^{-1}	$\sigma_V = 20$ km s^{-1}
$\langle W \rangle = 1$ km s^{-1}	$\sigma_W = 18$ km s^{-1}
$\langle T \rangle = 33$ km s^{-1}	$\sigma_T = 38$ km s^{-1}
$\langle \mu \rangle = 0.16''$ yr^{-1}	$\sigma_\mu = 0.11''$ yr^{-1}
$\langle d \rangle = 61.7$ pc	$\sigma_d = 47.6$ pc

3.5 Sample Age

The white dwarfs surveyed in this work are not similar to the white dwarf samples of Silvestri et al. (2001); Silvestri, Oswalt, & Hawley (2002), which clearly belong to the old disk kinematical population ($\sim 5 - 10$ Gyr). Neither is the sample similar to any of the white dwarf subgroups in Sion et al. (1988) with the exception of the DH and DP stars (magnetic white dwarfs). The sample of magnetic white dwarfs in Sion et al. (1988) was expanded from only 13 stars to 26 stars in Anselowitz et al. (1999) with the same results – these stars appear to have young disk kinematics. In fact, the subsample of moderate proper motion white dwarfs in Table 3.2 have nearly identical kinematical properties as magnetic white dwarfs, implying relatively young ages (~ 2 Gyr) (Sion et al. 1988; Anselowitz et al. 1999).

3.5.1 Cooling Age

However, it must be kept in mind that the sample of white dwarfs consists of a mixture of hot and cool degenerate stars. The cooling age of a typical hot white dwarf ($T_{\rm eff} > 11,000$ K) is less than 500 Myr but the main sequence progenitor age is not known. Hence the total ages of hot white dwarfs in the sample are potentially consistent with relatively young disk objects. But for cool white dwarfs in the sample, it is more likely that they are descended from intermediate age disk stars. For example a white dwarf with $T_{\rm eff} < 7500$ K is at least 1.5 Gyr old according to cooling theory (Bergeron, Saumon, & Wesemael 1995).

In Figure 3.2 is plotted the number of white dwarfs in the sample versus effective temperature index. Exactly 90% of the sample stars have temperatures above 8000 K – implying cooling ages less than 1.1 Gyr for typical hydrogen

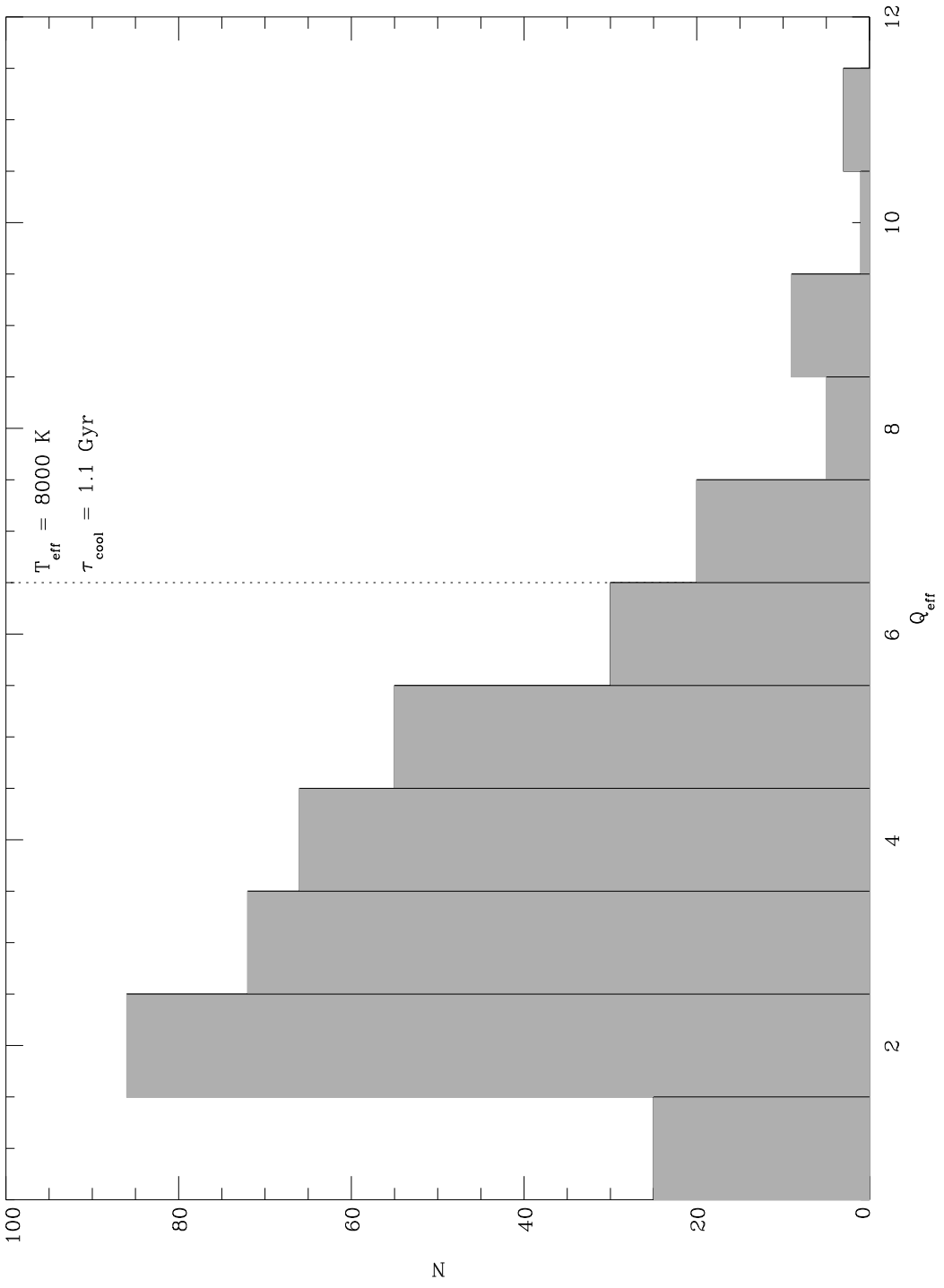

Figure 3.2: Number of sample white dwarfs versus effective temperature index. The dotted line represents a cooling age of 1.08 Gyr for a typical DA white dwarf (Bergeron, Saumon, & Wesemael 1995).

atmosphere white dwarfs (Bergeron, Saumon, & Wesemael 1995). Moreover, 67% of the sample have temperatures above 11,500 K and typical cooling ages less than 0.4 Gyr. Hence the cooling ages of the sample stars are consistent with the total age estimate inferred from kinematics; that of a relatively young disk population.

3.5.2 Total Age

Since one cannot know the main sequence progenitor ages for the white dwarf sample, caution must be taken not to overinterpret the kinematical results. In principle, any individual star of any age can have any velocity. It is possible to estimate total ages for white dwarfs if their mass is known by using the initial to final mass relation (Weidemann 1987, 1990, 2000; Bragaglia, Renzini, & Bergeron 1995). However, this is only feasible for DA white dwarfs (whose masses can be determined spectroscopically), white dwarfs with dynamical mass measurements, or those with trigonometric parallaxes (Bergeron, Saffer, & Liebert 1992; Bergeron, Ruiz, & Leggett 1997; Bergeron, Leggett, & Ruiz 2001). The sample in Table 3.1 contains many degenerates with no mass estimate and therefore no way to confirm or rule out relatively young total ages indicated by their kinematics. While their cooling ages are consistent with young disk objects, a conservative approach would be to explore a range of ages when interpreting the implications of the survey results. Realistically, a typical white dwarf in the sample is likely to be between $2 - 5$ Gyr old.

CHAPTER 4

Results

In this chapter, the individual and overall results of the search are presented. Data on detected companions include finding charts, optical and infrared photometry, proper motion measurements, and spectra. Basically two types of companions were detected – low mass main sequence stars and white dwarfs. Unresolved low mass stellar companions are analyzed separately. A brief description of the IRTF survey, the general method of detecting companions to white dwarfs by near infrared excess emission, and a reassessment of the objects reported in Zuckerman & Becklin (1992) and Schultz, Zuckerman, & Becklin (1996) is presented. A summary of all discovered companions is given. Individual systems of interest are discussed in detail in chapter 6.

4.1 All Companions

Table 4.1 lists all companions to white dwarf sample stars detected in this work or published in the literature. Many targets were thought to be single white dwarfs when this project began in the late 1980's but have subsequently been established to be binaries in various studies. Although only low mass stellar and substellar companions were directly sought in this study, the overall multiplicity of white dwarfs is of astrophysical interest for many reasons. The first column lists the name of the companion. This is generally the name of the white dwarf

primary plus the letter 'B' for a secondary, or 'C' for a tertiary. If a companion is previously known by another name, then that name is given along with a footnote at the end of the table indicating the white dwarf primary component of the system. The second column lists the known or suspected spectral type of the companion. For companions discovered in this work, spectral types were estimated from optical and infrared colors with the longest baselines (such as $V - K$) taking precedence over all else (§5.2.2). The third and fourth columns list the separation on the sky and position angle of resolved companions. If unresolved, an upper limit to the separation is given, whereas a designation of 'close' implies the system is a radial velocity variable. The final column lists references to the initial discovery, critical data and analysis of each companion.

In all, there are 83 objects in 75 stellar systems containing at least one white dwarf; 76 doubles, 6 triples, and 1 quadruple system. Of all the companions, 18 are white dwarfs and 65 are main sequence stars or brown dwarfs. There were 24 multiple systems independently discovered in this work, 20 of which are reported here for the first time and the remaining 4 previously published (Finley & Koester 1997; McCook & Sion 1999; Farihi 2004; Scholz et al. 2004). In addition, new data and new analysis of 32 binaries reported in Zuckerman & Becklin (1992) and Schultz, Zuckerman, & Becklin (1996) have resulted in more accurate descriptions of those systems.

Table 4.1: All Companions

Name	ST	a_{sky}	PA	References
GD 360B	DA	close	-	8
G1-45B	DC	close	-	5,9
G21-15B	DC	close	-	5,13
GD 429B	DC	close	-	9
PG 1241−010B	DC	close	-	8
PG 1428+373B	DC	close	-	14
PG 0922+162B	DA2	$4.4''$	287°	1,22
PG 1204+450B	DA3	close	-	5,12
PG 0945+245B	DAXP3	$< 0.03''$	-	23,24
PG 1115+166B	DB3	close	-	19,20
PG 1017+125B	DA4	$48.8''$	336.1°	1
GD 420B	DA5	close	-	12,13
PG 0901+140B	DA6	$3.6''$	173.6°	1
GD 559B	DC6	$28.7''$	180.8°	1,25
GD 322B	DC7	$15.6''$	235.6°	1
G261-43B	DC10	$1.4''$	167.9°	1,26
G21-15C	DC11	$58.6''$	124.4°	1
GD 392B	DC14	$45.8''$	103.9°	1,27
HD 147528[a]	dG0	$63.3''$	130.6°	1
HD 147513[b]	dG2	$432.4''$	72.3°	1,28
PG 0824+288B	dC	$< 0.5''$	-	29
GD 319B	dM	close	-	1,5,31,32
RE 1016−053C	dM1	$3.2''$	19.0°	1,10
RE 1016−053D	dM1	$3.2''$	19.0°	1,10
GD 683B	dM2	$111.5''$	173.4°	1

Table 4.1: All Companions

Name	ST	a_{sky}	PA	References
GD 984B	dM2	$< 0.5''$	-	1,3
LP 761-113[i]	dM2	$7.7''$	327.7°	1,25
PG 0933+729B[†]	dM2	$80.9''$	81.8°	1
PG 0950+185B	dM2	$1.1''$	100.3°	1,2,4,17
PG 1210+464B	dM2	$< 0.5''$	-	1,2,3,4
PG 1539+530B	dM2	$2.7''$	68.1°	1
PG 1643+143B	dM2	$< 0.5''$	-	1,3
PG 1659+303B	dM2	$154.8''$	326.5°	1
G130-6[d]	dM3	$174.7''$	9.8°	1,6
G163-51[c]	dM3	$279.1''$	159.2°	1,6
GD 51B	dM3	$< 0.5''$	-	1,3
LB 261B	dM3	$6.1''$	127.2°	1,2
LTT 0329B	dM3	$< 0.5''$	-	1,3,15
PG 1015+076B	dM3	$47.8''$	36.9°	1
PG 1123+189B	dM3	$1.3''$	336.1°	1,2,4
PG 1449+168B	dM3	$78.3''$	55.1°	1
PG 1608+118B	dM3	$3.0''$	291.1°	1,2
PG 2131+066B	dM3	$0.3''$	21.0°	1,3,4,35
RE 1629+780B	dM3	$< 0.5''$	-	1,3,34
Ton 1150B	dM3	$< 0.5''$	-	1,3,4
Ton S 392B	dM3	$1.2''$	3.5	1
G148-6[e]	dM3.5	$10.4''$	272.2°	1,7
GD 319C	dM3.5	$125.8''$	101.7°	1
KPD 2154+408B	dM3.5	close	-	1,3
LDS 678B	dM3.5	$27.3''$	306.7°	1,7

Table 4.1: All Companions

Name	ST	a_{sky}	PA	References
LDS 826B	dM3.5	6.6″	358.8°	1,18
PG 0824+288C	dM3.5	3.3″	121°	1,36
PG 0933+025B	dM3.5	$< 0.5''$	-	1,3,4
PG 2244+031B	dM3.5	2.4″	58.0°	1
GD 74B	dM4	99.9″	248.9°	1
GD 84B	dM4	73.7″	264.9°	1
GD 245B	dM4	close	-	1,2,3,30
LP 618-014B	dM4	$< 1''$	-	1
PG 1049+103B	dM4	$< 0.5''$	-	1,2,4
PG 1204+450C	dM4	83.4″	279.5°	1
PHL 790B	dM4	2.0″	89.3°	1,2,3
GD 13B	dM4.5	4.7″	216.7°	1,2
GD 123B	dM4.5	$< 0.5''$	-	1,2,3
GD 267B	dM4.5	8.9″	52.5°	1
GD 337B	dM4.5	$< 0.5''$	-	1,2,3,15
LHS 353[f]	dM4.5	503.3″	198.9°	1,7
LP 916-26[h]	dM4.5	53.6″	326.6°	1,18
LTT 3943B	dM4.5	close	-	1,2,8
PG 0308+096B	dM4.5	close	-	1,2,3,16
PG 0956+045B	dM4.5	2.0″	32.6°	1,2,4
PG 1026+002B	dM4.5	close	-	1,2,3,16
PG 1654+160B	dM4.5	3.5″	131.0°	1,2
RE 1016−053B	dM4.5	close	-	1,10,33
GD 60B	dM5	68.2″	132.8°	1
GD 543B	dM5	close	-	1,2,6,14

Table 4.1: All Companions

Name	ST	a_{sky}	PA	References
LHS 362[g]	dM5	198.5″	51.9°	1,37
LTT 2980B	dM6	close	-	1,2,3,9
GD 448B	dM7	close	-	1,2,21
Rubin 80B	dM7	$< 0.5''$	-	1,3,11
LDS 826C	dM8	102.7″	93.9°	1,38
LTT 8747B	dM8	$< 0.5''$	-	1,3,11
PG 1241−010C	dM9	3.2″	252.7°	1,2
GD 165B	dL4	3.7″	191.5°	2,39,40
GD 1400B[j]	dL6	$< 0.3''$	-	41

[†] candidate companion.

[a] CPM companion to PG 1619+123

[b] CPM companion to EGGR 274

[c] CPM companion to G163-50

[d] CPM companion to G130-5

[e] CPM companion to G148-7

[f] CPM companion to LHS 354

[g] CPM companion to LHS 361

[h] CPM companion to LP 916-27

[i] CPM companion to LP 761-114

[j] not included in survey (see §5.3.4 & §5.6.2).

(1) This work.

(2) Zuckerman & Becklin 1992.

(3) Schultz, Zuckerman, & Becklin 1996.

(4) Green, Schmidt, & Liebert 1986.

(5) Saffer, Livio, & Yungelson 1998.

(6) Greenstein 1984.

(7) Eggen & Greenstein 1965.

(8) Marsh, Dhillon, & Duck 1995.

(9) Maxted, Marsh, & Moran 2000.

(10) Vennes, Thorstensen, & Polomski 1999.

(11) Greenstein 1986a.

(12) Maxted, Marsh, & Moran 2002.

(13) Maxted & Marsh 1999.

(14) Marsh 2000.

(15) Probst 1983.

(16) Saffer et al. 1993.

(17) Greenstein 1986b.

(18) Oswalt, Hintzen, & Luyten 1988.

(19) Maxted et al. 2002.

(20) Bergeron & Liebert 2002.

(21) Maxted et al. 1998.

(22) Finley & Koester 1997.

(23) Liebert et al. 1993.

(24) Schmidt, Liebert, & Smith 1998.

(25) McCook & Sion 1999.

(26) Zuckerman et al. 1997.

(27) Farihi 2004.

(28) Alexander & Lourens 1969.

(29) Heber et al. 1993.

(30) Schmidt & Smith 1995.

(31) McAlister et al. 1996.

(32) Maxted et al. 2000b.

(33) Tweedy et al. 1993.

(34) Cooke et al. 1992.

(35) Reed, Kawaler, & O'Brien 2000.

(36) Green & Margon 1994.

(37) Dahn & Harrington 1976.

(38) Scholz et al. 2004.

(39) Becklin & Zuckerman 1988.

(40) Kirkpatrick et al. 1999b.

(41) Farihi & Christopher 2004.

4.2 Infrared Excess

Before going further into the results, a brief discussion of white dwarfs with infrared excess emission is necessary.

White dwarfs are generally a hot class of stellar object owing to the shape of observed mass functions in star forming regions, the fact that stellar lifetimes increase with decreasing mass and the finite age of the galaxy (hence finite cooling). Typically, white dwarfs have $T_{\rm eff} \geq 10,000$ K and hence blue or zero optical and infrared colors. Cooler white dwarfs will have colors that are just slightly red (Bergeron, Ruiz, & Leggett 1997; Leggett, Ruiz, & Bergeron 1998; Bergeron, Leggett, & Ruiz 2001). For example, a typical white dwarf with $T_{\rm eff} = 6750$ K will have $V - K = 1$, $J - K = 0.2$ (Bergeron, Saumon, & Wesemael 1995).

Very low mass stars and brown dwarfs have radii, $R \approx 1\ R_{\rm J}$, that are approximately 10 times larger than a typical white dwarf radius, $R \sim 1\ R_{\oplus}$ (Burrows et al. 1997). Due to this fact and despite very low effective temperatures and luminosities, an unresolved cool companion to a white dwarf can dominate the spectral energy distribution of the system at longer wavelengths, especially in the near infrared (Probst 1983; Zuckerman & Becklin 1987a,b). Therefore, a white dwarf with red colors in the near infrared or red portion of the optical spectrum can indicate the presence of an unresolved cool companion (Becklin & Zuckerman 1988; Zuckerman & Becklin 1992; Farihi & Christopher 2004).

4.2.1 Unresolved Companions

There are basically two methods for obtaining parameters for unresolved low mass stellar or substellar companions to white dwarfs – optical and/or near infrared photometry or optical spectroscopy. Near infrared spectroscopy is not typically

performed for two reasons; near infrared spectrographs were not common until recently, but more importantly, spectral types for low mass stars and cool dwarfs in general (M and L dwarfs) were established optically (Kirkpatrick & McCarthy 1994; Kirkpatrick et al. 1999b).

Optical spectroscopy can reveal unresolved companions to white dwarfs for a range of white dwarf to red dwarf luminosity ratios. If the white dwarf is cool enough and/or the red dwarf is bright enough, a composite spectrum can be seen even in the blue and visual portion of the optical spectrum (Greenstein 1986b; Finley, Koester, & Basri 1997). Red dwarf companions which are too dim, relative to their white dwarf hosts, in the blue or visual can still be seen at red optical wavelengths ($7000 - 10,000$ Å) (Maxted et al. 1998). In order to extract information on the companion, one can visually inspect the spectrum and compare to known spectral types. For better accuracy, one can fit the bluest portion of the spectrum with models and effectively subtract the contribution of the white dwarf, leaving only the companion spectrum for analysis (Raymond et al. 2003).

However, the lowest luminosity companions to white dwarfs do not contribute a relatively significant amount of light in the optical for accurate spectral typing or study if they are unresolved (Kirkpatrick, Henry, & Liebert 1993). Near infrared methods must be used for companions which are relatively invisible in the optical. Near infrared spectroscopy can verify the presence of a companion, but has only a limited ability to provide a spectral type for the reason mentioned above. The most successful method for doing so uses near infrared photometry. Using models, one can extrapolate the flux of the white dwarf into the near infrared and subtract its expected contribution, thereby obtaining photometry for any unresolved, very low luminosity companions (Zuckerman & Becklin 1987a;

Becklin & Zuckerman 1988; Zuckerman & Becklin 1992; Green, Ali, & Napiwotzki 2000; Farihi & Christopher 2004). The resulting near infrared colors (or infrared plus red optical colors or upper limits) can be compared with the colors of known isolated low luminosity objects such as late M dwarfs and L dwarfs to make a determination of spectral type (Kirkpatrick & McCarthy 1994; Kirkpatrick et al. 1999b).

In this work, both near infrared and optical colors resulting from photometry were used to determine spectral types for all unresolved companions, while optical spectroscopy was used to verify the presence of the companion, where possible. Most of the white dwarf primaries with unresolved cool companions are quite well studied and hence model extrapolation to longer wavelengths is likely to be reliable. The model grids of P. Bergeron (2002, private communication) for pure hydrogen and pure helium atmosphere white dwarfs were used to predict $RIJHK$ fluxes for white dwarfs in such systems. These fluxes, together with the measured composite fluxes, were then used to calculate $RIJHK$ magnitudes for the unresolved red dwarf component of the binary. The resulting optical and infrared colors were then compared to those of Kirkpatrick & McCarthy (1994) to determine spectral type. Unlike both Zuckerman & Becklin (1992) and Green, Ali, & Napiwotzki (2000), absolute K magnitudes of the companions were generally not used in estimating spectral types for reasons that will be discussed in §4.4.1 and §5.2.2.

4.3 New Companions

The companions discovered in this work – both those reported here for the first time or those discovered independently elsewhere – are almost exclusively common proper motion companions. There is only one white dwarf in this category

which is very likely to have a companion based on measured infrared excess emission and four visual binaries.

4.3.1 Finding Charts

Figures 4.1 – 4.20 are finding charts for companions reported here for the first time, including candidate companions. In the case of PG 1619+123, its newly identified common proper motion companion, HD 147528, is already known and hence no chart is provided here. The objects GD 392B, LDS 826C, & PG 0922+162B were discovered independently in the course of this survey but are previously published with finding charts (Finley & Koester 1997; Scholz et al. 2004; Farihi 2004). GD 559B is reported only in McCook & Sion (1999) with no other available reference.

For ease of use at the telescope, the charts are given at optical wavelengths when possible. In a few cases, the quality of a near infrared image is superior and used instead. Generally, these are all $\sim 3'$ square field of view CCD or near infrared array images taken at Lick Observatory and Steward Observatory. Coordinates are given for the companion if: (1) it is separated from the white dwarf primary by more than $20''$; (2) coordinates in the literature are inaccurate or difficult to find; (3) a finder chart is not published or difficult to find.

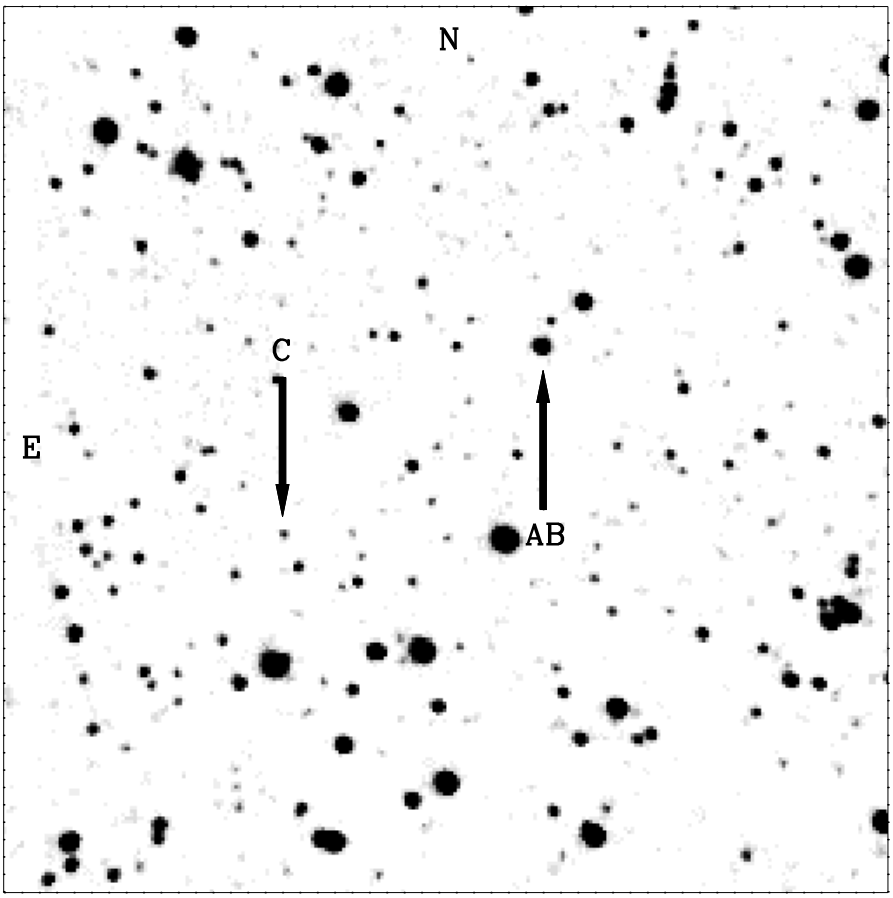

Figure 4.1: Near infrared finding chart for G21-15C, taken at J band with the Bok 2.3 meter telescope in July 2001. The image is 166″ square with 0.65″ pixels. The coordinates for the companion are $18^{h}27^{m}16.4^{s}$, $+04°04'09''$ J2000.

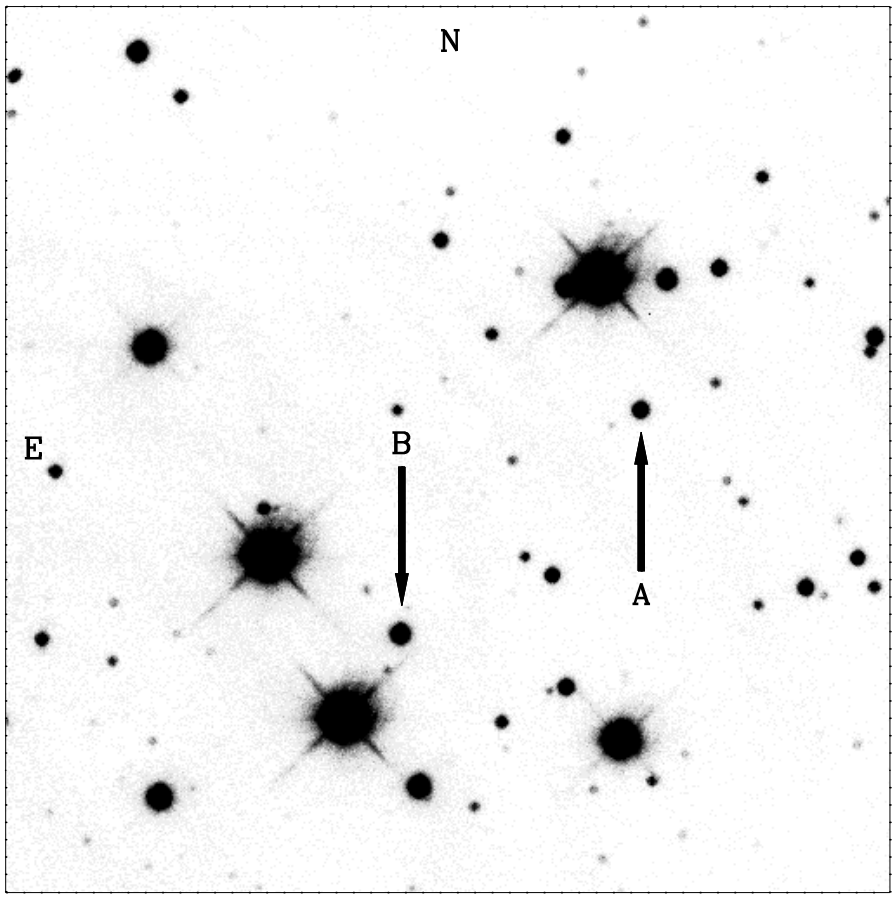

Figure 4.2: Optical finding chart for GD 60B, taken at I band with the Nickel 1 meter telescope in January 2003. The image is 184″ square with 0.36″ pixels. The coordinates for the companion are $04^{h}20^{m}15.2^{s}$, $+33°34'48''$ J2000.

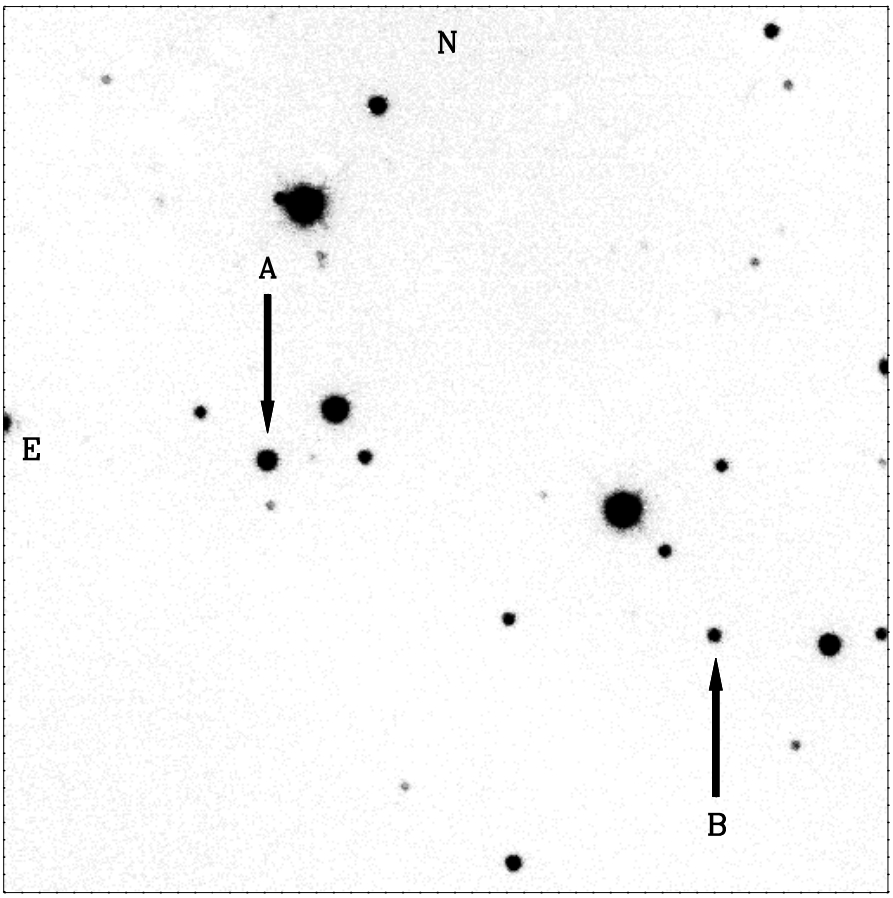

Figure 4.3: Optical finding chart for GD 74B, taken at R band with the Nickel 1 meter telescope in January 2003. The image is 184″ square with 0.36″ pixels. The coordinates for the companion are $06^{h}28^{m}55.8^{s}$, $+41°30'11''$ J2000.

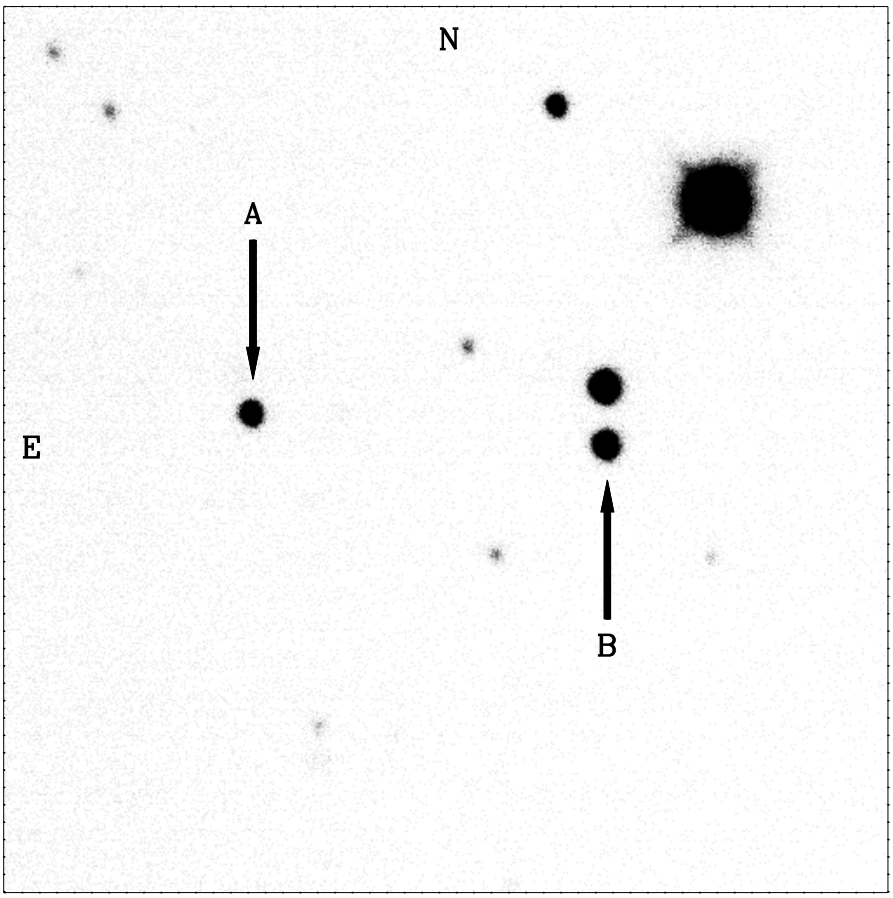

Figure 4.4: Optical finding chart for GD 84B, taken at R band with the Nickel 1 meter telescope in October 2001. The image is 184″ square with 0.36″ pixels. The coordinates for the companion are $07^{h}17^{m}54.6^{s}$, $+45°47'48''$ J2000.

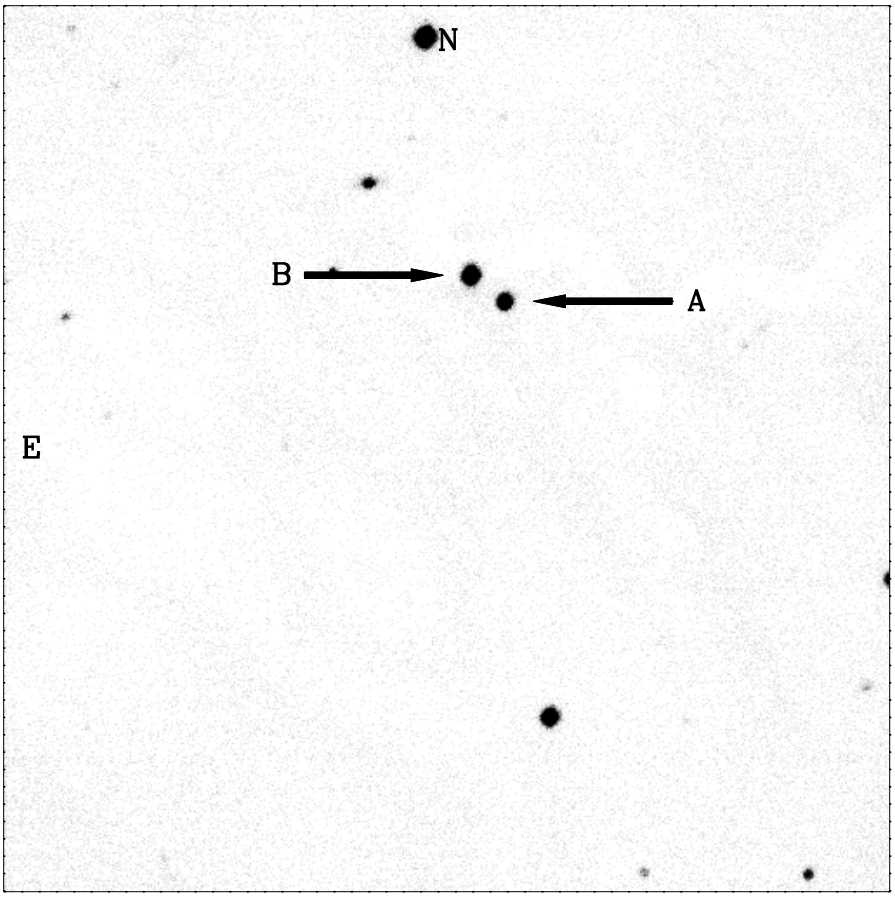

Figure 4.5: Optical finding chart for GD 267B, taken at I band with the Nickel 1 meter telescope in March 2003. The image is $184''$ square with $0.36''$ pixels.

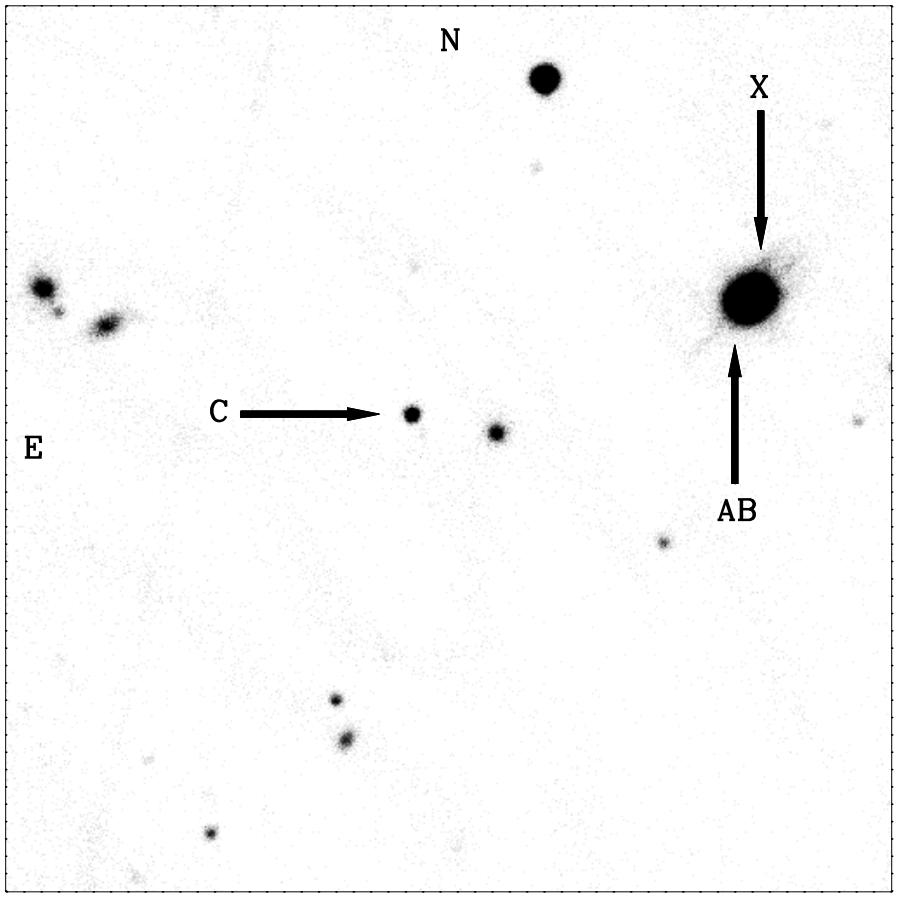

Figure 4.6: Optical finding chart for GD 319C, taken at I band with the Nickel 1 meter telescope in March 2002. The image is 184″ square with 0.36″ pixels. The coordinates for the companion are $12^{h}50^{m}12.7^{s}$, $+55°05'36''$ J2000. The object labelled 'X' is a foreground K dwarf located $\sim 2.5''$ away from GD 319AB.

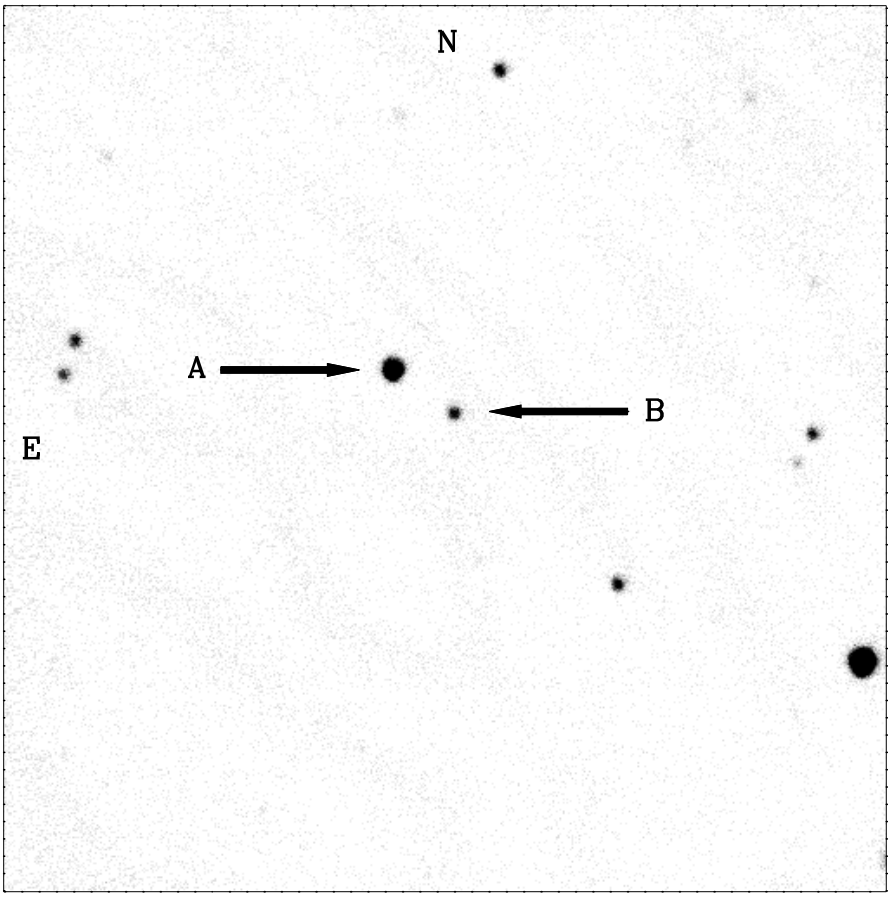

Figure 4.7: Optical finding chart for GD 322B, taken at I band with the Nickel 1 meter telescope in March 2002. The image is $184''$ square with $0.36''$ pixels.

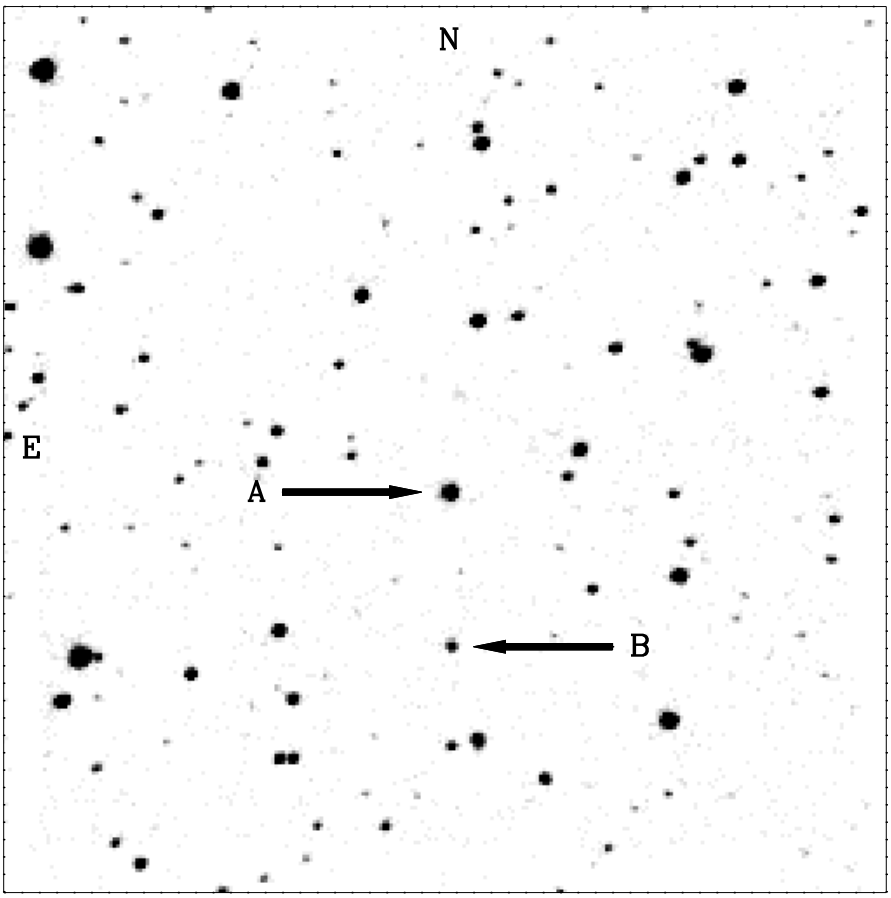

Figure 4.8: Near infrared finding chart for GD 559B, taken at J band with the Bok 2.3 meter telescope in October 1996. The image is $166''$ square with $0.65''$ pixels. The coordinates for the companion are $23^{\rm h}21^{\rm m}17.2^{\rm s}$, $+69°25'54''$ J2000.

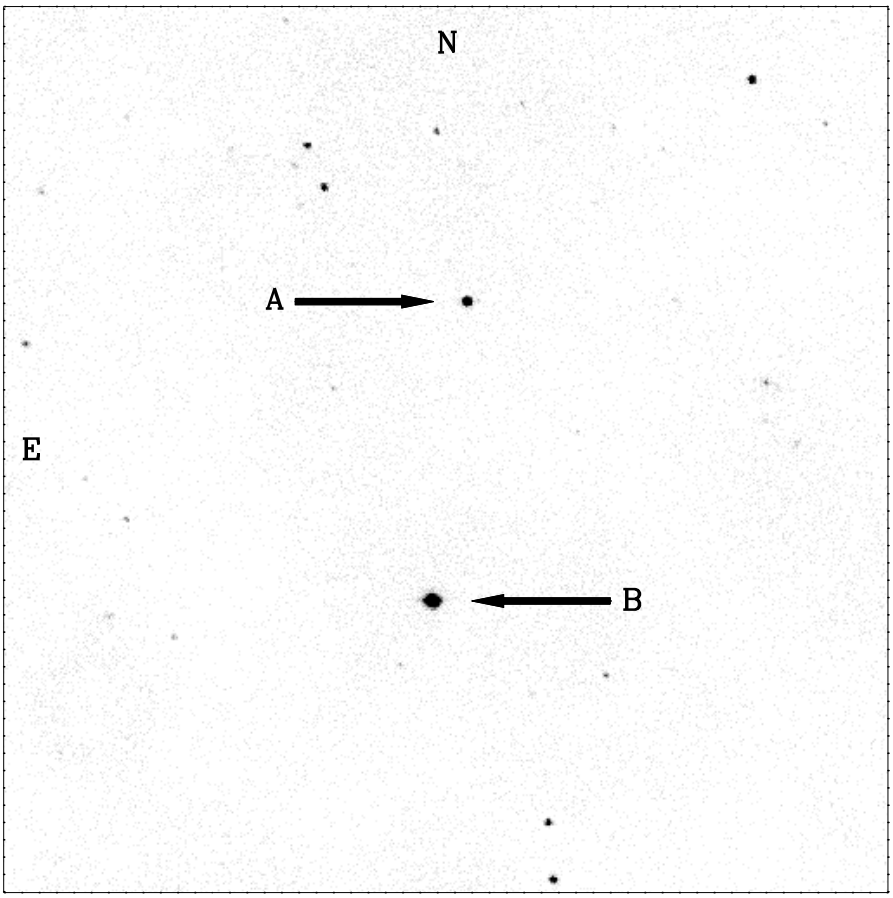

Figure 4.9: Optical finding chart for GD 683B, taken at I band with the Swope 1 meter telescope in November 2003. The image is $328''$ square with $0.44''$ pixels. The coordinates for the companion are $01^{h}08^{m}21.6^{s}$, $-35°36'33''$ J2000.

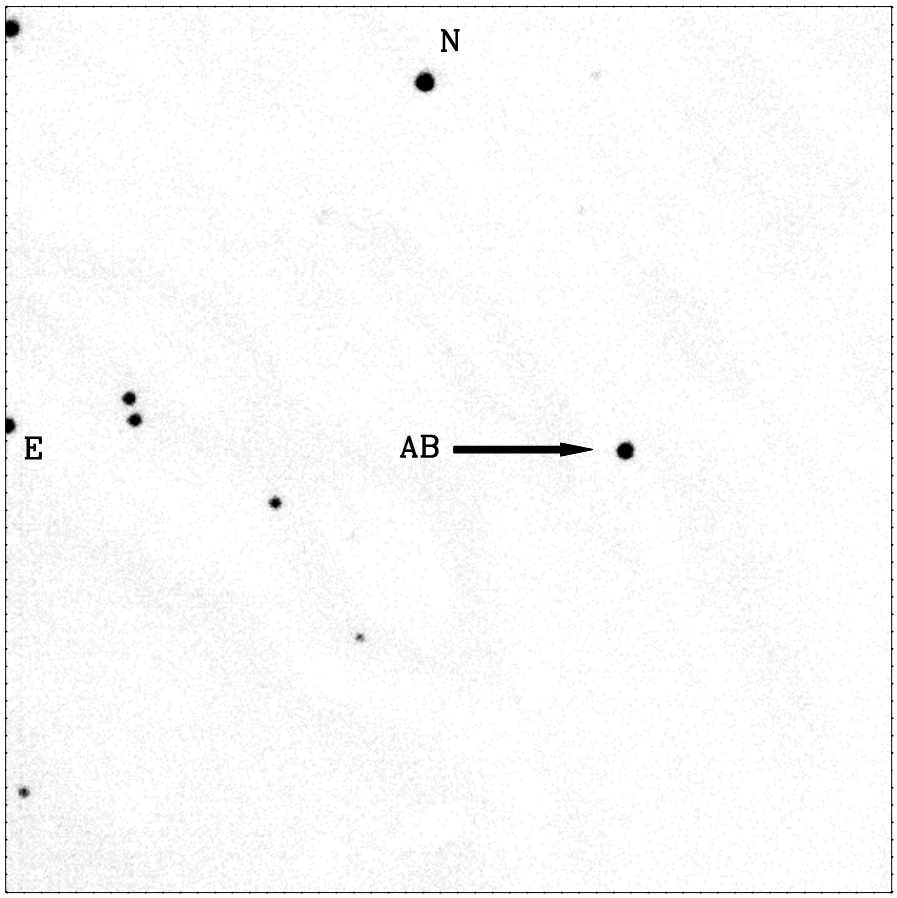

Figure 4.10: Optical finding chart for LP 618-14, taken at I band with the Nickel 1 meter telescope in June 2002. The image is 184″ square with 0.36″ pixels. The coordinates for the composite binary are $13^{h}36^{m}16.1^{s}$, $+00°17'33''$ J2000.

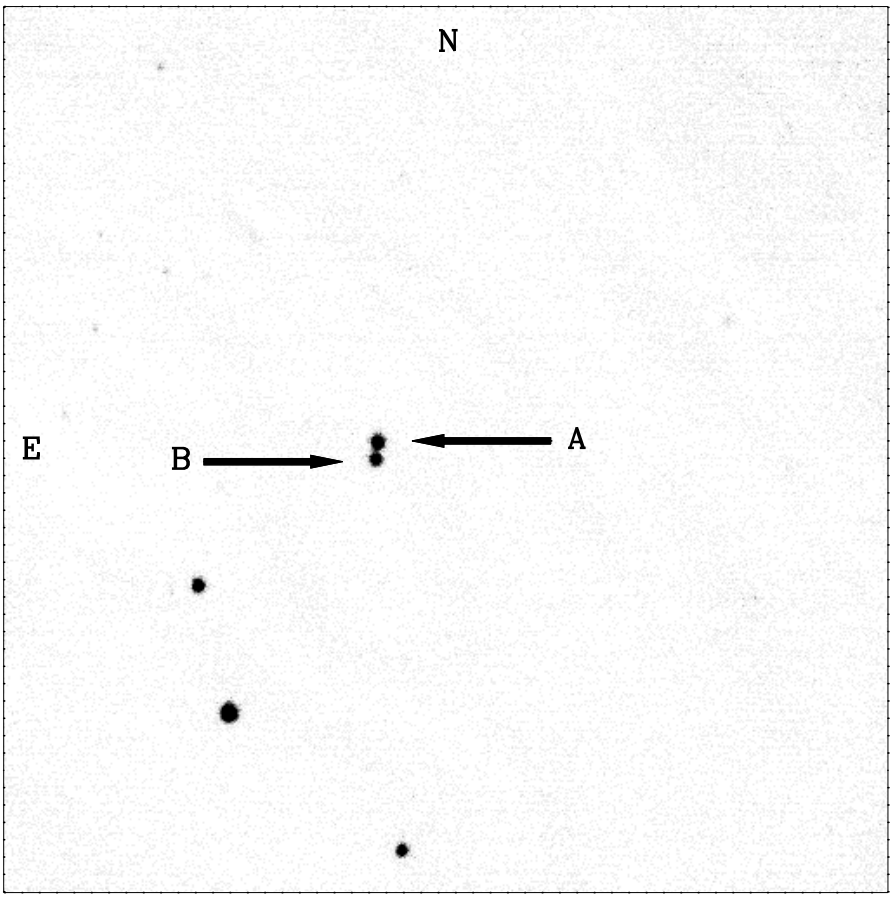

Figure 4.11: Optical finding chart for PG 0901+140B, taken at I band with the Nickel 1 meter telescope in April 2003. The image is 184″ square with 0.36″ pixels.

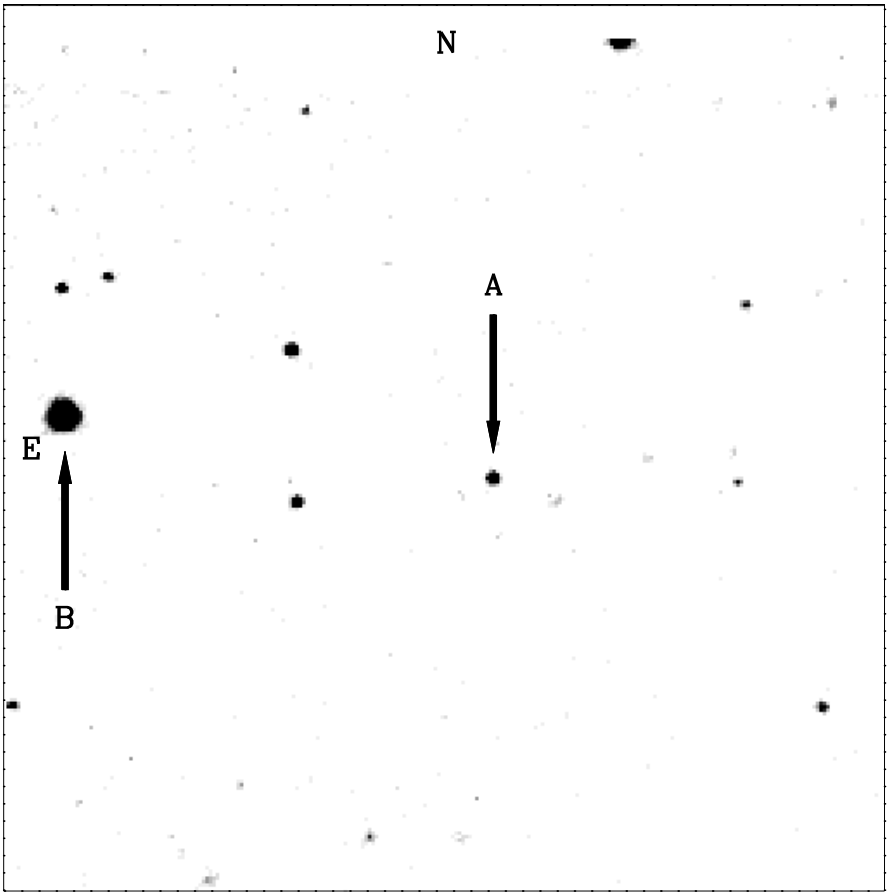

Figure 4.12: Near infrared finding chart for PG 0933+729B, taken at J band with the Bok 2.3 meter telescope in December 2002. The image is 166″ square with 0.65″ pixels. The coordinates for the companion are $09^{h}38^{m}39.8^{s}$, $+72°42'31''$ J2000.

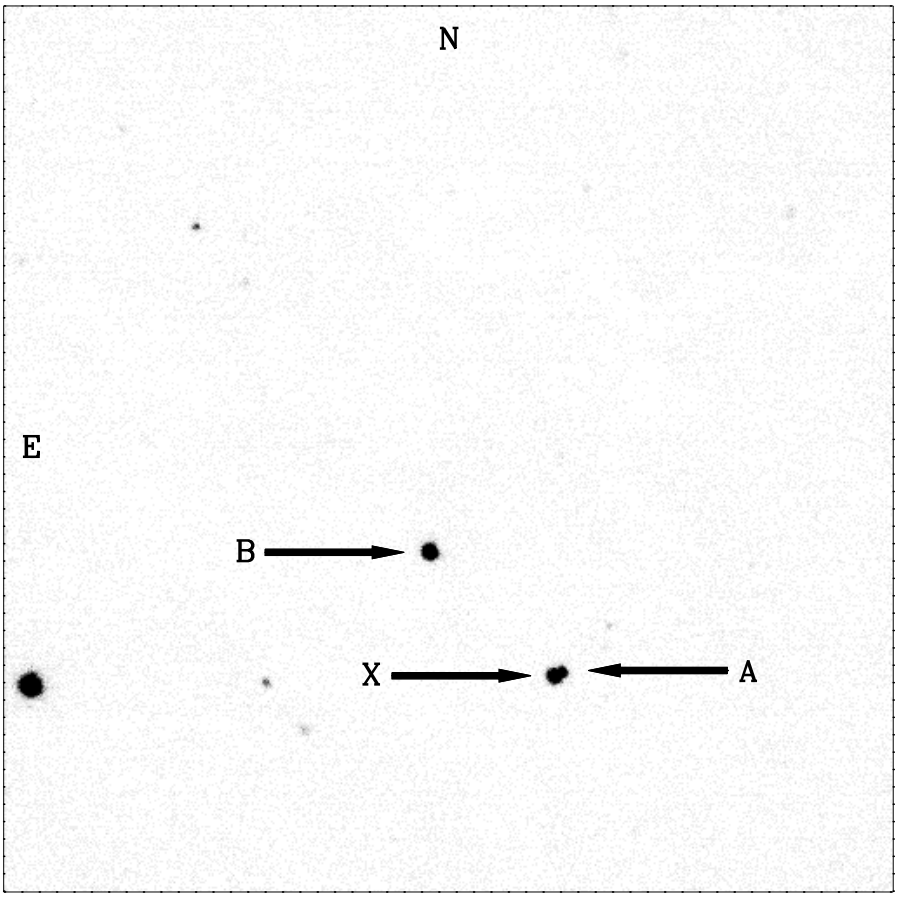

Figure 4.13: Optical finding chart for PG 1015+076B, taken at I band with the Nickel 1 meter telescope in March 2003. The image is 184″ square with 0.36″ pixels. The coordinates for the companion are $10^{h}18^{m}03.5^{s}$, $+07°21'50''$ J2000. The object labelled 'X' is a background G dwarf located 2.0″ away from PG 1015+076A.

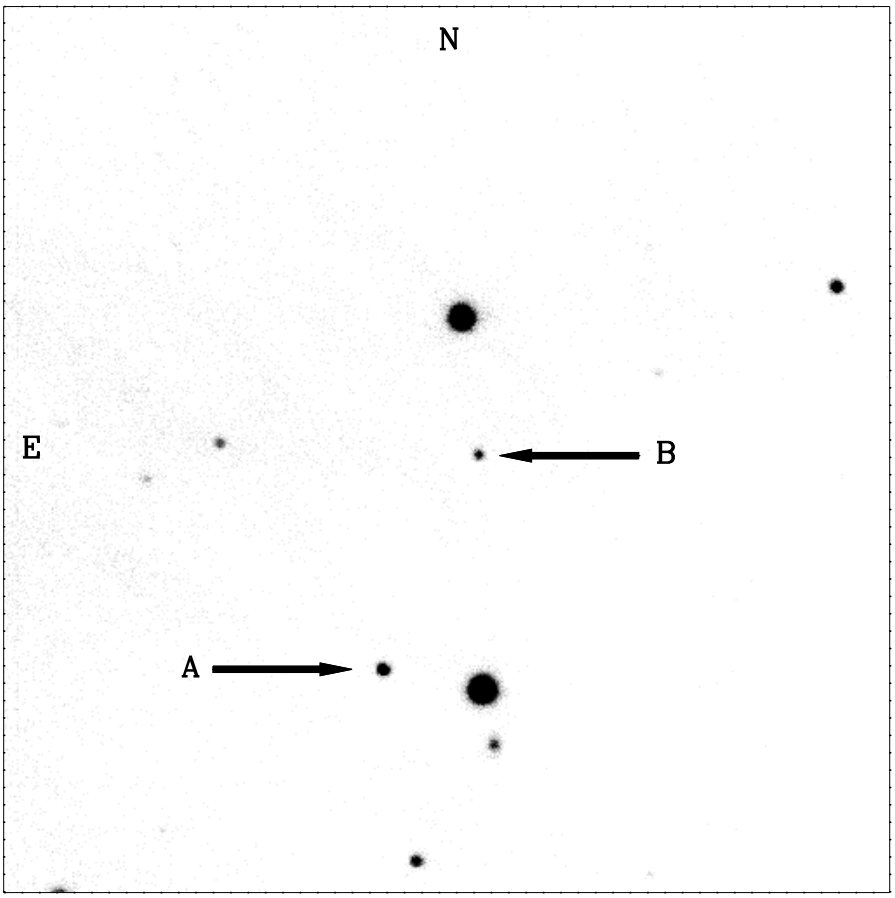

Figure 4.14: Optical finding chart for PG 1017+125B, taken at I band with the Nickel 1 meter telescope in January 2003. The image is 184″ square with 0.36″ pixels. The coordinates for the companion are $10^{h}19^{m}54.6^{s}$, $+12°17'18''$ J2000.

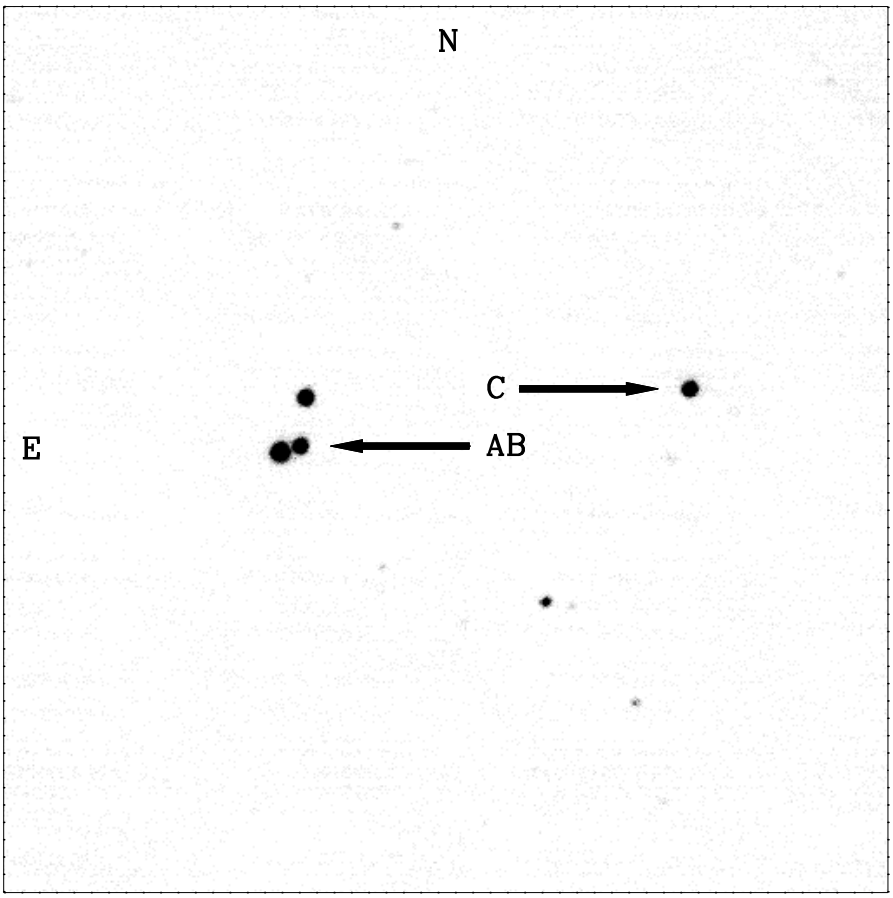

Figure 4.15: Optical finding chart for PG 1204+450C, taken at I band with the Nickel 1 meter telescope in April 2003. The image is 184″ square with 0.36″ pixels. The coordinates for the companion are $12^{h}06^{m}39.8^{s}$, $+44°50'09''$ J2000.

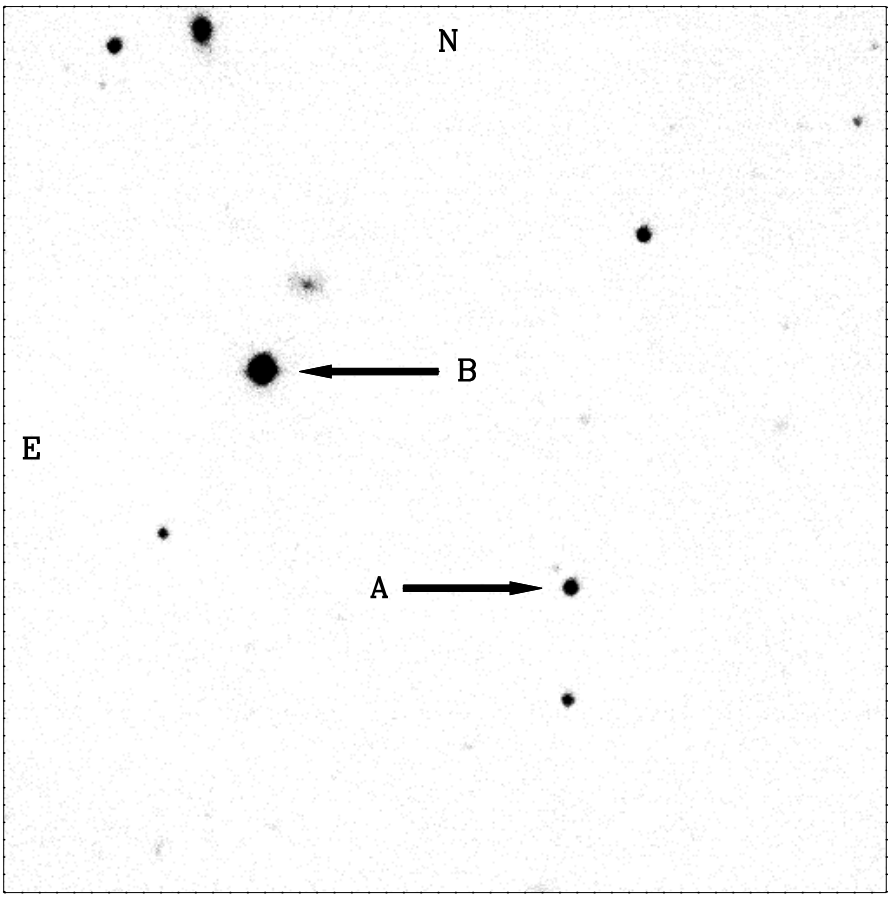

Figure 4.16: Optical finding chart for PG 1449+168B, taken at I band with the Nickel 1 meter telescope in April 2003. The image is 184″ square with 0.36″ pixels. The coordinates for the companion are $14^{h}52^{m}16.1^{s}$, $+16°38'48''$ J2000.

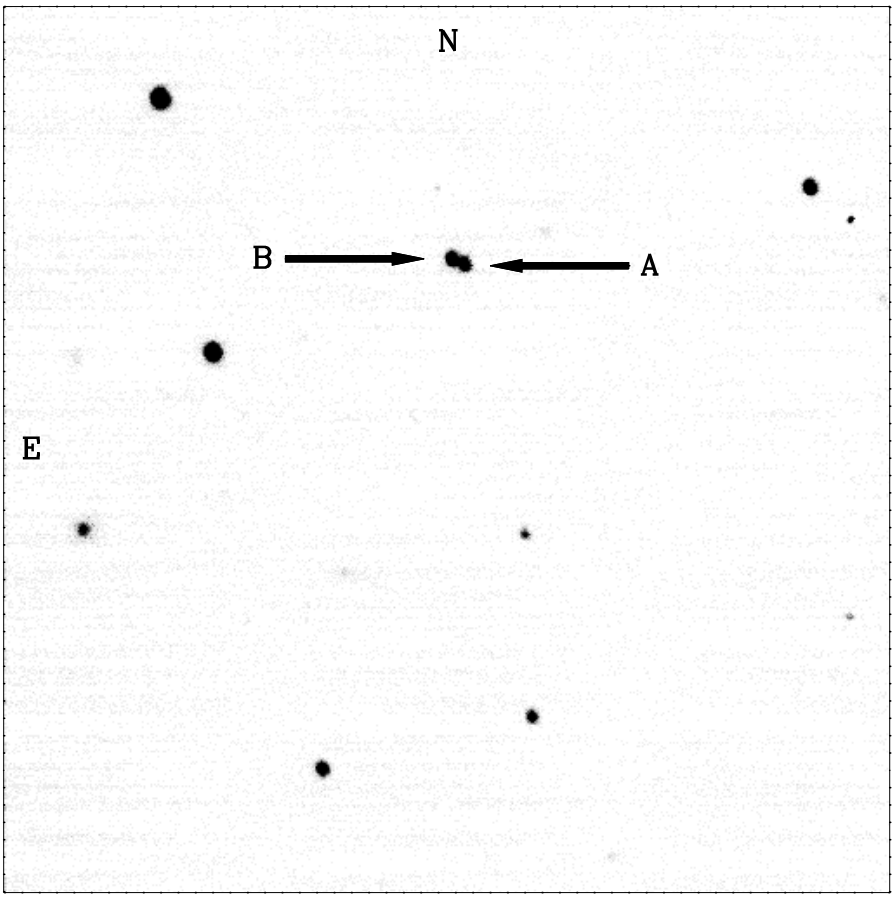

Figure 4.17: Optical finding chart for PG 1539+530B, taken at V band with the Nickel 1 meter telescope in April 2003. The image is 184″ square with 0.36″ pixels.

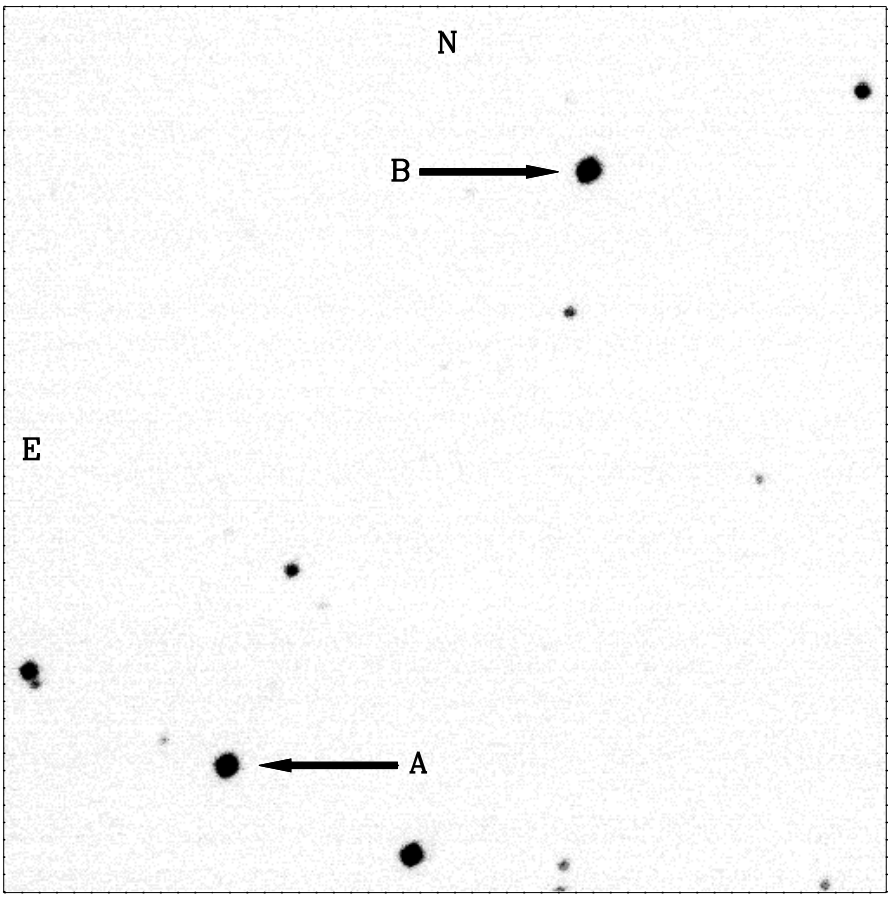

Figure 4.18: Optical finding chart for PG 1659+303B, taken at V band with the Nickel 1 meter telescope in April 2003. The image is 184″ square with 0.36″ pixels. The coordinates for the companion are $17^{h}01^{m}02.3^{s}$, $+30°17'45''$ J2000.

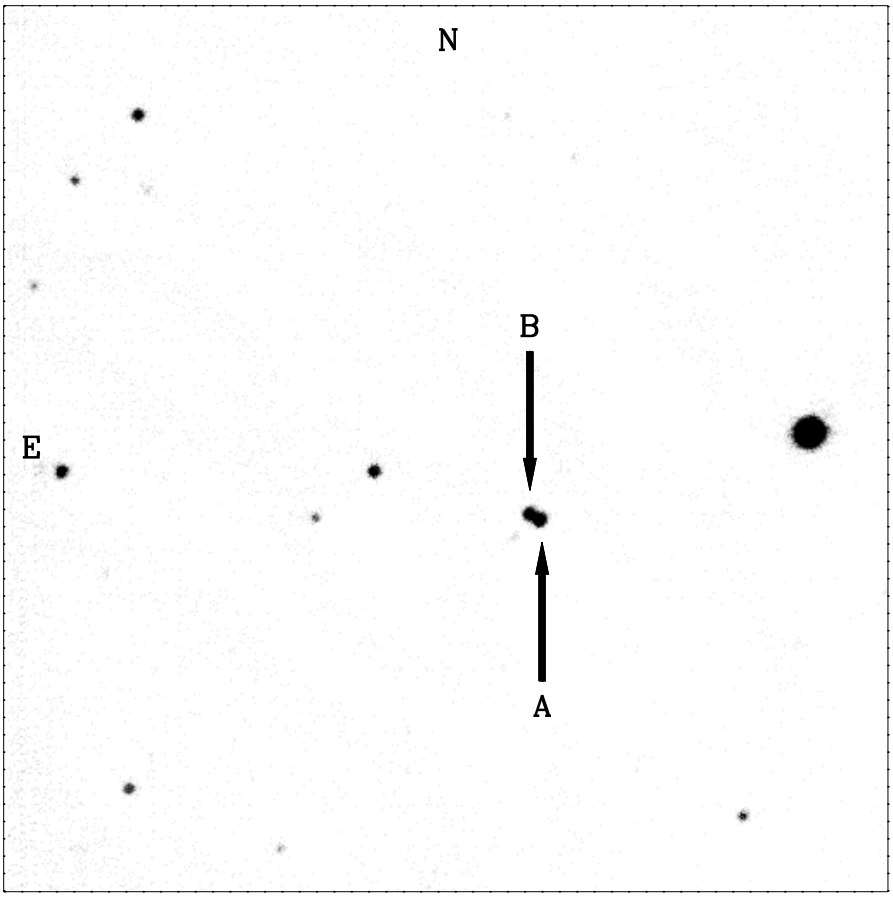

Figure 4.19: Optical finding chart for PG 2244+031B, taken at I band with the Nickel 1 meter telescope in July 2003. The image is 184″ square with 0.36″ pixels.

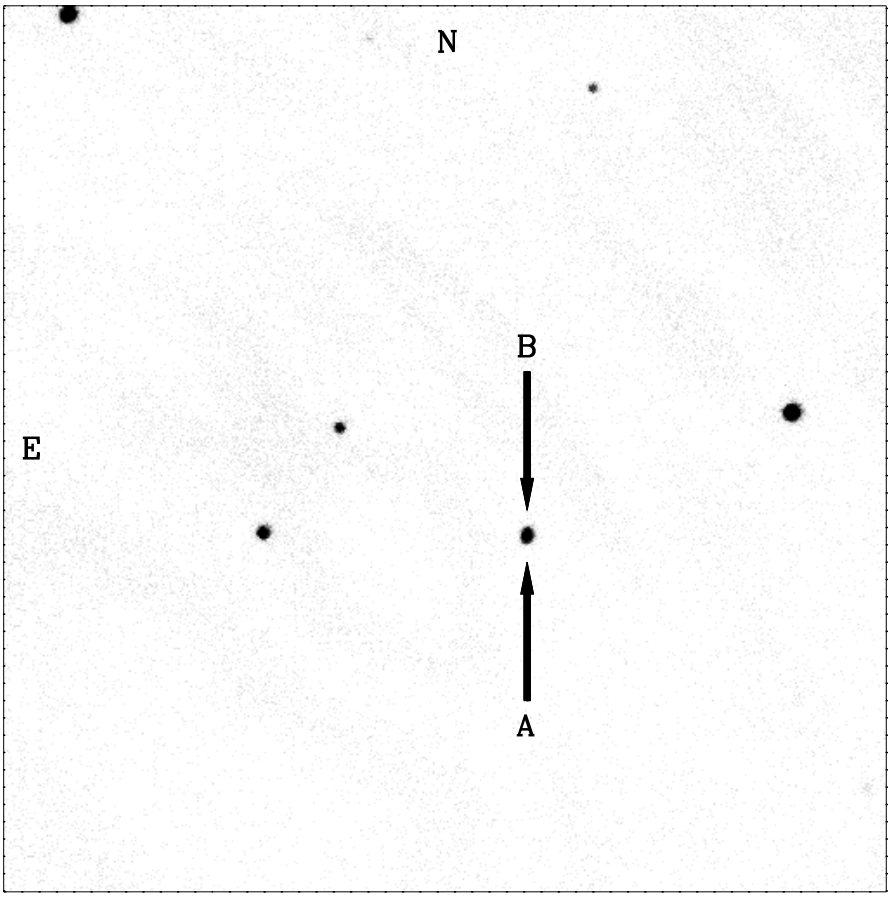

Figure 4.20: Optical finding chart for Ton S 392B, taken at I band with the Nickel 1 meter telescope in October 2003. The image is $184''$ square with $0.36''$ pixels. The coordinates for the binary are $03^{\rm h}59^{\rm m}04.9^{\rm s}$, $-23°12'25''$ J2000. At a separation of $\sim 1.2''$, the companion is just barely resolved in this image.

4.3.2 Proper Motion

Table 4.2 lists the measured proper motions for all confirmed and candidate commmon proper motion pairs discovered in this work. These values are the result of the mapping process discussed in §2.1.4. The map residuals were generally $\sim 0.01''$ yr^{-1}, but never greater than $0.02''$ yr^{-1}.

A very important item to note is that the uncertainty in the measured proper motions is not a total measurement error. This is because there was no independent astrometric calibration apart from the point sources in each individual mapped field. In essence only *relative proper motions* were measured, not the absolute positions of the stars. The uncertainties reported by GEOMAP are the root mean square of the map residuals and do not take into account the following factors: (1) any non zero motion of objects in the map; (2) the number of objects used in the map; (3) the signal to noise ratio for individual point sources and their measured coordinate centroids in the map. The fields used to measure proper motions were bewteen $166''$ and $300''$ in size, hence the number of field stars was limited, especially at higher galactic latitudes. Saturated stars are also unreliable because they can skew the centroiding process, as are faint field stars due to low signal to noise ratios. Therefore, the measurements given here should be considered only of limited accuracy for the above reasons. This is also the main reason that a few candidate companions have been retained for further investigation despite apparently discrepant measured proper motions (appendix).

Ironically, there was only a single common proper motion companion detected solely in the infrared and not also in the optical. Since the ostensible goal of this work was to detect companions too faint to be seen in the optical, it speaks volumes about the dearth of such objects. All other pairs were essentially detectable by "blinking" the first and second epoch Digitized Sky Survey scans (e.g.

in the northern hemisphere, the first and second epoch Palomar Observatory Sky Survey plates). These digitized scans were also used to measure proper motions when possible because the longer time baselines provide higher accuracy and the ability to measure smaller proper motions.

4.3.3 Visual Binaries

There are 3 new and 11 previously known visual binaries ($a < 10''$) studied here for which no proper motion measurement was made. In a few cases, there exists insufficient time baseline between available images in which the pair is resolved to measure proper motions, or the data avaible in proper motion catalogs is for the composite pair (whether unresolved or extended) or absent. But for most, the companionship of the visual pair is highly probable due to one or more of the following: (1) an unchanging visual separation and position angle or elongation axis between the pair over 15 to 50 years (this is essentially equivalent to a common proper motion determination because most if not all of these pairs have $\mu > 0.05''$ yr^{-1} and can be clearly seen moving with respect to background stars by "blinking" scans of two DSS epochs); (2) the common photometric distance implied by the spectral energy distributions of both components combined with the statistical likelihood of companionship based on proximity in the sky; (3) spectroscopic evidence presented here or elsewhere; (4) astrometric evidence presented elsewhere.

Table 4.2: Measured Proper Motions

Object	μ_α (yr^{-1})	μ_δ (yr^{-1})	Reference
G21-15AB	$-0.25''$	$-0.28''$	1
G21-15C	$-0.27''$	$-0.28''$	1
GD 60A	$+0.08''$	$-0.17''$	1
GD 60B	$+0.08''$	$-0.17''$	1
GD 74A	$-0.01''$	$-0.11''$	1
GD 74B	$-0.01''$	$-0.08''$	1
GD 84A	$-0.11''$	$-0.16''$	1
GD 84B†	$-0.06''$	$-0.21''$	1
GD 267A	$-0.08''$	$-0.10''$	1
GD 267B	$-0.07''$	$-0.10''$	1
GD 319AB	$-0.07''$	$-0.01''$	1
GD 319C	$-0.06''$	$-0.01''$	1
GD 322A	$+0.03''$	$+0.07''$	1
GD 322B	$+0.04''$	$+0.07''$	1
GD 392A	$+0.12''$	$+0.13''$	1
GD 392B	$+0.12''$	$+0.12''$	1

Table 4.2: Measured Proper Motions

Object	μ_α (yr^{-1})	μ_δ (yr^{-1})	Reference
GD 559A	$-0.13''$	$-0.01''$	2
GD 559B	$-0.13''$	$-0.01''$	2
GD 683A	$+0.00''$	$-0.06''$	3
GD 683B†	$+0.00''$	$-0.06''$	3
LDS 826AB	$-0.32''$	$-0.33''$	5
LDS 826C	$-0.32''$	$-0.35''$	1
PG 0901+140A	$-0.11''$	$-0.01''$	1
PG 0901+140B	$-0.11''$	$-0.01''$	1
PG 0922+162A	$-0.05''$	$-0.02''$	1
PG 0922+162B	$-0.05''$	$-0.02''$	1
PG 0933+729A	$-0.06''$	$-0.04''$	1
PG 0933+729B†	$-0.06''$	$-0.05''$	1
PG 1015+076A	$-0.00''$	$-0.03''$	3
PG 1015+076B	$-0.02''$	$-0.03''$	2
PG 1017+125A	$-0.03''$	$-0.02''$	1
PG 1017+125B	$-0.03''$	$-0.02''$	1

Table 4.2: Measured Proper Motions

Object	μ_α (yr^{-1})	μ_δ (yr^{-1})	Reference
PG 1204+450AB	$-0.06''$	$-0.01''$	1
PG 1204+450C	$-0.06''$	$-0.02''$	1
PG 1449+168A	$+0.00''$	$+0.06''$	1
PG 1449+168B	$+0.01''$	$+0.06''$	1
PG 1659+303A	$+0.02''$	$-0.07''$	1
PG 1659+303B	$+0.02''$	$-0.07''$	1
PG 1619+123	$+0.07''$	$-0.08''$	1
HD 147528	$+0.07''$	$-0.07''$	4

Note– Uncertainties for this work are generally $\sim 0.01''$ yr^{-1} (§4.3.2).

† candidate companion.

(1) This work.

(2) USNO B1.0 catalog.

(3) UCAC catalogs.

(4) Tycho 2 catalog.

(5) Reylé et al. 2002.

4.4 Known Companions

The majority of the objects together in Zuckerman & Becklin (1992) and Schultz, Zuckerman, & Becklin (1996) are unresolved white dwarf plus red dwarf binaries. As discussed above, the parameters of the two components must be deconvolved from one another. Most of these binaries were investigated with a thorough updated literature search, optical photometry and spectroscopy, to both confirm the identity and further constrain the properties of the low mass companion. The result being a higher confidence in their spectral classifications (i.e. temperature). For those partially or completely resolved pairs previously reported, all with $1'' < a < 9''$, §4.3.3 applies.

4.4.1 Later is Earlier

The title of this section refers to an apparent contradiction which results from optical flux contamination of a white dwarf by a low mass main sequence secondary. If a hot white dwarf ($T_{\rm eff} \geq 12,000$ K, spectral type DA4 and earlier) has a fairly early unresolved M companion (e.g. M2−M3), the measured optical fluxes can contain significant contribution from the secondary at V and sometimes even B. Since many white dwarfs in McCook & Sion (1987) were typed using UBV photometry and colors, this can lead to an underestimate of the primary star's temperature and luminosity, giving it the appearance of a DA5−DA7. There are still many examples of this in McCook & Sion (1999).

This phenomenon has two consequences. One is that any extrapolation of the white dwarf's flux toward longer wavelengths will overestimate its relative contribution there, when in fact most if not all of the red optical and near infrared flux will be due to the red dwarf component. Secondly, the resulting photometric

distance to the system, obtained from UBV considerations, will be too near. All this can and does lead to a red dwarf spectral type estimate that is too late.

Hence a white dwarf should not appear too late ($T_{\rm eff} < 12,000$ K) if it is suspected to have an unresolved red dwarf companion based on optical data – this is a red flag, so to speak. If the white dwarf appears later than about DA4, then the companion is likely to be earlier than around M4. Many very cool white dwarfs are not likely to be detected around the earliest M type dwarfs (because the white dwarf would go unrecognized), hence these systems should not largely populate white dwarf catalogs. Neither should many later M type dwarfs (M5 or later) be detected in UBV or through blue optical spectroscopy, which were and still are two staples in the study and identification of white dwarfs.

This is certainly not true in all cases. But in this work, it has been found to be a good guideline in determining what systems require followup work and closer inspection. It is also the main reason why some of the objects in Zuckerman & Becklin (1992) and Schultz, Zuckerman, & Becklin (1996) are being updated here to earlier spectral types, and hence higher masses.

4.5 Photometry

4.5.1 Measurement and Error

Circular aperture photometry was used to determine instrumental fluxes and magnitudes for all unresolved and resolved binary stars in this work (§2.3.3). Comparison with one or more standard stars yielded the true magnitudes listed in Tables 4.3 and 4.4. $BVRI$ photometry is on the Johnson-Cousins system and JHK photometry is on the Johnson-Glass system, collectively known as the Johnson-Cousins-Glass system (Bessel & Brett 1988; Bessel 1990). These

photometric systems define $m = 0.00$ at all wavelengths (which is generally Vega, but not always). The central wavelengths for these bandpasses are $\lambda_{\rm eff} = (0.44, 0.55, 0.64, 0.80, 1.22, 1.63, 2.20)$ μm for (B, V, R, I, J, H, K) respectively.

For binary pairs that were spatially well resolved from each other ($a > 3''$) and from neighboring stars, the flux measurement error was generally 5% or less for $m < M_c$, where $M_c \approx (19, 18, 17)$ for $(BVRI, JH, K)$, and $\sim 10\%$ or greater otherwise. For separations smaller than $\sim 3''$ between target star and neighbor or companion, overlapping point spread functions (PSFs) effectively contaminate flux measurements even in small apertures of $1-2$ pixels in radii. In these cases, the IRAF program DAOPHOT was used to simultaneously fit two or more PSFs within a given area, deconvolve and extract their individual fluxes. This method works quite well for pairs with $\Delta m \approx 3$ or less and generates errors equivalent to those quoted above. These errors take into account factors such as the number of full widths at half maxiumum separating a pair of stars, the residual flux after PSF fitting, and the number of point sources of a given SNR used to generate the PSF model.

Some binary systems lack data at one or multiple wavelengths due to unavoidable circumstances including, but not limited to; time constraints, poor weather, instrument problems, telescope pointing limits and telescope size.

4.5.2 Resolved Pairs

Table 4.3 lists all photometry for resolved binary components, including those stars requiring PSF deconvolution from neighbors or companions.

Table 4.3: Resolved Pair Optical & Infrared Photometry

Object	B	V	R	I	J	H	K	Ref
G21-15AB	14.03	13.92	13.94	13.96	14.10	14.16	14.16	1,5
G21-15C	20.05	19.00	18.44	17.82	17.53	17.05	16.88	1
G130-5	13.06	12.92	-	-	13.17	13.20	13.18	2,4
G130-6	13.25	11.69	12.15	10.77	7.86	7.25	7.04	2,3
G148-7	13.69	13.64	-	-	14.01	13.98	14.03	2,4
G148-6	15.72	14.09	-	-	9.96	9.39	9.14	2,3
G163-50	13.10	13.06	13.15	13.15	13.41	13.45	13.54	2,6
G163-51	14.10	12.58	11.50	10.14	8.80	8.14	7.93	2,6
GD 13A	14.83	14.94	15.06	15.18	15.42	15.47	15.61	1
GD 13B	20.15	18.75	17.61	15.49	13.99	13.41	13.21	1
GD 60A	15.19	15.16	15.28	15.43	15.46	15.54	15.59	1
GD 60B	19.54	18.05	16.85	14.67	12.91	12.50	12.15	1
GD 74A	14.96	14.93	15.09	15.20	15.53	15.60	15.72	1
GD 74B	19.21	17.74	16.70	14.95	13.57	13.03	12.79	1,2

Table 4.3: Resolved Pair Optical & Infrared Photometry

Object	B	V	R	I	J	H	K	Ref
GD 84A	15.27	15.19	15.12	15.12	15.10	15.04	14.89	1,4
GD 84B	16.96	15.53	14.46	12.79	11.48	10.87	10.55	1
GD 267A	14.76	14.93	15.08	15.17	15.54	15.63	-	1,2
GD 267B	19.13	17.76	16.62	14.51	13.04	12.45	12.17	1,2
GD 319AB	-	12.70	-	-	13.36	13.36	13.50	1,7
GD 319C	20.77	19.36	18.38	16.61	15.38	14.84	14.59	1
GD 322A	15.22	15.02	14.97	15.31	15.67	15.66	15.79	1
GD 322B	18.25	17.68	17.25	17.16	17.04	16.83	16.83	1
GD 392A	15.75	15.68	15.62	15.66	15.75	15.80	15.87	1,8
GD 392B	20.82	19.50	18.80	18.06	17.73	18.16	18.51	1,8
GD 559A	-	14.63	-	-	15.14	-	15.32	1,4
GD 559B	-	17.20	-	-	16.98	-	16.88	1,4
GD 683A	14.54	14.72	14.84	15.11	15.42	-	-	1,2,9
GD 683B	16.88	15.49	14.58	13.29	12.09	11.48	11.28	1,2

Table 4.3: Resolved Pair Optical & Infrared Photometry

Object	B	V	R	I	J	H	K	Ref
LB 261A	-	-	-	-	15.66	-	15.82	1
LB 261B	-	-	-	-	11.83	11.24	10.95	2
LDS 678A	12.36	12.32	12.28	12.24	12.35	12.36	12.42	2,3
LDS 678B	13.76	12.13	11.09	9.82	8.22	7.66	7.41	2,3,10
LDS 826A	-	14.42	14.34	14.22	-	-	-	1,3
LDS 826B	-	13.54	12.25	10.78	9.48	8.91	8.61	1,2,3
LDS 826C	-	-	18.41	15.89	13.05	12.37	11.88	1,2
LHS 354	12.40	12.33	12.38	12.38	12.62	12.68	12.74	2,3
LHS 353	15.89	14.23	12.91	11.21	9.60	9.05	8.75	2,3
LHS 361	16.75	15.65	15.08	14.53	13.92	13.67	13.62	2,3
LHS 362	17.29	15.33	13.84	11.90	10.08	9.51	9.18	2,3
LP 761-114	18.38	17.83	17.56	17.10	16.66	16.42	16.49	1
LP 761-113	14.84	13.57	12.59	11.29	10.18	9.62	9.37	1,2
LP 916-27	15.53	15.49	15.40	15.37	15.28	15.32	15.41	1,2
LP 916-26	16.77	15.33	14.17	12.26	10.79	10.20	9.91	1,2

Table 4.3: Resolved Pair Optical & Infrared Photometry

Object	B	V	R	I	J	H	K	Ref
PG 0824+288AB	-	14.22	-	-	12.74	-	11.84	1,4
PG 0824+288C	-	-	-	-	13.24	-	12.41	1
PG 0901+140A	16.27	15.93	15.87	15.85	15.87	15.82	15.80	1
PG 0901+140B	16.86	16.48	16.33	16.24	16.13	15.98	15.96	1
PG 0922+162A	-	16.26	-	-	16.82	16.94	17.07	1,11
PG 0922+162B	-	17.30	-	-	17.72	17.78	17.87	1,11
PG 0933+729A	-	15.71	-	-	16.11	-	-	2,4
PG 0933+729B†	-	-	-	-	12.22	11.61	11.38	2
PG 0956+045A	15.86	15.88	16.02	16.10	16.39	16.42	16.46	1
PG 0956+045B	-	19.42	18.50	16.26	14.74	14.18	13.92	1
PG 1015+076A	16.45	16.60	16.69	16.84	-	-	-	1
PG 1015+076B	18.50	17.30	16.26	14.73	13.60	12.96	12.75	1,2
PG 1017+125A	15.73	15.74	15.78	15.99	16.34	16.41	16.52	1
PG 1017+125B	17.03	16.83	16.79	16.88	17.08	17.11	17.15	1

Table 4.3: Resolved Pair Optical & Infrared Photometry

Object	B	V	R	I	J	H	K	Ref
PG 1204+450AB	14.85	15.04	15.14	15.34	15.70	15.85	16.03	1
PG 1204+450C	19.40	18.22	17.11	15.30	13.91	13.30	13.06	1,2
PG 1241−010AB	13.86	14.00	-	14.26	14.51	14.60	14.58	1,4
PG 1241−010C	-	-	-	18.56	15.60	14.92	14.44	1
PG 1449+168A	15.34	15.44	15.54	15.66	16.01	-	-	1,2
PG 1449+168B	16.83	15.49	14.44	12.94	11.77	11.25	10.97	1,2
PG 1539+530A	16.40	16.52	16.67	16.82	-	-	-	1
PG 1539+530B	17.54	16.25	15.25	13.98	12.03	12.21	12.90	1,2
PG 1619+123	14.67	14.66	14.74	14.82	15.00	14.99	15.01	1,2
HD 1457218	8.71	8.19	-	-	7.56	6.89	6.84	2,12
PG 1659+303A	15.07	14.99	15.06	15.12	15.33	15.32	15.36	1,2
PG 1659+303B	16.06	14.81	13.85	12.48	11.39	10.69	10.53	1,2
PG 1654+160A	16.42	16.55	16.61	16.56	-	-	-	1
PG 1654+160B	19.17	17.74	16.57	14.50	13.09	12.43	12.14	1,2

Table 4.3: Resolved Pair Optical & Infrared Photometry

Object	B	V	R	I	J	H	K	Ref
PG 1608+118A	15.25	15.29	15.38	15.50	-	-	-	1
PG 1608+118B	17.32	15.85	14.80	13.26	12.10	11.50	11.27	1,2
PG 2244+031A	16.15	16.46	16.57	16.73	17.02	17.09	17.27	1
PG 2244+031B	-	19.82	18.73	17.18	15.83	15.24	15.08	1
PHL 790A	15.09	15.32	15.37	15.54	15.93	16.06	16.21	1
PHL 790B	-	18.10	16.88	15.11	13.83	13.25	13.05	1,2
RE 1016−053AB	13.93	14.14	14.19	14.19	13.74	13.12	12.90	1,13
RE 1016−053CD	15.08	13.58	12.66	11.63	10.61	9.99	9.77	2,13

Note– All values are in magnitudes. Uncertainties for this work are 5% or less with a few exceptions (§4.5.1).

† candidate companion.

(1) This work.

(2) 2MASS.

(3) ARICNS.

(4) McCook & Sion 1999.

(5) Bergeron, Leggett, & Ruiz 2001.

(6) Landolt 1983.

(7) McAlister et al. 1996.

(8) Farihi 2004.

(9) Norris, Ryan, & Beers 1999.

(10) Bessell 1990.

(11) Finley & Koester 1997.

(12) Tycho 2 catalog.

(13) Vennes, Thorstensen, & Polomski 1999.

4.5.3 Composite Pairs

Binaries consisting of a white dwarf plus red dwarf which were indistinguishable from point sources were treated as a single star and aperture photometry performed accordingly. This is true also for those pairs with separations too small to be accurately fit with two PSFs ($a < 2''$) due to pixel scale, seeing conditions, $\Delta m > 3$, or all three.

In Table 4.4 are the measured optical and infrared magnitudes for all composite binaries. For each system, the table has three entries. (1) The first line is the composite photometry itself, with all measurement errors for this work being 5% or less in this range of magnitudes. (2) The next line gives the predicted magnitudes for the white dwarf (WD) component based on the most current hydrogen and helium atmosphere model grids of P. Bergeron (2002, private communication), which are considered more accurate than previous generations (Bergeron, Saumon, & Wesemael 1995; Bergeron, Wesemael, & Beauchamp 1995). The predicted white dwarf magnitudes are calculated by adding model colors (appropriate for its $T_{\rm eff}$, and log g if known) to a photometric bandpass that is essentially uncontaminated by its cool red dwarf companion – either U or B (or V in a few rare cases). If the calculation was done from U, a reference is given for the photometry. The temperature and surface gravity used as input for the models is taken from the most reliable sources available with the reference provided. (3) The last line gives the deconvolved magnitudes for the red dwarf (RD). This is generally only $IJHK$ due to large uncertainties at shorter wavelengths.

Based on comparisons with Kirkpatrick & McCarthy (1994), spectral types were estimated from $I-K$. Unlike $J-K$, which is highly degenerate across most of the M type dwarf spectral class, $I-K$ is essentially monotonically increasing from M2 until well into the L spectral class (Kirkpatrick & McCarthy 1994;

Kirkpatrick et al. 1999b).

Table 4.4: Composite Optical & Infrared Photometry

Object	B	V	R	I	J	H	K	Ref
GD 51AB	15.27	14.99	14.64	13.32	12.05	11.57	11.30	1,2
WD	15.62	15.67	15.77	15.90	16.24	16.31	16.42	3,9
RD	-	-	-	13.43	12.07	11.58	11.31	
GD 123AB	14.21	14.40	14.42	13.76	12.56	12.03	11.75	1,2
WD	14.22	14.41	14.54	14.71	15.13	15.23	15.36	3,4
RD	-	-	-	14.35	12.67	12.09	11.79	
GD 245AB	13.67	13.68	13.57	12.83	11.66	111.20	10.89	1,2,3
WD	13.70	13.78	13.80	13.94	14.36	14.43	14.54	10,11
RD	-	-	-	13.31	11.75	11.26	10.93	
GD 337AB	16.04	16.11	16.13	15.61	14.67	14.22	13.92	1,2
WD	16.04	16.12	16.23	16.36	16.71	16.78	16.89	3,4
RD	-	-	-	16.37	14.85	14.33	13.99	
GD 448AB	14.91	14.97	-	-	14.71	14.43	14.16	2,3
WD	14.96	15.01	15.10	15.22	15.51	15.58	15.67	7,12
RD	-	-	-	-	15.42	14.89	14.47	
GD 543AB	15.15	15.26	15.32	15.06	14.28	13.92	13.58	1,2
WD	15.14	15.26	15.38	15.53	15.91	15.99	16.11	1,7
RD	-	-	-	16.20	14.55	14.09	13.69	

Table 4.4: Composite Optical & Infrared Photometry

Object	B	V	R	I	J	H	K	Ref
GD 984AB	13.69	13.89	13.95	13.63	12.96	12.45	12.24	1,2
WD	13.83	14.11	14.25	14.45	14.90	15.02	15.15	3,13
RD	-	-	-	14.32	13.16	12.56	12.32	
KPD 2154+408AB	15.24	15.21	14.97	14.02	12.88	12.38	12.15	1,2
WD	15.24	15.33	15.44	15.57	15.93	16.00	16.12	5,14
RD	-	-	-	14.32	12.95	12.42	12.18	
LP 618-14AB	17.68	17.23	16.74	15.64	14.26	13.74	13.51	1,2,6
WD	17.68	17.46	17.30	17.16	17.17	17.14	17.14	1
RD				15.89	14.34	13.79	13.55	
LTT 0329AB	14.85	14.44	13.95	12.63	11.43	10.91	10.64	1,2
WD	15.05	15.03	15.11	15.21	15.49	15.54	15.63	8,15
RD	-	-	14.41	12.74	11.46	10.93	10.65	
LTT 2980AB	13.54	13.59	13.66	13.48	12.63	12.14	11.83	1,2
WD	13.59	13.60	13.69	13.80	14.09	14.15	14.25	16
RD	-	-	-	14.96	12.94	12.33	11.96	
LTT 3943AB	13.05	13.09	-	12.39	11.24	-	10.44	3,6
WD	13.10	13.17	13.27	13.40	13.73	13.80	13.90	8,17
RD	-	-	-	12.93	11.36	-	10.49	

Table 4.4: Composite Optical & Infrared Photometry

Object	B	V	R	I	J	H	K	Ref
LTT 8747AB	14.76	14.54	14.39	13.97	12.46	11.79	11.36	1,2,6
WD	14.76	14.54	14.39	14.24	14.16	14.06	14.09	1,5
RD	-	-	-	15.61	12.71	11.93	11.45	
PG 0308+096AB	15.25	15.31	15.33	14.79	13.72	13.18	12.93	1,2
WD	15.25	15.39	15.51	15.66	16.05	16.14	16.26	1,4
RD	-	-	-	15.44	13.86	13.25	12.98	
PG 0933+025AB	16.12	15.97	15.66	14.44	13.27	12.73	12.48	1,2
WD	16.12	16.22	16.33	16.47	16.83	16.90	17.01	3,4
RD	-	-	-	14.63	13.31	12.75	12.50	
PG 0950+185AB	15.59	15.40	14.98	13.78	12.69	12.01	11.79	1,2
WD	15.59	15.81	15.94	16.11	16.54	16.64	16.77	3,4
RD	-	-	15.56	13.92	12.72	12.03	11.80	
PG 1026+002AB	13.88	13.82	13.68	12.90	11.77	11.22	10.92	1,2
WD	13.88	13.86	13.95	14.04	14.32	14.38	14.46	3,4
RD	-	-	-	13.37	11.88	11.28	10.96	
PG 1049+103AB	-	15.65	-	-	13.27	12.83	12.48	2,3
WD	15.69	15.74	15.83	15.95	16.28	16.34	16.44	3,4
RD					13.34	12.87	12.51	

Table 4.4: Composite Optical & Infrared Photometry

Object	B	V	R	I	J	H	K	Ref
PG 1123+189AB	13.83	14.11	14.09	13.58	12.78	12.23	12.00	2,18
WD	13.87	14.16	14.30	14.49	14.95	15.07	15.20	4,18
RD	-	-	-	14.20	12.94	12.31	12.06	
PG 1210+464AB	15.53	14.94	14.19	13.05	12.08	11.41	11.17	1,2
WD	15.53	15.59	15.71	15.88	16.28	16.37	16.49	3,4
RD	-	-	14.50	13.13	12.10	11.42	11.18	
PG 1643+143AB	15.76	15.45	14.90	13.79	12.77	12.10	11.96	1,2
WD	15.76	15.91	16.03	16.19	16.59	16.68	16.80	3,4
RD	-	-	15.37	13.92	12.80	12.12	11.97	
PG 2131+066AB	16.35	16.56	16.49	16.06	15.19	14.64	14.43	1
WD	16.33	16.65	16.80	17.00	17.47	17.60	17.73	19,20
RD	-	-	-	16.65	15.33	14.71	14.48	
RE 1016−052AB	13.93	14.14	14.19	14.19	13.74	13.12	12.90	1,21
WD	13.93	14.23	14.37	14.57	15.02	15.14	15.27	21
RD	-	-	-	15.51	14.14	13.30	13.03	
RE 1629+780AB	12.95	13.03	12.83	12.05	11.00	10.38	10.15	2,22
WD	12.95	13.21	13.34	13.53	13.98	14.10	14.22	23
RD	-	-	-	12.37	11.07	10.42	10.18	

Table 4.4: Composite Optical & Infrared Photometry

Object	B	V	R	I	J	H	K	Ref
Rubin 80AB	15.86	15.57	15.37	14.88	13.59	13.08	12.73	1,2
WD	15.86	15.62	15.51	15.38	15.36	15.28	15.33	1,5
RD	-	-	-	15.96	13.83	13.23	12.83	
Ton 1150AB	15.80	15.21	14.75	13.75	12.64	12.02	11.76	1,2
WD	15.84	15.91	16.02	16.14	16.48	16.55	16.66	1,4
RD	-	-	15.15	13.88	12.67	12.04	11.77	
Ton S 392AB	15.64	15.77	15.85	15.58	14.96	14.59	14.26	1,2
WD	15.64	15.93	16.07	16.26	16.72	16.84	16.96	1,24
RD	-	-	-	16.41	15.20	14.74	14.35	

Note– All values are in magnitudes. Uncertainties for this work are 5% or less for this magnitude range (§4.5.1).

(1) This work.

(2) 2MASS.

(3) McCook & Sion 1999.

(4) Liebert, Bergeron, & Holberg 2004.

(5) Zuckerman et al. 2003.

(6) DENIS.

(7) Bergeron, Saffer, & Liebert 1992.

(8) Bragaglia, Renzini, & Bergeron 1995.

(9) Koester et al. 2001.

(10) Schwartz 1972.

(11) Schmidt, Smith, & Harvey 1995.

(12) Hintzen & Jensen 1979.

(13) Finley, Koester, & Basri 1997.

(14) Downes 1986.

(15) Greenstein 1974.

(16) Eggen & Greenstein 1965.

(17) Kawka et al. 2000.

(18) Marsh et al. 1997.

(19) Bond et al. 1984.

(20) Kawaler et al. 1995.

(21) Vennes, Thorstensen, & Polomski 1999.

(22) Schwartz et al. 1995.

(23) Napiwotzki, Green, & Saffer 1999.

(24) Greenstein 1979.

4.6 Spectroscopy

In this section, spectroscopy is presented for resolved binaries or composite white dwarf plus red dwarf pairs. The purpose of the spectroscopy was merely to identify the spectral class of the companions, rather than to determine precise spectral types. Standard stars and spectral flats were taken to ensure the target spectra were free of both detector and instrument response. None of the spectra were corrected for telluric features or extinction. In the case of white dwarfs, the purpose was to look for the presence or absence of highly pressure broadened hydrogen or helium lines – implying spectral classes DA, DB, or DC for no lines. In the case of red dwarfs, this means searching for the characteristic TiO and CaH bands of M dwarfs.

There exist a few potential sources of error and noise on particular instruments and observing runs which should be briefly discussed.

The Kast Dual Spectrograph sits atop Mount Hamilton, which is all too close to the city lights of San Jose. Sodium at 5880 Å can be seen very brightly in spectra taken with this instrument and can be difficult or impossible to remove completely in lower signal to noise observations. Hence positive and negative residuals often remain.

During one observing run with the Kast, only the red side of the spectrograph was used without any dichroic or blocking filter on the blue side. Hence second order blue light was present in the spectra of all objects excepting those red objects such as single M dwarfs. This effect on the continuum was mostly removed by calibrating with a standard star observed in the same arrangement, but not completely.

The one spectroscopic observing run with the Boller & Chivens Spectrograph

at Steward Observatory was over 3 nights with a very bright moon. The solar spectrum reflected from the moon can be seen quite brightly over the entire chip and was generally stable and removable. However, the regions around the Balmer lines were problematic in a few instances and some lower signal to noise spectra still contain residuals in the region around Hα, Hβ, and Hγ.

There are a few miscellaneous stars which were observed with LRIS because they were considered important yet too faint to obtain reliable spectra with a 3 meter class telescope. The observations were kindly performed by colleagues at other institutions. In a few cases, calibration stars were not observed and hence the flux calibration is not perfect and had to be adjusted as best possible.

4.6.1 White Dwarfs

In several of the binary systems reported here, the primary white dwarf is poorly documented in the literature, or missing all together. Spectra are presented here for those stars which do not have published spectra, are misclassified or missing from the literature, new white dwarf identifications, and those systems where binarity or other issues have precluded proper analysis. Also shown in this section are the optical spectra of all unpublished white dwarf wide binary companions discovered uniquely in the study. These spectra are displayed in Figures 4.21 – 4.28 in order of decreasing temperature.

4.6.2 Red Dwarfs

In Figures 4.29 – 4.41, the spectra of unpublished resolved M dwarf secondaries and tertiaries are presented. The spectra are displayed in order of decreasing temperature.

4.6.3 Composites

In Figures $4.42 - 4.50$, the composite spectra of white dwarf plus red dwarf pairs is presented (at least one of which has been resolved photometrically but not spectroscopically). The spectra are displayed in order of decreasing red dwarf temperature.

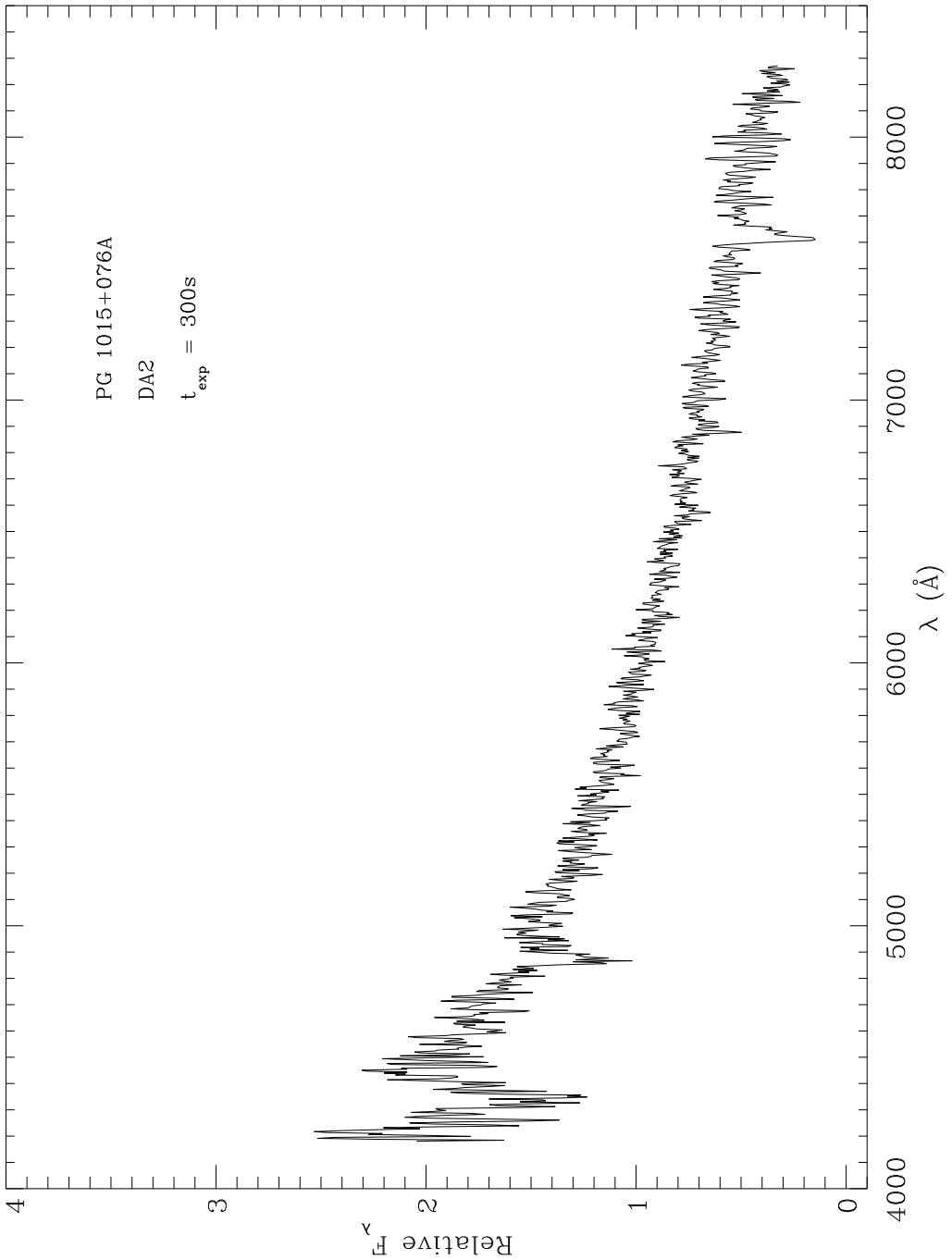

Figure 4.21: Optical spectrum of PG 1015+076A taken with the Boller & Chivens Spectrograph on the Bok 2.3 meter in April 2003.

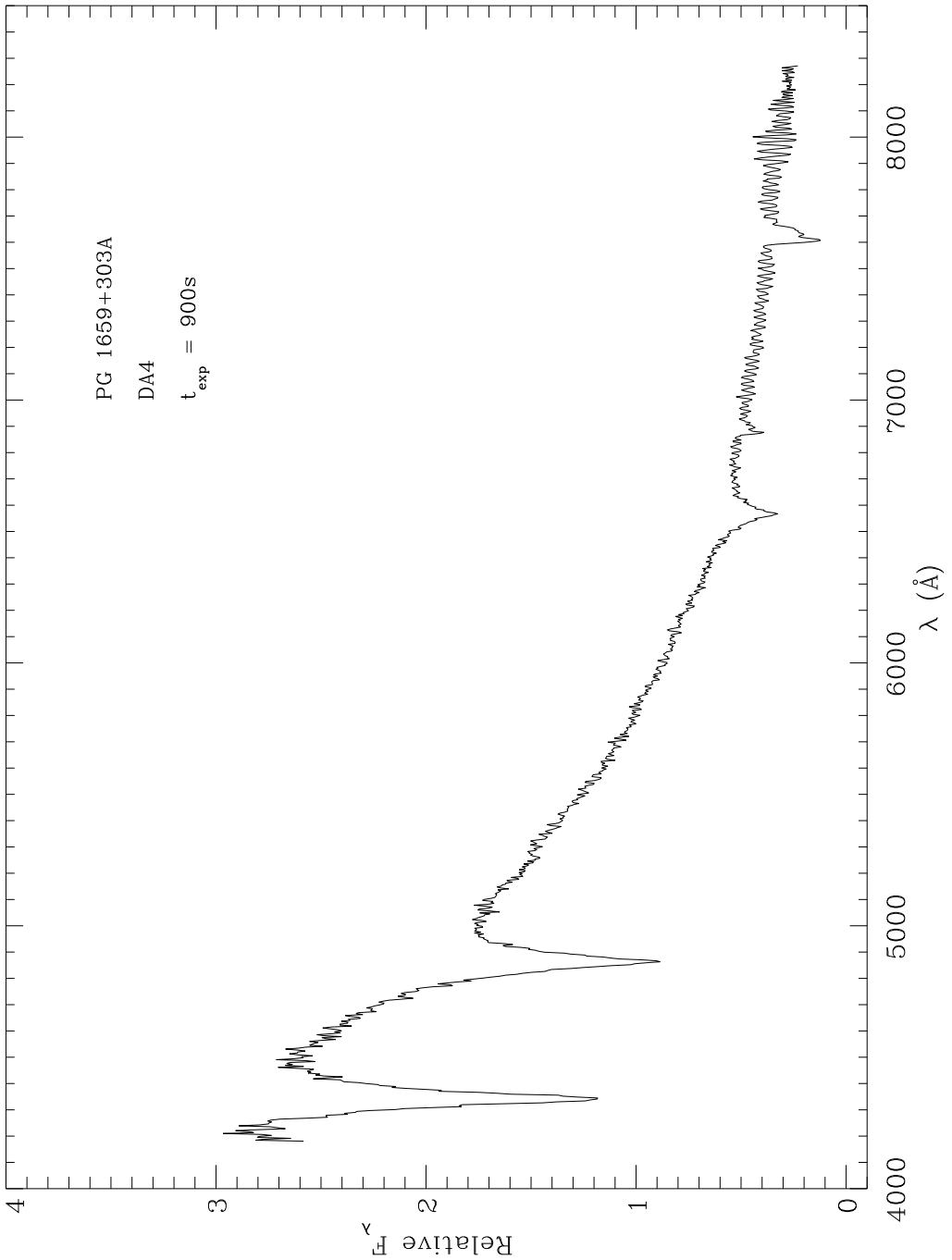

Figure 4.22: Optical spectrum of PG 1659+303A taken with the Boller & Chivens Spectrograph on the Bok 2.3 meter in April 2003.

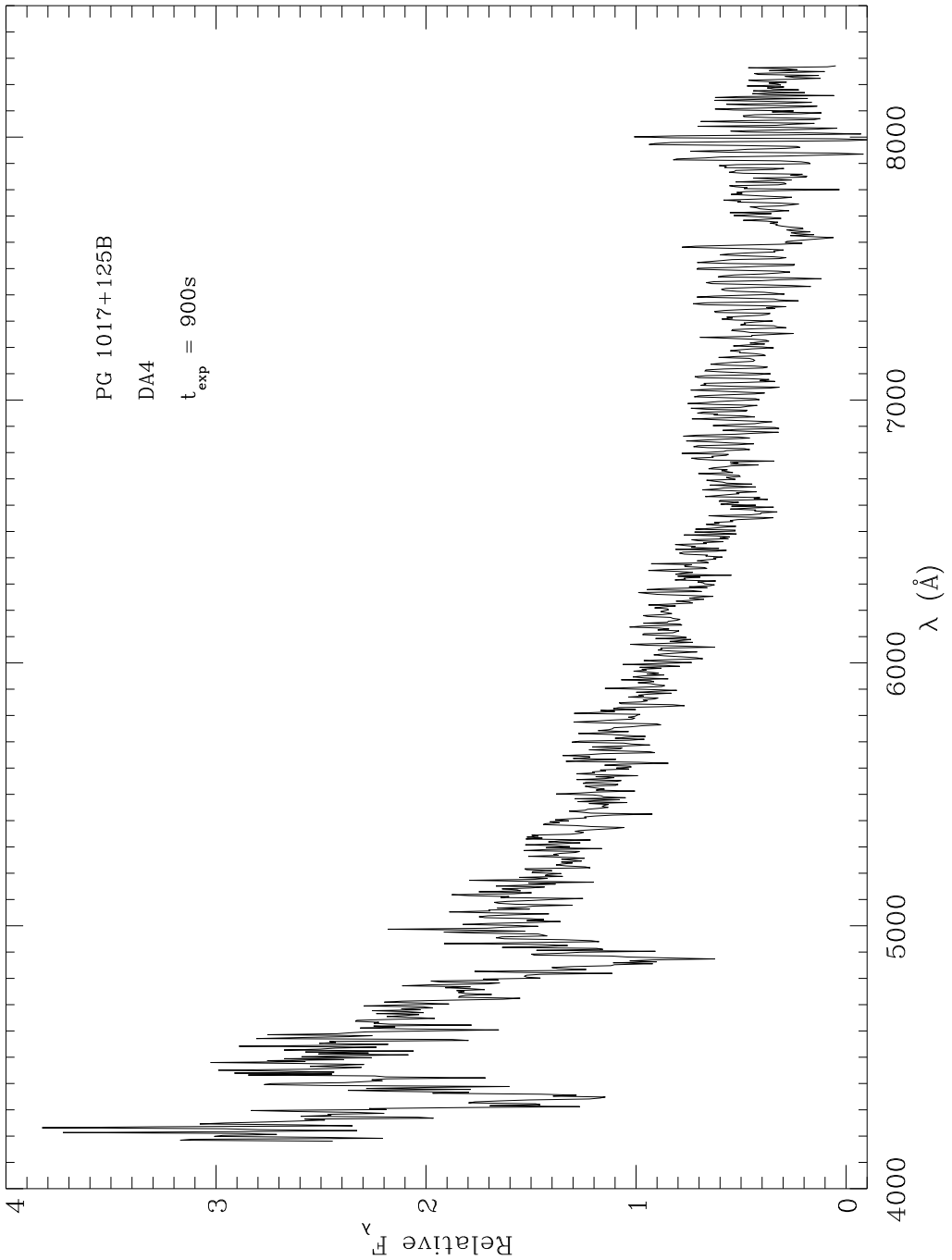

Figure 4.23: Optical spectrum of PG 1017+125B taken with the Boller & Chivens Spectrograph on the Bok 2.3 meter in April 2003.

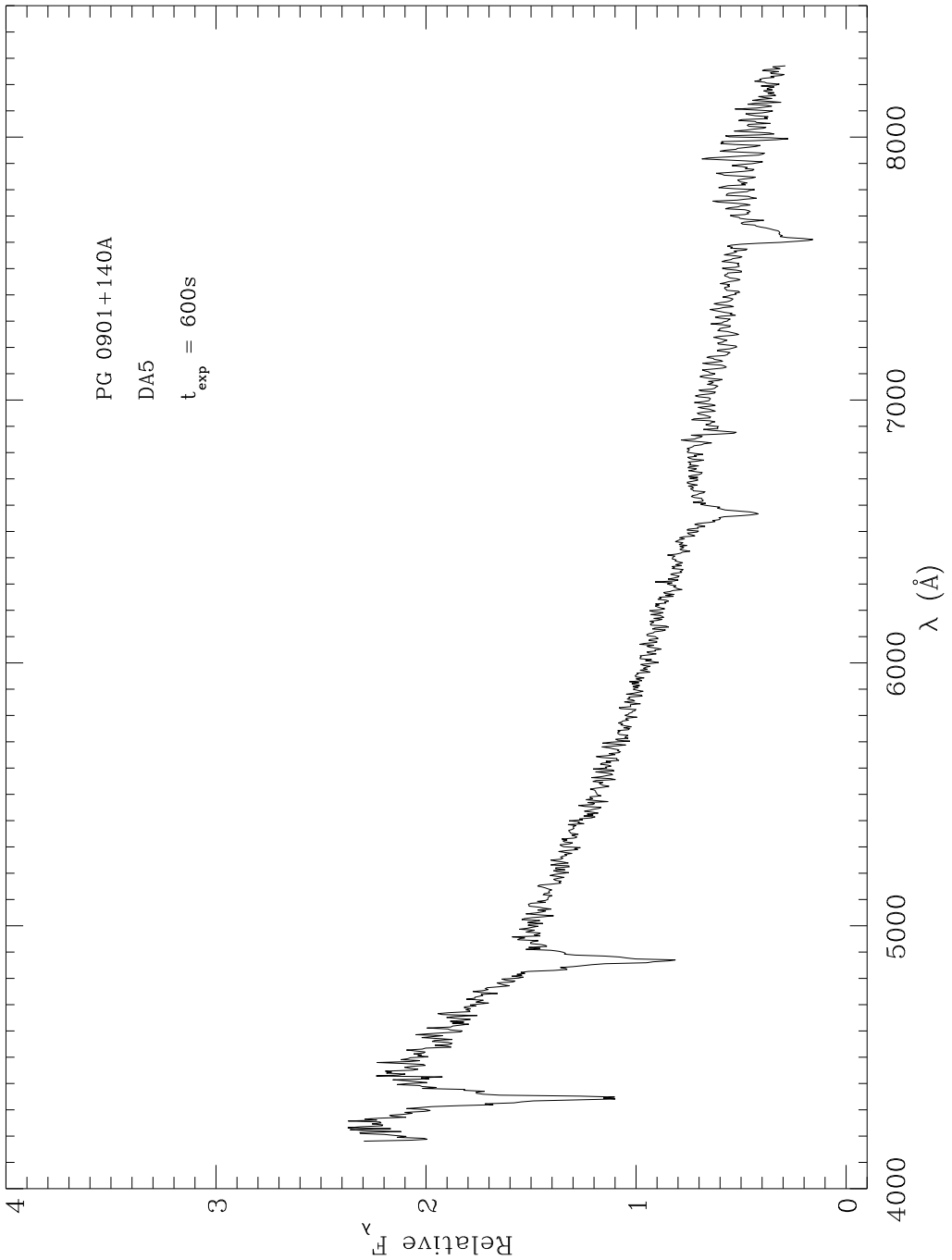

Figure 4.24: Optical spectrum of PG 0901+140A taken with the Boller & Chivens Spectrograph on the Bok 2.3 meter in April 2003.

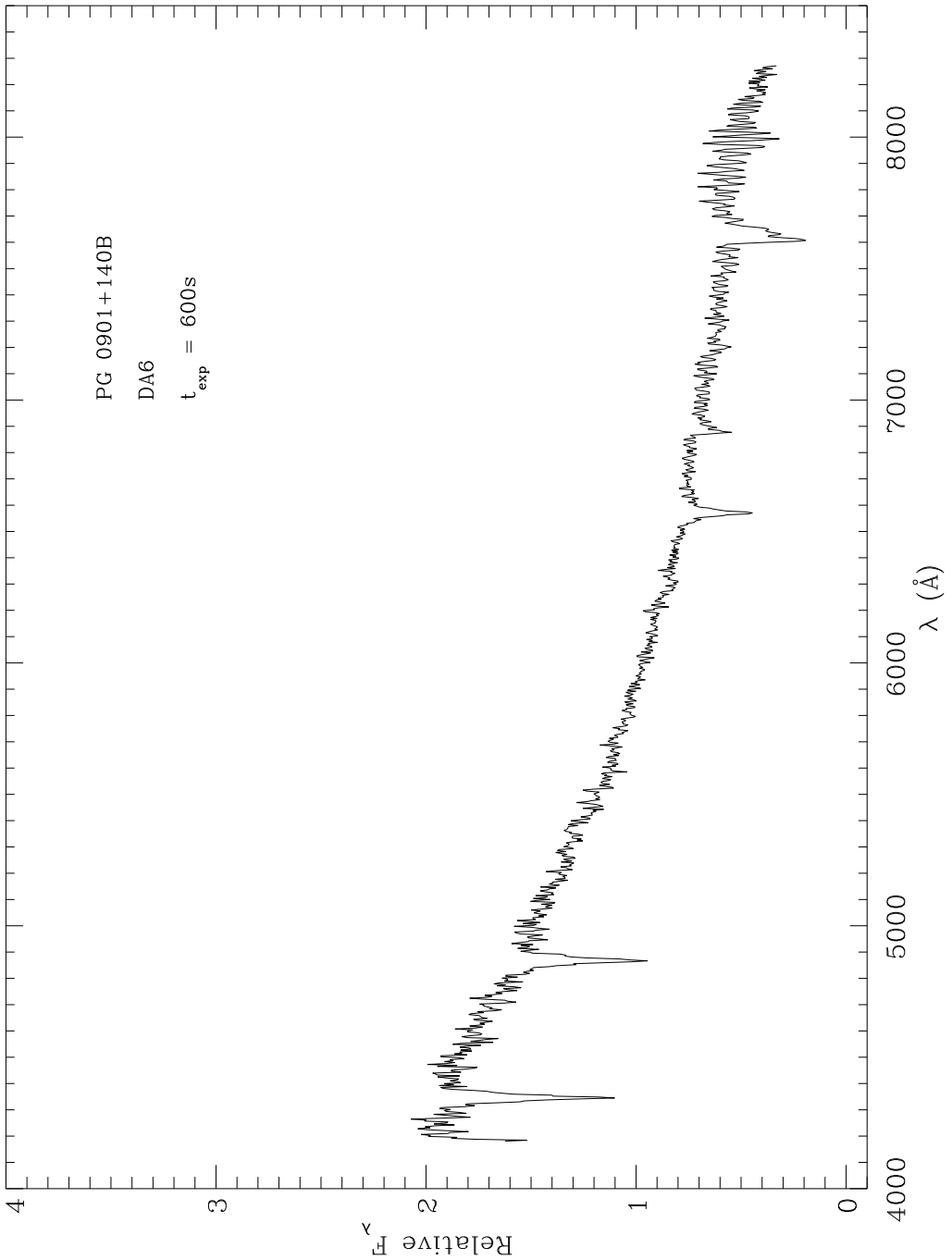

Figure 4.25: Optical spectrum of PG 0901+140B taken with the Boller & Chivens Spectrograph on the Bok 2.3 meter in April 2003.

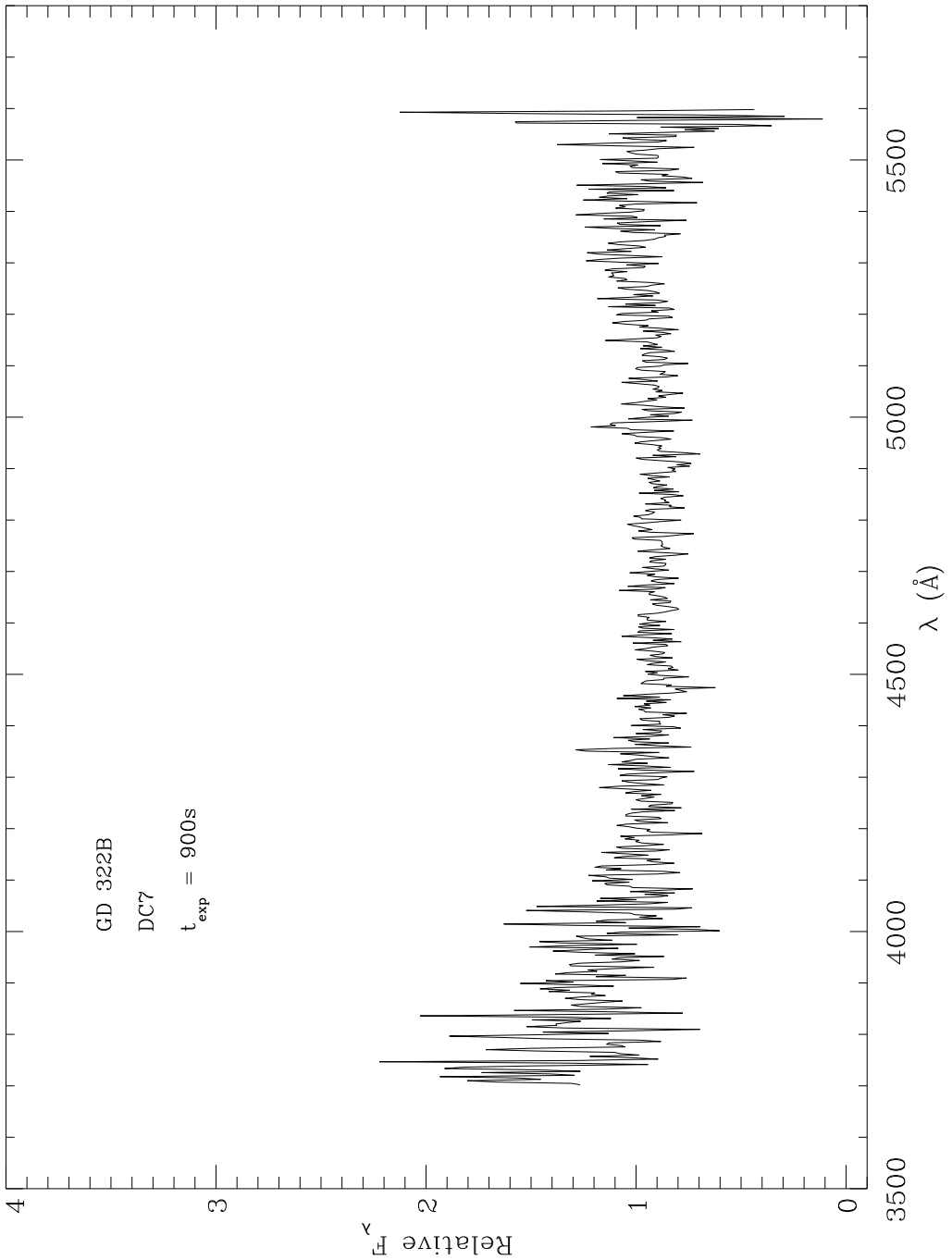

Figure 4.26: Blue optical spectrum of GD 322B taken with the Kast Spectrograph on the Shane 3 meter telescope in August 2002.

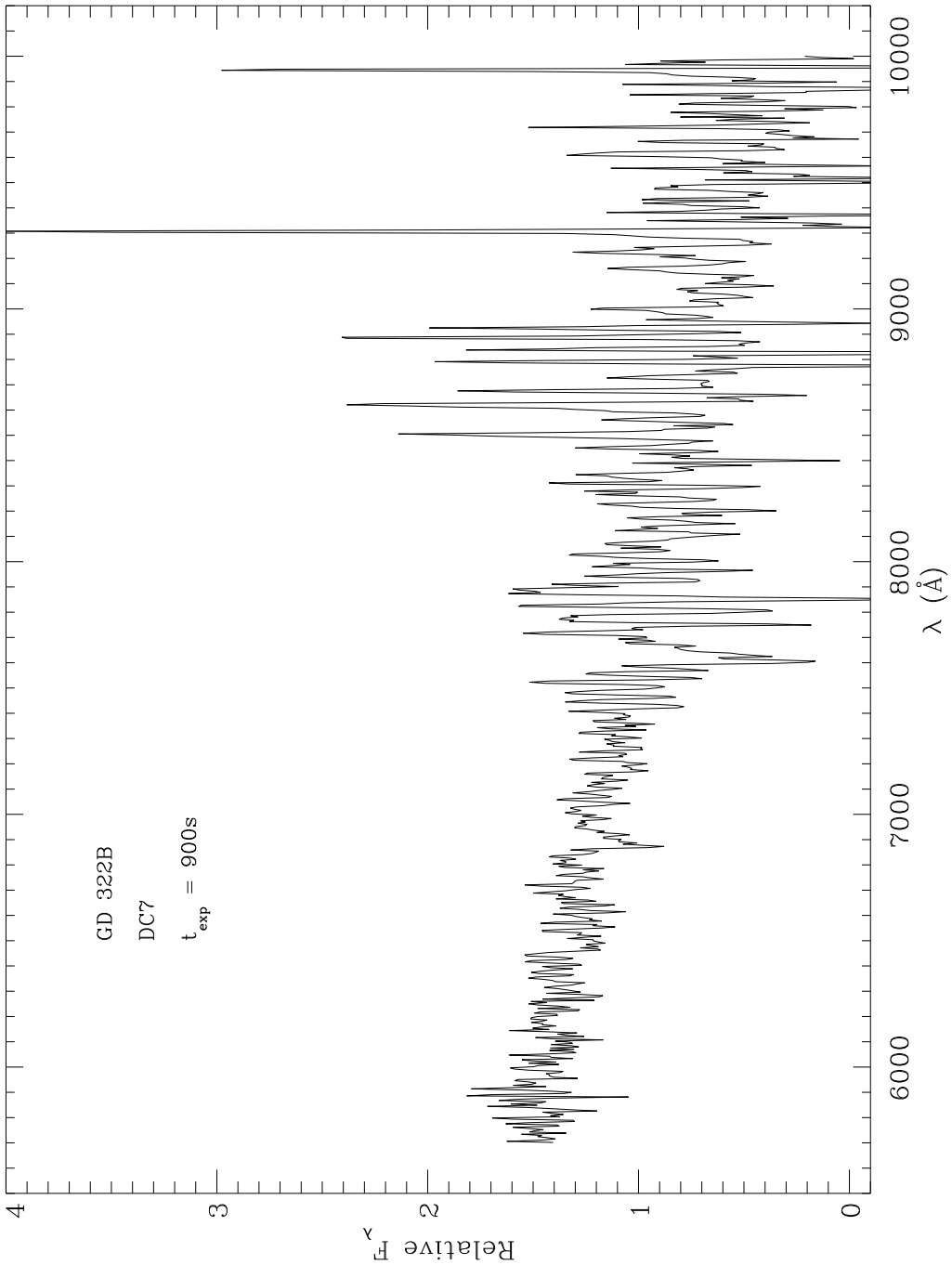

Figure 4.27: Red optical spectrum of GD 322B taken with the Kast Spectrograph on the Shane 3 meter telescope in August 2002.

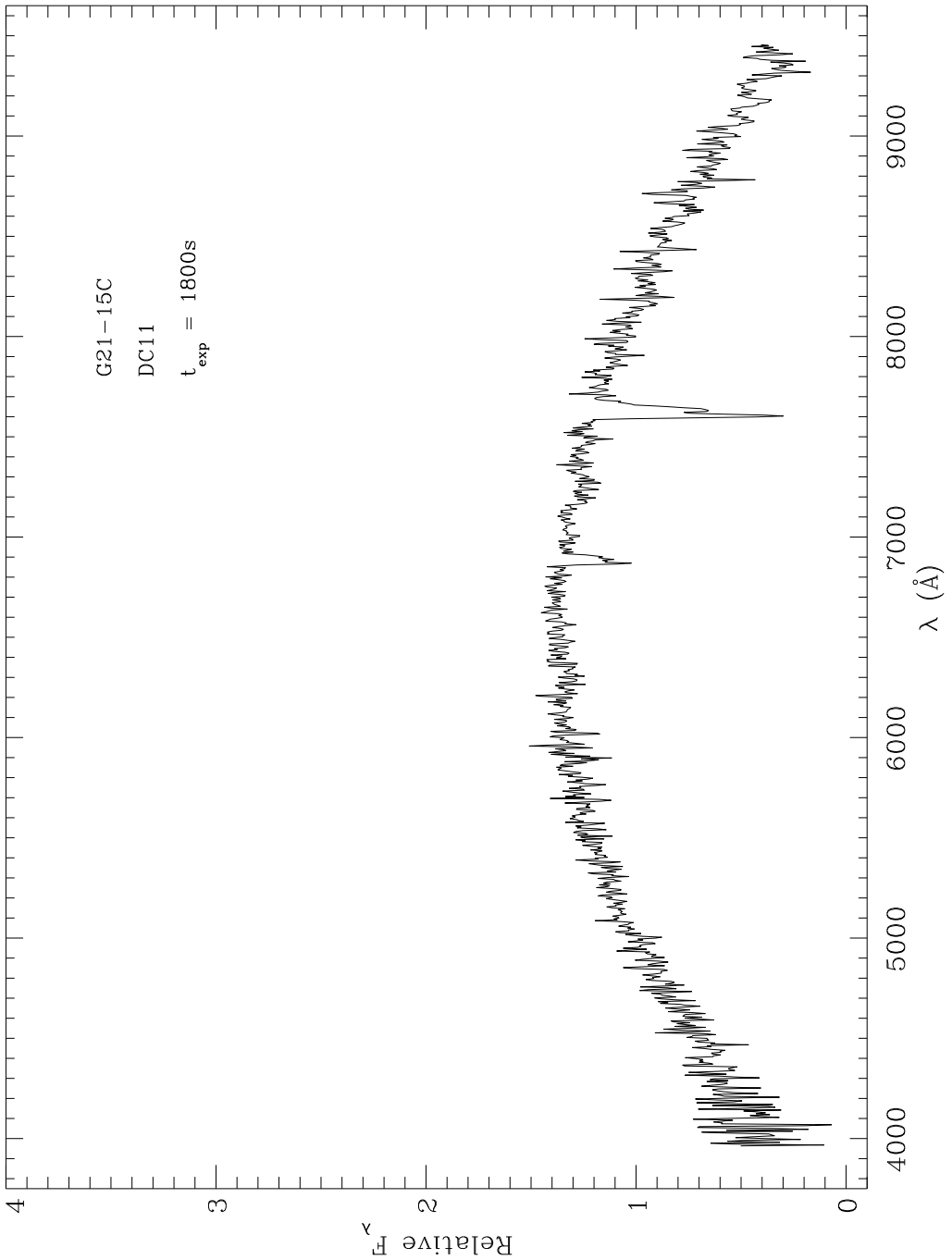

Figure 4.28: Optical spectrum of G21-15C taken with the Kast Spectrograph on the Shane 3 meter telescope in August 2003.

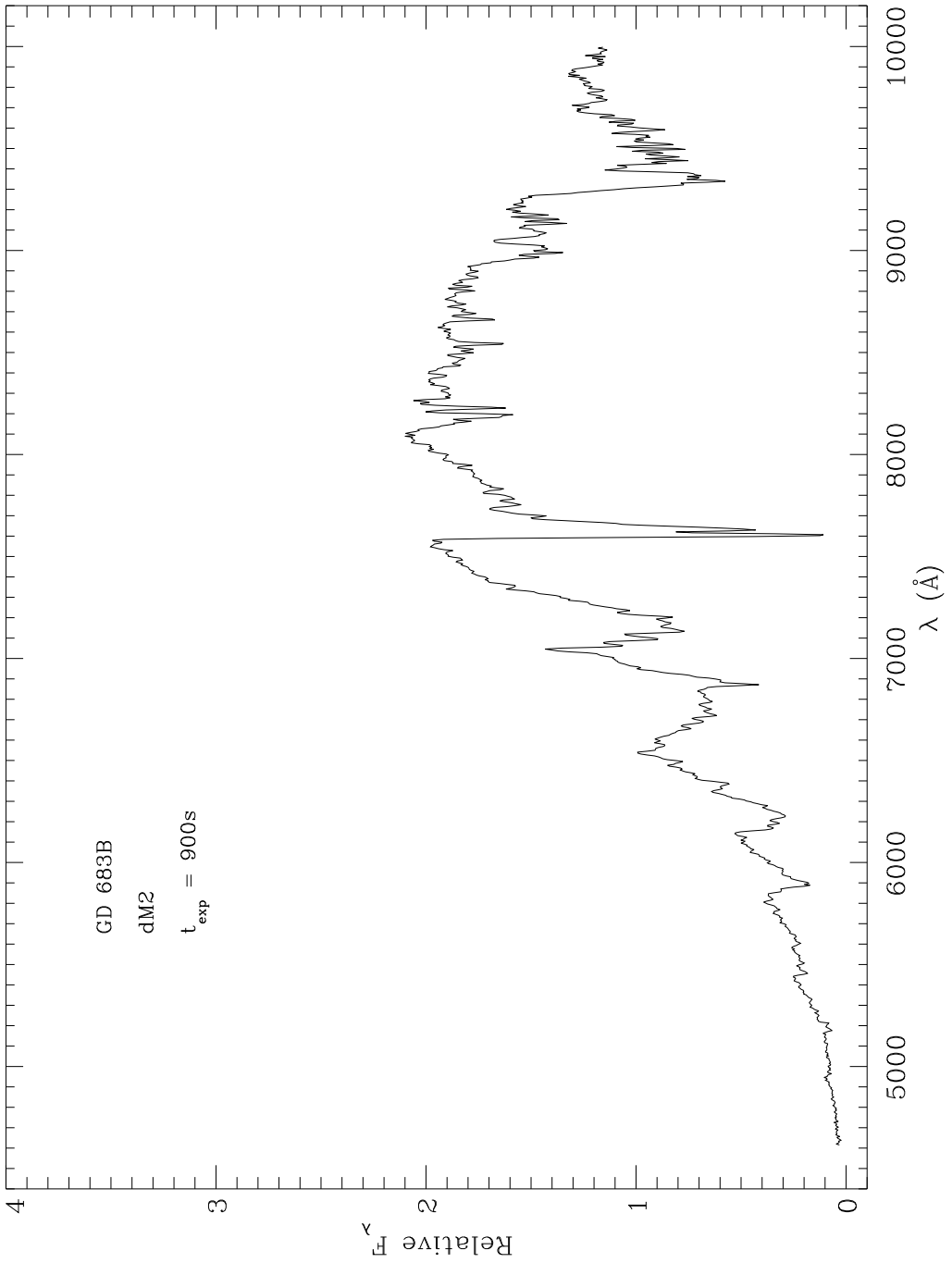

Figure 4.29: Optical spectrum of GD 683B taken with the Kast Spectrograph on the Shane 3 meter telescope in August 2003.

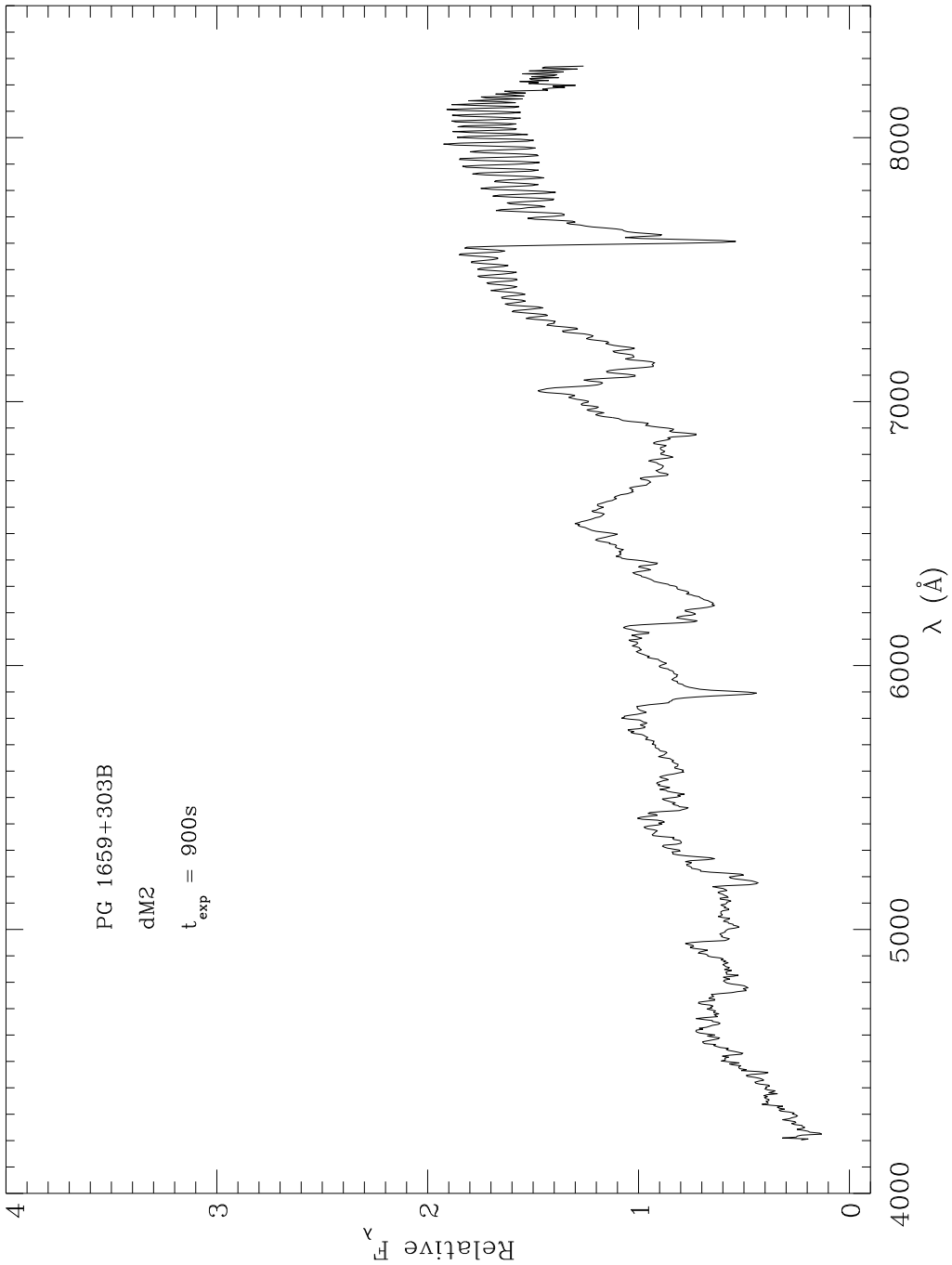

Figure 4.30: Optical spectrum of PG 1659+303B taken with the Boller & Chivens Spectrograph on the Bok 2.3 meter in April 2003.

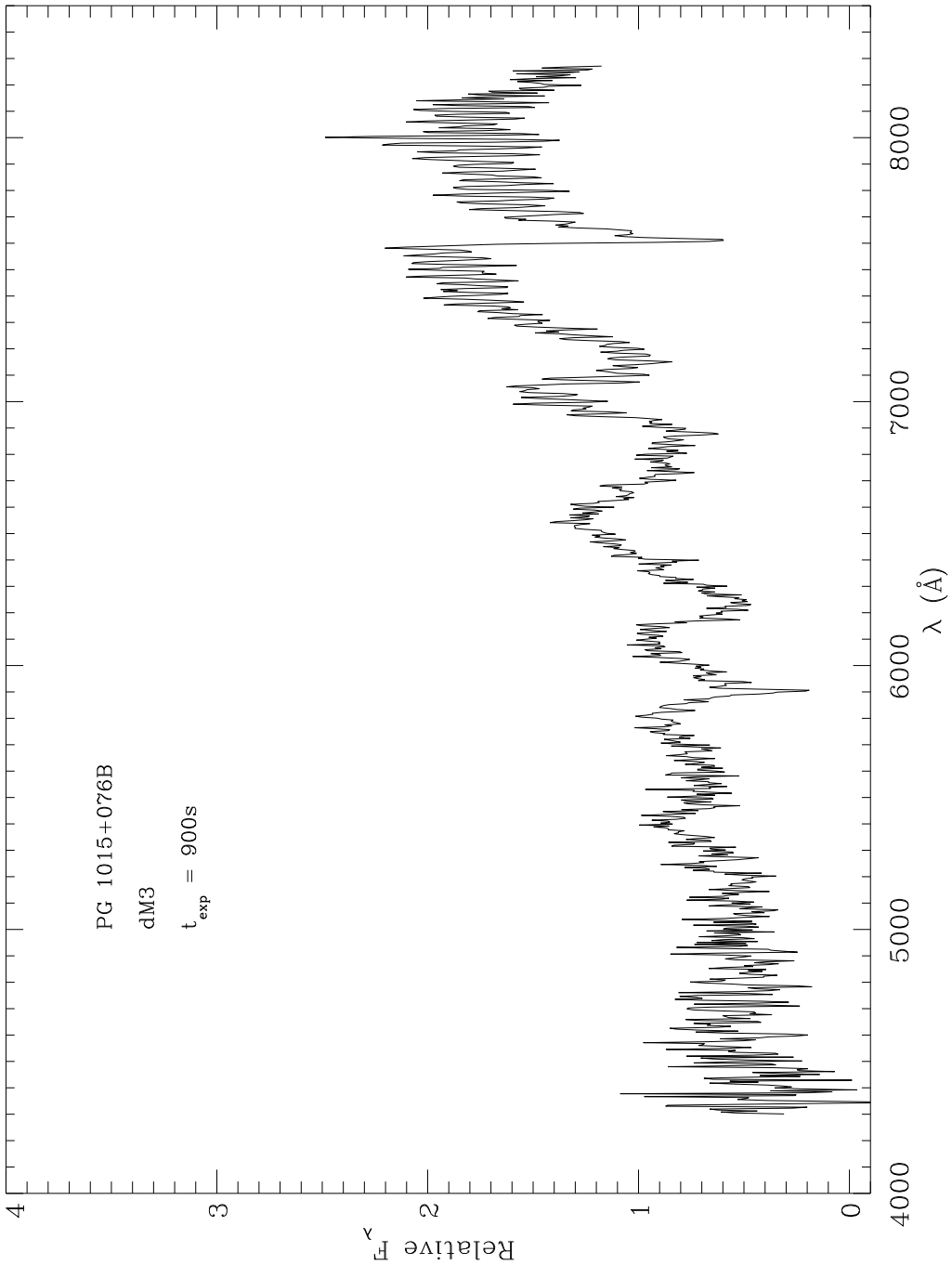

Figure 4.31: Optical spectrum of PG 1015+076B taken with the Boller & Chivens Spectrograph on the Bok 2.3 meter in April 2003.

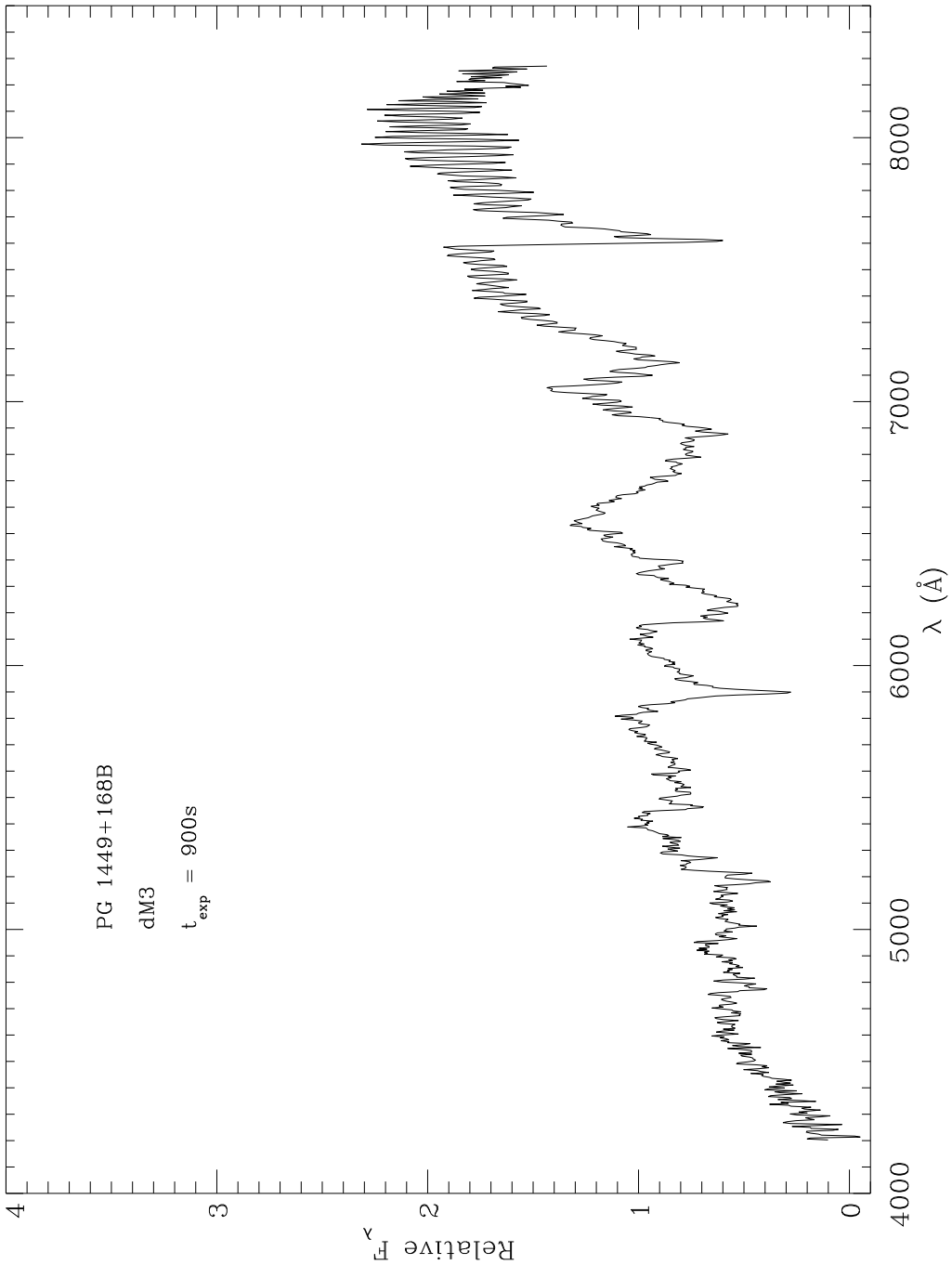

Figure 4.32: Optical spectrum of PG 1449+168B taken with the Boller & Chivens Spectrograph on the Bok 2.3 meter in April 2003.

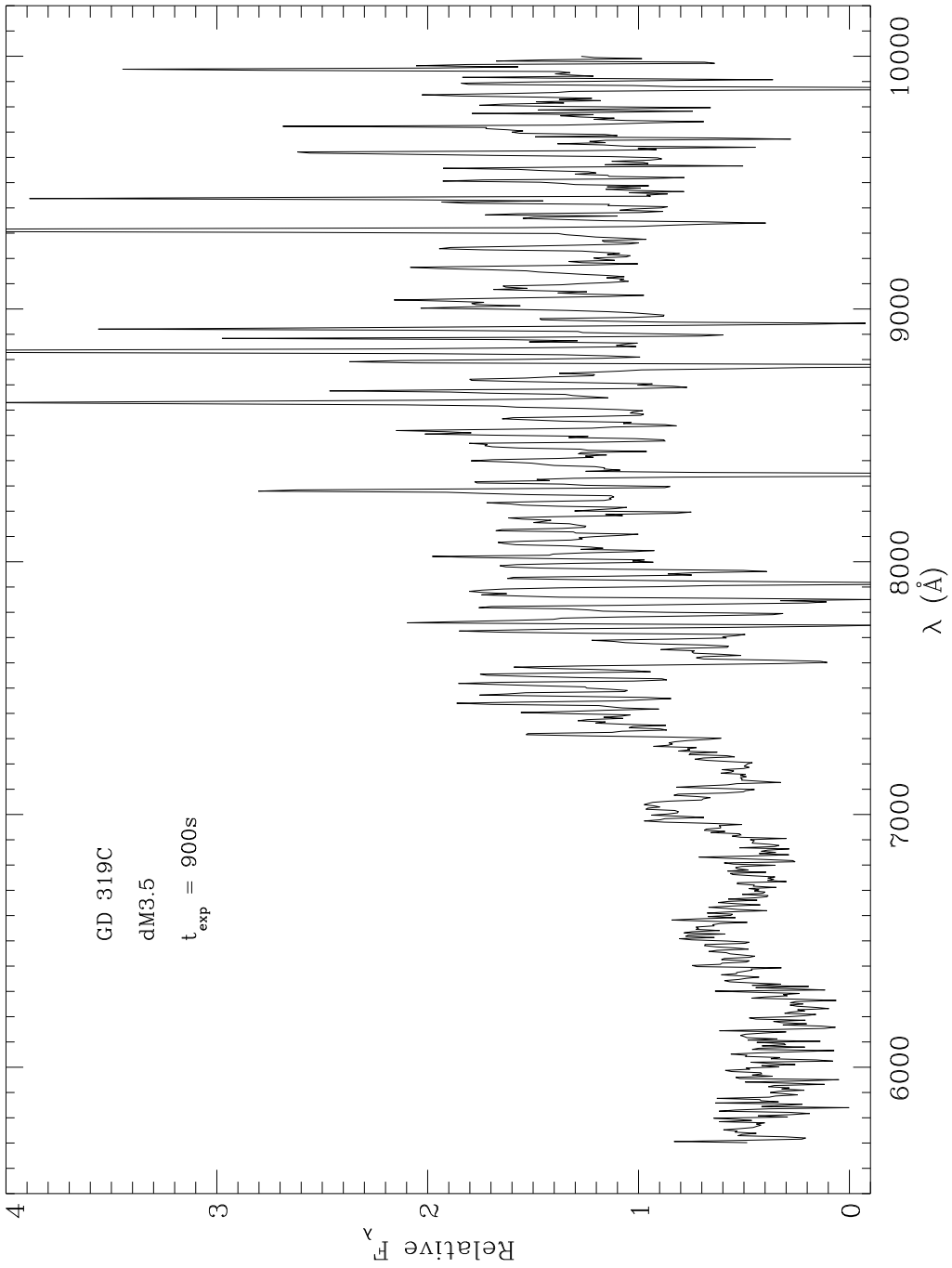

Figure 4.33: Red optical spectrum of GD 319C taken with the Kast Spectrograph on the Shane 3 meter telescope in August 2002.

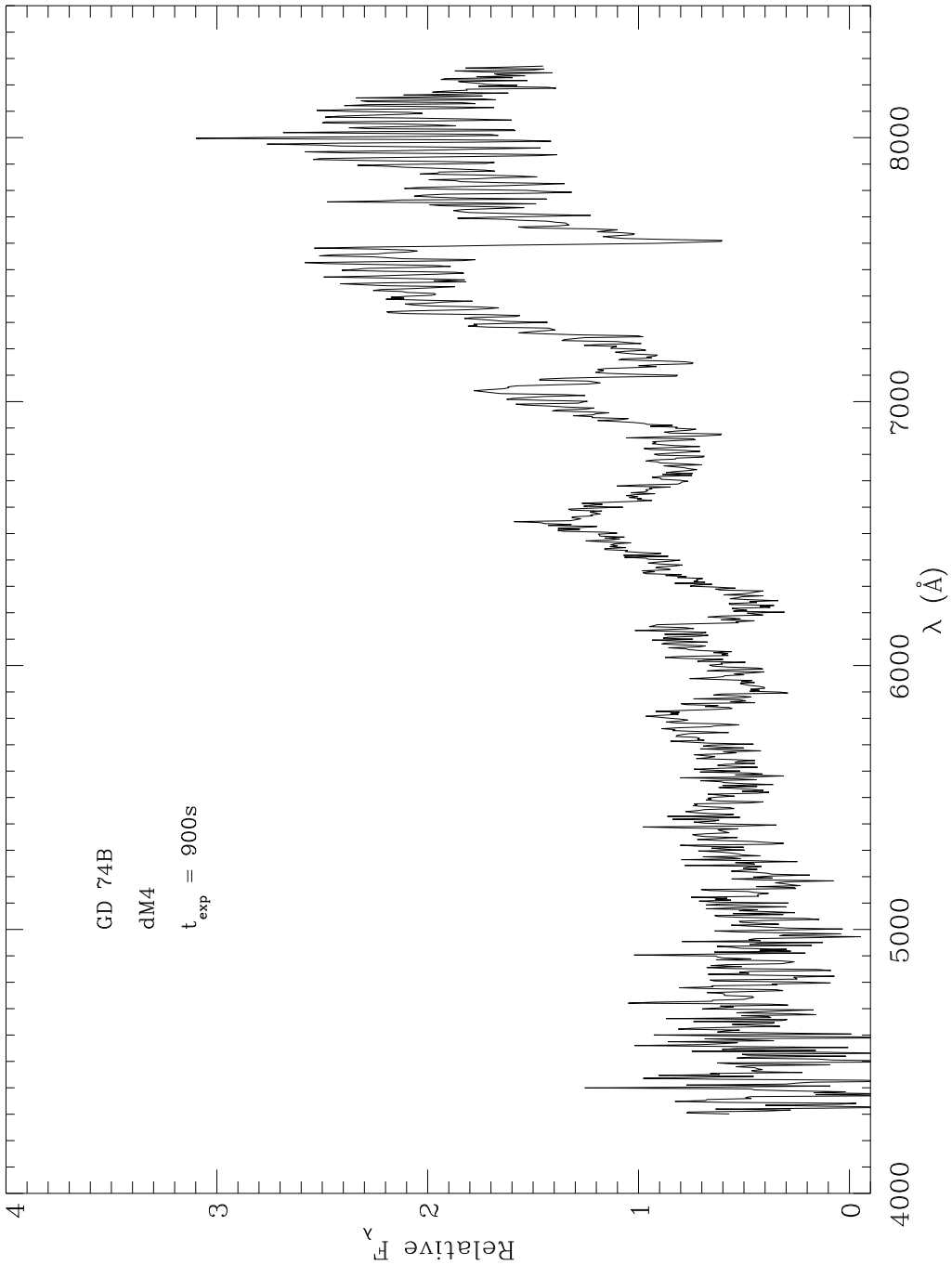

Figure 4.34: Optical spectrum of GD 74B taken with the Boller & Chivens Spectrograph on the Bok 2.3 meter in April 2003.

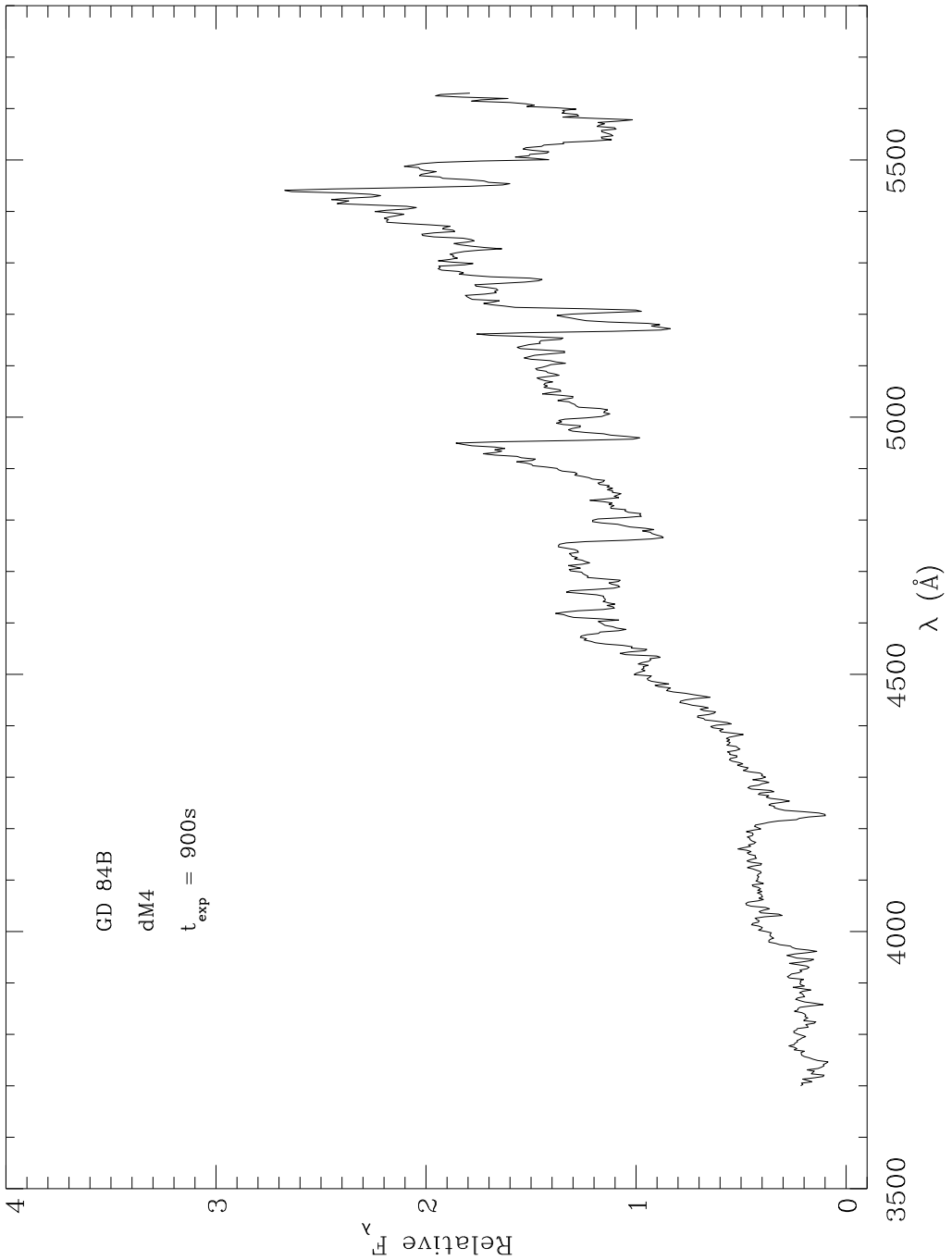

Figure 4.35: Blue optical spectrum of GD 84B taken with the Kast Spectrograph on the Shane 3 meter telescope in February 2002.

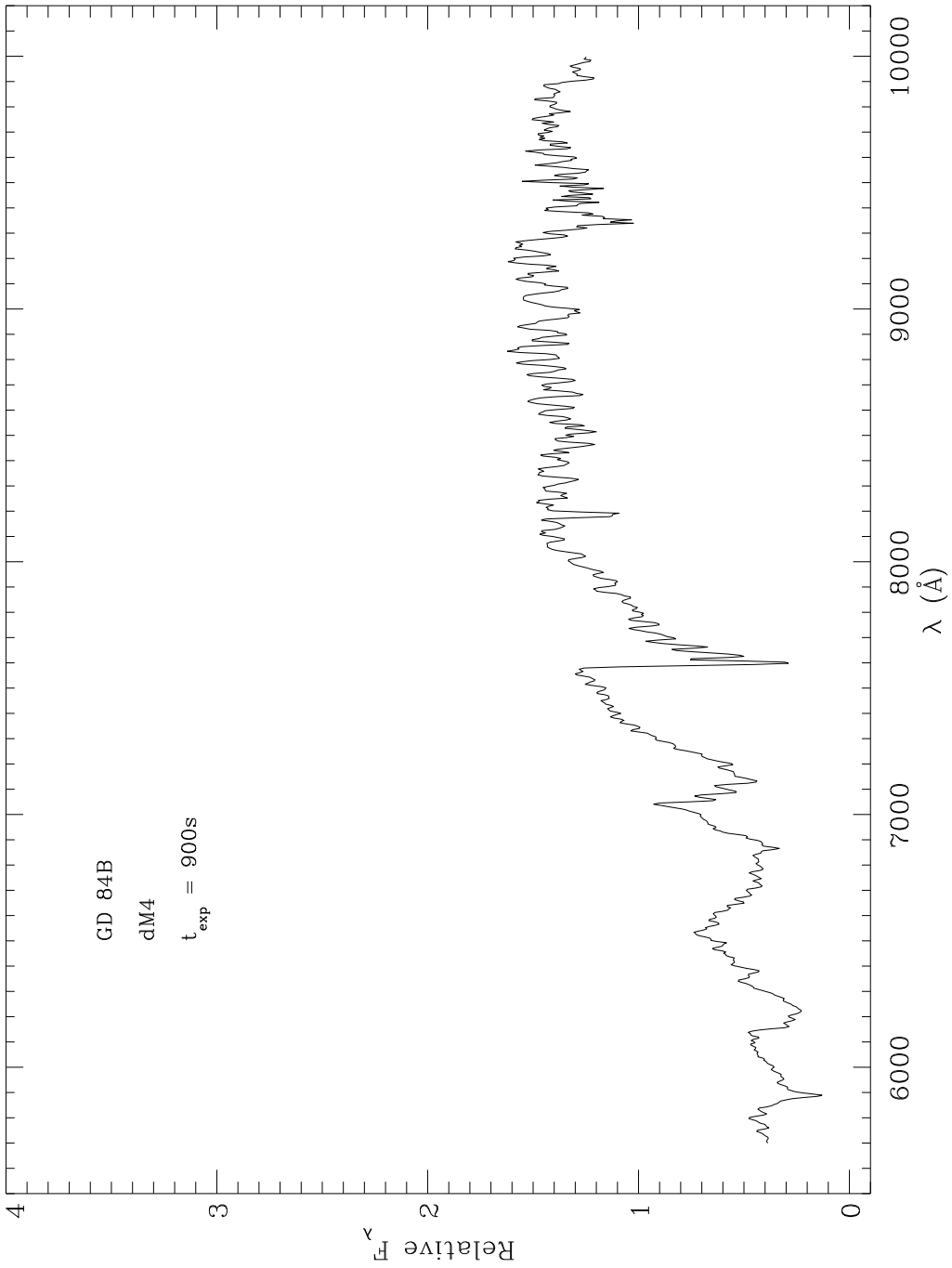

Figure 4.36: Red optical spectrum of GD 84B taken with the Kast Spectrograph on the Shane 3 meter telescope in February 2002.

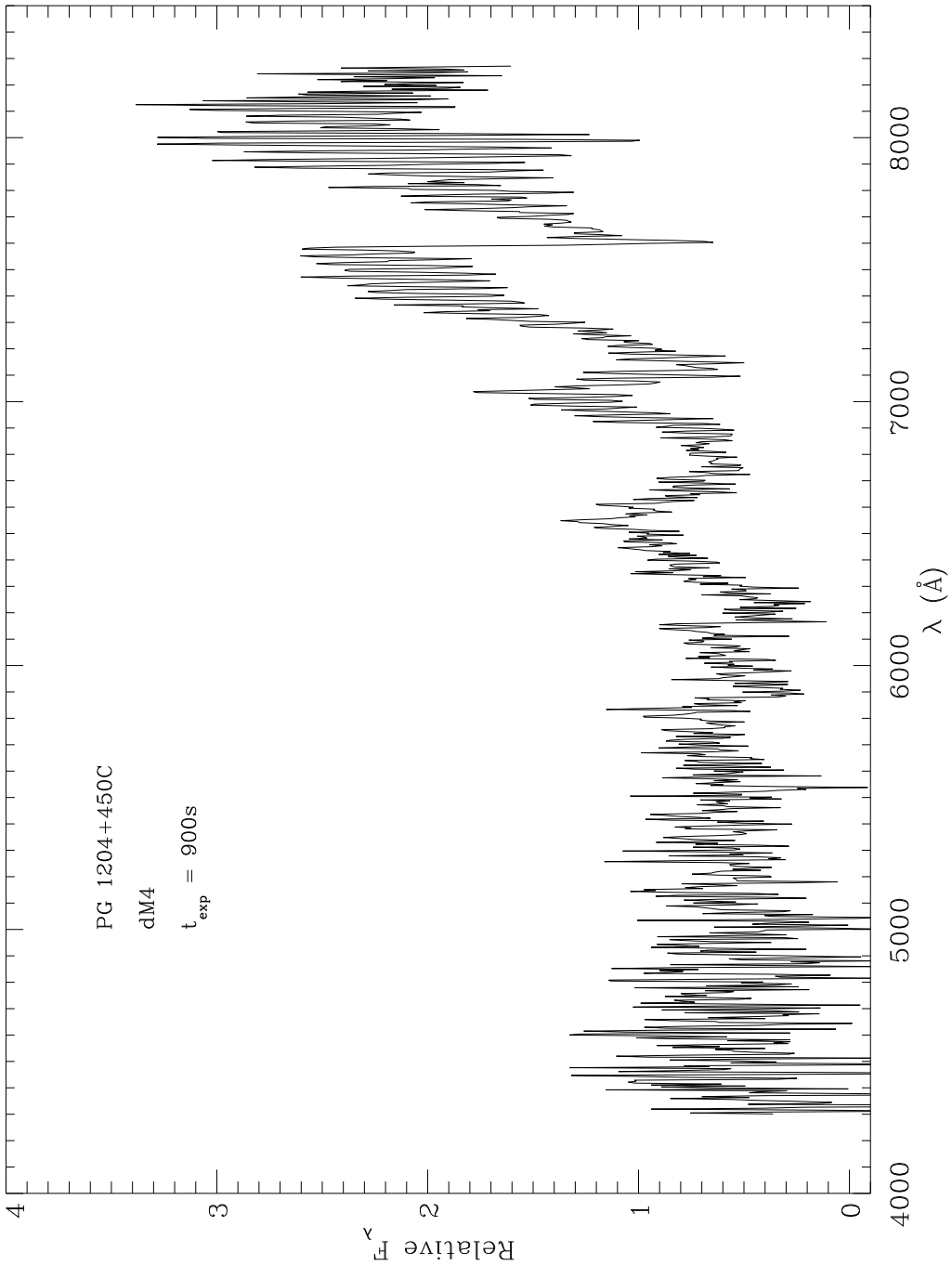

Figure 4.37: Optical spectrum of PG 1204+450C taken with the Boller & Chivens Spectrograph on the Bok 2.3 meter in April 2003.

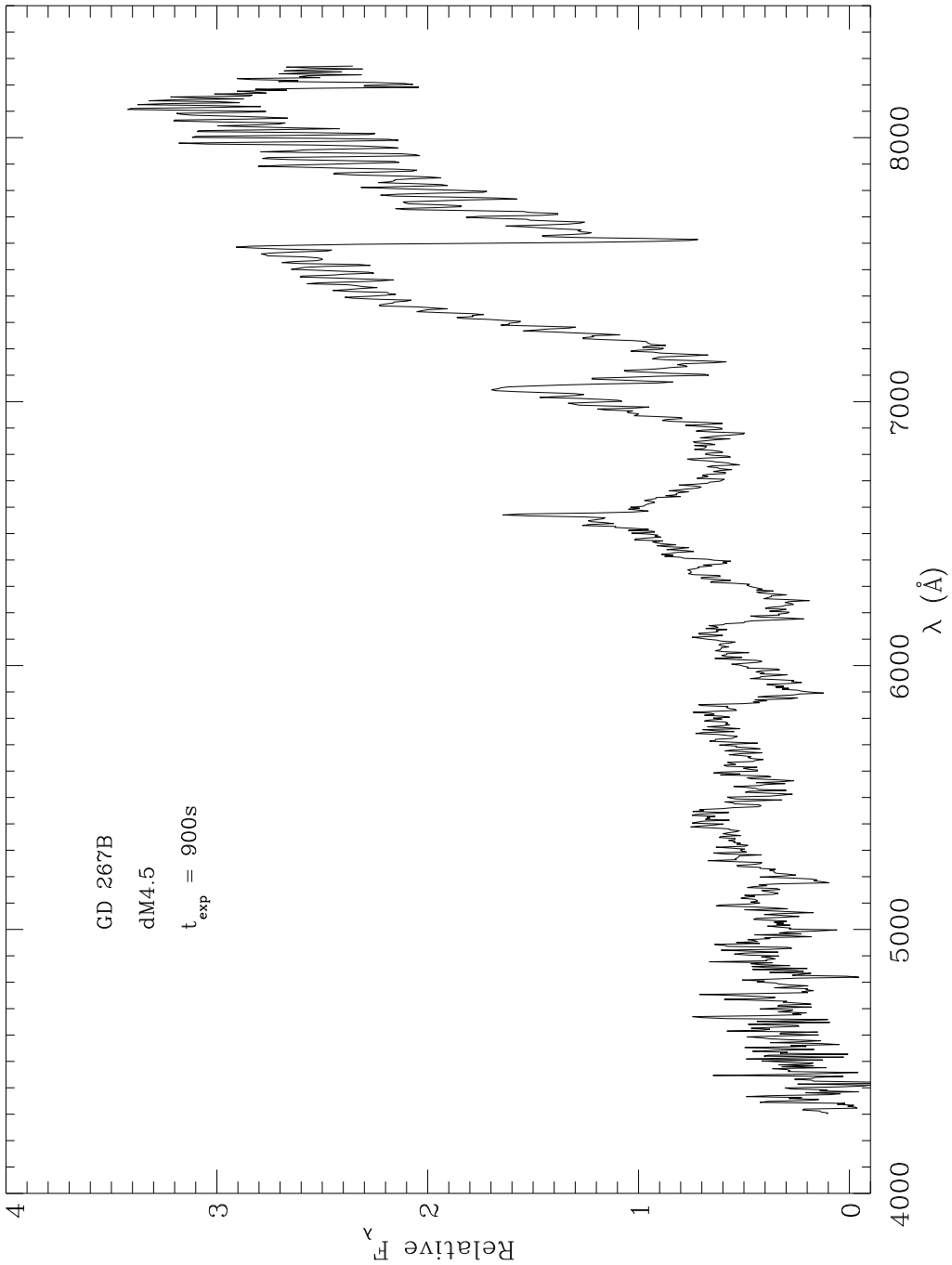

Figure 4.38: Optical spectrum of GD 267B taken with the Boller & Chivens Spectrograph on the Bok 2.3 meter in April 2003.

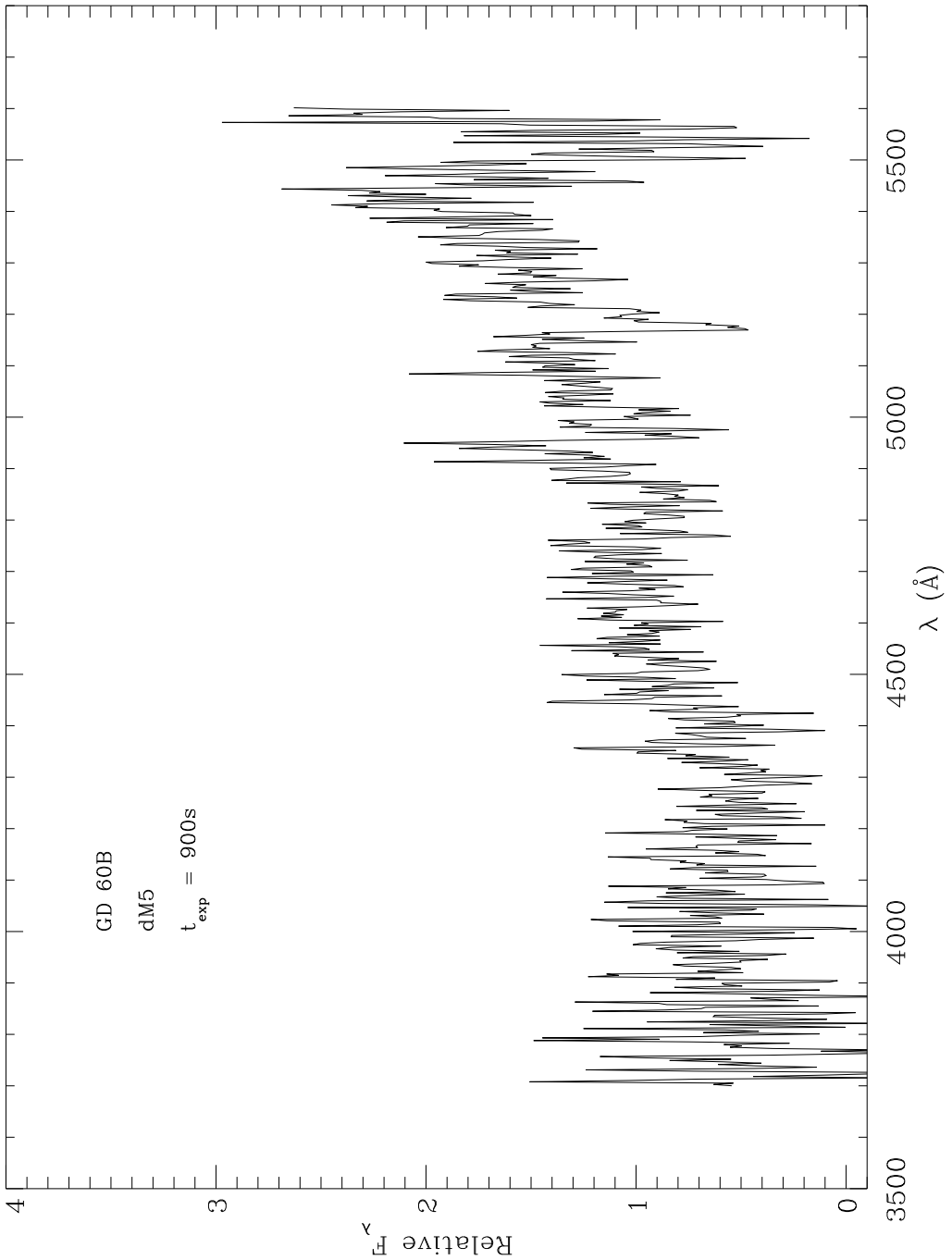

Figure 4.39: Blue optical spectrum of GD 60B taken with the Kast Spectrograph on the Shane 3 meter telescope in February 2002.

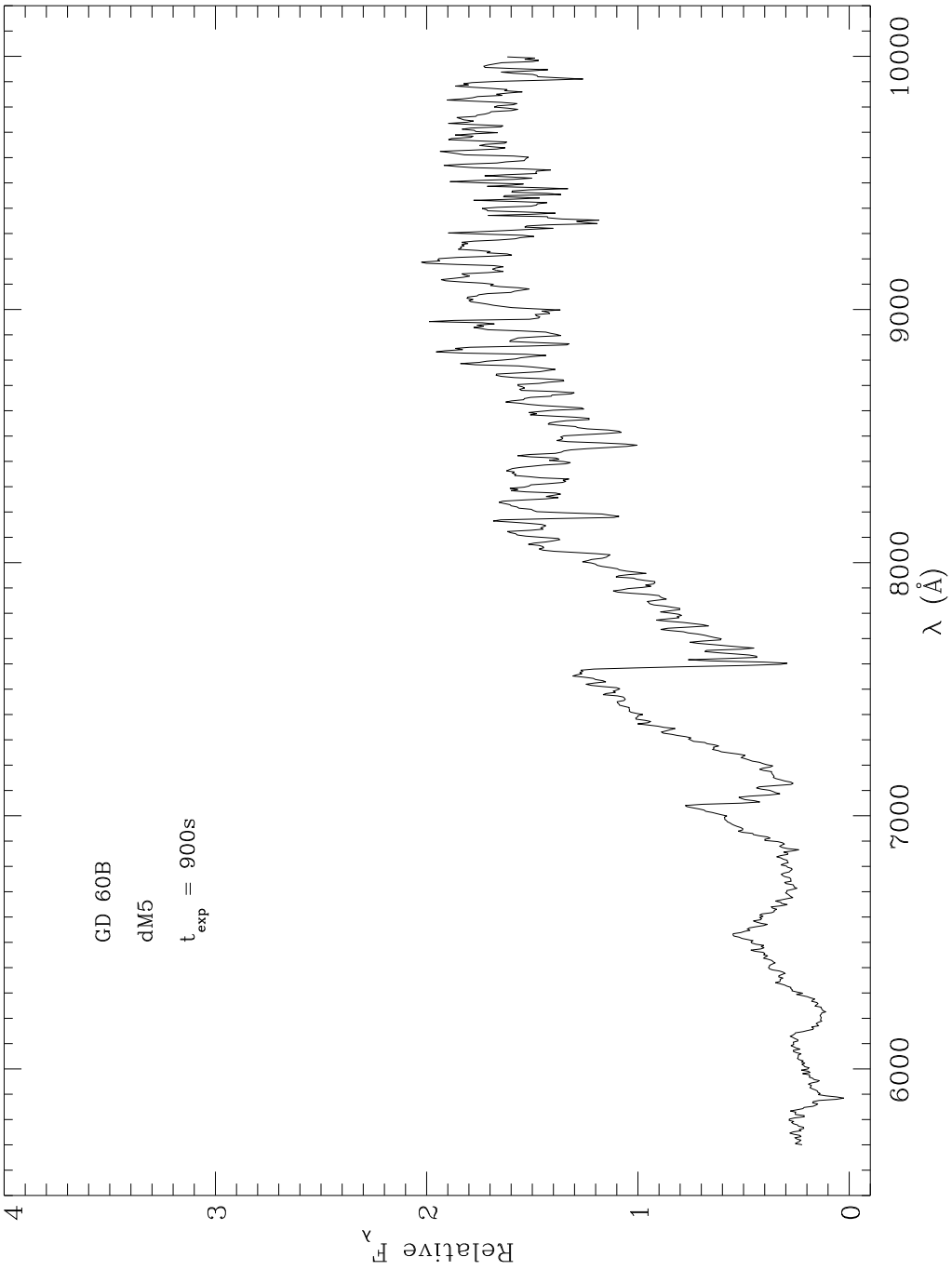

Figure 4.40: Red optical spectrum of GD 60B taken with the Kast Spectrograph on the Shane 3 meter telescope in February 2002.

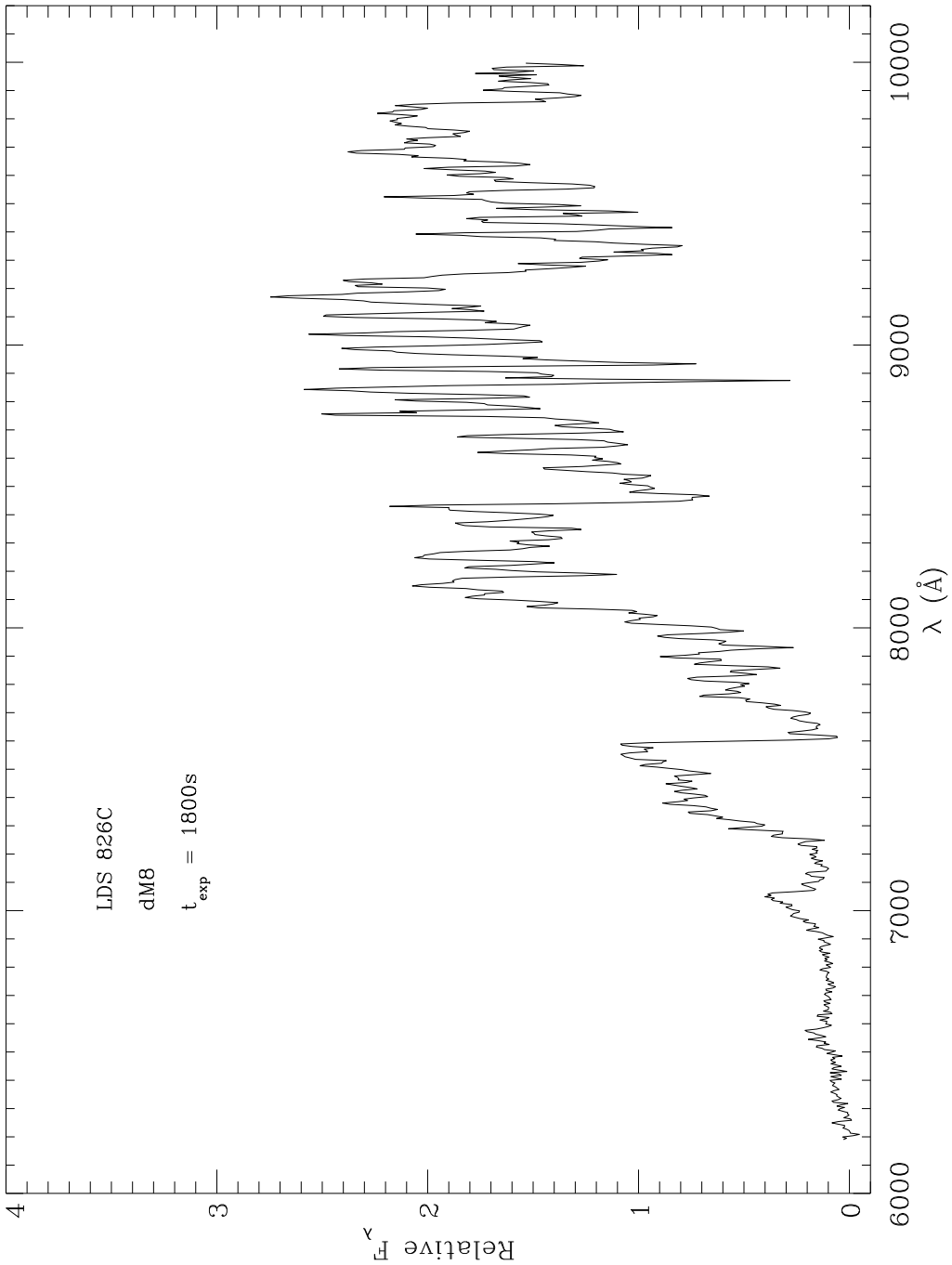

Figure 4.41: Optical spectrum of LDS 826C taken with the Kast Spectrograph on the Shane 3 meter telescope in August 2003.

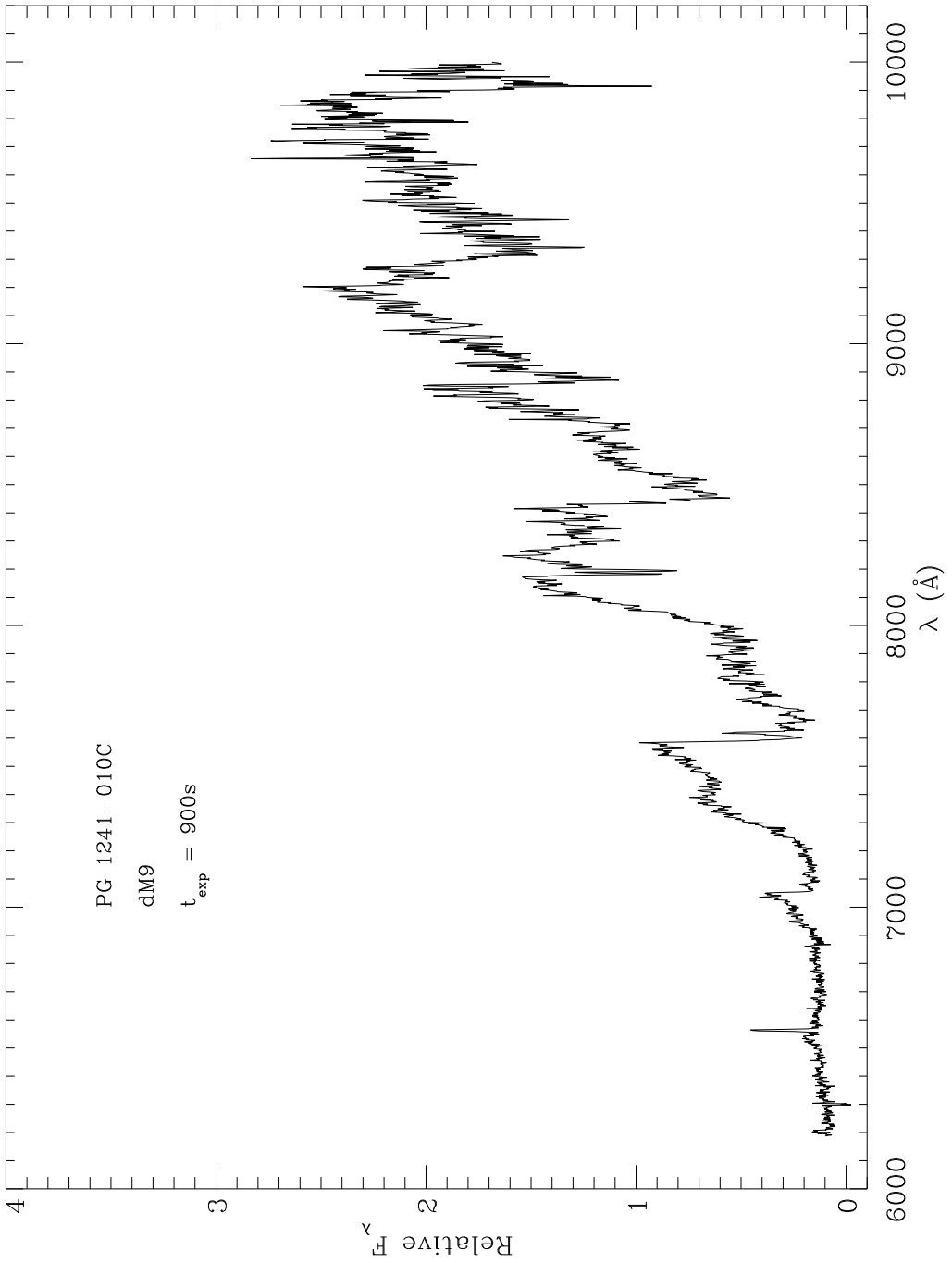

Figure 4.42: Optical spectrum of PG 1241−010C taken with the Low Resolution Imaging Spectrograph on the Keck I 10 meter telescope in May 2003.

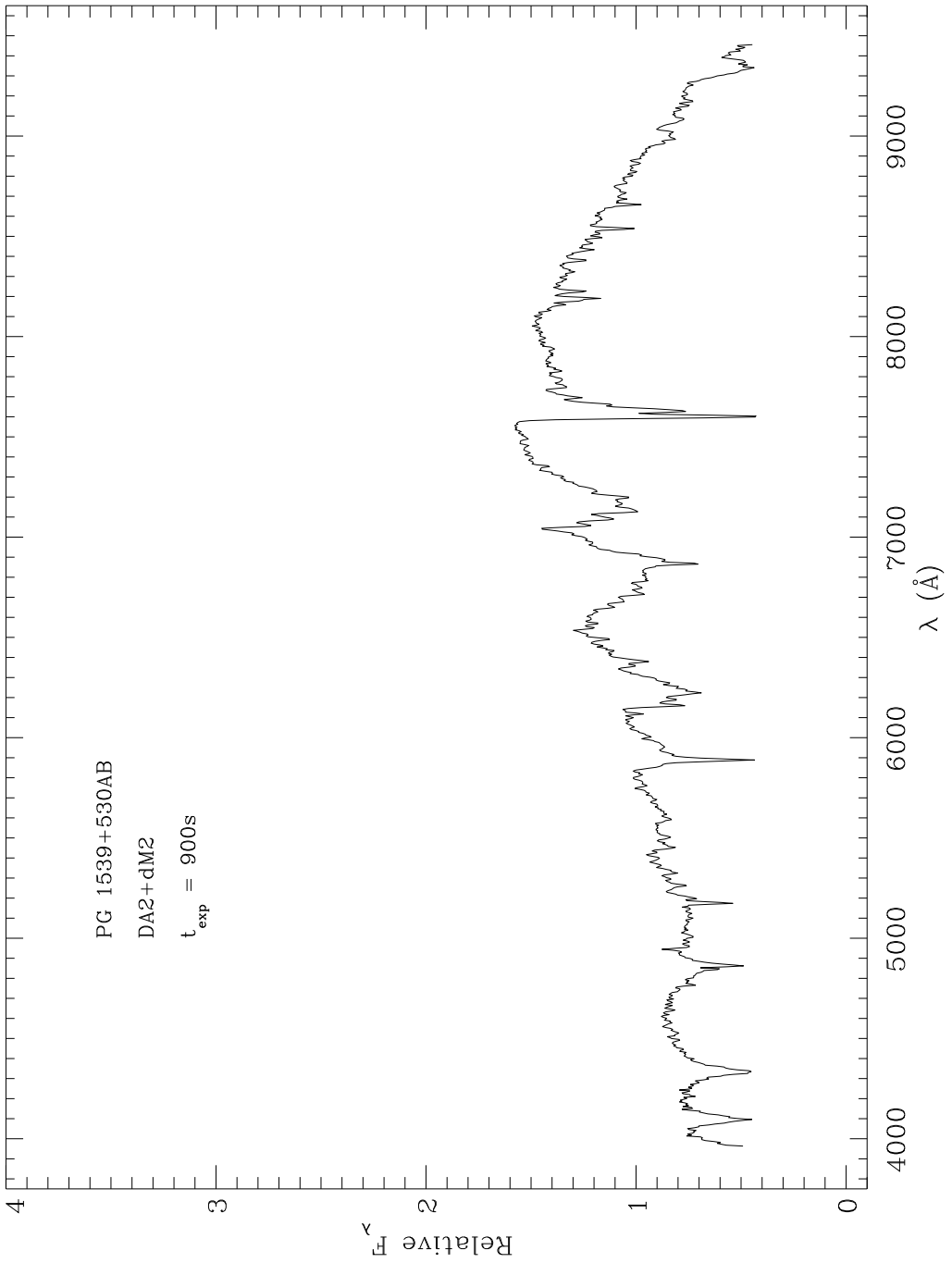

Figure 4.43: Optical spectrum of PG 1539+530AB taken with the Kast Spectrograph on the Shane 3 meter telescope in August 2003.

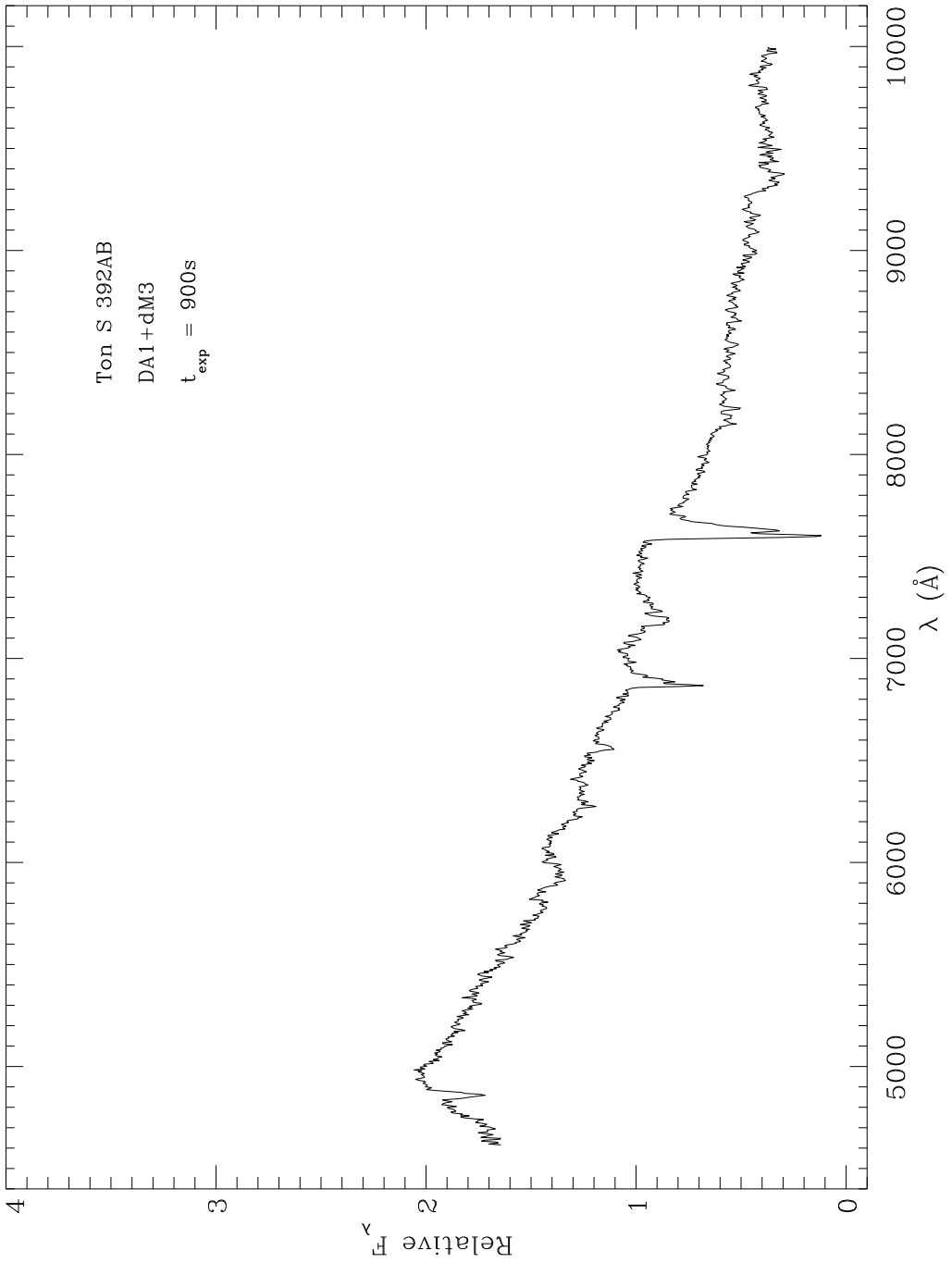

Figure 4.44: Optical spectrum of Ton S 392AB taken with the Kast Spectrograph on the Shane 3 meter telescope in August 2003.

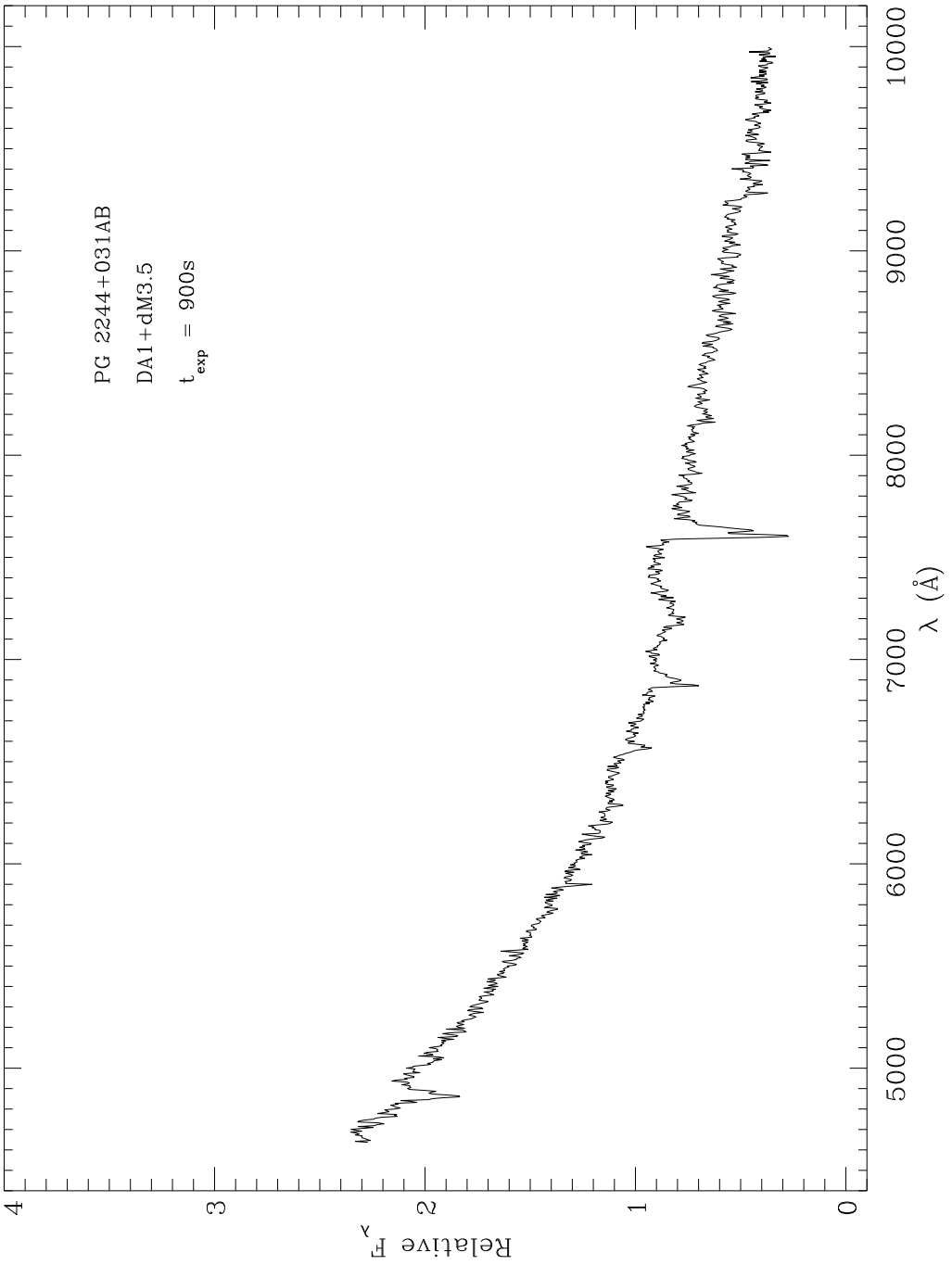

Figure 4.45: Optical spectrum of PG 2244+031AB taken with the Kast Spectrograph on the Shane 3 meter telescope in August 2003.

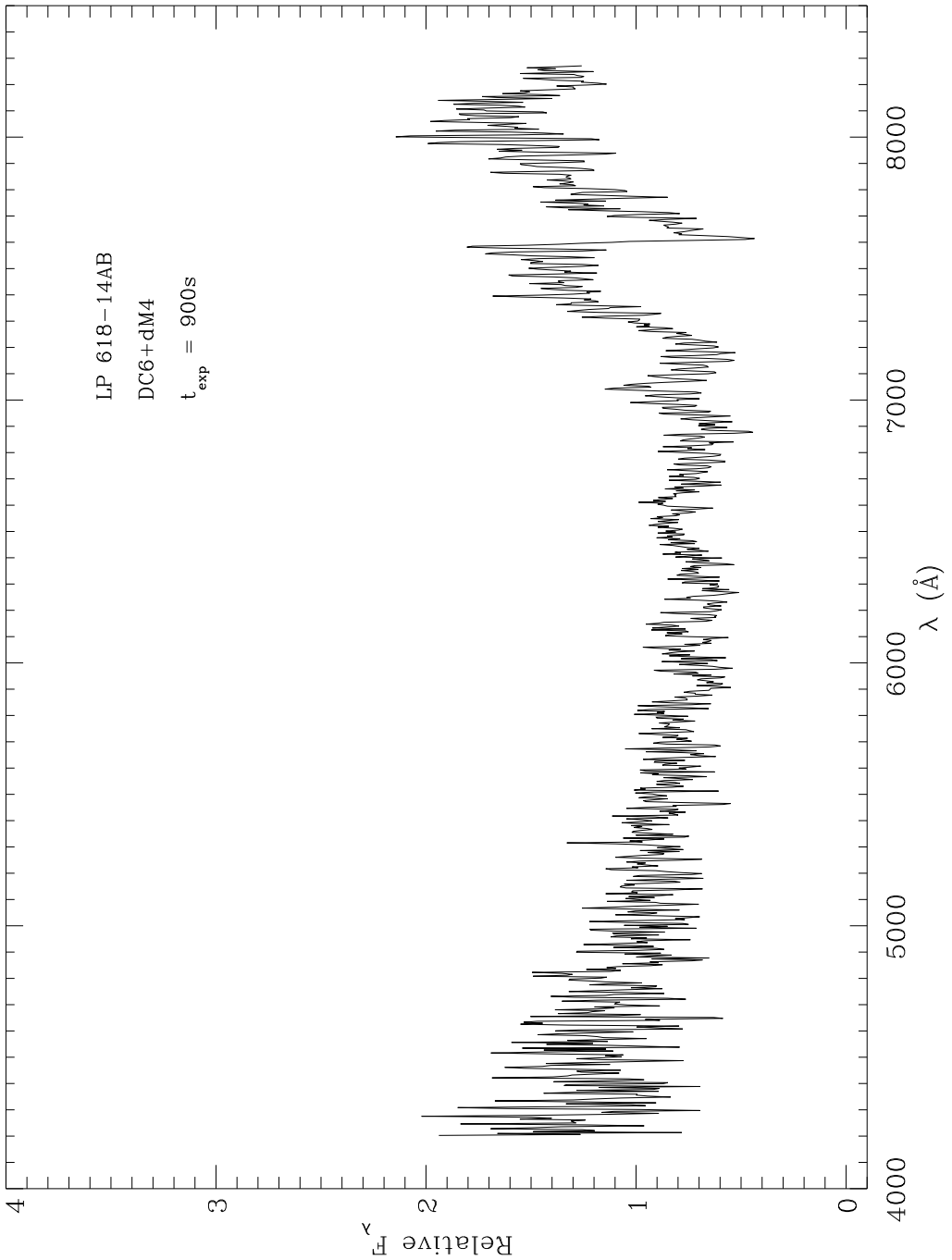

Figure 4.46: Optical spectrum of LP 618-14AB taken with the Boller & Chivens Spectrograph on the Bok 2.3 meter in April 2003.

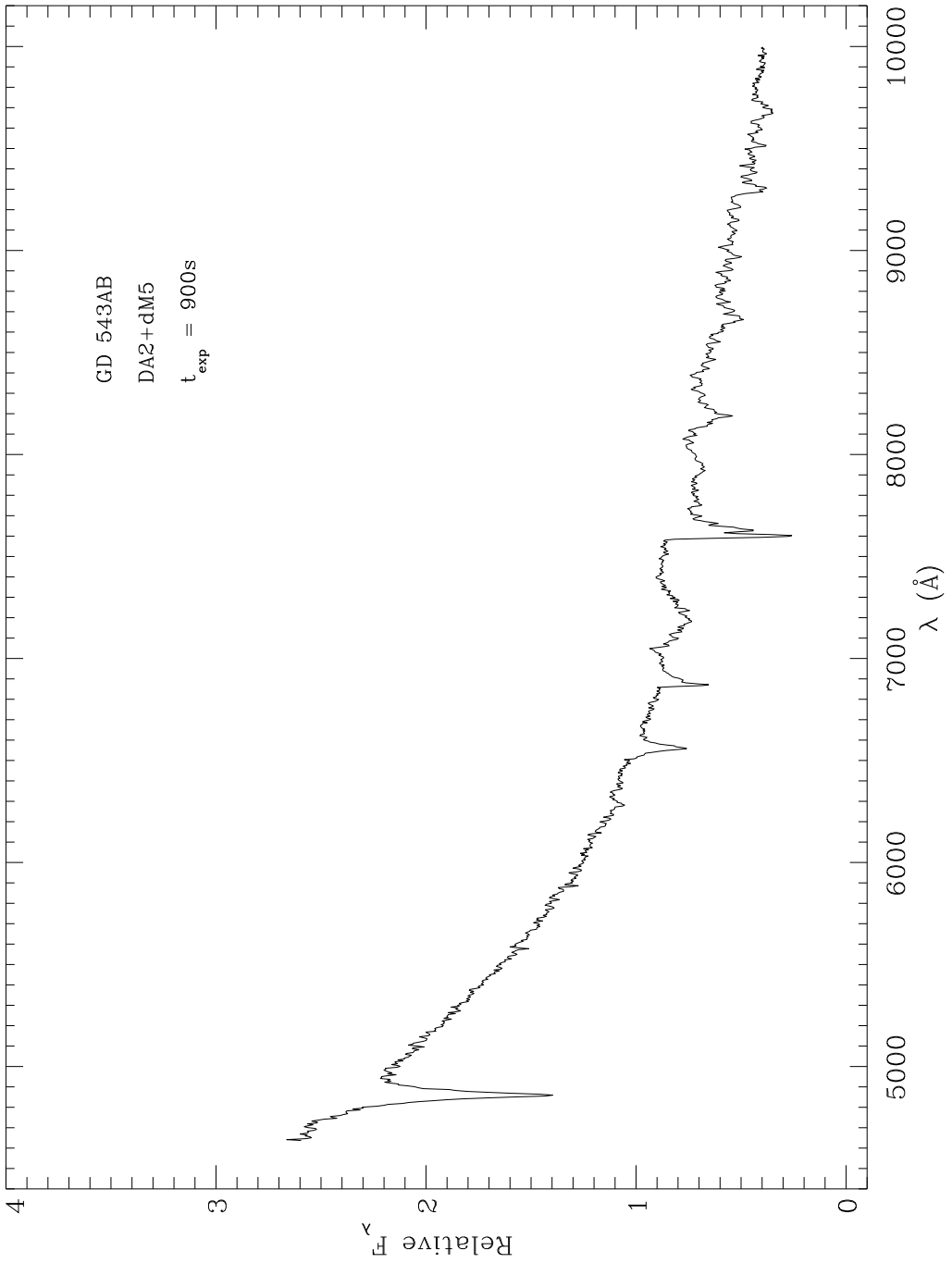

Figure 4.47: Optical spectrum of GD 543AB taken with the Kast Spectrograph on the Shane 3 meter telescope in August 2003.

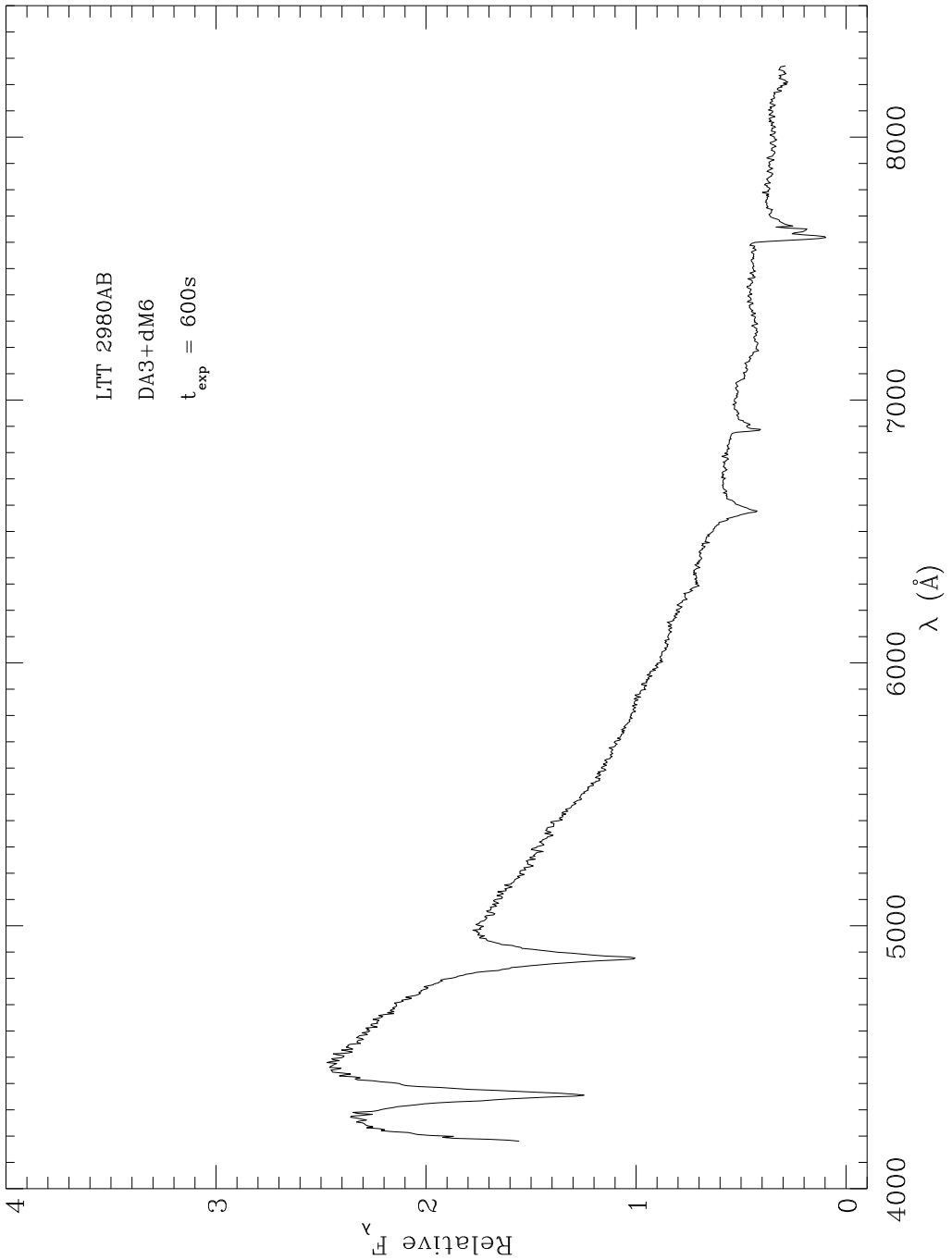

Figure 4.48: Optical spectrum of LTT 2980AB taken with the Boller & Chivens Spectrograph on the Bok 2.3 meter in April 2003.

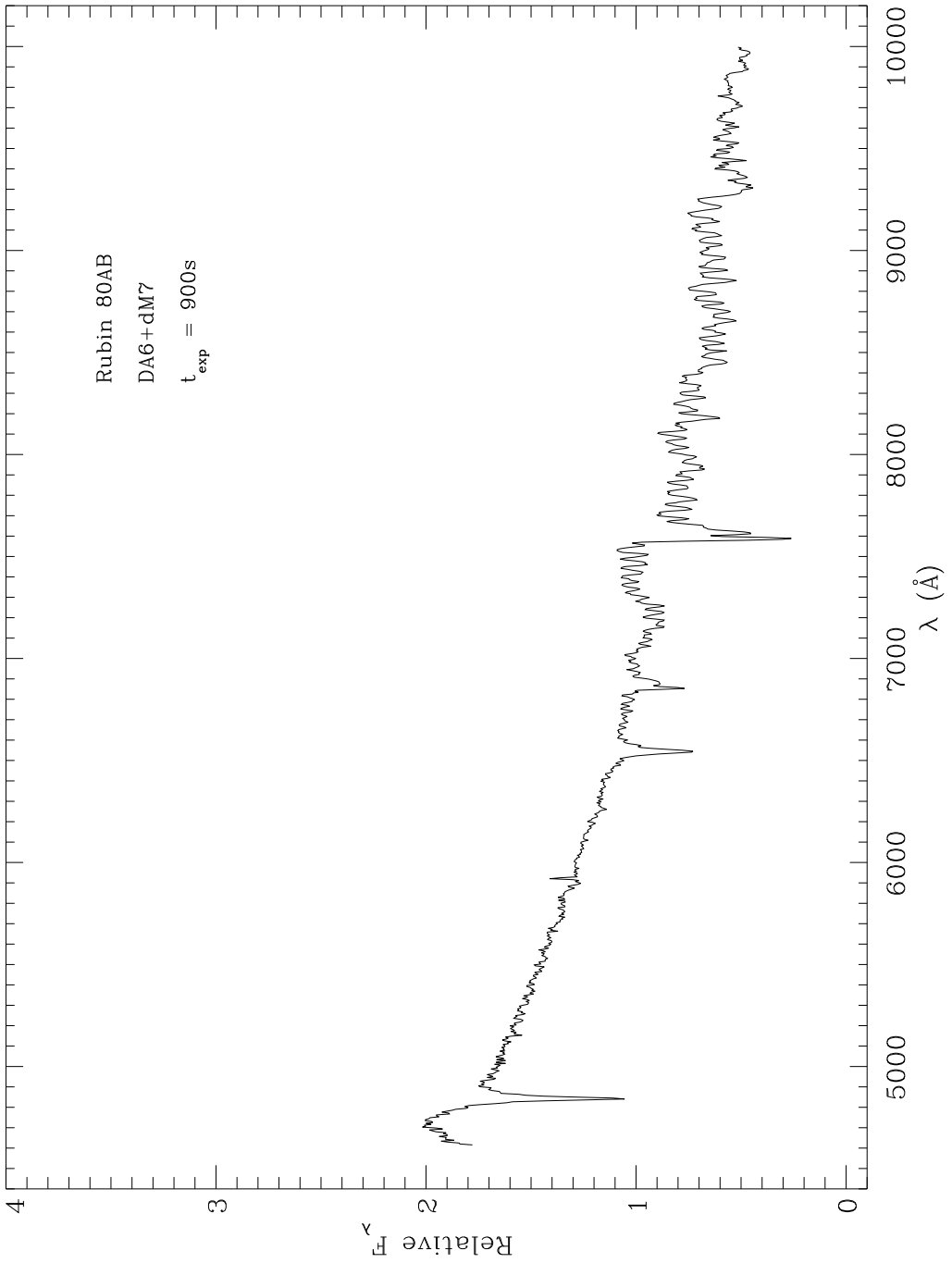

Figure 4.49: Optical spectrum of Rubin 80AB taken with the Kast Spectrograph on the Shane 3 meter telescope in August 2003.

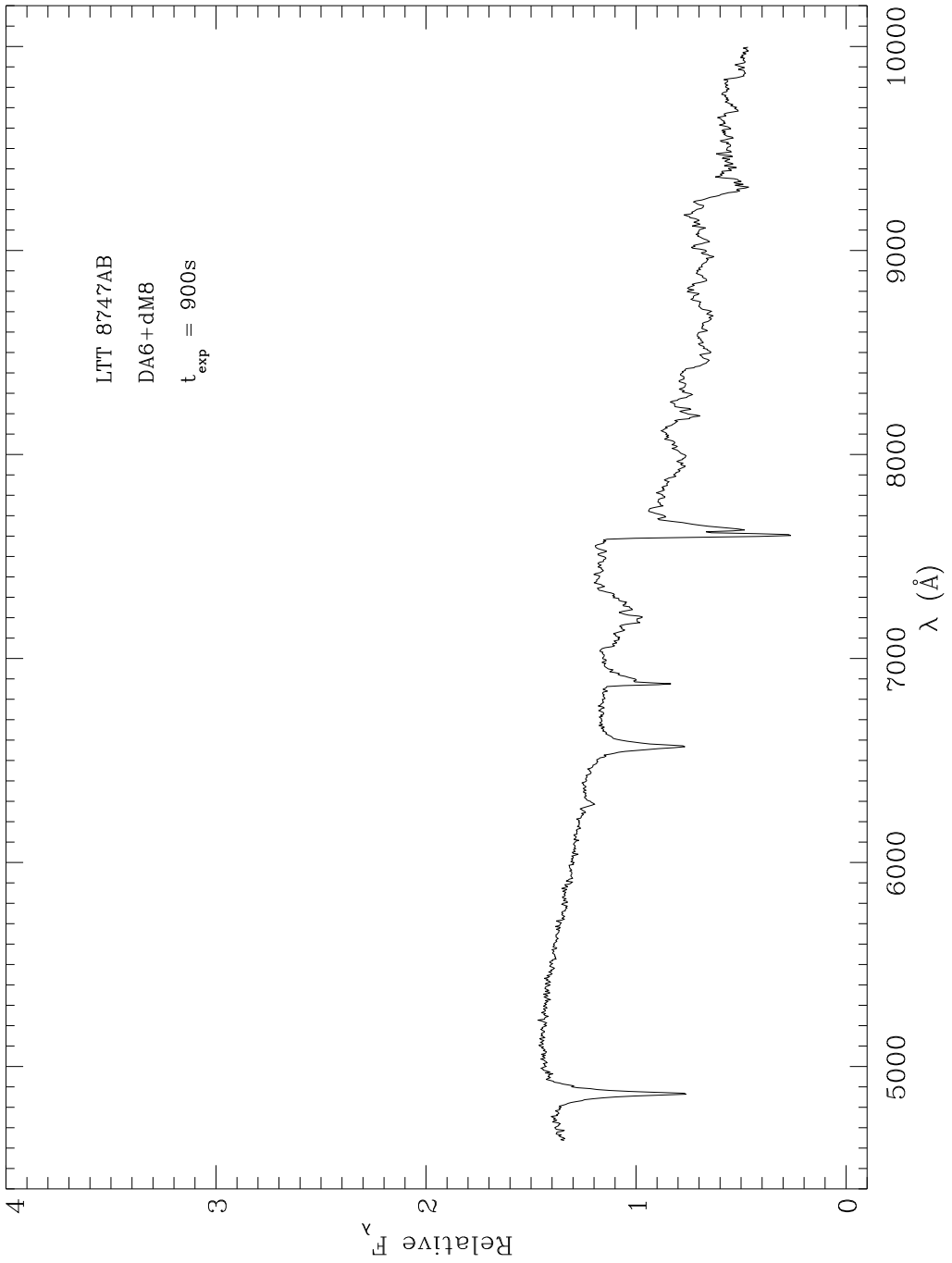

Figure 4.50: Optical spectrum of LTT 8747AB taken with the Kast Spectrograph on the Shane 3 meter telescope in August 2003.

4.7 Summary

Finally, Table 4.3 summarizes the primary, secondary, and tertiary (there is one quaternary also) components of the white dwarf multiple systems contained in the sample.

The first column gives the common name of the primary white dwarf component, followed by its spectral type in the second column. The third column gives the spectral type of a secondary or tertiary component. The fourth column is the distance to the system based on the best white dwarf distance determination. A few stars have trigonometric parallaxes, but the majority rely on photometric distances. The fifth column gives the projected separation in astronomical units or an upper limit if the system is unresolved. For radial velocity variables, a value of $a < 0.1$ AU is given. The last column gives the absolute K magnitude for red dwarf companions or the absolute V magnitude for white dwarf companions.

Table 4.5: Binary Summary Table

System	ST1	ST2	d	a (AU)	M_K or M_V
GD 360	DA2	DA	85.5	< 0.1	-
G1-45	DA5	DC	13.5	< 0.1	-
G21-15	DA4	DC	54.9	< 0.1	-
GD 429	DA4	DC	44.7	< 0.1	-
PG 1241−010	DA2	DC	88.7	< 0.1	-
PG 1428+373	DA5	DC	96.8	< 0.1	-
PG 0922+162	DA2	DA2	118.7	522	11.93
PG 1204+450	DA2	DA3	92.9	< 0.1	-
PG 0945+245	DA3	DAXP3	41.4	< 1.2	-
PG 1115+166	DA2	DB3	132.4	< 0.1	-
PG 1017+125	DA2	DA4	111.7	5450	11.59
GD 420	DA3	DA5	67.6	< 0.1	-
PG 0901+140	DA5	DA6	41.3	149	13.40
GD 559	DA3	DC6	63.9	1834	13.16
GD 322	DA3	DC7	60.3	941	13.65
G261-43	DA3	DC10	21.2	30	14.80
G21-15	DA4	DC11	54.9	3217	15.30
GD 392	DB4	DC14	57.8	2647	15.69
PG 1619+123	DA3	dG0	58.6	3709	3.00
EGGR 274	DA2	dG2	12.8	5535	3.39
PG 0824+288	DA1	dC	119.1	< 60	6.50
GD 319	sdB	dM	436.5	< 0.1	-
RE 1016−053	DAO1	dM1	108.1	346	5.35
RE 1016−053	DAO1	dM1	108.1	346	5.35
GD 683	DA2	dM2	95.5	10648	6.38

Table 4.5: Binary Summary Table

System	ST1	ST2	d	a (AU)	M_K or M_V
GD 984	DA1	dM2	120.2	< 60	6.92
LP 761-114	DC8	dM2	53.2	410	5.74
PG 0933+729	DA3	dM2	96.4	7797	6.46
PG 0950+185	DA2	dM2	201.4	222	5.28
PG 1210+464	DA2	dM2	139.3	< 70	5.46
PG 1539+530	DA2	dM2	173.0	467	5.84
PG 1643+143	DA2	dM2	150.0	< 75	6.09
PG 1659+303	DA4	dM2	53.5	8275	6.89
G130-5	DA3	dM3	17.6	3075	5.81
G163-50	DA3	dM3	25.8	7201	5.87
GD 51	DA2	dM3	83.6	< 42	6.70
LB 261	DA3	dM3	81.7	498	6.39
LTT 0329	DA3	dM3	63.4	< 32	6.63
PG 1015+076	DA2	dM3	179.5	8580	6.48
PG 1123+189	DA1	dM3	114.8	149	6.76
PG 1449+168	DA2	dM3	101.4	7939	5.94
PG 1608+118	DA2	dM3	89.9	270	6.50
PG 2131+066	DO1	dM3	398.1	119	6.48
RE 1629+780	DA1	dM3	57.3	< 29	6.39
Ton 1150	DA2	dM3	117.5	< 59	6.42
Ton S 392	DA1	dM3	278.0	334	7.23
G148-7	DA3	dM3.5	31.6	329	6.64
GD 319	sdB	dM3.5	436.5	54914	6.39
KPD 2154+408	DA2	dM3.5	92.5	< 0.1	7.35
LDS 678	DBQA5	dM3.5	11.2	306	7.16

Table 4.5: Binary Summary Table

System	ST1	ST2	d	a (AU)	M_K or M_V
LDS 826	DA5	dM3.5	20.0	132	7.10
PG 0824+288	DA1	dM3.5	119.1	393	7.03
PG 0933+025	DA2	dM3.5	133.7	< 67	6.87
PG 2244+031	DA1	dM3.5	407.4	978	7.03
GD 74	DA3	dM4	83.2	8309	8.19
GD 84	DQ6	dM4	33.1	2440	7.95
GD 245	DA	dM4	51.3	< 0.1	7.38
LP 618-014	DC6	dM4	86.3	< 86	8.87
PG 1049+103	DA2	dM4	109.1	< 55	7.32
PG 1204+450	DA2	dM4	92.9	7748	8.22
PHL 790	DA2	dM4	133.0	266	7.43
GD 13	DA2	dM4.5	82.4	387	8.63
GD 123	DA2	dM4.5	84.7	< 42	7.15
GD 267	DA2	dM4.5	75.5	672	7.78
GD 337	DA2	dM4.5	150.7	< 75	8.10
LHS 354	DA4	dM4.5	18.0	9064	7.47
LP 916-27	DB4	dM4.5	52.2	2800	6.32
LTT 3943	DA2	dM4.5	36.5	< 0.1	7.75
PG 0308+096	DA2	dM4.5	100.9	< 0.1	7.96
PG 0956+045	DA3	dM4.5	112.7	225	8.66
PG 1026+002	DA3	dM4.5	38.2	< 0.1	8.05
PG 1654+160	DB2	dM4.5	166.0	581	6.04
RE 1016−053	DAO1	dM4.5	108.1	< 0.1	7.86
GD 60	DA3	dM5	60.8	4147	8.34
GD 543	DA2	dM5	134.3	< 0.1	8.05

Table 4.5: Binary Summary Table

System	ST1	ST2	d	a (AU)	M_K or M_V
LHS 361	DC9	dM5	12.1	2394	8.77
LTT 2980	DA3	dM6	35.0	< 0.1	9.24
GD 448	DA3	dM7	92.0	< 0.1	9.65
Rubin 80	DA6	dM7	41.1	< 21	9.76
LDS 826	DA5	dM8	20.0	2054	10.37
LTT 8747	DA6	dM8	19.6	< 10	9.99
PG 1241−010	DA2	dM9	88.7	284	9.70
GD 165	DA4	dL4	31.5	117	11.66
GD 1400	DA4	dL6	39.3	< 12	12.13

Note– The absolute magnitudes listed in the final column are not measured quantities. They are based upon the photometric distance for the white dwarf primary. In a few cases, there exists a trigonometric parallax and the absolute magnitude for a companion may be considered accurate. Due to likely errors, a different approach is used to obtain absolute magnitudes and masses for red dwarf companions (§5.2.2).

CHAPTER 5

Analysis & Conclusions

In this chapter, analysis of the results is presented and conclusions are drawn from the entire data set. The initial mass function for low mass companions to intermediate mass stars is constructed, while examining possible biases due to potential changes in companion mass during the common envelope phase of stellar evolution. Although this work is somewhat unique, comparisons and contrasts with similar studies is made.

5.1 Companion Spectral Type Frequency

In Figure 5.1 is plotted the number of unevolved low mass companions versus spectral type for objects discovered in this work. Despite excellent sensitivity to late M dwarfs and early L dwarfs in all survey phases, very few were detected. For comparison, Figure 5.2 shows similar statistics for cool field dwarfs. Interestingly, Figures 5.1 & 5.2 are quite similar.

Hence, binary systems with small mass ratios ($q = M_2/M_1 < 0.05$) are rare for white dwarf progenitors (which typically have main sequence masses ~ 2 $M_\odot$). Although there exists some speculation regarding the possibility that brown dwarfs are ejected in the early stages of multiple system or cluster formation, there is currently no evidence of this occuring.

Although it is possible that very low mass companions ($M < 0.02$ $M_\odot$) to

intermediate mass stars become evaporated and/or cannibalized duing the AGB phase (just as the earth is predicted to experience in our own solar system), this is unlikely to be the case for the mass range in question here ($M > 0.04\ M_{\odot}$). In §5.5, the secondary masses in binaries which may have experienced a common envelope phase during the AGB of the white dwarf progenitor will be compared to those which did not.

In a way, the dearth of late M dwarfs alleviates a potential interpretation problem. Had it been the case that more late M dwarfs were detected and still only two L dwarfs, it might have been argued that the L dwarfs were cooling beyond the sensitivity of the search. Since all M dwarfs (and the first few L dwarf subclasses) at $\tau \geq 1$ Gyr are stellar according to theory, this concern does not exist. The measured dearth is real and is not caused by brown dwarf cooling and the resulting lower sensitivity.

5.2 The Companion Mass Function

Before constructing the observed mass function, there are some important issues to discuss. How will masses be determined? There do not exist dynamical masses available for these companions.

There are a few systems – close white dwarf plus red dwarf spectroscopic binaries – whose secondary masses have been estimated (Saffer et al. 1993; Marsh & Duck 1996; Maxted et al. 1998). This is not a mass measurement as it ultimately relies on models, and in fact, what is really measured in these systems is the mass ratio (hence the need for a white dwarf mass from models). But this method has been used successfully to estimate red dwarf masses that are consistent with both theory and existing dynamical mass measurements for low mass stars in the same

range of spectral types and temperatures.

5.2.1 Luminosity Versus Mass

For M spectral types, the works of Kirkpatrick, Henry, & McCarthy (1991); Henry & McCarthy (1993); Kirkpatrick & McCarthy (1994); Dahn et al. (2002) contain: (1) absolute magntudes as a function of spectral type; (2) mass versus luminosity relations; (3) spectral type as a function of mass based on all available dynamical measurements of very low mass stars. These empirical and semi-empirical relationships are for disk stars of intermediate age, which is appropriate for the sample of white dwarfs in this work. These relations have been used to provide masses for spectral types M1 through M9. It is unnecessary to extrapolate these empirical relations into the L dwarf regime, because only two white dwarf plus L dwarf systems are known and both companions have published mass estimates from models, based on likely age ranges (Kirkpatrick et al. 1999a; Farihi & Christopher 2004).

Figure 5.3 shows the first step in the construction process; mass versus K band luminosity relations from both models, empirical and semi-empirical results mentioned above. The models used are from Chabrier et al. (2000) and show tracks for ages of 1 and 5 Gyr, appropriate for young to intermediate disk ages. The minimum mass for hydrogen burning (HBMM) in these models is $M_{\rm HBMM} = 0.072\ M_{\odot}$. The track for 5 Gyr turns downward (relative to the track for 1 Gyr) before the stellar/substellar boundary because the lowest mass stars are still contracting onto the main sequence (Burrows et al. 1997, 2001; Chabrier et al. 2000). After the HBMM, the downturn is the result of brown dwarf cooling.

Dynamical masses have been measured down to spectral type M6 ($M = 0.10\ M_{\odot}$, Kirkpatrick & McCarthy 1994) for the ages appropriate here, but none lower.

Hence the empirical relation below this spectral type and corresponding mass is really semi-empirical. Adjustments had to be made according to the progess in this field over the past decade. For example, an extrapolation of the strictly empirical relation down to spectral type M9 predicts a clearly substellar mass of $M = 0.066\ M_{\odot}$. This is not currently accepted as correct for intermediate disk ages (Burrows et al. 1997; Chabrier et al. 2000).

5.2.2 Luminosity Versus Spectral Type

Figure 5.4 plots the absolute K magnitude versus spectral type for all the low mass stellar and substellar companions discovered in this work. Also plotted in the same figure is the combined empirical relation of Kirkpatrick & McCarthy (1994) and Dahn et al. (2002), both based on parallax measurements.

This figure demonstrates potentially inaccurate distances for many of the white dwarf primaries and is the major reason why absolute magnitude was not used as a proximate for mass in this work. Unlike previous work (Zuckerman & Becklin 1992) and similar studies (Green, Ali, & Napiwotzki 2000) – both of which employed M_K as an indicator of spectral class – this work uses spectral class itself. The reasons for this are twofold. First, in many cases photometric distances for white dwarfs are inaccurate for a variety of reasons that will not be discussed here in detail. In short, because white dwarfs have varying radii, their distances cannot be estimated with as much confidence as main sequence stars. Binarity can also cause a white dwarf to appear closer to the earth than it really is. In one recent study, it was concluded that, in general, the published photometric distance is an overestimate of the distance found by trigonometric parallax, though the sample size was quite small with only 6 stars (Smart et al. 2003). Secondly, M_K is a proximate for luminosity, not for temperature. Color

and spectral type are temperature indicators and do not require a precise distance determination. For stars, the temperature can be used with an HR diagram (i.e. an empirical radius versus temperature relation) to calculate a mass. This is, in essence, what has been done for this work.

There is no reason to indicate that these low mass stellar companions belong to the metal poor, Population II. With perhaps one or two exceptions discussed in chapter 6, all of these stars have published spectra (in this work or elsewhere) which are consistent with solar metallicity. Therefore the combined correlation between absolute magnitude and spectral type of Kirkpatrick & McCarthy (1994) and Dahn et al. (2002), for low mass field stars of intermediate disk age and solar metallicity, will suffice to confidently predict secondary masses.

5.2.3 Spectral Type Versus Mass

The last step is to combine the empirical and semi-empirical relations of Figures 5.3 and 5.4. Figure 5.5 shows the resulting correlation between spectral type and mass using the work discussed in the preceeding sections. Figure 5.6 is the histogram of the number of detections versus companion mass, using the correlation data in Figure 5.5.

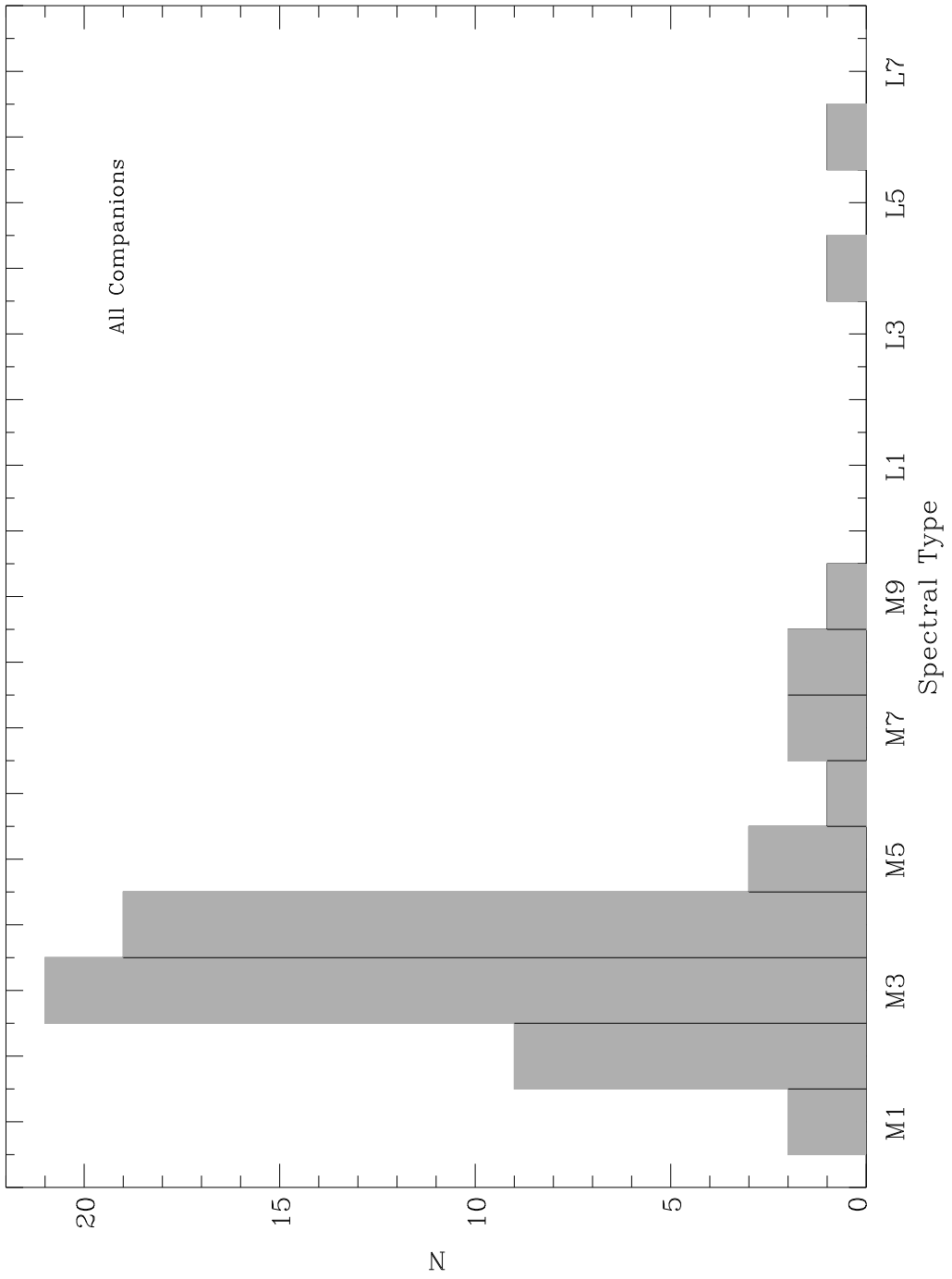

Figure 5.1: The number of red dwarf companions disovered in this study versus spectral type.

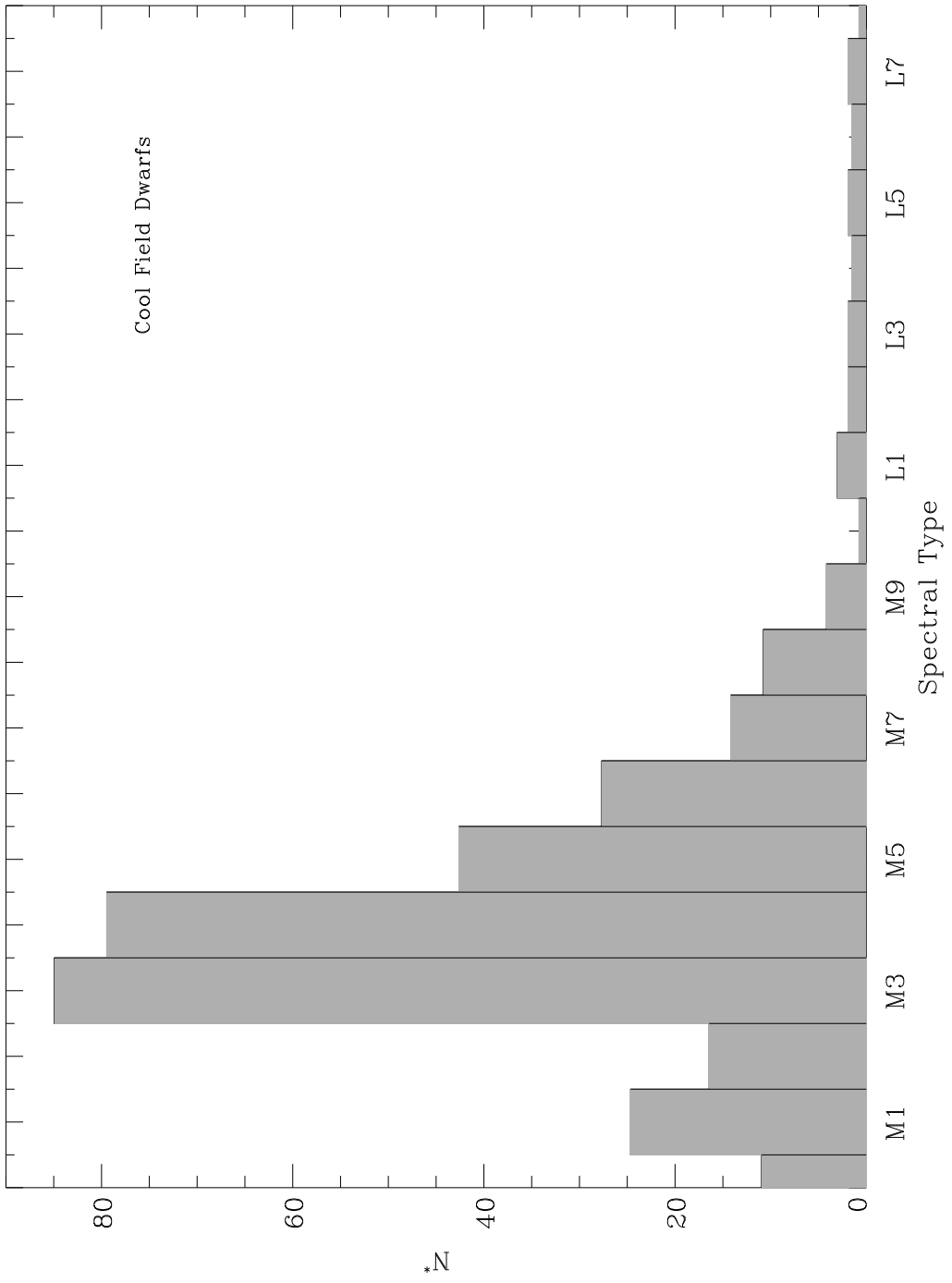

Figure 5.2: The number of cool field dwarfs within 20 pc versus spectral type. The statistics come from Reid & Hawley (2000); Cruz et al (2003) and have been corrected for volume, sky coverage, and estimated completeness

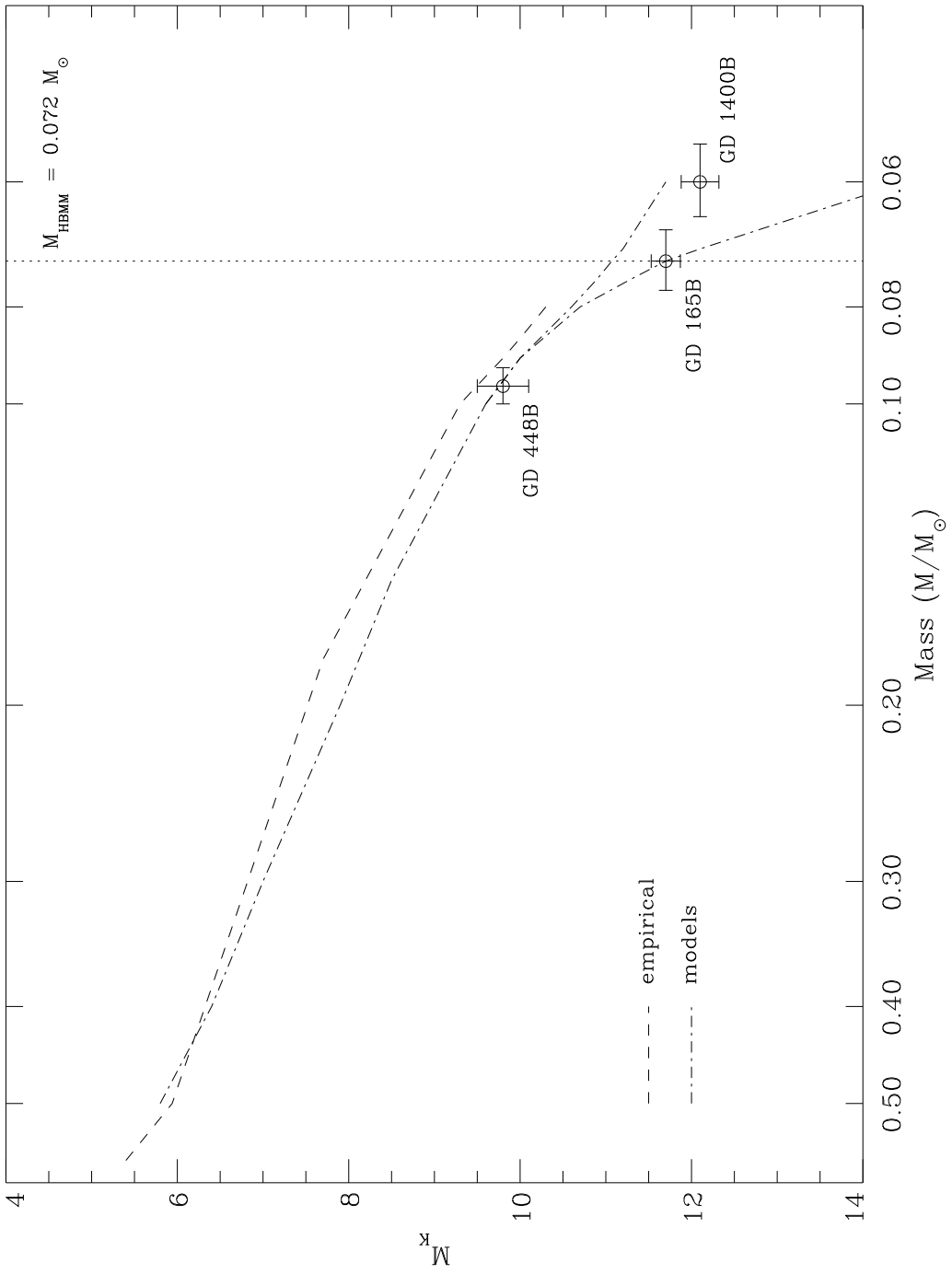

Figure 5.3: Empirical and model relations between absolute K band magnitude and mass. Three very cool companions to white dwarfs with mass estimates are shown along with 1 and 5 Gyr brown dwarf model cooling tracks.

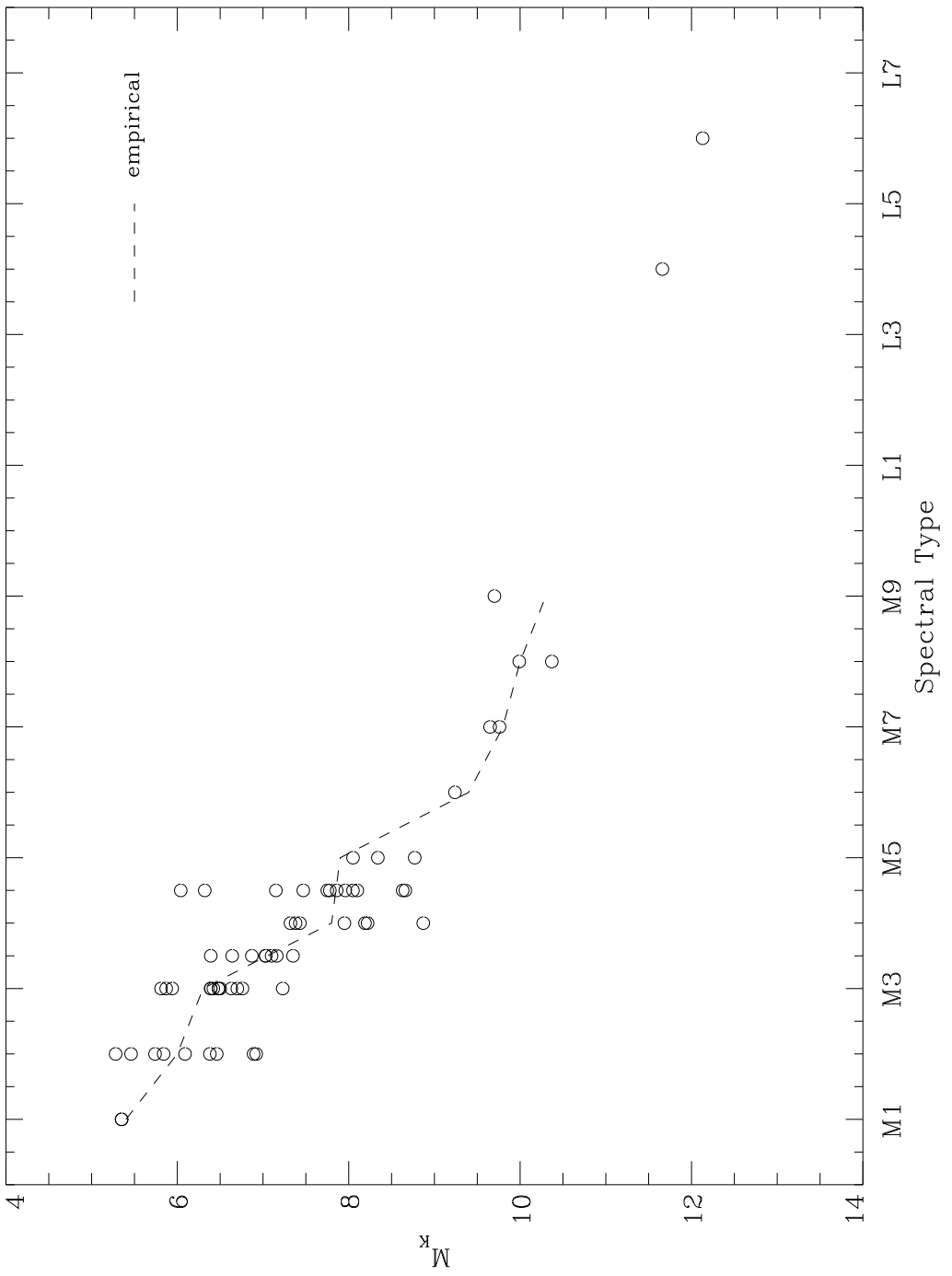

Figure 5.4: Absolute K magnitude versus spectral type for all low mass companions based on the white dwarf distance. The dashed line is the relation of Kirkpatrick & McCarthy (1994).

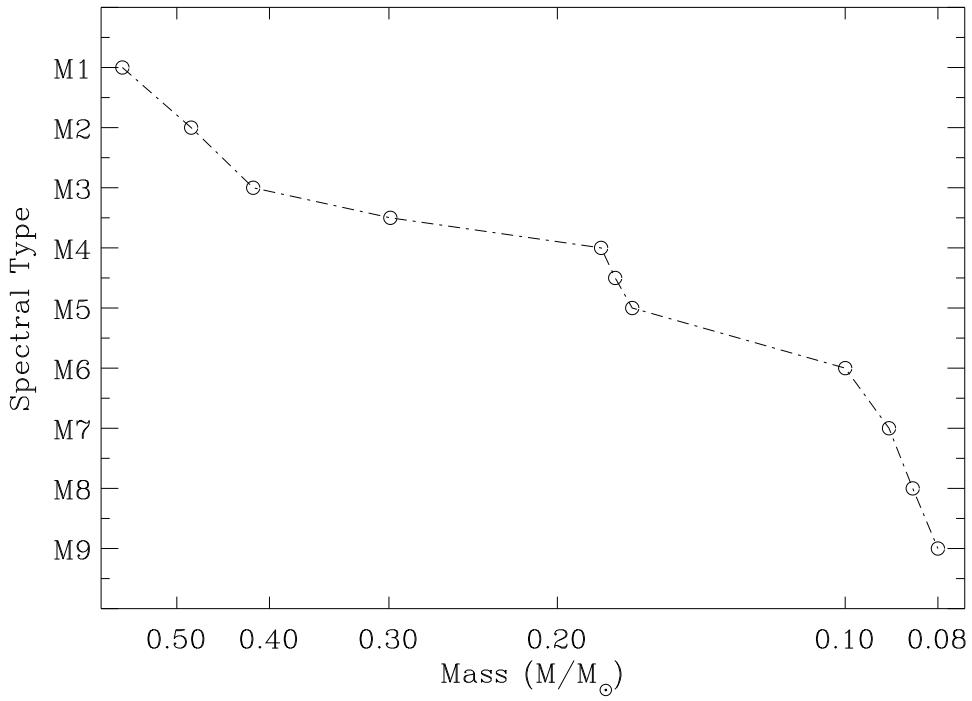

Figure 5.5: Spectral type correlation with mass used for constructing the companion mass function. Data points represent the nodes in the constructed correlation function. These points are from the empirical and semi-empirical relations of Henry & McCarthy (1993); Kirkpatrick & McCarthy (1994); Dahn et al. (2002), corrected for progress in the field and the best available models (Burrows et al. 1997; Chabrier et al. 2000).

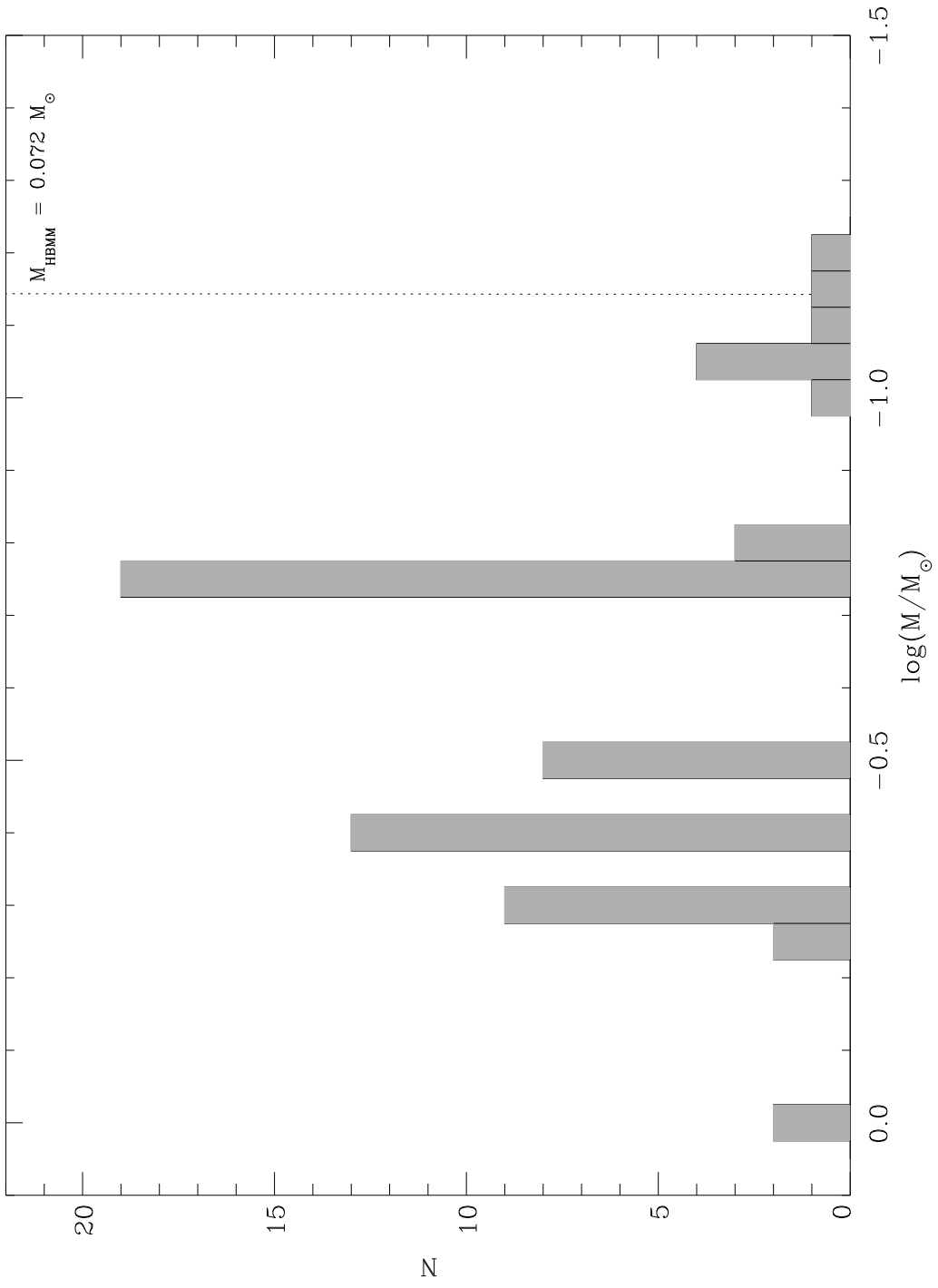

Figure 5.6: Detected companion mass function. The two wide G dwarf companions are included.

5.3 Sensitivities

In this section is discussed the overall mass sensitivity implied by the completeness of the survey in its various parts and intrinsic biases.

For low mass stellar companions, age is not an issue. But for substellar objects, any determination of mass sensitivity must include an age estimate. In §3.5 a likely age range for the sample was estimated to be $2 - 5$ Gyr based on the overall kinematics and cooling ages. Since the ages cannot be known with certainty, this range will be assumed, and calculations done for ages of 1 and 5 Gyr.

The average distance for the sample, was calculated to be 57 pc in §3.5. This distance will be used for determining overall mass completeness using the models of Chabrier et al. (2000). Obviously, the sensitivity changes for objects which are closer or farther and the standard deviation of the entire sample is significant at $\sigma_d = 47$ pc. Yet the masses, temperatres and spectral classes implied by the completeness limits for each phase of the survey (at the average distance of the sample stars) epitomize what was detectable. Table 5.1 summarizes these completeness limits.

5.3.1 IRTF

Zuckerman & Becklin (1992) report a completeness down to $K = 15$ mag. However, this completeness was limited by single detectors prior to the availability of near infrared cameras (Zuckerman & Becklin 1987a). All of the objects in Table 3.1 that were observed during this phase of the survey were imaged with arrays. For spatially resolved objects, a conservative completeness limit for these observations is $K = 16$ mag. Applying this limit at 57 pc for the 84 white

dwarfs observed in this early part of the survey (but not re-observed at Steward or Keck), these observations were complete to $M_K = 12.2$ mag. This corresponds to a spectral type near L6, $T_{\rm eff} \sim 1650$ K, and $M = 0.060 - 0.070\ M_\odot$ for $1 - 5$ Gyr (Reid et al. 1999; Kirkpatrick et al. 2000; Dahn et al. 2002; Chabrier et al. 2000; Vrba et al. 2004). GD 165B was discovered amongst the first observations in the program at $K = 14.2$ mag and has a mass estimated at $M = 0.072\ M_\odot$ (Kirkpatrick et al. 1999a).

5.3.2 Steward

The Steward survey was complete to $J = 18$ mag. For the 261 white dwarfs imaged in this program, this implies a completeness down to $M_J = 14.2$ mag at 57 pc. This corresponds to a spectral type around L7, $T_{\rm eff} \sim 1500$ K, and $M = 0.053 - 0.068\ M_\odot$ for $1 - 5$ Gyr (Reid et al. 1999; Kirkpatrick et al. 2000; Dahn et al. 2002; Chabrier et al. 2000).

5.3.3 Keck

The Keck survey was complete to $J = 21$ mag. For the 86 white dwarfs imaged in this program, this implies a completeness down to $M_J = 17.2$ mag at 57 pc. This corresponds to spectral types later than T8, $T_{\rm eff} < 750$ K, and $M \sim 0.020 - 0.040\ M_\odot$ for $1 - 5$ Gyr (Vrba et al. 2004; Leggett et al. 2002; Chabrier et al. 2000).

5.3.4 Infrared Excess

As mentioned in §2.5, all 372 sample stars were searched for infrared excess emission between $1 - 2\ \mu$m using the 2MASS all sky catalogue database. 2MASS provides a highly accurate, uniform and consistent method for this type of search.

Higher sensitivity to unresolved companions was not gained at Keck or Steward for two reasons: (1) the white dwarf was sometimes saturated in the attempt to image faint companions, especially at Keck; (2) infrared excess detection requires photometric accuracy, not deep imaging.

The averge temperature of a white dwarf in the sample is $T_{\rm eff} = 13,000$ K. This yields $M_H = 11.8$ mag, $M_K = 11.9$ mag for a white dwarf of typical mass (log $g = 8.0$, Bergeron, Saumon, & Wesemael 1995). The 2MASS all sky catalogue provides reliable photometry (SNR > 10, $\sigma > 0.1$) down to $H = 15.1$ mag and $K_s = 14.3$ mag for 100% of the sky and to $H = 15.6$ mag and $K_s = 14.8$ mag for 50% of the sky.

Taking the average of these H & K_s limiting magnitudes at 57 pc, an excess of 170% above the white flux would be detectable at $M_K = 10.8$ mag ($K_s = 14.5 mag$). This yields $M_K = 11.3$ mag for a cool companion, which is around spectral type L4. However, the sensitivity to excess emission is much greater at H. At 57 pc, an excess of 21% is detectable at $M_H = 11.6$ mag ($H = 15.3$), which yields $M_H = 13.5$ mag for a low mass companion. This corresponds to spectral type L8, $T_{\rm eff} \sim 1400$ K, and $M = 0.050 - 0.066\ M_\odot$ for $1 - 5$ Gyr (Reid et al. 1999; Kirkpatrick et al. 2000; Dahn et al. 2002; Chabrier et al. 2000).

The case of GD 1400B proves this point. Estimated at spectral type L6, it was detected using the 2MASS database in a manner identical to that performed for all 372 stars in the entire sample. Not included in the thesis sample, it was first identified by Wachter et al. (2003) in the initial phase of a search utilizing the 2MASS point source catalog to survey the entire sky near the positions of all white dwarfs in McCook & Sion (1999). Farihi & Christopher (2004) were the first to distinguish GD 1400 from the bulk of white dwarfs with near infrared excess emission and identify the companion.

Table 5.1: Survey Completeness for $d = 57$ pc, $\tau = 3$ Gyr

Survey	a_{in} (AU)	a_{out} (AU)	M_{abs} (mag)	ST	Mass ($M_{\odot}$)	N
IRTF	0	700	$M_K = 12.2$	L6	0.065	84
Steward	110	4700	$M_J = 14.2$	L7	0.060	261
Keck	55	1100	$M_J = 17.2$	T9†	0.030	86
All	0	110	$M_H = 13.5$	L8	0.058	372

Note– This table presents the average values. For some targets in the Steward survey, separations greater than 5000 AU were probed with less sensitivity. For some targets in the Keck survey, only separations less than 600 AU were searched, but with greater sensitivity.

† There are no objects yet known with spectral types later than T8. However, the average limiting magnitude of the Keck survey probed ~ 1.5 magnitudes deeper than that possessed by any known brown dwarf (Vrba et al. 2004; Leggett et al. 2002).

5.4 Biases

None of the searches were sensitive to companions beyond the field of view of the corresponding cameras. For the IRTF, only objects within roughly $12''$ of the white dwarf were detectable. The NIRC and Steward IR Camera fields of view are $19.2''$ and $83.2''$ in radius. This implies, on average, probing separations out to 4700 ± 3900 AU for the Steward survey but only out to 1100 ± 900 AU for the Keck survey. Therefore, the survey was biased against any low mass companions beyond ~ 8500 AU.

Generally speaking, M and L dwarfs were detectable at arbitrarily close physical separations (§5.3.4). However, T dwarfs are generally not detectable by infrared excess unless the white dwarf is quite cool or quite massive ($T_{\rm eff} < 7000$ K for $\log g = 8.0$, or $T_{\rm eff} < 9000$ K for $\log g = 8.5$). There were few stars in the sample meeting this criteria and therefore T dwarfs were only detectable if resolved.

In order that these cooler brown dwarfs be resolved at Keck required a separation on the sky of $\sim 1''$ (with typical Mauna Kea seeing) and at Steward $\sim 2''$ (with typical Kitt Peak seeing). However, no objects in this category were detected. Therefore, separations down to $55 - 110$ AU were probed for brown dwarfs not detectable by infrared excess.

On the brighter side, unresolved dwarf stellar companions earlier than around M1 ($M_V = 9.3$) were almost certainly selected against. Depending on the luminosity of the white dwarf, it is possible for a G−K dwarf or even an M0 dwarf to mask the presence of a nearby degenerate at optical wavelengths. These types of binaries are likely selected against in surveys which identify and catalogue nearby white dwarfs. This explains the drop off at the higher mass end of Figures 5.1 and

5.6. However, the study was not biased against wide yellow dwarf companions and two of the white dwarfs in the sample were found to have such secondaries.

5.5 Current Mass Versus Initial Mass

In order to measure the initial mass function for companions to intermediate mass stars, a critical question remains: are the red dwarf masses observed today the same as the initial masses when the binary was formed?

5.5.1 Post Common Envelope Binaries

When intermediate mass main sequence stars, the progenitors of white dwarfs, ascend the asymptotic giant branch, their photospheres expand by a factor of roughly 200. The relatively dense region of material being lost by wind and expansion is called its envelope. If such an AGB star has a relatively close main sequence companion within this ($R \sim 1 - 2$ AU) region, the pair is said to share a common envelope. Generally speaking, such a close binary pair will transfer much of its orbital energy (via angular momentum) into the common envelope through friction, resulting in the ejection of the envelope from the system and an inspiral to a smaller binary binding energy and separation (Paczynski 1976).

It has been theorized that a low mass companion may accrete up to 70% of its final mass during a common envelope phase or may evaporate completely during the inspiraling process, depending on the initial masses and separations of both components (Livio & Soker 1984). Hence, there is a possibility that the masses of red dwarf secondaries in close binaries are not their initial masses. There is no concensus on the topic unfortunately. There appears to be evidence in support of the idea that post common envelope binary secondaries do accrete a significant

amount of mass during the common envelope phase (Drake & Sarna 2003). Yet there also appears to be evidence as well that they emerge unaffected (Maxted et al. 1998).

5.5.2 Subgroup Comparisons

In Figures $5.7 - 5.11$ are displayed the number of low mass companions detected versus spectral type (same as Figure 5.1 for all companions) for various subgroups. The first subgroup (Figure 5.7) is all resolved binary companions. The second subgroup (Figure 5.8) is all known radial velocity variable binary companions – these are the post common envelope binaries. The third subgroup (Figure 5.9) is all unresolved binary companions that are not known to be radial velocity varibles. Hence this subgroup is an unknown and perhaps as many as 100%, or as few as 0% of these systems are post common envelope binaries. The fourth subgroup (Figure 5.10) supposes that subgroup three binaries are all wide ($a >$ 5 AU), whereas the fifth subgroup (Figure 5.11) supposes that subgroup three binaries are all close ($a < 0.1$ AU).

Do these figures provide any evidence that post common envelope binary secondaries have accreted a significant amount of mass (correlated here with spectral type)? If so, it is not obvious. Denoting the subgroups $1 - 5$ as above, the average spectral types in each subgroup are listed in Table 5.2. If anything, evidence may point to the contrary; that in fact, the average masses are *smaller* for the confirmed and potential post common envelope binaries.

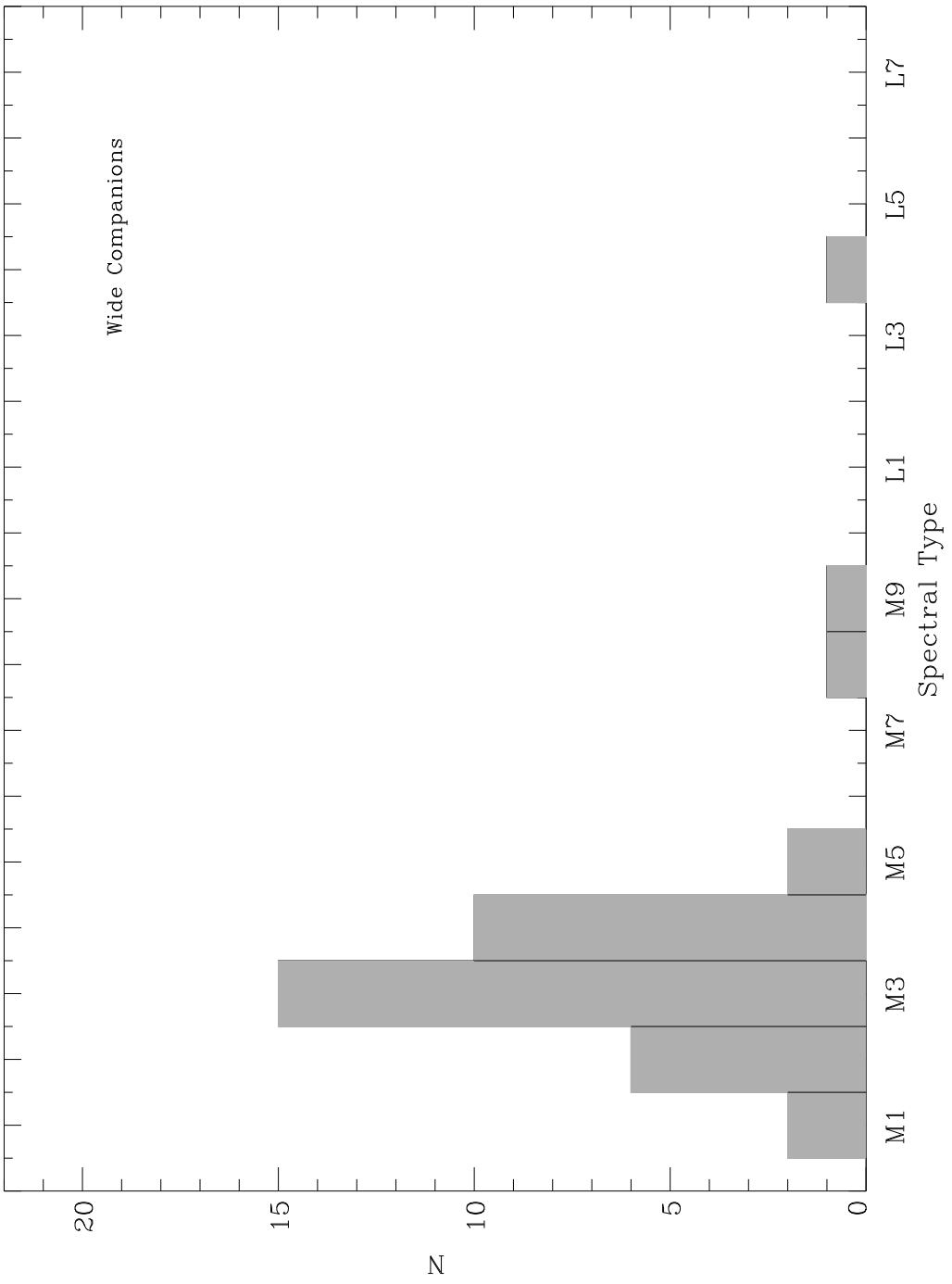

Figure 5.7: Same as Figure 5.1 but for wide binary companions only.

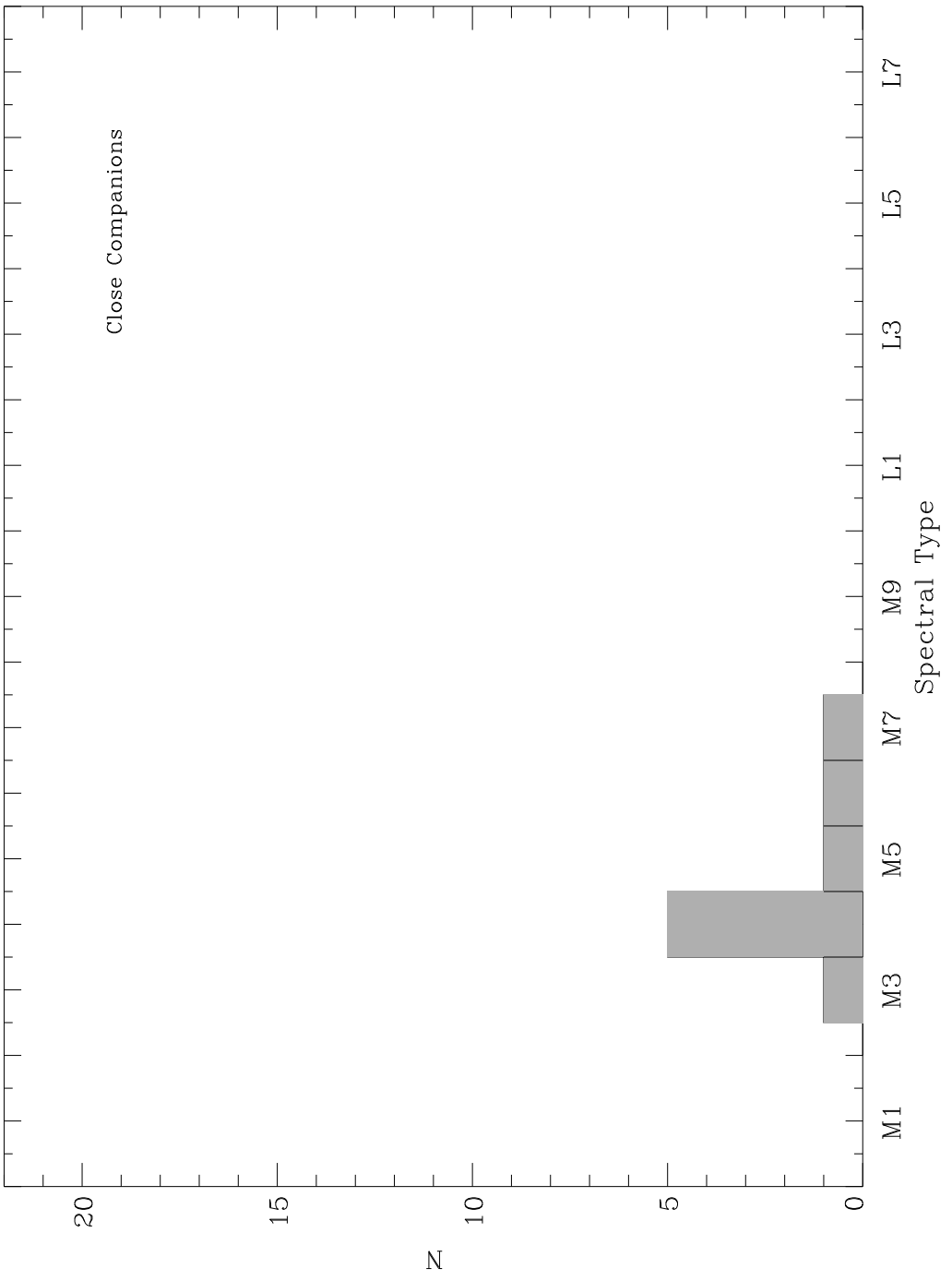

Figure 5.8: Same as Figure 5.1 but for known close binary companions only.

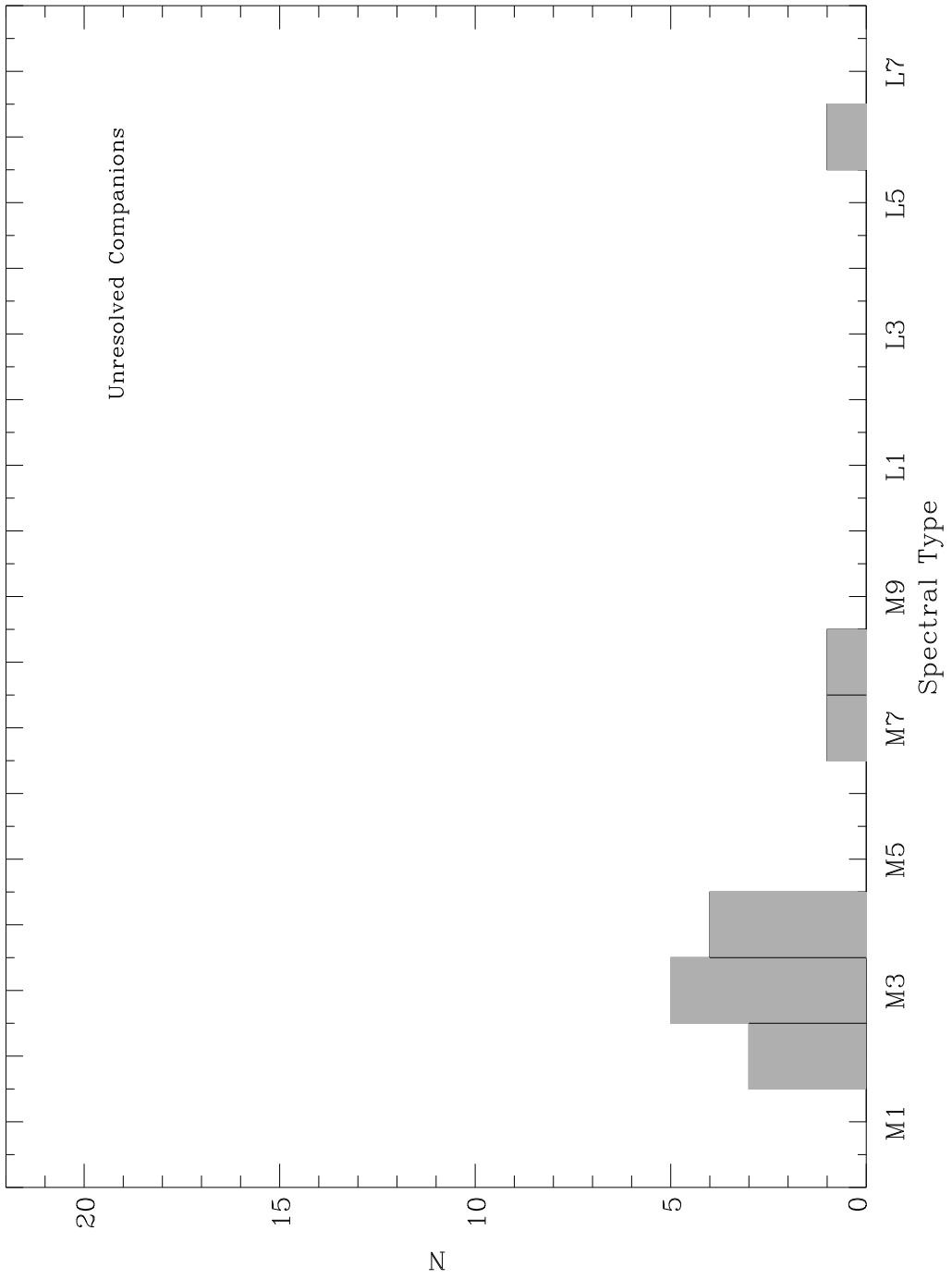

Figure 5.9: Same as Figure 5.1 but for unresolved companions which are not known to be radial velocity variables.

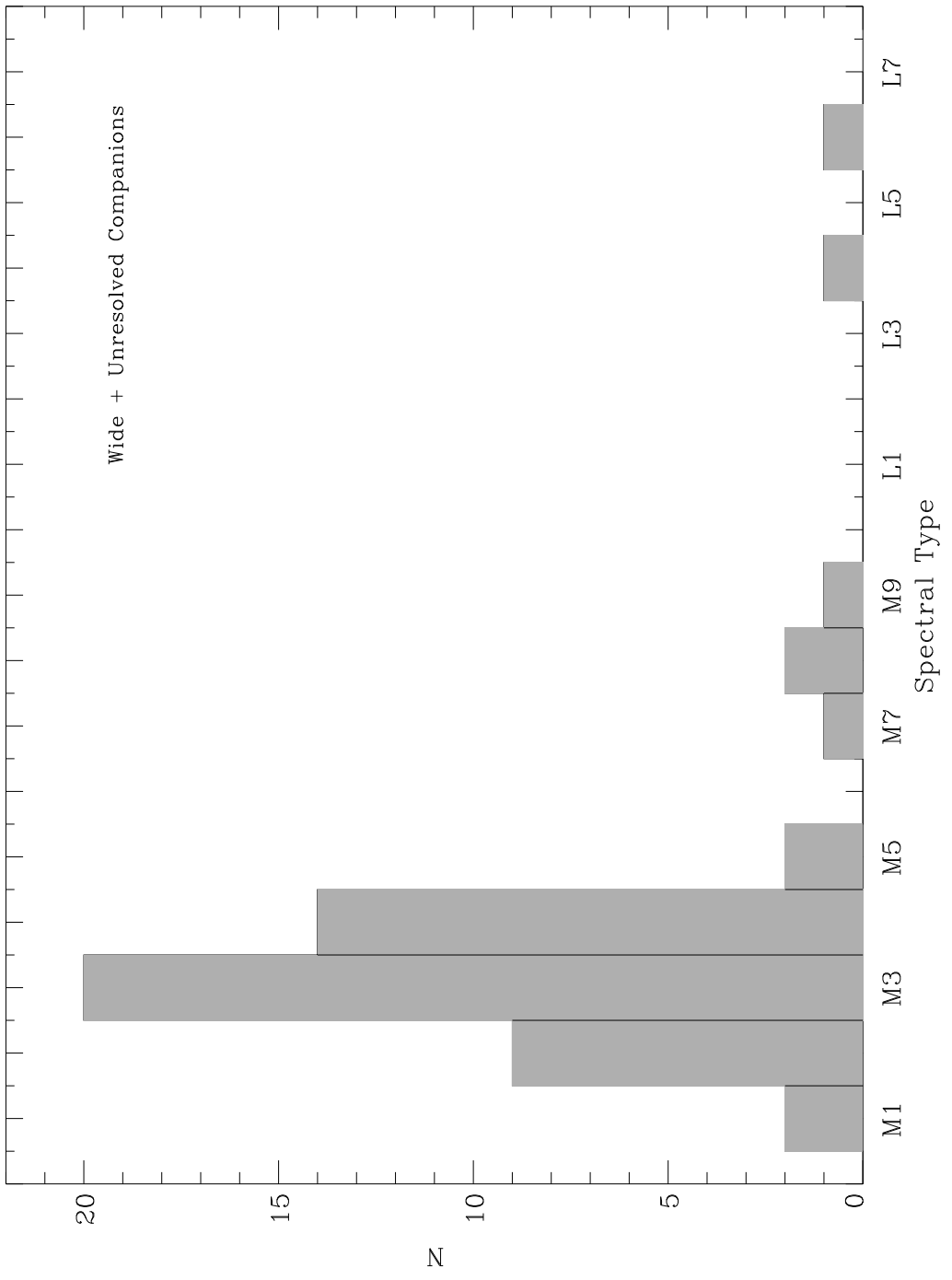

Figure 5.10: Same as Figure 5.1 but for all potential wide binary companions.

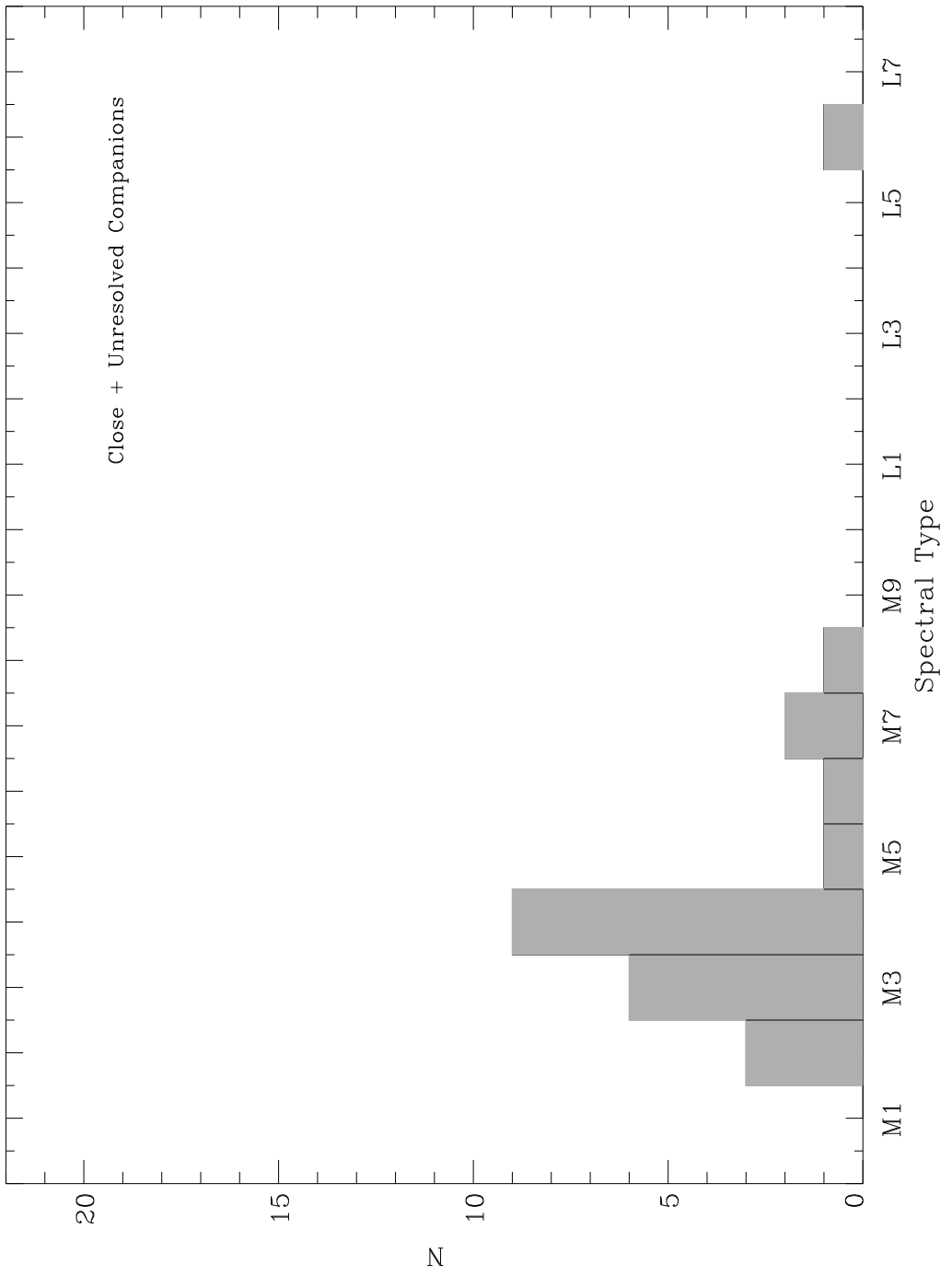

Figure 5.11: Same as Figure 5.1 but for all potential close binary companions.

Table 5.2: Subgroup Average Companion Spectral Types

Subgroup	Description	$< ST >$	N
0	All	M4.2	62
1	Resolved	M3.8	38
2	Close	M4.8	9
3	Unresolved / not Close	M4.6	15
4	Groups $1 + 3$	M4.1	47
5	Groups $2 + 3$	M4.7	24

5.6 Conclusions

Together, the various phases of this survey discovered over 40 previously unrecognized white dwarf binary and multiple systems. The wide field, common proper motion survey alone discovered at least 20 new white dwarf multiple systems. The conclusions follow.

5.6.1 The Initial Companion Mass Function

Based on the analysis of the §5.5.2, there is no reason why all the companion masses should not be included in the initial mass function. Therefore, Figure 5.6 is a good measure of the initial mass function for companions to intermediate mass stars.

5.6.2 Substellar Companion Fraction

Before proceeding to an estimate of the substellar companion fraction, GD 1400B must be discussed. Although not included in the thesis sample, it is a very important datum in the overall statistics of low mass companions to white dwarfs – a long, hard, and much sought after datum.

GD 1400 is a white dwarf not unlike white dwarfs in the thesis sample, with $T_{\rm eff} = 11,600$ K, $\log g = 8.1$, and a moderate proper motion of $\mu \approx 0.05''$ yr^{-1} (Koester et al. 2001; Fontaine et al. 2003; Zacharias et al. 2004). Hence its inclusion here is not inconsistent with the sample stars, nor the search methods and resultant sensitivities (§5.3.4). Due to these consistencies and the fact that GD 1400B is a vital statistic, it has been included in the analyses and conclusions.

The calculated fraction of white dwarfs with substellar companions, within the range of masses and separations to which this work was sensitive, is $f_{bd} =$

$0.4 \pm 0.1\%$. This represents the first measurement of the low mass tail of the companion mass function for intermediate mass stars, main sequence A and F stars (plus relatively few B stars) with masses in the range $1\ M_{\odot} < M < 8\ M_{\odot}$. This value is consistent with similar searches around solar type main sequence stars for comparable sensitivities in mass and separation (Oppenheimer et al. 2001; McCarthy & Zuckerman 2004)

5.6.3 Star Formation

Therefore the process of star formation hinders the production of very low mass ratio binaries, made clear by the relative dearth of both L dwarfs and late M dwarfs discovered in this work.

APPENDIX A

Individual Systems

In this chapter, topics related to individual systems of astrophysical interest are presented. In somewhat logical order, these are discussions of: unrelated proper motion stars; candidates which are not companions; candidates which may be companions; and noteworthy confirmed multiple systems. This chapter should be of particular interest to those doing research on white dwarfs, subdwarfs, wide and visual binaries, proper motion or all of the above.

A.1 Non Degenerates

The following is a list of stars in the sample which are not white dwarfs; many of the stars so noted in Table 3.1. For these stars, no reference in the literature can be found explicitly correcting the misclassification and the correct classification is presented here. They are listed as white dwarfs in the catalog of McCook & Sion (1999) and also in the same current online catalog.

A.1.1 G187-9

G187-9 is classified as type DC (McCook & Sion 1999), but it was classified more or less correctly as early as 1967 (Wagman 1967). It has spectral type M2 and $M_V = 11.27$ mag (Reid, Hawley, & Gizis 1995). A main sequence M2 star has

$M_V = 10.2$ mag and hence G187-9 is subluminous, and by definition a subdwarf. It also has a high proper motion of $\mu = 0.7''$ yr^{-1}.

A.1.2 GD 617 & PG 0009+191

GD 617 is classified as type DAB5 (Greenstein 1984; McCook & Sion 1999) but has been reclassified as a very hot subdwarf showing Balmer lines, neutral helium, and continuum flux from an unresolved F/G star (Lamontagne et al. 2000). Photometry verifies the probability of an unresolved main sequence companion. It has $V - K = +0.8$, which is too red for a single hot helium burning star. Hence GD 617 is very likely type sdB+F/G.

PG 0009+191 is classified as type DA (Green, Schmidt, & Liebert 1986; McCook & Sion 1987) but does not appear in McCook & Sion (1999). There exists nothing in the literature to indicate why it is absent from the white dwarf catalog, but the absence itself hints at probable non degeneracy. The spectrum of PG 0009+191 is shown in Figure 6.1 and it appears to be a hot subdwarf, type sdB.

A.1.3 PG 1126+185 & PG 0210+168

PG 1126+185 is classified as type DC8 (Green, Schmidt, & Liebert 1986; McCook & Sion 1999). It was reclassified as DC+G/K by Putney (1997), a puzzling combination of posited spectral types. It is not possible to detect a DC star (cool helium atmosphere white dwarf) around a main sequence G or K star, since the difference in brightness at V would be at least 6 magnitudes. Were it not for the blue continuum, the spectrum in Figure 2 of Putney (1997) makes a great case for a metal poor non degenerate star; weak lines of Mg, Fe, Na can be seen in addition to Balmer lines and Ca H & K. Figure 6.2 shows the spectrum taken

for this work, which is inferior but still displays many of these weak features. Photometry done here gives $V - K = 1.88$, which is consistent with a G/K type star. But PG 1126+185 also has $U - B = -1.12$, implying a very hot object and confirming the steep blue continuum seen in its spectrum. Smart et al. (2003) have measured a zero parallax for PG 1126+185 – clearly inconsistent with a white dwarf, given its relative brightness at $V = 14.0$ mag.

In order to explain both the blue continuum and the observed absoprtion features of PG 1126+185, a composite system consisting of one hot star and one cool star is needed. The luminosities should be comparable given the spectrum. A typical G star has $M_V \approx 5$ mag, but is there a hot star that has a comparable absolute V magnitude? Subdwarf B stars have $M_V \approx 4.5$ mag (Maxted et al. 2000b). Therefore, the most likely explanation for the spectrum of PG 1126+185 is a composite binary consisting of an sdB+G/K. This is also consistent with the zero parallax measurement.

PG 0210+168 shares a story similar to PG 1126+185. It was typed DC originally (Green, Schmidt, & Liebert 1986; McCook & Sion 1999) and then reclassified as DC+F/G by Putney (1997). Again, it is simply not possible to detect a DC white dwarf in the optical against the flux of an F or G star. In this case the brightness difference would be at least 8 magnitudes. Figure 2 of Putney (1997) clearly shows weak metal lines, a Balmer series, plus Ca H & K. Its spectrum is very similar to that of PG 1126+185 and shows a strong blue blue continuum as well. PG 0210+168 was not observed for optical photometry in the course of this work, so its UBV colors are not known, but with $V - K \approx 1.5$, it is quite certain that PG 0210+168 contains a cool star together with a hot star. Following the same reasoning as for PG 1126+185, the conclusion is that it is very likely an sdB+F/G composite binary.

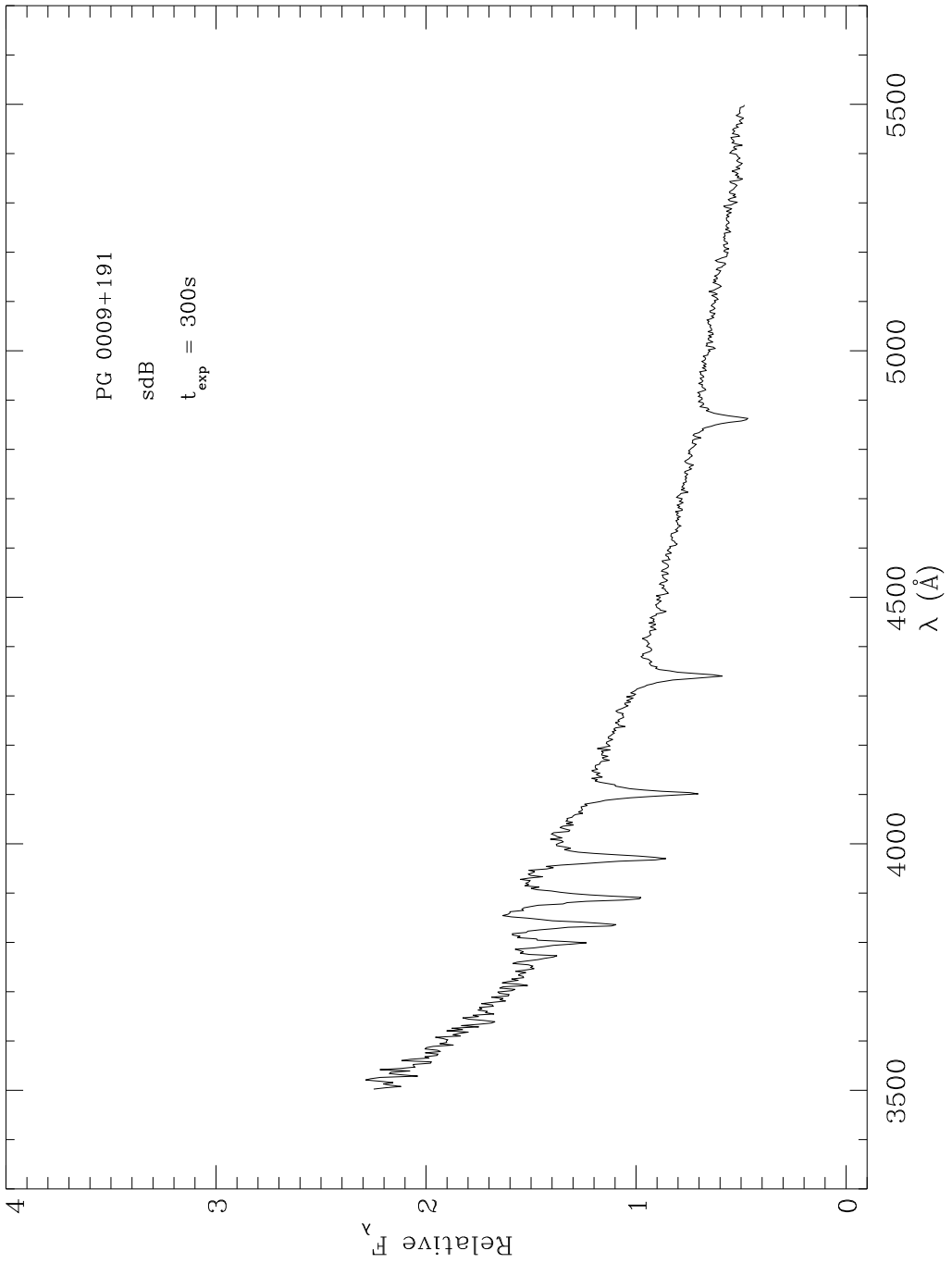

Figure A.1: Blue optical spectrum of PG 0009+190 taken with the Kast Spectrograph on the Shane 3 meter telescope in August 2002.

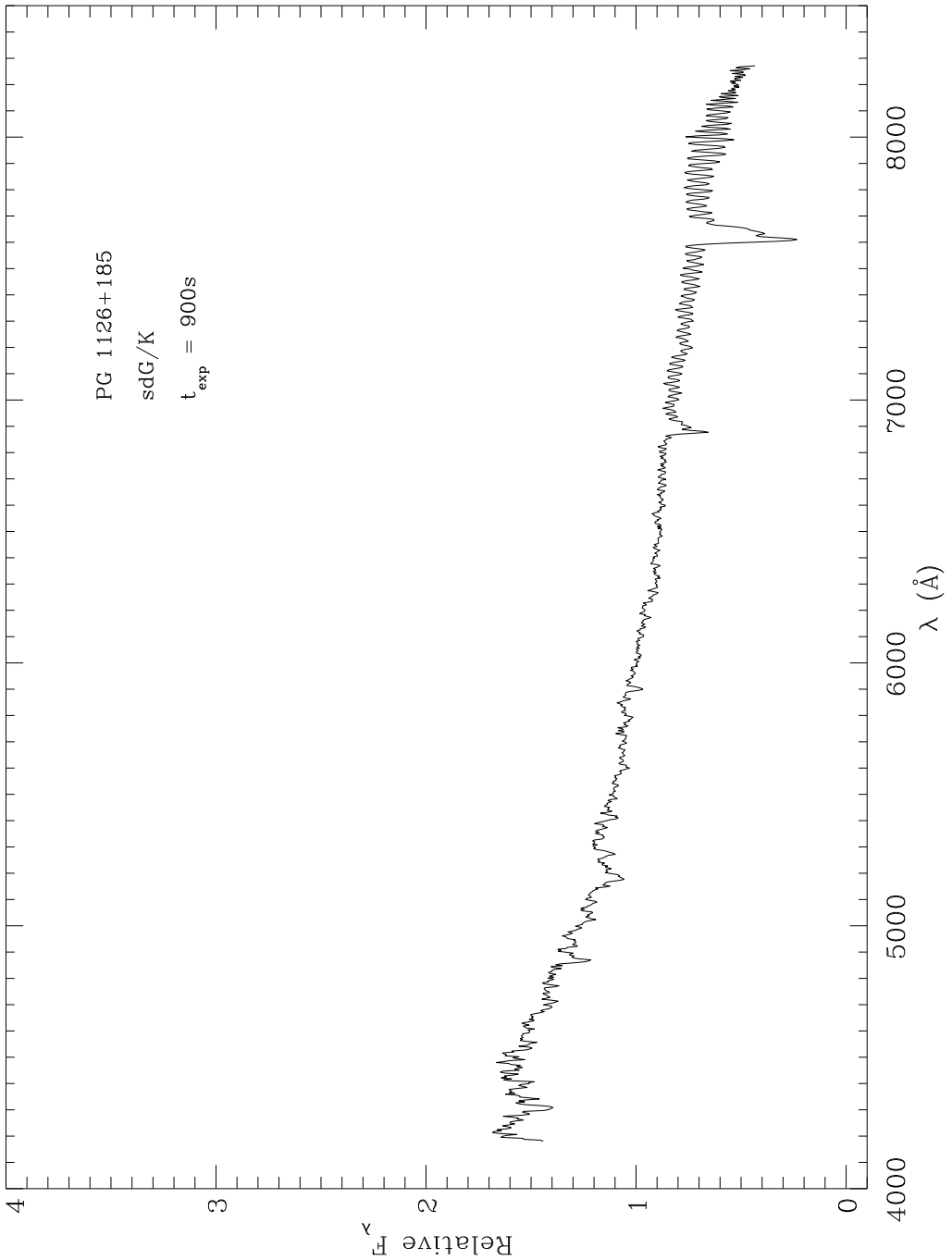

Figure A.2: Optical spectrum of PG 1126+185 taken with the Boller & Chivens Spectrograph on the Bok 2.3 meter in April 2003.

A.2 Uncommon Proper Motion

Common proper motion is a necessary but insufficient condition to establish physical companionship for wide binaries. In this section, evidence will be presented on several systems which justifies this claim.

Measuring proper motion accurately is a nontrivial task requiring good signal to noise on dozens if not hundreds of background, near zero motion sources. And still, what is almost always measured is relative proper motion; that is, the motion of an object relative to nearby stationary sources (Monet et al. 2003; Lépine, Shara, & Rich 2003). In searching for common proper motion companions, this issue is not really important. A wide binary pair should have the same absolute and relative proper motion, assuming zero orbital motion. However, the issues raised in §4.3.2 are valid and do contribute to measurement uncertainties. Given the limited accuracy of the proper motions measured for this work, many candidates were flagged which turned out to be background stars. This is a good thing. The error was on the side of caution and candidates were not thrown out.

In the end, only a reliable trigonometric parallax and/or orbital motion can determine binarity in widely separated pairs with certainty. This is illustrated by three white dwarf target primaries in the sample; G47-18, G66-36, & G116-16. All three of these stars are reported to be members of a wide binary containing a white dwarf in McCook & Sion (1999). However, further investigation proves these cases to be false positives. None of the following pairs are physically associated.

A.2.1 G47-18 & G116-16

G47-18 was reported as a common proper motion binary with the F6 dwarf HD 77408 (Eggen & Greenstein 1967). The white dwarf has $\mu = 0.324''$ yr^{-1} at

$\theta = 270.2°$ and $\pi = 0.049''$ (three measurements, McCook & Sion 1999). However, HD 77408 has $\mu = 0.420''$ yr^{-1} at $\theta = 269.5°$ and $\pi = 0.0199''$ (Perryman et al. 1997).

G116-16 was reported as a common proper motion binary with the G0 dwarf G116-14 (Eggen & Greenstein 1965). The white dwarf has $\mu = 0.252''$ yr^{-1} at $\theta = 180.1°$ and $\pi = 0.035''$ (Dahn et al. 1982). However, G116-14 has $\mu = 0.281''$ yr^{-1} at $\theta = 173.1°$ and $\pi = 0.0194''$ (Perryman et al. 1997).

A.2.2 G66-36

G66-36 was reported as a common proper motion binary with the G5 dwarf G66-35 (Oswalt 1981). First of all, G66-36 is not a white dwarf but a metal poor M2 star at $d = 25$ pc (Reid, Hawley, & Gizis 1995). Its proper motion is $\mu = 0.32''$ yr^{-1} at $\theta = 173°$ (McCook & Sion 1999). However, G66-35 has $\mu = 0.297''$ yr^{-1} at $\theta = 187.1°$ and $\pi = 0.0152''$ (Perryman et al. 1997). It is noteworthy that this is a case of a subdwarf being mistaken for a white dwarf and two stars with different proper motion being mistaken for companions.

A.3 Proper Motion Confusion

It is primarily the motion of the Sun through the Galaxy which is responsible for the proper motion of nearby stars (Binney & Tremaine 1987; Binney & Merrifield 1998). This is why proper motion is inversely proportional to distance and why reduced proper motion diagrams are useful. Although important for high velocity stars such as old disk and halo objects (which are relatively rare in the solar neighborhood), the tangential linear velocity determines proper motion to a slightly lesser degree than the distance. Therefore, it is possible in principle for

two moderate velocity stars in the same region of the sky to have nearly identical proper motions, both in magnitude and direction. This has in fact been observed in the course of this work at a two different levels.

The first level of proper motion confusion is due to limited accuracy, as exemplified above. Any measurement with relatively large uncertainty leads to a relatively large potential for overlap with other measurements. This is true of any data. But this poses a secondary problem in the case of common proper motion searches because stars in the same region of the sky tend to have similar (though not the same) proper motions due to the solar motion. This fact helps in mapping out the Galaxy, but confuses common proper motion searches especially when moderate motions are considered ($\mu \sim 0.1''$ yr^{-1}).

The second level (adding to and further complicating the first level) of proper motion confusion occurs when the motion, apparent magnitude, and color place two stars in a similar region or sequence in a reduced proper motion diagram. Absolute or reduced proper motion is defined analogously to absolute magnitude.

$$H = m + 5\log\mu + 5 \tag{A.1}$$

An example of a reduced proper motion diagram would be a plot of H_V versus $V - I$. Such a plot produces a diagram very similar to an HR diagram, and can reveal up to three kinematical main sequences; that of the local disk (dwarf), thick disk (subdwarf), and halo (extreme subdwarf) populations (Reid 1997). A definite white dwarf sequence may also be seen if the diagram includes magnitudes down to $V \sim 18$.

However, because proper motion is influenced by tangential linear velocity, the sequences in a reduced proper motion diagram will be contaminated by stars with velocities which are significantly higher or lower than their kinematical population

averages. This is why old, metal poor disk stars (subdwarfs) have been a longtime contaminant in white dwarf searches (Salim & Gould 2002). Therefore faint, high velocity stars can also confuse common proper motion searches in an identical manner.

A.3.1 GD 248

In early 2002, a candidate common proper motion companion to DC5 white dwarf GD 248 was identified at a separation of $93''$ and position angle of $9°$. A measurement utilizing digitized POSS plates separated by nearly 40 years seemed to indicate common proper motion. Another measurement using near infrared images separated by almost 5 years gave similar results but with uncertainty three times as large (Table 6.1). Both GD 248 and its candidate companion appeared to fall along the cool white dwarf sequence (specifically, the cool helium atmosphere white dwarf sequence) in a color-magnitude diagram, a color-color diagram, and a reduced proper motion diagram (Bergeron, Saumon, & Wesemael 1995; Bergeron, Ruiz, & Leggett 1997). This indicated the possibility that the candidate companion was perhaps the coolest helium atmosphere white dwarf yet discovered.

A spectrum covering $5700 - 10,000$ Å obtained with the Kast Spectrograph (Figure 6.1) on the Shane 3 meter telescope in August 2002 failed to reveal any reliable, non telluric features . Unfortunately, the exposure time was not long enough to get a decent signal on the blue side and light pollution precluded any search for Na at 5880 Å. However, a spectrum covering $4900 - 10,000$ Å taken with LRIS (Figure 6.2) on the Keck I 10 meter telescope revealed Na at 5880 Å, a strong MgH band at 5100 Å, and a variety of other fairly weak features – all indicative of a metal poor late K or very early M star (Reid & Hawley 2000).

It was quickly concluded that the candidate companion to GD 248 was an ultra high velocity background star and not a companion. At an estimated distance of ~ 800 pc (assuming $M_V = 10.1$ mag, 2 magnitudes below the main sequence for spectral type K7), its tangential velocity of $v_{\rm tan} \approx 530$ km s^{-1} is just under the escape velocity of the Galaxy (Binney & Tremaine 1987). In hindsight, one can see a discrepancy in the measured proper motions of GD 248 and the candidate companion, though the measurements agree within the errors. A more precise measurement has been performed on the non physical pair and their error ellipses differ by exactly $1\sigma = 0.008''$ yr^{-1} (S. Lépine 2002, private communication).

A.3.2 GD 304, PG 1026+002, & PG 1038+633

Candidate common proper motion companions to the white dwarfs GD 304 ($a = 104''$, PA$= 33°$), PG 1026+002 ($a = 37''$, PA$= 37°$), & PG 1038+633 ($a = 114''$, PA$= 21°$) were identified during the course of the survey. Table 6.1 lists the measured proper motions, V magnitudes and $V - K$ colors for all the primaries and candidate companions. As in the case of GD 248, all of these stars, if true physical companions, appeared to be cool white dwarfs based on apparent magnitude, color, and proper motion

Ultimately, spectra revealed that the candidate companions to PG 1026+002, & PG 1038+633 were high velocity background stars of similar tempterature to the candidate companion to GD 248. The candidate companion to GD 304 has a much redder $V - K$ color than the other three objects in Table 6.1 and from the beginning was suspected of being a high velocity background star. Their spectra are shown in Figures $6.3 - 6.6$.

Assuming $M_V = 9.8$ mag (1 magnitude below the main sequence for spectral type M0) for the candidate companion to PG 1026+002, its tangential velocity

is $v_{\rm tan} \approx 390$ km s^{-1}. Using $M_V = 9.1$ mag for the candidate companion to PG 1038+633 (1 magnitude below the main sequence for a K7 star), its tangential velocity is $v_{\rm tan} \approx 400$ km s^{-1}. These values are less than that of the candidate companion to GD 248, but still quite high. For the candidate companion to GD 304 however, a slightly more modest tangential velocity of $v_{\rm tan} \approx 210$ km s^{-1} is calculated assuming a main sequence absolute magnitude of $M_V = 10.8$ mag for spectral type M3.

In all four cases of these high velocity background stars, a spectrum was an absolutely critical discriminant; the only measurement short of a parallax that could demonstrate these pairs are not physically bound.

Table A.1: High Velocity Background Star Data

Object	V	$V-K$	μ_α (yr^{-1})	μ_δ (yr^{-1})	ST
GD 248	15.1	+0.0	$-0.05''$	$-0.11''$	DC5
background star	19.6	+3.4	$-0.06''$	$-0.13''$	sdK/M
GD 304	15.3	−0.8	$+0.06''$	$-0.01''$	DA2
background star	20.5	+4.7	$+0.05''$	$-0.01''$	dM
PG 1038+633	14.8	−1.0	$-0.08''$	$-0.04''$	DA2
background star	18.9	+3.2	$-0.08''$	$-0.04''$	dK/M
PG 1026+002	13.8	+2.9	$+0.06''$	$-0.08''$	DA3+dM
background star	19.7	+3.5	$+0.05''$	$-0.07''$	sdK/M

Note– Uncertainties for the proper motion values are $0.01''$ yr^{-1} (§4.3.2).

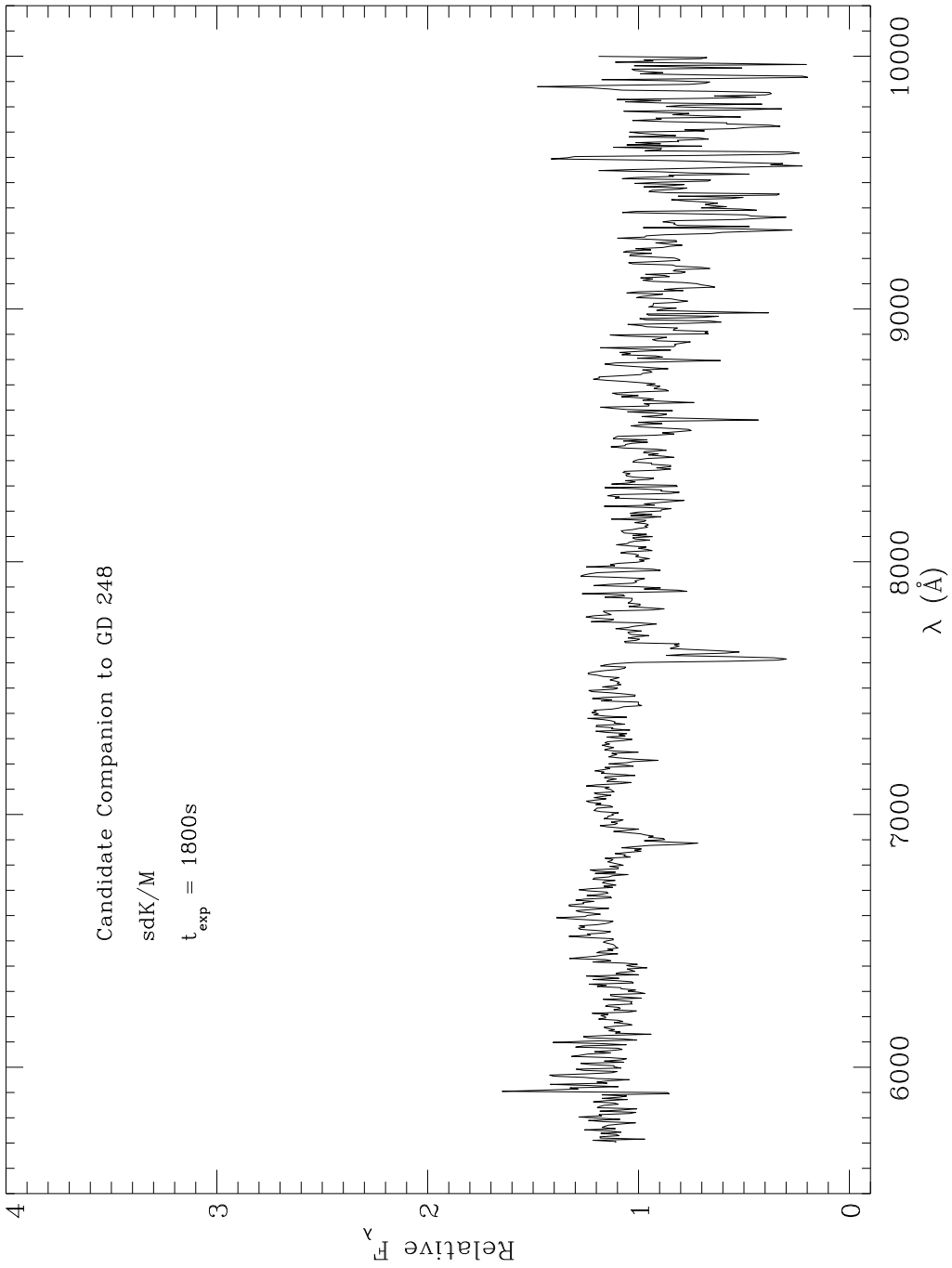

Figure A.3: Red optical spectrum of the candidate companion to GD 248 taken with the Kast Spectrograph on the Shane 3 meter telescope in August 2002.

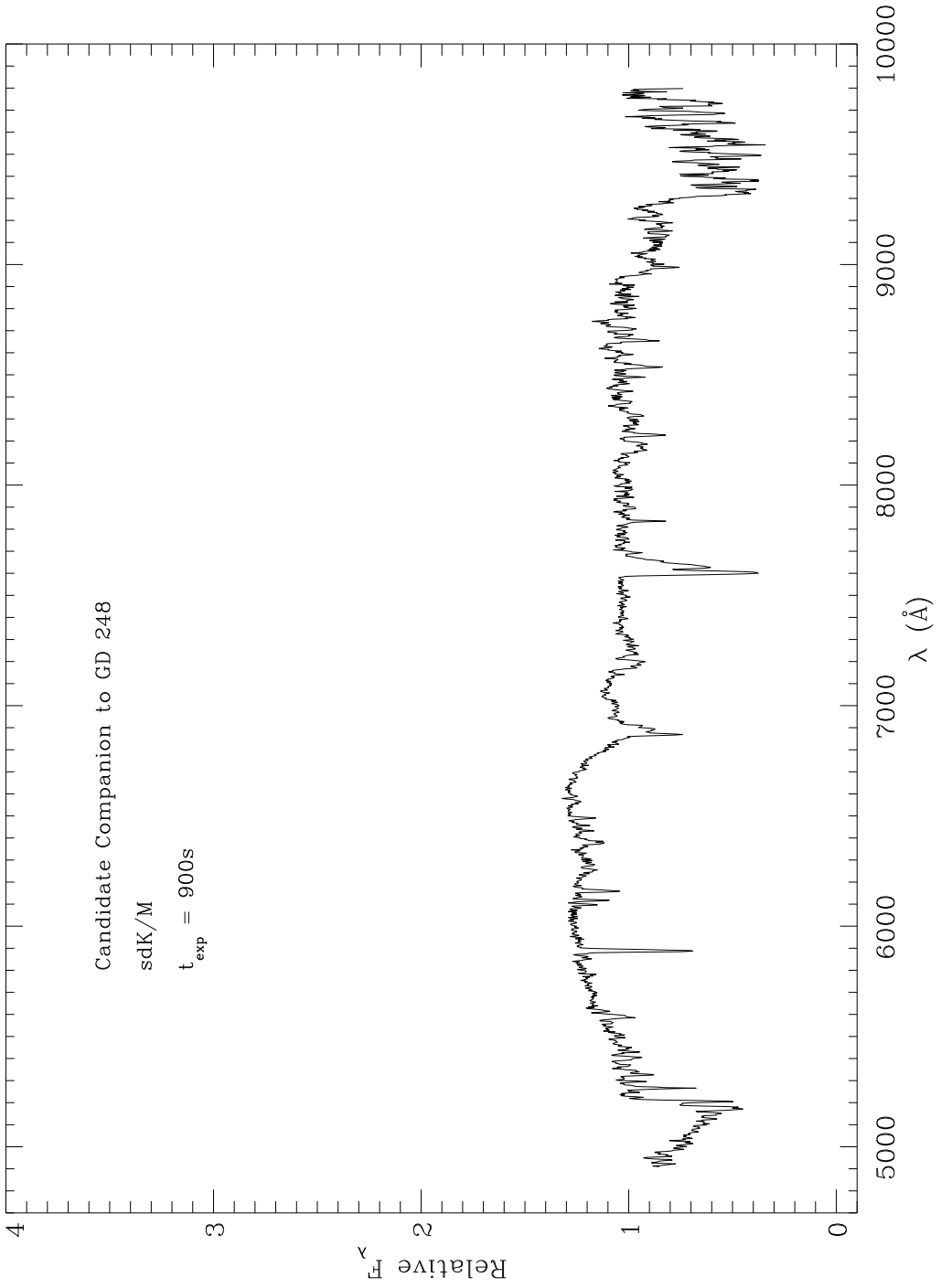

Figure A.4: Optical spectrum of the candidate companion to GD 248 taken with the Low Resolution Imaging Spectrograph on the Keck I 10 meter telescope in September 2002.

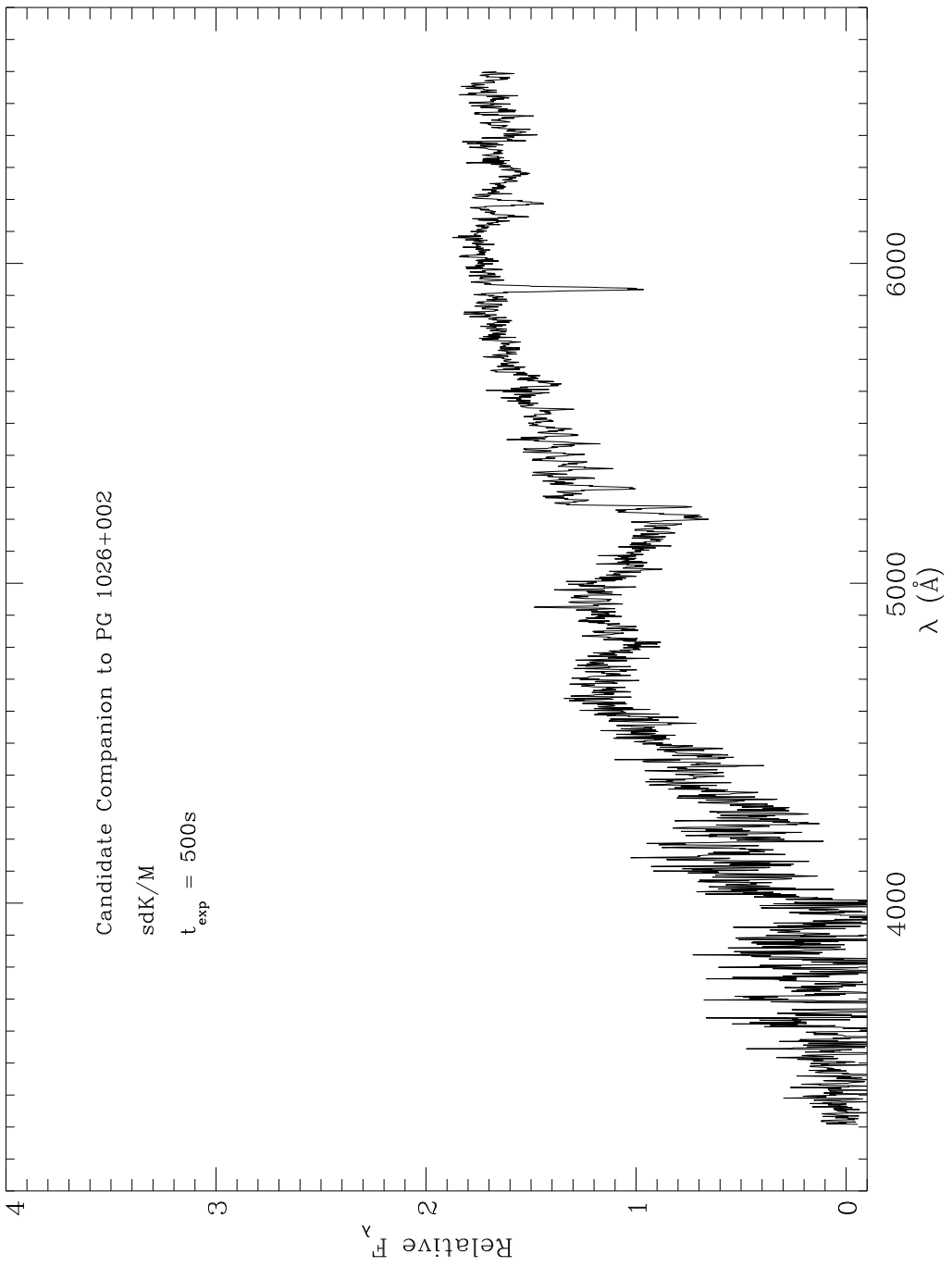

Figure A.5: Blue optical spectrum of the candidate companion to PG 1026+002 taken with the Low Resolution Imaging Spectrograph on the Keck I 10 meter telescope in May 2003.

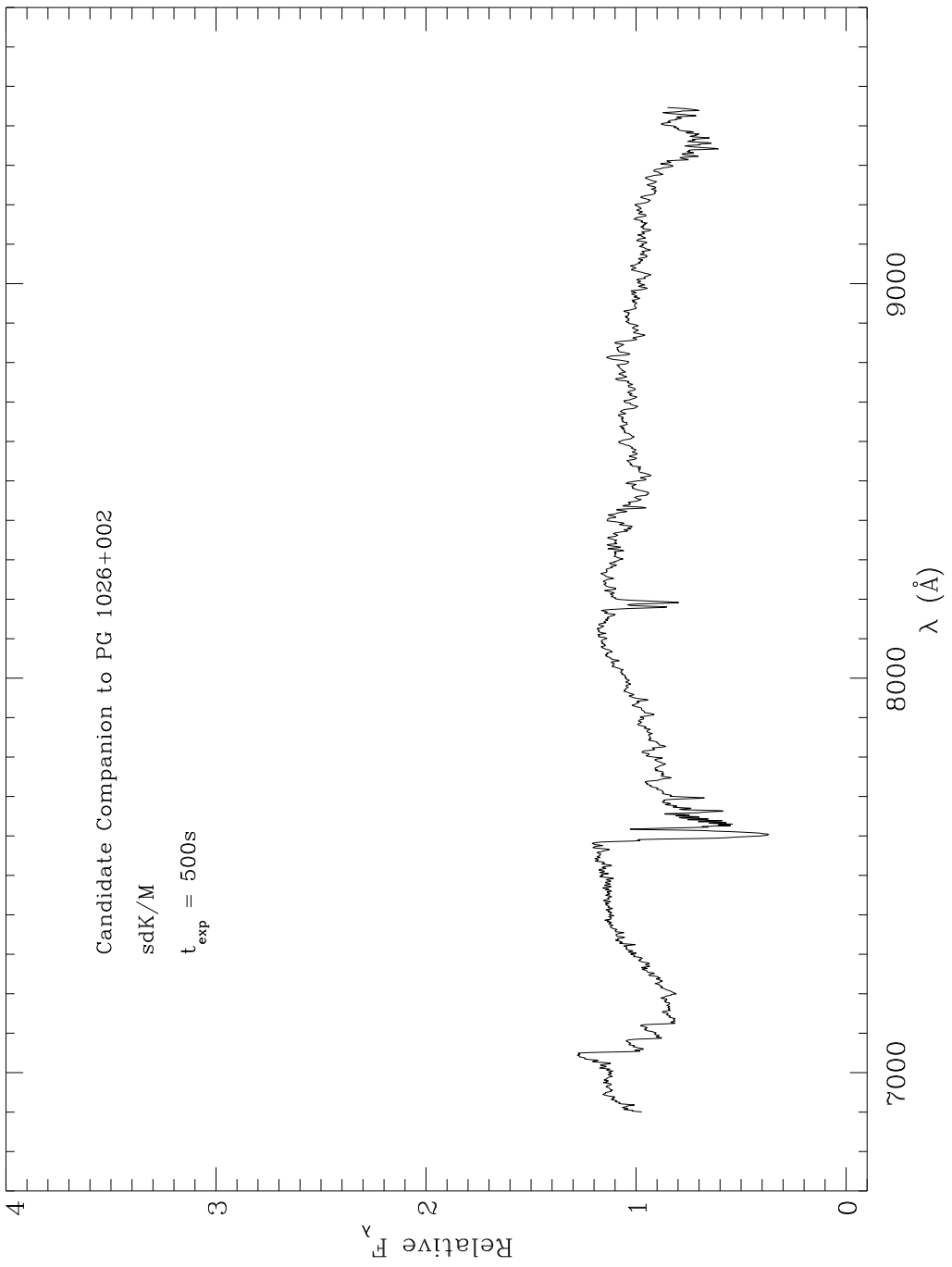

Figure A.6: Red optical spectrum of the candidate companion to PG 1026+002 taken with the Low Resolution Imaging Spectrograph on the Keck I 10 meter telescope in May 2003.

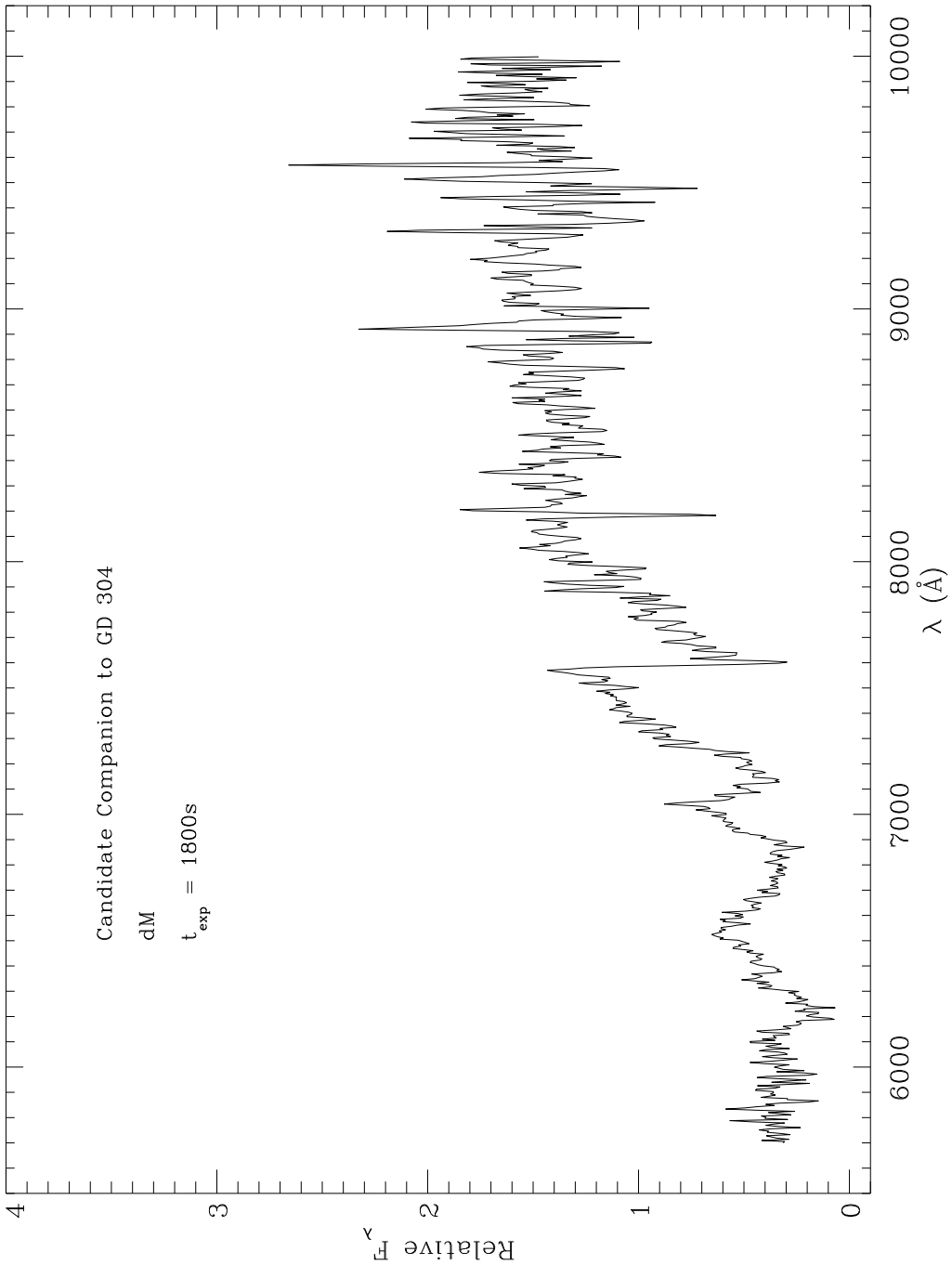

Figure A.7: Optical spectrum of the candidate companion to GD 304 taken with the Kast Spectrograph on the Shane 3 meter telescope in February 2002.

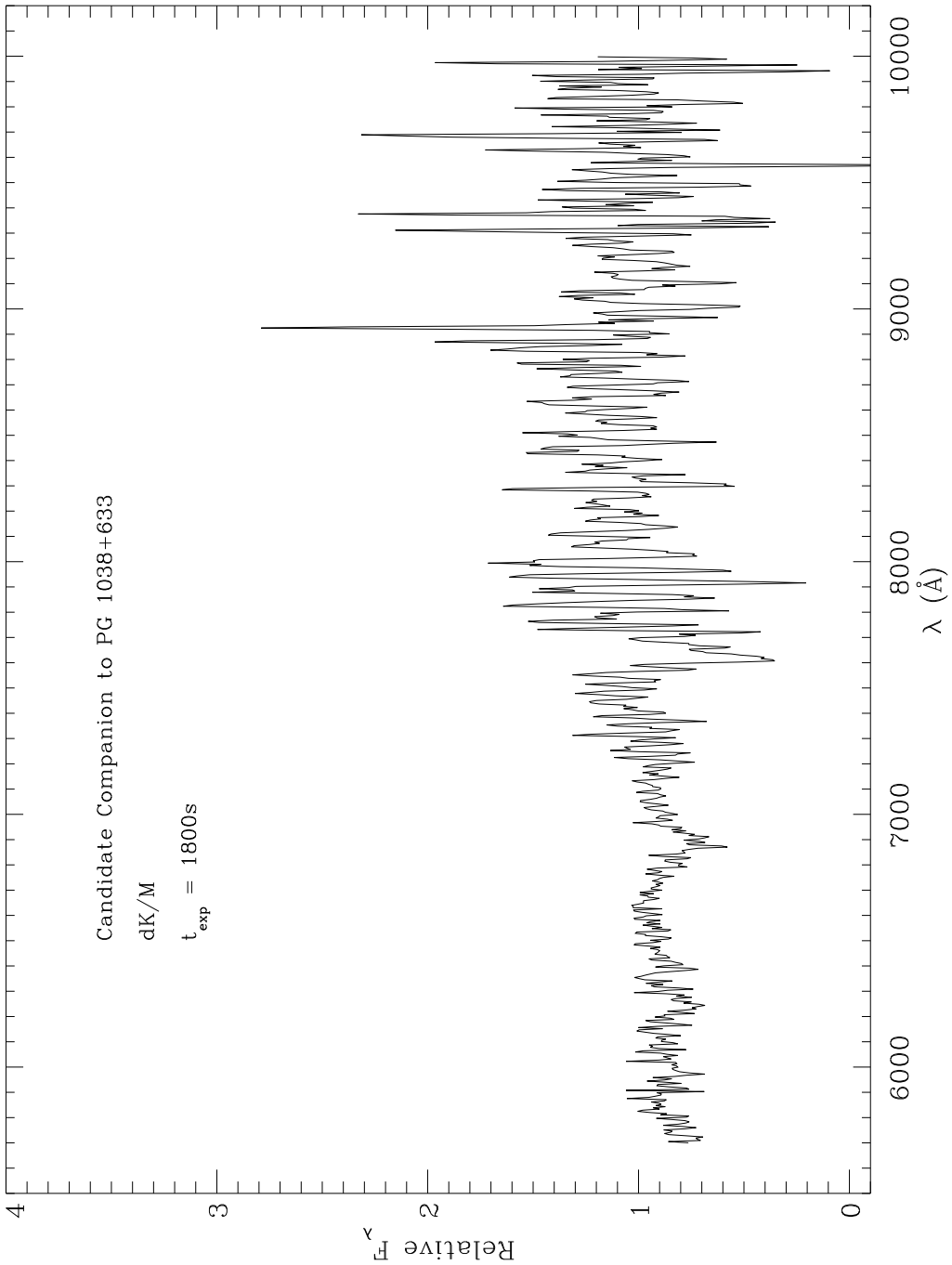

Figure A.8: Optical spectrum of the candidate companion to PG 1038+633 taken with the Kast Spectrograph on the Shane 3 meter telescope in February 2002.

A.4 Candidate Companions

There are a few candidate common proper motion companions that will be discussed individually. These objects show common proper motion of varying degree of agreement plus colors and/or spectra which are consistent with companionship. However, because background (and possibly foreground) stars can mimick common proper motion companions, as seen in the previous section, some caution is due.

A.4.1 GD 84

GD 84B is perhaps the most tentative companion due to the relative lack of agreement in the measured proper motion of GD 84 and itself. Even with the errors taken into account, their values are still discrepant by $\sim 0.02''$ yr^{-1}. A more precise measurement could not be made for the candidate companion because it is passing in front of another star in the digitized POSS I scans. Even so, the measurements in Table 6.2 appear precise enough with a roughly 9 year baseline.

However, there is something to consider. Weidemann & Koester (1995) give spectral type DQ5.6 for GD 84 ($T_{\rm eff} = 9000$ K), which yields $M_V = 12.59$ mag and a photometric distance of $d = 33$ pc for $\log g = 8.0$ (Bergeron, Saumon, & Wesemael 1995). The M dwarf, verified by its optical spectrum in Figures $4.35 - 4.36$, appears to be a normal solar metallicity star. Using $K = 10.55$ mag from Table 4.3 and $M_K = 7.80$ mag for spectral type M4, its photometric distance is $d = 35$ pc (Kirkpatrick & McCarthy 1994). If this is correct, why would the proper motions be discrepant? The projected separation between the two stars is $a = 2440$ AU at the white dwarf distance, much too large for orbital motion to explain any difference. The only other possible explanation would be

a gravitational perturbation by close encounter. This seems unlikely.

On the other hand, if the spectral type of GD 84B is M3.5, its photometric distance becomes $d = 50$ pc. This value is not inconsistent with companionship, especially considering the fact that the distance to GD 84 is not known. Sion et al. (1988) give type DBA6 and $T_{\rm eff} = 10,800$ K for GD 84, yielding $M_V = 12.06$ mag and $d = 42$ pc for $\log g = 8.0$. With the same temperature but $\log g = 7.75$ ($M = 0.46\ M_{\odot}$), this becomes $M_V = 11.46$ mag and $d = 56$ pc. Additionally, it is conceivable that metallicity effects, though not obvious in its spectrum, will make the photometric distance closer for GD 84B. Hence the object GD 84B is retained for these reasons, until companionship can be ruled out firmly.

A.4.2 GD 683

GD 683 and GD 683B have nearly identical proper motion measurements in the UCAC1 catalog (see Table 4.2, Zacharias et al. 2000). But for some unknown reason in the UCAC2 catalog, the proper motion of GD 683B changes to approximately half of its former value and GD 683 is completely absent (Zacharias et al. 2004). Because of this strange discrepancy, a less accurate measurement was made for this work. Table 6.2 gives the values measured for GD 683 and GD 683B, which are nearly identical.

Furthermore, using $K = 11.28$ mag from Table 4.3 and $M_K = 6.00$ mag for spectral type M2 (solar metallicity), the photometric distance for GD 683B is $d = 114$ pc (Kirkpatrick & McCarthy 1994). There are two temperature and surface gravity determinations for the DA white dwarf GD 683, the average of which gives $T_{\rm eff} = 30,000$ K and $\log g = 7.79$. These values give $M_V = 9.31$ mag and a photometric distance of $d = 121$ pc (Bergeron, Saumon, & Wesemael 1995), consistent with companionship between the pair. The object GD 683B is

retained as a candidate due to the discrepancy with the UCAC2 catalog.

A.4.3 PG 0933+729

The object PG 0933+729B is retained as a candidate because there exists no optical photometric nor spectroscopic data at present. The high declination of PG 0933+729 places it out of reach of the Nickel 1 meter telescope at Lick Observatory (this telescope has limited pointing due to the fact that it was built in an old dome originally designed for a much smaller telescope). It has photographic magnitudes of $B_{pg} = 16.6$ mag & $R_{pg} = 14.4$ mag in the USNO catalog. Together with the near infrared magnitudes in Table 4.3, this implies a $V - K$ color for an early M dwarf (type M2 or earlier) and a photometric distance of roughly $d \approx 120$ pc. The white dwarf is type DA3, $T_{\rm eff} = 17,400$ K at $d \approx 90$ pc (Liebert, Bergeron, & Holberg 2004). The candidate is retained until companionship can be ruled out with certainty.

Table A.2: Candidate Binary Proper Motions

Object	μ_α (yr^{-1})	μ_δ (yr^{-1})
GD 84A	$-0.11 \pm 0.01''$	$-0.16 \pm 0.02''$
GD 84B	$-0.06 \pm 0.01''$	$-0.21 \pm 0.02''$
GD 683A	$-0.04 \pm 0.01''$	$-0.06 \pm 0.01''$
GD 683B	$-0.03 \pm 0.01''$	$-0.06 \pm 0.01''$
PG 0933+729A	$-0.06 \pm 0.01''$	$-0.04 \pm 0.01''$
PG 0933+729B	$-0.06 \pm 0.01''$	$-0.05 \pm 0.01''$

A.5 Outstanding Doubles & Triples

In this section particular details on interesting and unique systems is presented. New information gleaned in this work – specifically, data on previously unknown companions – provides more accurate descriptions and parameterizations of many single and a few double degenerates. In several cases of confirmed white dwarf plus red dwarf binaries, the photometric distance to the white dwarf does not agree with the photometric distance to the red dwarf. In cases where the red dwarf appears overluminous, this may be explained by binarity. However, there are several cases where the red dwarf appears significantly underluminous. Although a metal poor M companion would be subluminous with respect to the main sequence, it is more likely that the distance to the white dwarf is inaccurate as none of the M dwarf companions appear to have metal poor spectra.

A.5.1 G21-15

G21-15 is a triple degenerate, only the second known. Its hierarchy is similar to the only other known triple degenerate WD 1704+481 (Maxted et al. 2000a), with one close double degenerate (Saffer, Livio, & Yungelson 1998) plus the widely separated cool white dwarf reported here. Maxted & Marsh (1999) report a 6.6 d period in the single lined DA spectroscopic binary.

This system has a trigonometric parallax $\pi = 0.0182 \pm 0.0023''$ and hence its distance is known at $d = 54.9 \pm 7.1$ pc (Bergeron, Leggett, & Ruiz 2001). Treating the primary DA as a single star, the photometric analysis of Bergeron, Leggett, & Ruiz (2001) yields $T_{\rm eff} = 12,240$ K, $\log g = 7.00$, $M = 0.23\ M_{\odot}$, and $M_V = 10.19 \pm 0.28$ mag. The spectroscopic analysis of the primary gives $T_{\rm eff} = 14,800$ K, $\log g = 7.61$, and $M = 0.39\ M_{\odot}$ (Bragaglia, Renzini, & Bergeron 1995; Maxted

& Marsh 1999; Bergeron, Leggett, & Ruiz 2001). The spectroscopic method produces the wrong absolute magnitude but more accurately determines mass, which is an intermediate value of the masses of the individual double degenerate components (Bergeron et al. 1991).

If one assumes that the two white dwarfs are equally luminous, the mass of each component, $M \approx 0.4\ M_{\odot}$ (Bergeron, Leggett, & Ruiz 2001), is still less than the cutoff for CO core white dwarfs. Hence it is possible that the close binary consists of two low mass, He core white dwarfs (Bergeron, Saffer, & Liebert 1992; Marsh, Dhillon, & Duck 1995). This scenario is consistent with the spectroscopy, photometry, and parallax. But this fails to correctly predict the single lined DA nature of the system, unless one of the stars is a yet undetected DB, which is very unlikely (Bergeron, Saffer, & Liebert 1992; Bergeron & Liebert 2002).

The other possibility is two white dwarfs with different luminosities; some combination of different masses and temperatures. But does there exist such a scenario which is consistent with all observations? The answer is yes. In order to display a single lined DA spectrum with a 6.6 d period, whose Balmer line profiles yield $\log g \approx 7.6$, $M \approx 0.4\ M_{\odot}$, one needs a relatively low mass hot component and a relatively high mass cool component. The observational data can be reproduced by assuming two DA stars at 55 pc, one with $M = 0.60\ M_{\odot}$ ($\log g = 8.0$), $T_{\rm eff} = 10,000$ K, $M_V = 12.15$ mag, and the other with $M = 0.35\ M_{\odot}$ ($\log g = 7.4$), $T_{\rm eff} = 15,000$ K, $M_V = 10.38$ mag. Therefore the most likely nature of the double degenerate is one white dwarf composed of helium and the other white dwarf composed of carbon and oxygen.

The optical and infrared colors of G21-15C (Table 4.3) are consistent with a helium atmosphere (it is too red for a hydrogen atmosphere) degenerate with $T_{\rm eff} = 4750$ K. The trigonometic parallax gives $M_V = 15.30 \pm 0.28$ mag and

indicates a radius corresponding to $\log g \approx 8.0$, or $M = 0.57\ M_{\odot}$. The cooling age of a helium atmosphere white dwarf with such parameters is 6.6 Gyr (Bergeron, Saumon, & Wesemael 1995). Its kinematics are consistent with a disk star of age $\tau = 5 - 10$ Gyr (Table 3.1).

It is somewhat surprising that such an old disk white dwarf is not more massive than $M = 0.57\ M_{\odot}$. If correct, this implies the total age of G21-15C, and hence the entire system, is likely to be closer to 8 Gyr. The initial to final mass relation for white dwarfs indicates that degenerate stars less massive than 0.6 $M_{\odot}$ have descended from main sequence progenitors less massive than 2 $M_{\odot}$ (Weidemann 1987, 1990, 2000; Bragaglia, Renzini, & Bergeron 1995). Such a progenitor should have had a main sequence lifetime of more than 1.5 Gyr (Girardi et al. 2000), yielding a total age for G21-15C of $\tau > 8.1$ Gyr.

Designating the brighter, helium white dwarf G21-15A and the fainter, putative carbon/oxygen white dwarf G21-15B, the cooling age of G21-15C can be used as a constraint on the overall age of the system and place upper limits to the masses of both main sequence progenitor components of the double degenerate. Using $T_{\rm eff} = 15,000$ K for G21-15A and $T_{\rm eff} = 10,000$ K for G21-15B, they have been cooling for 0.1 and 0.6 Gyr respectively (Bergeron, Saumon, & Wesemael 1995). If the above analysis is correct, the entire system is at least 8.1 Gyr old and hence the progenitors of G21-15A & B were very nearly solar mass stars (Girardi et al. 2000).

However, a helium core white dwarf is born as it ascends the red giant branch for the first time, its outer layers stripped before helium burning can begin (Bergeron, Saffer, & Liebert 1992; Marsh, Dhillon, & Duck 1995). G21-15A began this ascent at least 8 Gyr ago, corresponding to a star with $M \leq 1.10\ M_{\odot}$ (Girardi et al. 2000). G21-15B most likely completed all its post main sequence evolution

7.5 Gyr ago and hence came from a slightly larger progenitor with $M = 1.15\ M_{\odot}$ (Girardi et al. 2000).

Now a complete picture, albeit speculative, of the entire evolution of the double degenerate can emerge. The progenitors of G21-15A & B were probably two nearly solar mass stars with an orbital period on the order of 100 d ($a \sim$ 0.5 AU). The more massive component B left the main sequence first, without any mass transfer in the relatively wide binary during its first red giant phase. Upon ascending the asymptotic giant branch, component B forms a common envelope around the binary and the orbit shrinks significantly due to loss of angular momentum. The resulting close separation is enough to cause component A to overfill its Roche lobe as a first ascent giant and become a helium core white dwarf (Nelemans et al. 2001).

A.5.2 GD 319

GD 319 is a triple system consisting of an sdB with a close unseen companion (Saffer, Livio, & Yungelson 1998) plus the widely separated M3.5 dwarf reported here. The lower limit for the mass of the unseen companion is $M \geq 0.9\ M_{\odot}$, which is in a 0.6 d orbit around the sdB (Maxted et al. 2000b).

Although not a white dwarf, GD 319 was included in the survey due to its presence in McCook & Sion (1987). It was later reclassified as type sdB by Saffer, Livio, & Yungelson (1998), who also first detected its radial velocity variations. sdB stars such as GD 319 are thought to be helium burning stars with very thin hydrogen envelopes which eventually cool to become white dwarfs with mass around 0.5 $M_{\odot}$ (Saffer et al. 1994). These hot subdwarfs may form analogously to low mass white dwarfs, their surface hydrogen layers removed by a close companion (Iben & Livio 1993). Hence, GD 319 is perfectly representative of a white

dwarf system.

There is a K star located $\approx 3''$ away from GD 319, but it was shown to be astrometrically unrelated (McAlister et al. 1996). Most photometry reported in the literature for GD 319 is contaminated by the K star. The values for GD 319AB in Table 4.3 are measurements from images in which both stars were well resolved from one another and there should be no such contamination (McAlister et al. 1996). The near infrared photometry was performed on images taken at Keck Observatory and the results indicate the K star is a foreground object.

Although the mass of the close companion GD 319B is unknown, the lower limit indicates that it is very likely an M dwarf, with a mass in the range $0.09-0.60$ $M_{\odot}$ (unless the inclination is less than 9°). It is difficult to say whether the near infrared photometry of the sdB+dM reveals an infrared excess. The measured $V-K=-0.80$ is slightly less blue as one would expect for a 30,000 K star but an effective temperature for GD 319 has not been established in the literature. In any case, were the unseen companion a dK and not a dM star, one would expect a defnite excess at K band. To illustrate, an M0V star has $M_K \approx 5.0$ mag (Kirkpatrick & McCarthy 1994), while an sdB has $M_V \approx 4.5$ mag (Maxted et al. 2000b) plus $V-K \sim -1$ for a 30,000 K object (Bergeron, Saumon, & Wesemael 1995). Their combined contribution at 2.2 μm would be $M_K \approx 4.5$ mag – an excess of ~ 1 mag. Because an early M dwarf would cause a significant excess at K band and this excess is not seen (at least not at that level) the unseen companion is almost certainly an M dwarf.

The wide tertiary component, GD 319C, can be used to constrain the distance to the system. This is helpful because at d 400 pc, GD 319 is too far away for a parallax measurement. Using both optical and near infrared absolute magnitudes for an M3.5 dwarf from Kirkpatrick & McCarthy (1994), the average distance

modulus for GD 319C is $m - M = 7.39 \pm 0.10$ or $d = 300 \pm 14$ pc. This yields $M_V = 5.3$ mag for GD 319A. By the aforementioned lack of obvious infrared excess, this further constrains the spectral type of GD 319B to later than M3.5, implying a mass in the range $0.3\ M_\odot > M \geq 0.09\ M_\odot$. This in turn limits the inclination of the orbit by $\sin i > 0.09/0.3 = 0.3$, which yields $i > 17.5°$.

A.5.3 GD 392

Because GD 392B is a possible low mass, helium core white dwarf, it may belong to a triple degenerate system (Farihi 2004). Due to the lack of significant near infrared flux in GD 392B, the tertiary would have to be a white dwarf or a neutron star. Its trigonometric parallax should be published soon (H. Harris 2004, private communication) and is mentioned here simply as a potential seventh triple system discovered in this survey.

A.5.4 LDS 826

LDS 826 is a triple system consisting of a white dwarf plus red dwarf visual pair together with the widely separated M8 dwarf reported here and in Scholz et al. (2004). The data analyzed for this work indicate the system is a DA5.5+M3.5+dM8, which differs slightly from that given in Scholz et al. (2004).

The white dwarf component, LDS 826A, is a well studied, high proper motion, nearby cool white dwarf. Bergeron, Liebert, & Fullbright (1995) find $T_{\rm eff} = 8780$ K (DA5.5), $\log g = 8.29$, and $M = 0.76\ M_\odot$ using the spectroscopic method. It is listed in the ARICNS database for nearby stars at $d = 21.1$ pc but does not have a trigonometric parallax measurement. Holberg, Oswalt, & Sion (2002) list LDS 826A among white dwarfs within 20 pc and give spectral type DA5.5, $V = 13.56$ mag, $M_V = 13.95$ mag, and an adopted distance of $d = 12.4$ pc. There must be

an error somewhere in these values because they are inconsistent with one another and with other measurements. ARICNS has $V = 14.42$ mag for LDS 826A and $V = 13.54$ mag for LDS 826B, the M3.5 dwarf companion just $6.6''$ away. LDS 826B is very likely the source of the erroneous V magnitude in Holberg, Oswalt, & Sion (2002) since McCook & Sion (1999) list a photographic magnitude of 14.5 mag for the white dwarf from the LHS catalogue and Eggen & Greenstein (1965) similarly give a photographic magnitude of 14.6 mag. If one replaces the V magnitude in Holberg, Oswalt, & Sion (2002) with that from ARICNS, the resulting distance modulus reproduces their value of $d = 12.4$ pc. However, the absolute magnitude in Holberg, Oswalt, & Sion (2002) is almost certainly in error as well. LDS 826B can easily contaminate flux measurements of the white dwarf at R & I band, where it is $2 - 3.5$ magnitudes brighter respectively, resulting in an underestimate of its true effective temperature. Silvestri et al. (2001) report $V - I = 0.56$ and $T_{\rm eff} = 6750$ K for LDS 826A (but strangely, in the same table with the color and temperature is listed spectral type DA5), while ARICNS similarly has $R - I = 0.39$; these colors are obviously contaminated by the nearby M dwarf. The absolute magnitude listed in Holberg, Oswalt, & Sion (2002) is appropriate for a white dwarf temperature close to 6500 K and not 9000 K (Bergeron, Saumon, & Wesemael 1995). The R & I measurements in Table 4.3 were performed with zero contamination as described in §4.5, are consistent with the V magnitude in ARICNS, and the resulting $R - I = 0.20$ color is in excellent agreement with models for a $T_{\rm eff} = 9250$ K, DA5.5 star. Using this effective temperature and $\log g = 8.29$ from Bergeron, Liebert, & Fullbright (1995) for LDS 826A, models predict $M_V = 12.91$ mag (Bergeron, Saumon, & Wesemael 1995) and $d = 20.0$ pc.

The 20.0 pc distance estimate is in very good agreement with the photometric distance to LDS 826B. Using both optical and near infrared absolute magnitudes

for an M3.5 dwarf from Kirkpatrick & McCarthy (1994), the average distance modulus for LDS 826B is $m - M = 1.47 \pm 0.08$ or $d = 19.7 \pm 0.7$ pc.

At 20.0 pc, LDS 826C has $M_K = 10.37$ mag which is very close to the expected absolute magnitude of an M9 dwarf as opposed to an M8 ($\langle M_K \rangle = 10.0$ mag) as typed here (Kirkpatrick & McCarthy 1994; Dahn et al. 2002). Scholz et al. (2004) report a spectral type of M8.5. However, the $I - K = 4.01$ color of LDS 826C is not as red as would be expected for an M9 or even an M8.5. Absolute magnitudes vary, but the color relations are quite tight; $\langle I - K \rangle = 4.47 \pm 0.08$ for 2 M8.5 and 5 M9 dwarfs, whereas $\langle I - K \rangle = 4.08 \pm 0.09$ for 5 M8 dwarfs (Kirkpatrick & McCarthy 1994; Dahn et al. 2002). Scholz et al. (2004) report several sets of photometry for LDS 826C, some of which are photographic and hence unreliable. The 3 data sets which contain both optical CCD I band and near infrared photometry give $I-K = 4.10\pm0.05$. There is also one measurement of $R = 18.36$ mag. All of these photometric data agree within one sigma of the photometry in Table 4.3. LP 771-21 is an M8 dwarf with $I - K = 3.99$, and $M_K = 10.38$ mag from a reliable trigonometric parallax (Dahn et al. 2002). Its color and absolute magnitude very closely match that of LDS 826C at $d = 20.0$ pc. Therefore, the M8.5 spectral type reported by Scholz et al. (2004) might be half a spectral type too late. The spectrum of LDS 826C in Figure 4.41 is consistent with M8.

In contrast to the suggestion made in Scholz et al. (2004), LDS 826C cannot be a brown dwarf. According to models, LDS 826A has been cooling for approximately 1.4 Gyr (Bergeron, Saumon, & Wesemael 1995). At this minimum age, a $T_{\rm eff} \sim 2400$ K object such as LDS 826C is a low mass star with $M > 0.080\ M_\odot$ (Chabrier et al. 2000).

Lastly, it is worth mentioning that LDS 826A has shown some radial velocity

variablity but not at a level considered significant (Maxted & Marsh 1999).

A.5.5 PG 0824+288

PG 0824+288 is a triple system consisting of double lined DA plus dwarf carbon star spectroscopic binary in a visual pair with the M3.5 dwarf reported here (Heber et al. 1993). The spectroscopic binary has been searched unsuccesfully for radial velocity variability (Maxted, Marsh, & Moran 2000).

An astrometric measurement of the blended ($a \sim 3$) visual double between POSS I & II epochs reveals the pair moving together with the proper motion listed in Table 3.1. The visual binary was first suspected by Green & Margon (1994), but remained unconfirmed until now.

The white dwarf, PG 0824+288A, is very hot at $T_{\rm eff} \approx 50,000$ K (Finley, Koester, & Basri 1997; Marsh et al. 1997). One can estimate its distance by first noting that the visual magnitude of the composite spectroscopic binary, $V = 14.22$ mag, is estimated to have a 25% contribution from the dwarf carbon star, PG 0824+288B (Heber et al. 1993). This yields $V = 14.53$ mag for the white dwarf. Two spectroscopic analyses of PG 0824+288A exist which give significantly different mass estimates but similar effective temperatures; Marsh et al. (1997) give $T_{\rm eff} = 51,900$ K and $\log g = 8.00$, while Finley, Koester, & Basri (1997) give $T_{\rm eff} = 50,500$ K and $\log g = 7.43$ (Marsh et al. 1997). The absolute magnitudes predicted by models for these two spectroscopic parameter fits are quite different; $M_V = 9.09$ mag (122 pc) versus $M_V = 8.12$ mag (191 pc).

The nearby visual M dwarf companion, PG 0824+288C, has an estimated spectral type of M3.5 (Green & Margon 1994). This is perfectly consistent with its estimated color, $V - K \approx 4.8$, calculated from the $\Delta g = 3.0$ mag difference between the components of the visual pair (Green & Margon 1994), plus the

measured K magnitude. This spectral type can be used to contrain the distance to the PG 0824+288 system. Comparing the J & K values in Table 4.3 with the absolute magnitudes of an M3.5 dwarf from Kirkpatrick & McCarthy (1994), the average distance modulus is $m - M = 5.31$, or $d = 115$ pc. This value is inconsistent with the mass and radius determined by Finley, Koester, & Basri (1997). Therefore, it appears more likely that PG 0824+288A is a $\log g = 8.0$ white dwarf with a relatively high mass of $M = 0.70\ M_{\odot}$ at $d \approx 120$ pc.

A.5.6 PG 1204+451

PG 1204+450 is a triple system consisting of a double lined DA spectroscopic binary plus the widely separated M4 dwarf companion reported here (Saffer, Livio, & Yungelson 1998; Maxted, Marsh, & Moran 2002). The spectroscopic binary consists of an approximate DA2+DA3 with a 1.6 d period and a mass ratio of $M_A/M_B = 0.87$ (Maxted, Marsh, & Moran 2002).

The brightest component, PG 1204+450A, was thought to be a relatively low mass white dwarf with spectroscopic parameters $T_{\rm eff} = 23,000$ K and $M = 0.48$ $M_{\odot}$ if treated as a single star (Bergeron, Saffer, & Liebert 1992). Maxted, Marsh, & Moran (2002) have resolved the Hα line core into two components and give effective temperature estimates and luminosity weighted masses for the individual components of $T_{\rm eff} = 31,000$ K, $M = 0.46\ M_{\odot}$ for PG 1204+450A and $T_{\rm eff} = 16,000$ K, $M = 0.52\ M_{\odot}$ for PG 1204+450B. One should keep in mind that these are estimates and that it is not possible to perform a spectroscopic fit of the Balmer lines for the individual components.

Liebert, Bergeron, & Holberg (2004) give $T_{\rm eff} = 22,600$ K, $M = 0.52\ M_{\odot}$ in a recent update of their previous work (Bergeron, Saffer, & Liebert 1992), again treating the double degenerate as a single star. If these newer parameters are

more accurate, the individual component masses inferred by Maxted, Marsh, & Moran (2002) should change similarly to 0.50 and 0.57 $M_{\odot}$ for components A and B respectively, using the same weighting (2.05:1) and mass ratio.

The wide M4 companion, PG 1241+450C, should be able to constrain the effective temperatures and absolute magnitudes of PG 1241+450 A & B by constraining the distance to the system. Using both optical and near infrared absolute magnitudes for an M4 dwarf from Kirkpatrick & McCarthy (1994), the average distance modulus for PG 1241+450C is $m - M = 5.30 \pm 0.11$ or $d = 115 \pm 6$ pc. This implies an absolute magnitude for PG 1241+450AB of $M_V = 9.74$ mag. If the flux ratio at V is similar to the estimated luminosity ratio from Maxted, Marsh, & Moran (2002), this implies $M_V = 10.17$ mag and $M_V = 10.95$ mag for components A and B respectively. Using these absolute magnitudes and the newly estimated masses from the previous paragraph, models predict $T_{\rm eff} = 22,000$ K for PG 1204+450A and $T_{\rm eff} = 16,500$ K for PG 1204+450B (Bergeron, Saumon, & Wesemael 1995).

A.5.7 PG 1241−010

PG 1241−010 is a triple system consisting of a close double degenerate plus the visual M9 companion reported here. The close binary is a single lined DA in a 3.3 d orbit (Marsh, Dhillon, & Duck 1995).

The brightest component, PG 1241−010A, is a low mass white dwarf with spectroscopic parameters $T_{\rm eff} = 24,000$ K and $M = 0.31$ $M_{\odot}$ if treated as a single star (Bergeron, Saffer, & Liebert 1992). At the time, this was the lowest mass ever reported for a white dwarf. As in the case of G21-15 above, this implies that the close binary is likely to be composed of one relatively hot helium core white dwarf plus another relatively cool and more massive carbon and oxygen

core white dwarf.

Liebert, Bergeron, & Holberg (2004) give $T_{\rm eff} = 23,800$ K, $M = 0.40\ M_{\odot}$ in a recent update of their previous work (Bergeron, Saffer, & Liebert 1992), again treating the double degenerate as a single star. This is a somewhat significant difference from $M = 0.31\ M_{\odot}$ and is hopefully more accurate due to improvements over the intervening years. Yet even at this slightly higher mass, it appears that PG 1241−010A is a low mass, helium white dwarf in a close orbit with a cooler, higher mass degenerate (Bergeron, Saffer, & Liebert 1992). The spectroscopically determined absolute magnitude for PG 1241−010, $M_V = 9.3$ mag (Bergeron, Saffer, & Liebert 1992; Liebert, Bergeron, & Holberg 2004), is almost certainly an underestimate due to the presence of not one but two white dwarfs. Unfortunately, parameter estimates for the individual components do not exist in the literature

PG 1241−010C, at estimated spectral type M9, was first recognized by (Zuckerman & Becklin 1992) and is one of the latest known confirmed companions to a white dwarf. Previous to this work, only GD 165B, GD 1400B and perhaps LDS 826C were known to be as late or later (Becklin & Zuckerman 1988; Farihi & Christopher 2004; Scholz et al. 2004). The photometric distance to the tertiary may be used as a constraint on the distance to the system and perhaps provide a limit to the brightness of the fainter white dwarf component, PG 1241−010B. However, the spectral type of PG 1241−010C was estimated by visual comparison to the standards of (Kirkpatrick, Henry, & McCarthy 1991; Kirkpatrick et al. 1999b), and there is a possibility it is as early as M8 (but not earlier). Its I band magnitude was very difficult to measure due to the $\Delta I > 4$ mag difference from PG 1241−010AB just $3''$ away. In any case, its colors (Table 4.3) are consistent with spectral types M8−M9 (Kirkpatrick & McCarthy 1994; Dahn et

al. 2002). Comparing its apparent K magnitude with absolute magnitudes of M8 and M9 spectral standards, the resulting distance modulus is bounded by $4.14 < m - M < 4.44$ or $d = 72 \pm 5$ pc. This gives $M_V = 9.71 \pm 0.15$ mag for PG 1241−010AB.

This photometric distance to the tertiary is interesting because it implies a distance much closer than previously suspected. A single 24,000 K DA white dwarf with $\log g = 7.5$ ($M = 0.41\ M_\odot$) has $M_V = 9.65$ mag according to models (Bergeron, Saumon, & Wesemael 1995), implying that PG1241−010B contributes almost nothing to the overall V band flux. A distance around 72 pc is also inconsistent with the previous spectroscopic mass determination of $M = 0.31\ M_\odot$ ($M_V = 9.2$ mag) for PG 1241−010AB. Assuming the above distance bounds and the spectroscopic temperature of PG 1241−010A are correct (but using $\log g = 7.5$), the maximum contribution from PG 1241−010B is $M_V = 12.3$ mag, implying $T_{\rm eff} < 10,000$ K for a $\log g = 8.0$ white dwarf.

However, it is possible that PG 1241−010C is a binary itself. This would indicate a distance up to 109 pc (two identical M8 dwarfs) and be more consistent with the spectroscopically determined parameters of PG 1241−010AB.

A.5.8 G261-43

G261-43A is a DA3 white dwarf with a trigonometric parallax of $\pi = 0.471''$ (McCook & Sion 1999). McMahan (1989) reports and compares three independent determinations of effective temperature and surface gravity, all of which agree very well at $T_{\rm eff} = 15,400$ K, $\log g = 7.9$. Models predict $M = 0.57\ M_\odot$ and $M_V = 11.04$ mag, compared with $M = 0.61\ M_\odot$ and $M_V = 11.19$ mag from its parallax (Bergeron, Saumon, & Wesemael 1995). Hence, G261-43 is a DA white dwarf with a typical mass (Bergeron, Saffer, & Liebert 1992).

The binary nature of G261-43 was first reported by Zuckerman et al. (1997). An almost certain white dwarf itself, G261-43B is located only $1.4''$ away and quite faint relative to its primary ($\Delta V \approx 3.5$ mag). This is almost certainly the reason it was discovered in the near infrared where the contrast much lower at $\Delta K < 2$ mag.

The roughly estimated effective temperature of G261-43B ($\sim$ 5000 K, Zuckerman et al. 1997) is probably a bit too low given the photometry. Although the near infrared photometric measurements had good signal to noise, the optical measurements were difficult due to the brightness ratio of primary to secondary (B. Zuckerman 2004, private communication). Using the three most reliable magnitudes available (I = 15.7 mag, J=15.34mag,K= 15.05 mag) and the resulting $I - J = 0.36$ & $J - K = 0.29$ colors, hydrogen atmosphere models predict $T_{\rm eff} = 6000$ K almost exactly, regardless of log g (Bergeron, Saumon, & Wesemael 1995). Combining this effective temperature with the trigonometric parallax gives log $g = 8.39$ and $M = 0.84\ M_{\odot}$ for G261-43B (Bergeron, Saumon, & Wesemael 1995). Therefore, the difference in radii between components A & B is likely to be significant (Zuckerman et al. 1997).

If this analysis is correct, the main sequence progenitor of G261-43A spent 4.4 Gyr on the main sequence. This is the difference between the 4.58 Gyr cooling age of G261-43B minus its own cooling age of 0.18 Gyr (Bergeron, Saumon, & Wesemael 1995). A main sequence star with such a lifetime, including post main sequence evolution, should have a mass just greater than 1.3 $M_{\odot}$ (Girardi et al. 2000).

A.5.9 PG 0901+140

PG 0901+140 is a visual double degenerate with a separation on the sky of 3.6″. Despite several studies and comparable luminosities between its two components ($\Delta V \approx 0.5$ mag), the binarity has never been mentioned in the literature (Green, Schmidt, & Liebert 1986; Bergeron et al. 1990; Liebert, Bergeron, & Holberg 2004).

Liebert, Bergeron, & Holberg (2004) give $T_{\rm eff} = 9200$ K, $\log g = 8.29$, and $M_V = 12.91$ mag for PG 0901+140 by spectroscopic analysis, assuming it is a single star. Comparison of hydrogen atmosphere model colors to the optical and near infrared photometry in Table 4.3 yields $T_{\rm eff} = 9500$ K for the brighter component PG 0901+140A, and $T_{\rm eff} = 8250$ K for the fainter component PG 0901+140B (Bergeron, Saumon, & Wesemael 1995). These effective temperatures are quite consistent with the combined effective temperature determination, whereas the spectroscopically determined mass ($M = 0.79\ M_\odot$, Liebert, Bergeron, & Holberg 2004) is an intermediate value of the masses of the individual double degenerate components (Bergeron et al. 1991). Assuming a luminosity ratio of 1.6:1 between components A & B (from the 0.5 mag average of ΔV and ΔR), a reasonable guess at the individual masses is $M = 0.78\ M_\odot$ for PG 0901+140A and $M = 0.81\ M_\odot$ for PG 0901+140B. If approximately correct, this would place the system at a little more than 40 pc.

Further speculation is not worthwhile, since the component parameters of the resolved double degenerate can be determined from individual spectra. Such a determination would be very useful for the white dwarf initial to final mass relation – analogous to the analysis of PG 0922+162 by Finley & Koester (1997).

A.5.10 LP 618-14

LP 618-14 was identified by S. Salim (2002, private communication) during a survey intended to find previously unidentified white dwarfs in the new Luyten two tenths catalog (Salim & Gould 2002). Its reduced proper motion placed in within the white dwarf sequence while its Sloan colors were a little too red for a single degenerate star.

Its spectrum in Figure 4.46 reveals the blue continuum of a cool DA or DC star plus the TiO bands of a red dwarf. Unfortunately, the spectrum has sufficiently low signal to noise as to preclude a more precise estimate of the white dwarfs effective temperature. Also the UBV photometry was performed on images acquired under less than ideal weather conditions. The $U - B = -0.45 \pm 0.15$ color of LP 618-14 is consistent with a large range of effective temperatures; $6000 - 13,000$ K for a hydrogen atmosphere white dwarf with $\log g = 8.0$, up to 15,000 K for $\log g \leq 7.5$, but only $6000 - 8000$ K for $\log g \geq 8.5$ or for a helium atmosphere at any value of $\log g$ (Bergeron, Saumon, & Wesemael 1995). Additionally, it is not known whether the red dwarf contributes significantly at B band. A good blue spectrum and photometric UBV data would end this ambiguity.

The luminosity contribution of the two components is further confused by the "later is earlier" (§4.4.1) possibility because the distance to the system is not nailed down. The reduced proper motion indicates LP 618-14 should be within 50 pc of the sun ($\mu = .32''$ yr^{-1}), but this interpretation is thwarted by predicting a spectral type later than M7 for the red dwarf companion ($M_K \geq 10.0$ mag). This appears to be inconsistent with the spectrum in Figure 4.46. Alternatively, if one constrains the spectral type of the secondary to no later than M5, the system is located at $d > 100$ pc with a very high tangential velocity ($v_{tan} > 150$ km s^{-1}). This results in a white dwarf with a relatively large radius at ~ 9000 K; a helium

core degenerate with $M < 0.4\ M_{\odot}$ (Bergeron, Saumon, & Wesemael 1995). This is a real possibility for any white dwarf in a close binary (Marsh, Dhillon, & Duck 1995) but further investigation is required before firm conclusions may be drawn.

A.5.11 LP 761-114

LP 761-114 is first mentioned in Oswalt et al. (1996) as a white dwarf in a wide binary system, where it is reported as the lowest luminosity star in a sample used to place a lower limit to the age of the Galactic disk. Silvestri, Oswalt, & Hawley (2002) and Holberg, Oswalt, & Sion (2002) corroborate this interpretation, reporting $V = 17.45$ mag, $V - I = 1.75$, $T_{\rm eff} = 4020$ K, and a photometric distance of $d = 15.3$ pc.

First of all, the M2 dwarf common proper motion companion absolutely rules out a distance of less than 20 pc (Kirkpatrick & McCarthy 1994). Secondly, this system suffers from the same type of problem as does LDS 826 (§6.5.4); its visual early M dwarf neighbor can easily contaminate photometric measurements of the cool white dwarf. The M star $7.7''$ distant positively dominates the binary flux ratio at all wavelengths, including U band where it is over 2 magnitudes brighter than the white dwarf. It gets much worse toward longer wavelengths with $\Delta V = 4.26$ mag, $\Delta I = 5.81$ mag. This is a somewhat unusual arrangement – in a typical white dwarf plus M dwarf binary, the degenerate star dominates the UBV flux.

The photometry presented for LP 761-114 in Table 4.3 was measured with near zero contamination as described in §4.5, and tells a slightly different story than the existing analyses in the literature (Oswalt et al. 1996; Silvestri, Oswalt, & Hawley 2002; Holberg, Oswalt, & Sion 2002). The V magnitude measured here is 0.4 mag fainter than what is reported in the aforementioned studies; a clear

sign that previous measurements were contaminated by the relatively bright M companion. The measured color of $V - I = 0.73$ is much bluer than previously reported and further confirmation of pollution by the glaring neighbor.

The resulting optical and near infrared colors of LP 761-114 are not consistent with a 4000 K helium atmosphere white dwarf (Oswalt et al. 1996). Comparing its colors (e.g. $U - B = -0.31$, $V - J = 1.17$) with models of cool helium and hydrogen atmosphere white dwarfs, one finds very good agreement with a hydrogen atmosphere degenerate at $T_{\rm eff} = 6000$ K (Bergeron, Saumon, & Wesemael 1995). The near infrared measurements were extremely difficult due to $6.5 - 7$ mag brightness difference between components and possesses the lowest (but still reliable) signal to noise ratio of all the photometry done on this system.

Is this new interpretation consistent with the photometric distance to the M2 dwarf companion? Comparing the optical and near infrared magnitudes of LP 761-113 with spectral standard absolute magnitudes from Kirkpatrick & McCarthy (1994), the average distance modulus is $m - M = 3.38 \pm 0.04$ or $d = 47.4 \pm 0.9$ pc. This would yield an absolute magnitude of $M_V = 14.45$ mag for the white dwarf, indicating $\log g = 8.17$ or $M = 0.70\ M_\odot$ – a perfectly reasonable mass for a white dwarf that has been cooling for more than 3.2 Gyr (Bergeron, Saumon, & Wesemael 1995).

A.5.12 PG 1539+530

PG 1539+530 is listed as a DA2 in McCook & Sion (1987) but is mysteriously absent from McCook & Sion (1999). The PG catalog lists type DA2 for this star and in the comments column of Table 5 is the note "DBL" (Green, Schmidt, & Liebert 1986). The removal of an object from the white dwarf catalog is usually a sign of misclassification, but in this case the original classification is the correct

one.

The composite spectrum of PG 1539+530AB is shown in Figure 4.43. It clearly displays the spectral features of an early M dwarf plus a few pressure broadened Balmer lines typical of hot white dwarfs. The Hα line has been completely masked by the brighter M companion, but at least 3 more hydrogen lines are visible out to a partial Hϵ.

The pair has been resolved at a separation of 2.7″ on the sky. The M dwarf component, PG 1539+530B, has colors and a spectrum consistent with spectral type M2. The white dwarf component, PG1539+530A, has optical and near infrared colors consistent with a $T_{\rm eff} = 25,000$ K DA star and is actually fainter than its companion at V band and longward. Comparison of the photometry in Table 4.3 with the optical and near infrared absolute magnitudes for M2 dwarfs yields a photometric distance of $d = 162 \pm 4$ pc for PG 1539+530B (Kirkpatrick & McCarthy 1994). At this distance, a 25,000 K DA white dwarf has $M_V = 10.47$ mag, log $g = 8.09$ and a mass of $M = 0.69\ M_\odot$ according to models (Bergeron, Saumon, & Wesemael 1995).

A.5.13 PG 2244+031

PG 2244+031 is noted as a DA1 with a composite spectrum in the PG catalog (Green, Schmidt, & Liebert 1986). This work designates the system as a visual binary consisting of the DA1 white dwarf PG 2244+031A plus an M3.5 dwarf companion at 2.4″, PG 2244+031B. The composite optical spectrum of the binary is shown in Figure 4.45.

However, there is significant confusion and inaccuracy regarding the coordinates, identity, finding chart, and designated WD number for PG 2244+031 in both McCook & Sion (1999) and the current online version of the white dwarf cat-

alog. There are four objects in the following discussion and they will be referred to as objects $1-4$ to help alleviate the existing confusion.

Object 1, PG 2244+031 (WD 2244+031) was first reported as type DC by Green (1980) and this paper contains the only published finding chart for any of the four objects. The coordinates given in Table 3 of Green (1980) for object 1 more or less correctly identify the position of PG 2244+031AB. Those correct coordinates are $22^{\rm h}44^{\rm m}49^{\rm s}$, $+03^\circ05'54''$ B1950 or $22^{\rm h}47^{\rm m}22^{\rm s}$, $+03^\circ21'45''$ J2000.

Object 2, HS 2244+0305 (WD 2244+030) is designated as a DA1 (Homeier et al. 1998) with coordinates identical to those of object 1 listed above, but is listed separately from PG 2244+031 in the most current version of the white dwarf catalog. This is an error; WD 2244+031 and WD 2244+030 are the same object.

Object 3 is the star which is identified in the finding chart of Green (1980) for PG 2244+031. This chart points to coordinates $22^{\rm h}44^{\rm m}16^{\rm s}$, $+03^\circ06'20''$ B1950 or $22^{\rm h}46^{\rm m}48^{\rm s}$, $+03^\circ22'10''$ J2000 and a completely different object from PG 2244+031. Photometry was performed on object 3 and it has $B-V=0.44$ and $V-K=1.37$. These values are consistent with the colors of a G0 star, perhaps a sdG0. A spectrum of object 3 was not taken due to the suspicion of being the incorrect object based on the combination of inconsistent coordinates and its colors. Perhaps object 3 is the star which Green (1980) observed and noted as having a DC spectrum. As explained in the first few sections of this chapter, it is not uncommon that a metal poor subdwarf is mistaken for a DC white dwarf.

Object 4 is the star corresponding to the coordinates in the PG catalog for PG 2244+031. These coordinates neither match the finding chart of Green (1980) nor the coordinates in Table 3 of Green (1980). The PG coordinates are $22^{\rm h}44^{\rm m}25^{\rm s}$, $+03^\circ08'52''$ B1950 or $22^{\rm h}46^{\rm m}57^{\rm s}$, $+03^\circ24'41''$ J2000 (Green, Schmidt, & Liebert 1986). No finding chart is provided as the identity and coordinates of object 3

in Green (1980) and object 4 in Green, Schmidt, & Liebert (1986) are assumed to be one and the same. However, photometry was performed on object 4 and it has $B - V = 0.50$ and $V - K = 1.51$. These values are consistent with the colors of a G5 star, perhaps a sdG5. Again, a spectrum of object 4 was not taken due to the suspicion of being the incorrect object based on the combination of inconsistent coordinates and its colors.

To summarize, the objects PG 2244+031, WD 2244+031, HS 2244+0305, & WD 2244+030 are identical to the DA1+M3.5 visual binary described here as PG 2244+031AB. All published coordinates for these objects are in error with the exception of those in Green (1980), and more accurately in Homeier et al. (1998). The only correct finding chart in the literature is the one shown here in Figure 4.19.

A.5.14 GD 74

GD 74A is well cited in the literature but only one study has produced a distance estimate. Bergeron, Saffer, & Liebert (1992) gives $T_{\rm eff} = 16,900$ K, $\log g = 7.99$, $M = 0.59\ M_{\odot}$, and $M_V = 11.11$ mag for GD 74A. If correct, this would place the DA white dwarf at just under 60 pc.

However, the optical and near infrared colors inferred from the photometry in Table 4.3 indicate an effective temperature higher than 17,000 K for GD 74. With colors such as $V - K = 0.79$, hydrogen atmosphere white dwarf models predict a temperature much closer to 25,000 K. Such a DA2 star with $\log g = 8.0$ would have a photometric distance closer to 85 pc (Bergeron, Saumon, & Wesemael 1995).

What does the photometric distance to its M4 common proper motion companion indicate? Comparison of the photometry in Table 4.3 with the optical

and near infrared absolute magnitudes for M4 dwarfs yields a photometric distance of $d = 97 \pm 6$ pc for GD 74B (Kirkpatrick & McCarthy 1994). These two distances may be truly different, the two stars coincidentally having the same proper motion. But it is also possible that GD 74A is farther away than previously suspected; it may be a double degenerate or simply have $\log g < 8.0$. At $M_V = 10.0$ mag, GD 74A could be a single 25,000 K DA star with $M = 0.54\ M_\odot$ (Bergeron, Saumon, & Wesemael 1995).

A.5.15 GD 123

GD 123A is a DA white dwarf that has been repeatedly studied in the literature, with a well corroborated effective temperature near 30,000 K. The average of five independent spectroscopic analyses gives $T_{\rm eff} = 29,500$ K, $\log g = 7.92$, and $M_V = 9.86$ mag (Finley, Koester, & Basri 1997; Marsh et al. 1997; Vennes et al. 1997; Napiwotzki, Green, & Saffer 1999; Liebert, Bergeron, & Holberg 2004). This would place the GD 123 system near 81 pc.

The binarity of GD 123 was first found by Green, Schmidt, & Liebert (1986) who noted a composite spectrum of a DA4+K. Optical and near infrared analysis done here indicates that GD 123B is an M4.5 dwarf. The photometric distance to GD 123B is $d = 67 \pm 2$ pc (Kirkpatrick & McCarthy 1994), which indicates it may be slightly overluminous, raising the possibility of a third cool component in the GD 123 system.

A.5.16 GD 337

GD 337A is reported as a DA2 white dwarf in McCook & Sion (1999). This was recently corroborated by Liebert, Bergeron, & Holberg (2004) who give $T_{\rm eff} = 22,400$ K, $\log g = 7.80$, and $M_V = 10.23$ mag. A photometric distance of 151 pc

is inferred from these data.

Probst (1983) first detected the still unresolved companion by its near infrared excess emission. The presence of a late type confirmed has been confirmed by its observed composite spectrum (Green, Schmidt, & Liebert 1986; Greenstein 1986b). The analysis here places GD 337B at spectral type M4.5. Comparing its inferred optical and near infrared magnitudes with the absolute magnitudes of M4.5 dwarfs from Kirkpatrick & McCarthy (1994), its photometric distance is $d = 180 \pm 5$ pc.

GD 337 also has three parallax measurements in McCook & Sion (1999), all of which give $\pi \leq 0.004''$ yet with substantial uncertainties as to make them indicative but not firm. These data may substantiate the greater distance implied by the companion, they may not. If the GD 337 system is as distant as 180 pc, GD 337A may be a double degenerate.

A.5.17 GD 984

GD 984A is a well studied hot DA white dwarf. At least five independent spectroscopic studies have been carried out, yielding average parameters of $T_{\rm eff} = 49,000$ K, $\log g = 7.85$, and $M_V = 8.95$ mag (Finley, Koester, & Basri 1997; Marsh et al. 1997; Vennes et al. 1997; Napiwotzki, Green, & Saffer 1999; Koester et al. 2001). If correct, this would place the system near 108 pc.

There is some spread in the derived effective temperatures and surface gravities for GD 984A, perhaps due to its unresolved companion, GD 984B. The M2 dwarf contaminates the Balmer lines of the white dwarf as blue as Hγ, making the spectroscopic parameter fit less certain (Finley, Koester, & Basri 1997). The spread in temperature estimates ranges from $43,000 - 57,000$ K and surface gravity from $\log g = 7.7 - 8.2$ (Marsh et al. 1997; Koester et al. 2001).

What does the photometric distance to GD 984B say? Comparing its optical and near infrared photometry in Table 4.4 with the absolute magnitudes for an M2 dwarf, the average distance is $d = 185 \pm 2$ pc (Kirkpatrick & McCarthy 1994). There is a significant difference between this distance for GD 984B and the preceding value derived for the GD 984A. Since there is a fair amount of room for uncertainty in the parameters of the white dwarf, it is quite possible this farther distance is the correct one. At 185 pc, GD 984A would have $M_V = 7.77$ mag. Even with an effective temperature of 60,000 K, this would imply a radius too large for a single white dwarf with $M \geq 0.5\ M_\odot$. At $T_{\rm eff} = 50,000$ K, this implies $\log g = 7.23$ or $M = 0.43\ M_\odot$ (Bergeron, Saumon, & Wesemael 1995). Therefore, if GD 984A has a distance near 185 pc, it is almost certainly a double degenerate or low mass, helium white dwarf.

A.5.18 LTT 8747

LTT 8747A is a nearby cool DA star ripe for a trigonometric parallax measurement. The ARICNS database gives a *photometric* parallax of $0.051 \pm 0.006''$ but it is not included in a recent list of white dwarfs within 20 pc (Holberg, Oswalt, & Sion 2002). The reason stated in Holberg, Oswalt, & Sion (2002) for exclusion is that it belongs to a group of white dwarfs which "all have trigonometric parallaxes smaller than $0.05''$" while citing McCook & Sion (1999). This may be an error because the ARICNS value of $0.051''$ is cited in McCook & Sion (1999) as a *trigonometic* parallax and no other value or measurement exists in the literature.

The photometric parallax may be reliable as it is based only on UBV magnitudes and colors. Zuckerman et al. (2003) report $T_{\rm eff} = 7660$ K and $\log g = 7.80$ from $UBVRI$ photometry and parallax (which must be the same *photometric* parallax mentioned above). This effective temperature is likely a bit too low as

LTT 8747B contributes to the I band flux, causing the white dwarf to appear slightly cooler.

The analysis here finds $T_{\rm eff} = 8500$ K is quite consistent with both the UBV and Stromgren colors of LTT 8747A (both published and those measured in this work) (Eggen & Greenstein 1965; McCook & Sion 1999). This results in a photometric distance of $d = 22.6$ pc for $\log g = 8.0$, possibly closer if its mass is greater than 0.60 $M_{\odot}$. Still, alltogether the existing analyses indicate a distance very close to 20 pc.

The possible radial velocity variable companion (Schultz, Zuckerman, & Becklin 1996; Maxted, Marsh, & Moran 2000), LTT 8747B is certainly a late M dwarf by both its contribution to the composite spectrum in Figure 4.50 (at least one band of VO can be seen) and by the $J - K = 1.10$ composite color of the binary (Kirkpatrick, Henry, & McCarthy 1991; Kirkpatrick & McCarthy 1994; Kirkpatrick et al. 1999b). The inferred colors of LTT 8747B indicate an M8 dwarf with an uncertainty of 1 spectral type (Kirkpatrick & McCarthy 1994; Dahn et al. 2002). If it has an absolute K magnitude typical of an M8V, then $d = 19.4$ pc is inferred. At this distance LTT 8747A would have $M_V = 13.10$ mag, $\log g = 8.20$, and $M = 0.73$ $M_{\odot}$ for $T_{\rm eff} = 8500$ K (Bergeron, Saumon, & Wesemael 1995).

A.5.19 PG 0308+096

PG 0308+096 is a post common envelope binary consisting of a DA2 white dwarf and the M4.5 dwarf reported here in a 0.3 d orbit (Saffer et al. 1993). A recent spectroscopic analysis gives $T_{\rm eff} = 25,900$ K, $\log g = 8.08$, and $M_V = 10.37$ mag for PG 0308+096A (Liebert, Bergeron, & Holberg 2004). The distance inferred from these white dwarf parameters is $d = 101$ pc.

Comparing the optical and near infrared magnitudes of PG 0308+096B with the absolute magnitudes for M4.5 dwarfs from Kirkpatrick & McCarthy (1994), the resulting photometric distance is 114 pc. Hence it is possible that PG 0308+06A has a slightly larger radius, and is less massive than implied by spectroscopy.

A.5.20 PG 0950+185

PG 0950+185 is a visual double containing a hot DA white dwarf plus the M2 dwarf reported here 1.1″ distant (Green, Schmidt, & Liebert 1986; Greenstein 1986b). The only spectoscopic analysis in the literature gives $T_{\rm eff} = 31,800$ K, $\log g = 7.68$, $M = 0.50\ M_{\odot}$, and $M_V = 9.29$ mag for PG 0950+185A (Liebert, Bergeron, & Holberg 2004). The distance inferred from these parameters is $d = 201$ pc.

If this is correct, the implied absolute K magnitude of $M_K = 5.28$ mag for PG 0950+185B is significantly brighter than the expected value of $M_K = 6.00$ mag for a single M2 dwarf (Kirkpatrick & McCarthy 1994). The difference between the standard optical and near infrared magnitudes of an M2 dwarf at 201 pc and the apparent magnitudes of PG 0950+185B are 0.59 mag at I, 0.60 mag at J, 0.70 mag at H, and 0.72 mag at K. Hence, there appears to be excess flux at all reliably measureable wavelengths. If the 201 pc distance is accurate, it is likely that PG 0950+185B is a binary M2 dwarf consisting of two nearly equal luminosity stars.

A.5.21 PG 0956+045

PG 0956+045 is a visual visual double containing a DA3 white dwarf plus the M4.5 dwarf reported here 2.0″ distant (McCook & Sion 1999). The only specto-

scopic analysis in the literature gives $T_{\rm eff} = 18,200$ K, $\log g = 7.81$, $M = 0.52$ $M_{\odot}$, and $M_V = 10.62$ mag for PG 0956+045A (Liebert, Bergeron, & Holberg 2004). The distance inferred from these parameters is $d = 113$ pc.

Using both optical and near infrared absolute magnitudes for an M4.5 dwarf from Kirkpatrick & McCarthy (1994), the average distance modulus for PG 0956+045B is $m - M = 6.25 \pm 0.17$ or $d = 178 \pm 15$ pc. There are two puzzling aspects of this result: one is the mismatch in photometric distances between the white dwarf and red dwarf components in the binary, and the second is relatively large standard deviation in the distance modulus.

The V and R magnitudes for PG 0956+045B are unusual and do not seem to match what might be expected from an mid M type dwarf. Specifically, they are significantly fainter than an extrapolation from the $IJHK$ magnitudes would predict and color indices involving V and/or R appear to be inconsistent with those involving only the other bands. It is possible that the V band magnitude for PG 0956+045B is somewhat inaccurate due to both low signal to noise plus additional uncertainty from deconvoling its PSF from the much brighter PG 0956+045A. However, the R band measurement had a signal to noise ratio over 200, and is both reliable and robust – the measurement was repeated in numerous ways, always with near zero residuals after PSF subtraction and predicting the correct relative instrumental magnitude for PG 0956+045A (certainly within the typical 0.05 mag standard error). As an example of the resulting discrepancy, the $I - K = 2.34$ color is consistent with a spectral type of M4 and one might expect something near $R - I \approx 1.6$ for this spectral type (Kirkpatrick & McCarthy 1994). But PG 0956+045B has $R - I = 2.24$ and, by itself, predicts a spectral type between M6−M6.5 (Kirkpatrick & McCarthy 1994). A spatially resolved optical spectrum of PG 0956+045B might shed light on this issue.

Returning to the mismatch of photometric distances, there are three distinct possiblities. One is that the flux of the red secondary may have contaminated the spectoscopic analysis of Liebert, Bergeron, & Holberg (2004), causing PG 0956+045A to appear cooler that it actually is. A hotter, more luminous white dwarf would be more consistent with a distance of around 180 pc. But its measured colors such as $V - K = -0.58$ are consistent with a white dwarf of $T_{\rm eff} \sim 17,000$ K (Bergeron, Saumon, & Wesemael 1995). The second possibility is that PG 0956+045B is an M dwarf at 113 pc with $M_K = 8.66$ mag, corresponding to a spectral type near M5.5 for the main sequence. This seems unlikely since such an M dwarf should have $I - K \approx 3.0$ (Kirkpatrick & McCarthy 1994). A variation of this second prospect could be made by invoking a subdwarf to explain the discrepancy between the colors of the secondary and the absolute magnitude implied by $d = 113$ pc. While this is certainly possible, it is unlikely based on the disk like kinematics of the PG 0956+045 system (Table 3.1). The third possible explanation is simply that the white dwarf distance has been underestimated due to binarity.

A combination of the above factors could explain the discrepancy between the inferred distances of PG 0956+045A & B. In any case, the difference between their distance moduli is greater than 0.9 and is worthy of further exploration.

A.5.22 PG 1015+076

PG 1015+076A is a DA2 star that has been repeatedly misclassified as a much cooler white dwarf due to the presence of a background main sequence star 2.0″ distant (Green, Schmidt, & Liebert 1986; Zuckerman et al. 2003). The background star has $V - K = 1.61$ and is probably a G type star. The spectrum of PG 1015+076A in Figure 4.21 is almost certainly contaminated at some level by

the continuum light of the nearby G star. This is why it does not have as steep a slope as would be expected from a DA2 white dwarf and also why Hβ and Hγ are diluted while Hα is nearly absent. The optical photometry for PG 1015+076A and background G star was performed without mutual contamination. Its optical colors from Table 4.3 (plus $U-B=-0.98$) indicate $T_{\rm eff} \approx 25,000$ K for the white dwarf (Bergeron, Saumon, & Wesemael 1995).

PG 1015+076B is the M3 dwarf common proper motion companion to PG 1015+076A. Comparing its optical and near infrared magnitudes in Table 4.3 with the expected absolute magnitudes of a typical M3, the average distance modulus is $m-M=6.44\pm0.06$, implying $d=194\pm6$ (Kirkpatrick & McCarthy 1994). At this distance PG 1015+076A should have $M_V = 10.16$ mag, which corresponds to log $g = 7.89$ or $M = 0.59\ M_\odot$ for $T_{\rm eff} = 25,000$ K (Bergeron, Saumon, & Wesemael 1995).

A.5.23 PG 1210+464

PG 1210+464 is an unresolved binary DA+dM, evidenced by its composite spectrum and infrared excess Green, Schmidt, & Liebert (1986); Zuckerman & Becklin (1992); Schultz, Zuckerman, & Becklin (1996). The white dwarf, PG 1210+464A, has spectroscopic parameters $T_{\rm eff} = 27,700$ K, log $g = 7.85$, and $M_V = 9.87$ mag (Liebert, Bergeron, & Holberg 2004). Hence, its photometric distance is around $d = 139$ pc.

Its companion, PG 1210+464B is estimated to be spectral type M2 based on its deconvolved $R-I$ and $I-K$ colors. Comparing its optical and near infrared magnitudes in Table 4.4 with the expected absolute magnitudes of a typical M2 dwarf, the average distance is $d=111\pm4$ (Kirkpatrick & McCarthy 1994). The ~ 0.5 mag difference in the expected versus observed K magnitude

of PG 1210+464B is not huge, but there is further evidence that it may be overluminous. The composite $J - K = 0.91$ color of the binary is a bit too red for a single early M star companion. Deconvoling the red dwarf flux from the contribution of the white dwarf gives $J - K = 1.02$ for PG 1210+464B. Based on these two pieces of evidence, it appears likely that there is a third component in the system contributing (minimally) to the flux at K band. This scenario is more consistent with the 139 pc phtometric distance to PG 1210+464A.

A.5.24 PG 1654+160

PG 1654+160 is a relatively rare DB+dM system; the only such system out of 61 white dwarf plus M dwarf pairs discovered or described in this work. PG 1654+160A itself is an uncommon object, a DBV (Winget et al. 1984; Beauchamp et al. 1999).

Spectroscopic investigation indicates the pulsating helium atmosphere white dwarf has parameters in the range $T_{\rm eff} = 24,300 - 27,800$ K, $\log g = 7.95 - 8.00$, depending on whether there is a trace amount of hydrogen in its atmosphere versus none. Helium atmosphere models predict that a white dwarf with $T_{\rm eff} = 26,000$ K and $\log g = 8.0$ would have $M_V = 10.38$ mag and $M = 0.61\ M_\odot$ (Bergeron, Saumon, & Wesemael 1995). If correct, this would place the PG 1654+160 system at a distance near 171 pc.

Recent astroseismological analysis of data acquired using the Whole Earth Telescope may corroborate the spectroscopically determined parameters of PG 1654+160A. Detection of nearly equal spacing between pulsation periods was found to be consistent with with the expected mean period spacing of a normal mass ($M \approx 0.6\ M_\odot$) DB white dwarf pulsating in nonradial $\ell = 1$ modes (Handler et al. 2003).

However, the photometric distance to the M4.5 dwarf companion is positively inconsistent with this interpretation. Comparing the optical and near infrared magnitudes of PG 1654+160B with absolute magnitudes expected of an M4.5 dwarf yields a distance modulus of $m - M = 4.49 \pm 0.11$ or $d = 79 \pm 4$ pc (Kirkpatrick & McCarthy 1994).

This serious discrepancy calls into question the binary nature of the apparent common proper motion pair. It is quite easy to see the elongated pair moving together while blinking the digitized POSS I & II red sensitive plates. Both the relative proper motion and the elongation are readily visible using the blue and infrared sensitive scans, but the contrast is best for the red plates where the components have nearly equal brightness. However, the pair is not well resolved in either of the two POSS epochs, and therefore accurate photocenters (centroids) are not possible for any of these digitized scans. The position angle corresponding to the elongation axis appears constant over the 46 year baseline between POSS epochs and consistent with the 131.0° value (epoch 2003.3) in Table 4.1. Using a single centroid for the elongated pair in the POSS I & II red sensitive plate scans, a proper motion of $\mu = 0.085''$ yr^{-1} at $\theta = 137°$ is obtained over a 39 year baseline. This value is somewhat greater than the USNO B1.0 value in Table 3.1 but consistent with an object whose photocenter is perturbed depending on whether blue (white dwarf dominated centroid), red (maximum elongation) or infrared (red dwarf dominated centroid) POSS plates are used for astrometry. If the two stars are unrelated, the pair should have separated by as much as $4.5''$ since the epoch 1950.4 POSS I red plate was observed. The conclusion based on this analysis is that the visual pair is almost certainly a physical binary based on its common proper motion.

Still remaining is the 1.75 mag discrepancy between the expected magnitude

of an M4.5 dwarf at 79 pc versus 171 pc. If PG 1654+160B is as far away as 171 pc, it would have to consist of 5 equally luminous stars to explain this difference. Since the probability of this is vanishing, the only possibility remaining is that PG 1654+160A is located much closer to 79 pc. If correct, this implies $M_V = 12.13$ mag for the DB white dwarf. While this absolute magnitude is completely reasonable for cool white dwarfs, it is utterly out of the ordinary for such a hot degenerate. At $d = 79$ pc, PG 1654+160A would be an ultramassive white dwarf with $M > 1.19\ M_\odot$ for a DB with $T_{\rm eff} = 26,000$ K. Only a lower limit can be given as the models used here do not exceed $\log g = 9.0$ (Bergeron, Saumon, & Wesemael 1995).

Clearly, the PG 1654+160 system requires follow up observations and analysis in order to constrain both its distance and the parameters of its components.

A.5.25 PG 1659+303

PG 1659+303A is a DA white dwarf with spectroscopically determined parameters $T_{\rm eff} = 13,600$ K, $\log g = 7.95$, and $M_V = 11.35$ mag (Liebert, Bergeron, & Holberg 2004). If correct, this places the system at $d = 53$ pc.

The $V - K = 4.28$ color of PG 1659+303B places it between spectral types M2−M2.5. Its measured spectrum in Figure 4.30 is consistent with this interpretation and gives no indication of subsolar metallicity (i.e. it is not a subdwarf). Comparing the expected optical and near infrared absolute magnitudes for these types with the apparent magnitudes in Table 4.3, the average distance falls in the range $d = 67 - 82$ pc (Kirkpatrick & McCarthy 1994). As in previous examples, this may imply that PG 1659+303A is a double degenerate or a low mass white dwarf. In fact, the entire distance range above is incompatible with a single 13,600 K DA white dwarf with $M \geq 0.5\ M_\odot$ (Bergeron, Saumon, & Wesemael

1995).

It is possible that the common proper motion measured for both PG 1659+303A & B is coincidental. This would explain the above distance discrepancy. But until further evidence is obtained, it is reasonable to regard the common proper motion as a strong indicator of a physically bound system.

A.5.26 Rubin 80

Rubin 80A is listed as a DA6 in McCook & Sion (1999) while referencing an unpublished spectrum taken around 1979. But caution is warranted because an unresolved low mass companion can contaminate both spectra and colors, thus causing a white dwarf to appear cooler than it is. Greenstein (1986a) first noted the companion to Rubin 80A in its composite spectrum as well as commenting that the companion affected his measured colors of the white dwarf. Zuckerman et al. (2003) gives $T_{\rm eff} = 7765$ K based on $UBVRI$ colors, but this might be too cool due to the inclusion of the RI bands in the determination. Examining only the $U - B = -0.57$ and $B - V = +0.28$ colors (this work finds $U - B = -0.55$, $B - V = +0.29$), an effective temperature near 8000 K ($\log g = 8$) is implied by both color indices independently (Bergeron, Saumon, & Wesemael 1995). Hence it appears the DA6 type is likely to be accurate, assuming the flux of Rubin 80B does not contribute at B (a safe assumption).

However, the blue continuum slope of Rubin 80 (Figure 4.49) is slightly steeper than LTT 8747 ($T_{\rm eff} = 8500$ K, Figure 4.50), which is consistent with Rubin 80A having a higher effective temperature than LTT 8747. Both stars were observed on the same night with the same instrument, setup and calibration. Possible errors in flux calibration were searched for unsuccessfully and a variety of standard star sensitivity functions were used, all producing the similar results.

In order to deconvolve the $IJHK$ magnitudes of the companion, an effective temperature of 9000 K was used for the values in Table 4.4. While this may be too high, it turns out to be more consistent with the resulting parameters for the red dwarf companion, Rubin 80B. Two possibile temperatures for the white dwarf are explored below.

If Rubin 80A is a $T_{\rm eff} = 9000$ K DA white dwarf with $\log g = 8.0$, then it should have $M_V = 12.55$ mag (Bergeron, Saumon, & Wesemael 1995). This implies a distance of 41 pc. At this distance, the implied absolute K magnitude of Rubin 80B is $M_K = 9.76$ mag, which agrees quite well with that expected for a typical M7 dwarf (Kirkpatrick & McCarthy 1994; Dahn et al. 2002). The deconvolved $J - K = 1.00$ color of Rubin 80B implies a spectral type of M7 or later, while the $I - J = 2.13$ implies a spectral type as early as M5.5. Which is right? First of all, although the compsosite spectrum of Rubin 80 suffers from fringing, at least one VO band is visible. This implies a spectral type of M6.5 or later and is consistent with the near infrared colors (Kirkpatrick, Henry, & McCarthy 1991; Kirkpatrick & McCarthy 1994). The deconvolved I band measurement contains a fair amount of uncertainty due to the model white dwarf magnitude being only 0.5 mag fainter than the composite value; it is highly sensitive to small changes in either the composite and/or model value. Therefore, the estimated spectral type given here is M7 and is further corroborated by the likely white dwarf distance.

If instead Rubin 80A has $T_{\rm eff} = 8000$ K and this effective temperature is used to deconvolve the $IJHK$ magnitudes for Rubin 80B, the result is $I - J = 2.42$ and $J - K = 1.03$. This is quite consistent with the expected colors of an M7 dwarf (Kirkpatrick & McCarthy 1994). However, the implied distance for a DA white dwarf with $\log g = 8.0$ and $T_{\rm eff} = 8000$ K is 33 pc (Bergeron, Saumon,

& Wesemael 1995). This distance implies an absolute K magnitude for Rubin 80B of $M_K = 10.31$ mag – much too faint for its colors (Kirkpatrick & McCarthy 1994; Dahn et al. 2002). In fact, if the white dwarf does have $T_{\rm eff} = 8000$ K, it would have to be a low mass white dwarf ($M = 0.40\ M_\odot$) or double degenerate in order to predict an absolute K magnitude bright enough for spectral type M7 or earlier (Bergeron, Saumon, & Wesemael 1995). In fact, the equivalent widths for the Hα & Hβ lines together are 26% larger in LTT 8747A than in Rubin 80A. This may be hard evidence in favor of a lower surface gravity for Rubin 80A, since both it and LTT 8747A have similar effective temperatures.

Table 6.3 summarizes the possibilities for the Rubin 80 system. In any case it should be close enough for a trigonometric parallax.

Table A.3: Alternate Parameters for Rubin 80A & B

Object	$T_{\rm eff}$	log g	V	I	J	K	d (pc)
WD	9000 K	8.0	15.62	15.38	15.36	15.33	41.1
RD	-	-	-	15.96	13.83	12.83	40.7
WD	8000 K	8.0	15.58	15.21	15.08	14.97	32.6
RD	-	-	-	16.33	13.91	12.88	41.7
WD	8000 K	7.6	15.58	15.21	15.08	14.97	41.7
RD	-	-	-	16.33	13.91	12.88	41.7

Note– The distance column for the red dwarf contains the distance expected for an M7 dwarf of solar metallicity (Kirkpatrick & McCarthy 1994; Dahn et al. 2002)

A.5.27 Ton S 392

TS 392A is a very hot DA white dwarf that is not well studied. The only published paper which studies TS 392A is Greenstein (1979), who notes the white dwarf is a "very hot" narrow lined DA. The coordinates in McCook & Sion (1999) are inaccurate by almost $3'$. Accurate coordinates are given in Figure 4.20 and have been checked against a photographic finding chart provided by J. Greenstein (B. Zuckerman 2002, private communication).

The near infrared excess of TS 392 was noticed in January 1992 at the IRTF, but remained unpublished until now. Wachter et al. (2003) were the first to publish near infrared magnitudes for TS 392 which indicate the presence of a cool stellar companion.

The spectrum in Figure 4.44 has a turnover near the blue end of the spectrum that is almost certainly not real. Possible errors in flux calibration were searched for unsuccessfully. Attempting to correct the turnover to the expected continuum resulted in a sensitivity function that produced grossly incorrect shapes for all other stars taken on the same night with the same instrument and setup. In fact, all the other stars similarly observed appear to have accurately flux calibrated spectra, but there is a possibility of a calibration error that went undetected. TS 392 was observed at a high airmass of $\sec z = 2.40$ and this may be the source of the error. In any case, the spectrum verifies a fairly steep blue continuum from a hot DA white dwarf with weak Hα & Hβ absorption plus TiO band from its $\sim 1''$ distant M dwarf companion.

Virtually nothing was known or published about this system until now, so distance estimates and parameter determinations should be considered somewhat preliminary. Treating TS 392A as a $T_{\rm eff} = 50,000$ K white dwarf, the deconvolved magnitudes of TS 392B result in colors consistent with an M3 dwarf, ± 1

spectral type (Kirkpatrick & McCarthy 1994). However, assuming $M = 0.50\ M_{\odot}$ ($\log\ g = 7.5$) for such a DA1 predicts a distance of $d = 342$ pc, which is a bit closer than expected ($d = 409$) for an M3 companion (Kirkpatrick & McCarthy 1994; Bergeron, Saumon, & Wesemael 1995) This discrepancy might be explained by a higher effective temperature for the white dwarf. It does not seem worthwhile to speculate further until more accurate parameters for the white dwarf are determined.

Bibliography

Alexander, J., & Lourens J. 1969, MNSSA, 28, 95

Allen, P., Koerner, D., McElwain, M., Murphy, G., Reid, I., Gizis, J., & Kirkpatrick, J. 2003, Proceedings of IAU Symposium 211, ed. E. Martín (San Francisco: ASP), 303

Anselowitz, T., Wasatonic, R., Matthews, K., Sion, E., & McCook, G. 1999, PASP, 111, 702

Barrado y Navascés, D., Bouvier, J., Stauffer, J., Lodieu, N., & McCaughrean, M. 2002, A&A, 395, 813

Basri, G., Marcy, G., & Graham, J. 1996, ApJ, 458, 600

Bate, M. 2000, MNRAS, 314, 33

Bate, M,. Bonnell, I., & Bromm, V. 2002, MNRAS, 332, 65

Beauchamp, A., Wesemael, F., Bergeron, P., Fontaine, G., Saffer, R., Liebert, J., & Brassard, P. 1999, ApJ, 516, 887

Becklin, E. & Zuckerman, B. 1988, Nature, 336, 656

Beers, T., Chiba, M., et al. 2000, AJ 119, 2866

Béjar, V., Martín, E., Zapatero-Osorio, M., Rebolo, R., Barrado y Navascués, D., et al. 2001 ApJ, 556, 830

Bergeron, P., Kidder, K., Holberg, J., Liebert, J., Wesemael, F., & Saffer, R. 1991, ApJ, 443, 764

Bergeron, P., Leggett, S., & Ruiz, M. 2001, ApJS, 133, 413

Bergeron, P., & Liebert, J. 2002 ApJ, 566, 1091

Bergeron, P., Liebert, J., & Fulbright, M. 1995, ApJ, 444, 810

Bergeron, P., Ruiz, M., & Leggett, S. 1997, ApJS, 108, 339

Bergeron, P., Saffer, R., & Liebert, J. 1992, ApJ, 394, 228

Bergeron, P., Saumon, D., & Wesemael, F. 1995, ApJ, 443, 764

Bergeron, P., Wesemael, F. & Beauchamp, A. 1995, PASP, 107, 1047

Bergeron, P., Wesemael, F., Fontaine, G., & Liebert, J. 1990, ApJ, 351, L21

Bessell, M. 1990, PASP, 102, 1181

Bessell, M. 1990, A&AS, 83, 357

Bessell, M. S., & Brett, J. M. 1988, PASP, 100, 1134

Binney, J., & Merrifield, M. 1998, in Galactic Astronomy, (New Jersey: Princeton)

Binney, J., & Tremaine, S. 1987, in Galactic Dynamics, (New Jersey: Princeton)

Bond, H. 1985, Proceedings of the 7th N. American Workshop on Cataclysmic Variables and Low Mass X-Ray Binaries, (Dordrecht: D. Reidel), 15

Bond, H., Grauer, A., Green, R., & Liebert, J. 1984, ApJ, 279, 751

Bond, H., & Livio, M. 1990, ApJ, 355, 568

Bouvier, J., Stauffer, J., Martín, E., Barrado y Navascués, D., Wallace, B., & Béjar, V. 1998, A&A, 336, 490

Bragaglia, A., Renzini, A., & Bergeron, P. 1995, ApJ, 443, 735

Briceño, C., Luhman, K., Hartmann, L., Stauffer, J., & Kirkpatrick, J. 2003, Proceedings of IAU Symposium 211, ed. E. Martín (San Francisco: ASP), 81

Burgasser, A. 2001, Ph.D. Thesis, Caltech

Burgasser, A., Kirkpatrick, J., Reid, I., Brown, M., Miskey, C., & Gizis, J. 2003, ApJ, 586, 512

Burrows, A., Marley, M., Hubbard, W., Lunine, J., Guillot, T., Saumon, D., et al. 1997, ApJ, 491, 856

Burrows, A., Hubbard, W., Lunine, J., & Liebert, J. 2001, RvMP, 73, 719

Butler, P., Marcy, G., Vogt, S., & Fischer, D. 2000, IAU Symposium 202

Carson, J., Eikenberry, S., Brandl, B. & Wilson, J. 2003, Proceedings of IAU Symposium 211, ed. E. Martín (San Francisco: ASP), 271

Chabrier, G., Baraffe, I., Allard, F., & Hauschildt, P. 2000, ApJ, 542, 464

Chabrier, G., & Méra, D. 1997, A&A, 328, 83

Chabrier, G., Segretain, L., & Méra, D. 1996, ApJ, 468, L21

Close, L., Siegler, N., & Freed, M. 2003, Proceedings of IAU Symposium 211, ed. E. Martín (San Francisco: ASP), 249

Close, L., Siegler, N., Potter, D., Brandner, W., & Liebert, J. 2002, ApJ, 567, L53

Cooke, B., et al. 1992, Nature, 355, 61

Cruz, K., Reid, I., Liebert, J., Kirkpatrick, J., & Lowrance, P. 2003, AJ, 126, 2421

Dahn, C., & Harrington, R. 1976, ApJ, 204, L91

Dahn, C., Harrington, R., et al. 1982, AJ, 87, 419

Dahn, C., et al. 2002, AJ, 124, 1170

Downes, R. 1986, ApJS, 61, 569

Drake, J., & Sarna, M. 2003, A&A, 594, 55

Duquennoy, A., & Mayor, M. 1991, A&A, 248, 485

Eggen, O., & Greenstein, J. 1965, ApJ, 141, 83

Eggen, O., & Greenstein, J. 1967, ApJ, 150, 927

Einstein, A. 1905, Annalen der Physik, 17, 132

Farihi, J. 2004, ApJ, 610, 1013

Farihi, J., & Christopher, M. 2004, AJ, 128, 1868

Farihi, J., Becklin, E., & Zuckerman, B. 2003, Proceedings of IAU Symposium 211, ed. E. Martín (San Francisco: ASP), 289

Finley, D., & Koester, D. 1997, ApJ, 489, L79

Finley, D., Koester, D., & Basri, G. 1997, ApJ, 488, 375

Fischer, D., & Marcy, G. 1992, ApJ, 396, 178

Fleming, T., Green, R., Jannuzi, B., Liebert, J., et al. 1993, AJ, 106, 1729

Fontaine, G. Bergeron, P., Billères, M., & Charpinet, S. 2003, ApJ, 591, 1184

Girardi, L., Bressan, A., Bertelli, G., & Chiosi, C. 2000, A&AS, 141, 371

Gizis, J. 2003, Proceedings of IAU Symposium 211, ed. E. Martín (San Francisco: ASP), 303

Gizis, J., Kirkpatrick, J., Burgasser, A., Reid, I., Monet, D., Liebert, J., & Wilson, J. 2001, ApJ, 551, L163

Gizis, J., Reid, I., Knapp, G., Liebert, J., Kirkpatrick, J., Koerner, D., & Burgasser, A. 2003, AJ, 125, 3302

Gizis, J., Reid, I., & Monet, D. 1999, AJ, 118, 997

Green, R. 1980, ApJ, 238, 685

Green, P., Ali, B., & Napiwotzki, R. 2000, ApJ, 540, 992

Green, P., & Margon, B. 1994, ApJ, 423, 723

Green, R., Schmidt, M., & Liebert, J. 1986, ApJS, 61, 305

Greenstein, J. 1974, ApJ, 189, L131

Greenstein, J. 1979, ApJ, 227, 244

Greenstein, J. 1984, ApJ, 276, 602

Greenstein, J. 1986, ApJ, 304, 334

Greenstein, J. 1986, AJ, 92, 867

Handler, G. 2003, MNRAS, 340, 1031

Hambly, N., Hodgkin, S., Cossburn, M., & Jameson, R. 1999, MNRAS, 303, 835

Hawarden, T., Leggett, S., Letawsky, M., Ballantyne, D., & Casali, M. 2001, MNRAS, 325, 563

Heber, U., Bade, N., Jordan, S., & Voges, W. 1993, A&A, 267, L31

Henry, T., & McCarthy, D. 1990, ApJ, 350, 334

Henry, T., & McCarthy, D. 1993, AJ, 106, 773

Hillenbrand, L., & Carpenter, John M. 2000, ApJ, 540, 236

Hintzen, P., & Jensen, E. 1979, PASP, 91, 492

Hinz, J., McCarthy, D., Simons, D., Henry, T., Kirkpatrick, J., & McGuire, P. 2002, AJ, 123, 2027

Høg, E., et al. 2000, A&A, 355, 27

Holberg, J., Oswalt, T., & Sion, E. 2002, ApJ, 571, 512

Homeier, D., Koester, D., et al. 1998, A&A, 338, 563

Hunt, L., et al. 1998, AJ, 115, 2594

Iben, I., & Livio, M. 1993, PASP, 105, 1373

Jameson, R., Dobbie, P., Hodgkin, S., & Pinfield, D. 2002, MNRAS, 335, 853

Jahreiß, H., & Wielen, R. 1997, Hipparcos '97, ed. B. Battrick (Noordwijk: ESA), 675

Jeans, J. 1924, MNRAS, 85, 2

Kawaler, S., et al. 1995, ApJ, 450, 350

Kawka, A., Vennes, S., Dupuis, J., & Koch, R. 2000, AJ, 120, 3250

Kirkpatrick, J., Allard, F., Bida, T., Zuckerman, B., Becklin, E. E., Chabrier, G., & Baraffe, I. 1999a, ApJ, 519, 834

Kirkpatrick, J., Henry, T., & Liebert, J. 1993, ApJ, 406, 701

Kirkpatrick, J., Henry, T., & McCarthy, D. 1991, ApJS, 77, 417

Kirkpatrick, J., & McCarthy, D. 1994, AJ, 107, 333

Kirkpatrick, J., Reid, I., Liebert, J., Cutri, R., Nelson, B., Beichman, C., Dahn, C., Monet, D., et al. 1999b, ApJ, 519, 802

Kirkpatrick, J., Reid, I., Liebert, J., Gizis, J., Burgasser, A., Monet, D., Dahn, C., et al. 2000, AJ, 120, 447

Koester, D., et al. 2001, A&A, 378, 556

Kroupa, P., Tout, C., & Gilmore G. 1990, MNRAS, 244, 76

Kumar, S. 1963, ApJ, 137, 1121

Lamontagne, R., Demers, S., Wesemael, F., Fontaine, G., & Irwin, M. 2000, AJ, 119, 241

Landolt, A. 1983, AJ, 88, 439

Leggett, S. 1992, ApJS, 82, 351

Leggett, S., Geballe, T., Fan, X., Schneider, D. 2000, ApJ, 36, L35

Leggett, S., Golimowski, D., Fan, X., Geballe, T., et al. 2002, ApJ, 564, 452

Leggett, S., Ruiz, M., & Bergeron, P. 1998, ApJ, 497, 294

Lépine, S., Shara, M., & Rich, M. 2003, AJ, 126, 921

Liebert, J., Bergeron, P., & Holberg, J. 2004, ApJ, in press

Liebert, J., Bergeron, P., Schmidt, G., & Saffer, R. 1993, ApJ, 418, 426

Livio, M. 1996, ASP Conference Series 90, eds. E. Milone & J. Mermilliod (San Francisco: ASP), 291

Livio, M., & Soker, N. 1984, MNRAS, 208, 783

Lowrance, P. 2001, Ph.D. Thesis, UCLA

Lucas, P., & Roche, P. 2000, MNRAS, 314 858

Luhman, K., Rieke, G., Young, E., Cotera, A., Chen, H., Rieke, M., Schneider, G., & Thompson, R. 2000, ApJ, 540, 1016

Macintosh, B. 1994, Ph.D. Thesis, UCLA

Magazzù, A., Rebolo, R., Zapatero-Osorio, M., Martín, E., & Hodgkin, S. 1998, ApJ, 497 L47

Marcy, G., & Butler, P. 1994, ASP Conference Series 64, ed. J. Caillault (San Francisco: ASP), 587

Marley, M., Saumon, D., Guillot, T., Freedman, R., Hubbard, W., Burrows, A., & Lunine, J. 1996, Science, 272, 1919

Marois, C., Nadeau, D., Doyon, R., Racine, R., &, Walker, G. 2003, Proceedings of IAU Symposium 211, ed. E. Martín (San Francisco: ASP), 275

Marsh, T. 2000, NewAR, 44, 119

Marsh, M., et al. 1997, MNRAS, 286, 369

Marsh, T., Dhillon, V., & Duck, S. 1995, MNRAS, 275, 828

Marsh, T., & Duck, S. 1996, MNRAS, 278, 565

Martín, E., Basri, G., & Zapatero-Osorio, M. 1999, AJ, 118, 1005

Martín, E., Basri, G., Zapatero-Osorio, M., Rebolo, R., & López, R. 1998, ApJ, 507, L41

Martín E., Barrado y Navascués, D., Baraffe, I., Bouy, H., & Dahm, S. 2003, ApJ, 594, 525

Martín, E., Brandner, W., Bouvier, J. Luhman, K., Stauffer, J., Basri, G., Zapatero-Osorio, M., Barrado y & Navascués, D. 2000, ApJ, 543, 299

Matthews, K., & Soifer, B. 1994, Infrared Astronomy with Arrays: the Next Generation, ed. I. McLean (Dordrecht: Kluwer), 239

Maxted, P., Burleigh, M., Marsh, T., & Bannister, N. 2002, MNRAS, 334, 833

Maxted, P. & Marsh, T. 1999, MNRAS, 307, 122

Maxted, P., Marsh, T., & Moran, C. 2000, MNRAS, 319, 305

Maxted, P., Marsh, T., & Moran, C. 2002, MNRAS, 332, 745

Maxted, P., Marsh, T., Moran, C., Dhillon, V., & Hilditch, R. 1998, MNRAS, 300, 1225

Maxted, P., Marsh, T., Moran, C., & Han, Z. 2000, MNRAS, 314, 334

Maxted, P., Moran, C., Marsh, T., & Gatti, A. 2000, MNRAS, 311, 877

McAlister, H., Mason, B., Hartkopf, W., Roberts, L., & Shara, M. 1996, AJ, 112, 1169

McCarthy, C., & Zuckerman, B. 2004, AJ, 127, 2871

McCook, G., & Sion, E. 1987, ApJS, 65, 603

McCook, G., & Sion, E. 1999, ApJS, 121, 1

McLean, I., et al. 1993, SPIE, 1946, 513

McMahan, R. 1989, ApJ, 336, 409

Mihalas, D., & Binney, J. 1981, in Galactic Astronomy, (San Francisco: W. H. Freeman & Co.)

Monet, D., et al. 2003, AJ, 125, 984

Nagashima, C., Dobbie, P., Nagayama, T., Nakajima, Y., et al. 2003, MNRAS, 343, 1263

Najita, J., Tiede, G., & Carr, J. 2000, ApJ, 541, 977

Nakajima, T., Durrance, S., Golimowski, D., & Kulkarni, S. 1994, ApJ, 428, 797

Nakajima, T., Oppenheimer, B., Kulkarni, S., Golimowski, D., Matthews, K., & Durrance, S. 1995, Nature, 378, 463

Napiwotzki, R., Green, P., & Saffer, R. 1999, ApJ, 517, 399

Nelemans, G., Yungelson, L., Portegies Zwart, S., & Verbunt, F. 2001, A&A, 365, 491.

Norris, J., Ryan, S., & Beers, T. 1999, ApJS, 123, 639

Oppenheimer, B., Golimowski, D., Kulkarni, S., Matthews, K., Nakajima, T., Creech-Eakman, M., & Durrance, S. 2001, AJ, 121, 2189

Oswalt, T., Smith, J., Wood, M., & Hintzen, P. 1996, Nature, 382, 692

Oswalt, T. 1981, Ph.D. Thesis, Ohio State University

Oswalt, T., Hintzen, P., & Luyten, W. 1988, ApJS, 66, 391

Paczynski, B. 1976, Proceedings of IAU Symposium 73, eds. P. Eggleton, S. Mitton, & J. Whelan (Dordrecht: D. Reidel), 75

Perryman, M., et al. 1997, A&A, 323, L49

Potter, D., Martín, E., & Cushing, M. 2003, Proceedings of IAU Symposium 211, ed. E. Martín (San Francisco: ASP), 265

Prato, L., Simon, M., Mazeh, T., McLean, I., Norman, D., & Zucker, S. 2002, ApJ, 569, 863

Probst, R. 1983, ApJS, 53, 335

Putney, A. 1997, ApJS, 112, 527

Raymond, S., et al. 2003, AJ, 125, 2621

Rebolo, R., Martín, E., Basri, G., Marcy, G., & Zapatero-Osorio, M. 1996, ApJ, 469, L53

Reed, M., Kawaler, S., & O'Brien, M. 2000, ApJ, 545, 429

Reid, I. 1997 ASP Conference Series 127, ed. R. Humphreys (San Francisco: ASP), 63

Reid, I., & Gizis, J. 1997 AJ, 114, 1992

Reid, I., Gizis, J., Kirkpatrick, J., & Koerner, D. 2001, AJ, 121, 489

Reid, I., & Hawley, S. 2000, in New Light on Dark Stars, (New York: Springer)

Reid, I., Hawley, S., & Gizis, J. 1995, AJ, 110, 1838

Reid, I., Kirkpatrick, J., Liebert, J., Burrows, A., Gizis, J., Burgasser, A., et al. 1999, ApJ, 521, 613

Reipurth, B., & Clarke, C. 2001, AJ, 122, 432

Reylé, C., Robin, A., Scholz, R., & Irwin, M. 2002, A&A, 390, 491

Rieke, M., Rieke, G., Green, E., Montgomery, E.,& Thompson, C. 1993, SPIE, 1946, 179

Saffer, R., Bergeron, P., Koester, D., & Liebert, J. 1994, ApJ, 432, 351

Saffer, R., Livio, M., & Yungelson, L. 1998, ApJ, 502, 394

Saffer, R., Wade, R., Liebert, J. et al. 1993, AJ, 105, 1945

Salim, S., & Gould, A. 2002, ApJ 575, 83

Salpeter, E. 1955, ApJ, 121, 161

Schmidt, G., Liebert, J., & Smith, P. 1998, AJ, 116, 451

Schmidt, G., & Smith, P. 1995, ApJ, 448, 305

Schmidt, G., Smith, P., & Harvey, D. 1995, AJ, 110, 398

Scholz, R., et al. 2004, MNRAS, 347, 685

Schroeder, D., Golimowski, D., Brukardt, R., Burrows, C., et al. 2000, AJ, 119, 906

Schultz, G. 1999, Ph.D. Thesis, UCLA

Schultz, G., Zuckerman, B., & Becklin E. 1996, ApJ, 460, 402

Schwartz, R. 1972, PASP, 84, 28

Schwartz, M., Becklin, E., & Zuckerman, B. 2003, Proceedings of IAU Symposium 211, ed. E. Martín (San Francisco: ASP), 185

Schwartz, R., Dawkins, D., Findley, D., & Chen, D. 1995, PASP, 107, 667

Siegler, N., Close, L., Mamajek, E., & Freed, M. 2003, ApJ, 598, 1265

Silvestri, N., Oswalt, T., & Hawley, S. 2002, AJ, 124, 1118

Silvestri, N., Oswalt, T., Wood, M., Smith, J., Reid, I., & Sion, E. 2001, AJ, 121, 503

Smart, R., et al. 2003, A&A, 404, 317

Sion, E., Fritz, M., McMullin, J., & Lallo, M. 1988, AJ, 96, 251

Stauffer, J., Barrado y Navascués, D., Bouvier, J., et al. 1999, ApJ, 527, 219

Stauffer, J., Schultz, G., & Kirkpatrick, J. 1998, ApJ, 499, L199

Tej, A., Sahu, K., Chandrasekhar, T., & Ashok, N. 2002, ApJ, 578, 523

Tinney, C. 1999 ASP Conference Series 165, eds. B. Gibson, T. Axelrod, & M. Putman (San Francisco: ASP), 419

Trimble, V. 1986, Nature, 320, 311

Trimble, V. 1987, ARA&A, 25, 425

Tweedy, R., Holberg, J., Barstow, M., Bergeron, P., et al. 1993, AJ, 105, 1938

Vennes, S., Thejll, P., Galvan, R., & Dupuis, J. 1997, ApJ, 480, 714

Vennes, S., Thorstensen, J., & Polomski, E. 1999, ApJ, 523, 386

Vrba, F., et al. 2004, AJ, 127, 2948

Wachter, S., Hoard, D., Hansen, K., Wilcox, R., Taylor, H., & Finkelstein, S. 2003, ApJ, 586, 1356

Wagman, N. 1967, AJ, 72, 957

Weidemann, V. 1987, A&A, 188, 74

Weidemann, V. 1990, ARA&A, 28, 103

Weidemann, V. 2000, A&A, 363, 647

Weidemann, V., & Koester, D. 1995, A&A, 297, 216

White, R., & Ghez, A. 2001, ApJ, 556, 265

Wielen, R. 1974, Highlights of Astronomy, Volume 3, (Dordrecht: D. Reidel), 395

Winget, D., Robinson, E., Nather, R., & Balachandran, S. 1984, ApJ, 279, L15

Woitas, J. 1999, Ph.D. Thesis, MPIA

Woitas, J., & Leinert, C. 1998, Abstracts of Contributed Talks and Posters presented at the Annual Scientific Meeting of the Astronomische Gesellschaft, B16

Zacharias, N., et al. 2000, AJ, 120, 2131

Zacharias, N., et al. 2004 AJ, 127, 3043

Zapatero-Osorio, M., Béjar, V., Rebolo, R., Martın, E., & Basri, G. 1999, ApJ, 524, L115

Zuckerman, B., & Becklin, E. 1987a, ApJ, 319, 99

Zuckerman, B., & Becklin, E. 1987b, Nature, 330. 138

Zuckerman, B., & Becklin, E. 1992, ApJ, 386, 260

Zuckerman, B., Becklin, E., Macintosh, B., & Bida, T. 1997, AJ, 113, 764

Zuckerman, B., Koester, D., Reid, I., & Hünsch, M. 2003, ApJ, 596, 477